Preparation and characterisation of new materials for electrolytes used in Direct Methanol Fuel Cells

Alfonso Martínez Felipe

Supervisors

Amparo Ribes Greus

Corrie T. Imrie

Science is organized knowledge. Wisdom is organized life.

Immanuel Kant (1724 - 1804)

I was just guessing at numbers and figures,
pulling the puzzles apart.
Questions of science, science and progress,
do not speak as loud as my heart.

Coldplay

Declaration

This is a thesis submitted to the University of Aberdeen for consideration for the degree of Doctor in Philosophy and to the Univesitat Politècnica de València for consideration for the degree of Doctor in Chemical Engineering, in the framework of an agreement between both universities for the joint supervision of my PhD studies.

It has not been previously submitted for any degree and, except where due reference is made, is believed to be wholly original. The research has been carried out by myself, except where acknowledged, in the Department of Chemistry of the University of Aberdeen and in the Univesitat Politècnica de València.

Some of the chapters are presented in the style of journal articles. Even though the experimental work has been carried out by me, the other authors have contributed to the discussion of the results and advices.

Alfonso Martinez Felipe
September 2009

Summary

The aim of this PhD thesis is the preparation and study of new materials to be used as electrolytes in Direct Methanol Fuel Cells (*DMFC*) in order to reduce crossover of methanol. Different materials have been prepared, including polymer dispersed liquid crystals, crosslinked polymers with high protonic conductivity and polymeric liquid crystals. Moreover, a methodology to characterise potential new materials for their application in *DMFC* has been developed. The absorption properties of water and methanol in the materials have been studied in different conditions and compared with the results obtained for commercial Nafion membranes used in DFMC. The absorption and diffusion properties of water and methanol through the materials have been studied by means of Fourier Transform Infrared Spectroscopy and thermal analysis techniques. The methodology provides important information to analyse the interactions between the different functional groups of the polymers and the solvents commonly used in *DMFC*. Finally, a device has been designed and set-up to analyse the effect on crossover of methanol of the electro-osmotic drag and the polarisation of the polymeric electrolytes.

Acknowledgments

First of all I would like to acknowledge my two supervisors, for their excellent guidance during all these years.

Thanks Corrie for all your effort and support in this long way. Thanks for giving me the chance to learn and see things from so many different points of view.

Thanks a lot Amparo for believing in me from the start, until the end, and show me the way of excellence in research and teaching. Thanks for bringing me at the start of a brilliant future. For your strength is my inspiration.

Thanks to my family; to my mother and all the Charos and Jose Marias in my life; por vuestro amor y apoyo durante todos estos años en la cercanía y la distancia. For those who have always been with me, and those who are not anymore.

Infinite thanks to Marta; for all the love that we share and the time that I owe you. For all your comprehension. For all the evenings in the world. Thanks for creating bridges across the sea. Because the future is bright if you are by my side.

Thanks to my workmates in UPV. Well, to my brothers and sisters of long days. Moltes gràcies de tot cor Laura, Rosana, Jose i Fran, per ser la meua segona família. Per fer que els moments durs lluisquen tant i els brillants siguen inoblidables. Thanks Roberto and Cristina, for believing in our beautiful project. Thanks all to form the most brilliant group of people I'll ever find. Everything is possible if we work together. Also thanks to all the students who have shared any single bit of my thesis with me. You all have made me be the person I am now.

Thanks to all my friends; for your time, words and music along the years. For keeping this light on and help me grow as the person I am now.

Thanks also to all the persons in UPV who have helped me during this long distance, in one or another way.

Thanks also to all the people in the Department of Chemistry of the University of Aberdeen. Thanks again Peter, for your time and advices. Thanks for your practical demonstrations about pressure in closed systems. Especial thanks also for Dr. Lu and his patience, for showing me the first words in the language of synthesis. Also thanks to Brian Paterson, for his help with the thermal analysis, and Russel Gray for his NMR advices. Thanks a lot Val and the rest of people from the Department who made my life easier in my long trips.

I cannot forget all these persons that I met in Aberdeen, which made me feel like home when I was away. Thanks from my heart Toby. Thanks dear old friends who shared my first days in Aberdeen, Ioaniss, Ash, Simmy. Thanks to all of you that I had the luck to meet during these years, Chris, Simon, James, Colin, Carl, Nasos…There is always a good reason to come back to the North Pole.

Thanks to all of you, the future is ours.

General aims of the PhD thesis

In recent years the interest in alternative energy sources has increased enormously mainly due to environmental and political reasons. One of the most promising alternatives to conventional energy sources is the use of low temperature fuel cells. In particular, fuel cells using bio-alcohols produced by renewable sources (Direct Methanol Fuel Cells-*DMFC* and Direct Ethanol Fuel Cells-*DEFC*) are particularly suitable for portable applications. *DMFC* and *DEFC* reach high efficiencies with low environmental impact, and they are not affected by some of the restrictions derived from the use of hydrogen (for example, production, storage, delivery, safety procedures, etc)

However, the technology related to *DMFC* and *DEFC* still presents some serious limitations. One of the most important problems related to *DMFC* and *DEFC* is the so-called crossover phenomenon, which consists of the transport of unreacted alcohol from the anode to the cathode through the polymeric electrolyte. The alcohol transferred by crossover reacts with the oxygen at the cathode following a conventional combustion reaction which does not contribute to the electrical power generation. Crossover can account for up to 30% decrease in fuel efficiency and a loss of cathode voltage by the formation of a mixed potential.

Crossover is mainly attributed to the links between the transport processes of protons, water and methanol through the polymer electrolyte and also to the electroosmotic drag. Membranes used in low temperature fuel cells usually consist of ionomeric polymers which consist of hydrophobic backbones and contain some proton exchange groups, usually ionic groups and often based on sulfonic acid. The hydrophobic backbone provides mechanical integrity to the membrane while the ionic groups increase the proton conductivity required in the fuel cell. In the presence of water, a hydrophobic/hydrophilic microphase separation occurs and the proton conductivity takes place through interconnected ionic channels. It has been shown that the morphology of the membranes used in *DMFC* has a strong effect on the diffusion of water and methanol and also on the proton conductivity. The diameter and length of the ionic channels, the concentration and distribution of ionic charges and also the water content affect the proton conductivity and methanol permeability of the membrane.

In particular, water content is of special importance in determining the morphology of the membrane and hence the proton conductivity and the methanol solubility. Normally, high water content leads to high methanol permeation rates, especially due to the so-called vehicular transport mechanism. However, it is difficult to obtain high proton conductivities in relatively dry membranes, since the proton conductivity is strongly dependent on the formation of ionic clustering, which is related to the presence of water in the membrane. Therefore, attempting to reduce crossover by reducing water content results in a consequent reduction in the proton conductivity. Thus, in designing new membranes for *DMFC* (and also for *DEFC*) a balance between the degree of sulfonation, of the hydrophilic/hydrophobic ratio and water content must be achieved, since the methanol permeability and proton conductivity are interconnected.

Attempts to control the swelling of *DMFC* membranes and the methanol solubility have been made by changing the membranes structures by chemical (crosslinking) or physical (blending) modification, or by the introduction of inorganic particles or hydrophobic moieties. However, these approaches have not improved to any great extent the behaviour of the commercial materials used in hydrogen fuel cells.

The main aim of this PhD thesis is to prepare and characterise new polymeric materials that could be used as electrolytes in *DMFC*. The work is focused on the preparation of phase separated systems which may show high proton conductivities and low methanol permeabilities, independent of water content, in order to minimize the crossover phenomenon. In particular, liquid crystalline and crosslinked polymers have been prepared in order to allow some control over the morphology of the new materials. The role of liquid crystallinity in the polymers is to provide a means of controlling the membranes's morphology, which does not depend on water content.

A range of different materials have been studied in this thesis: perfluorosulfonic commercial materials, polymer dispersed liquid crystals containing cellulose acetate (*PDLC*), poly(vinyl alcohol) crosslinked membranes and liquid-crystalline side-chain polymers containing sulfonic groups (*SCLCP)*. This selection of membranes having very different compositions allows for the comparison of some general features of membrane design including stability, the presence of protonic conducting groups, and the complexity of the preparation method and the possibility of morphological control.

These considerations are important in selecting the proper configuration for new *DMFC* electrolytes, and are summarised in *Table 1*, together with the corresponding chapter where it is studied in this PhD thesis:

Table 1. Some General features of the materials investigated in this Thesis

	Perfluorinated membranes	PDLC	PVA crosslinked	SCLCP
Chapter	3	4	5	6
Thermal Stability	High	Low	High	Medium
Complexity (fabrication)	-	Low	Medium	High
Morphological control	Hydrophilic / hydrophobic separation	Mesomorphism	Crosslinking	Mesomorphism
Proton conductivity	Yes	No	Yes	Yes

Chapters 3 and 5 study some aspects related to materials which have already been used as *DMFC* electrolytes. In these materials the morphology is driven by the phase separation between the hydrophobic backbone and the hydrophilic domains created by the presence of ionic groups. Since the phase separation is directly related to the presence of the proton conducting groups, it is possible to assume that this is a coupled system.

Chapter 4 shows the results for dispersed liquid crystals based on a cellulose acetate substrate. The study of this system is helpful in comparing the effect of physical interactions and chemical bonds in the phase morphology of membranes. The results can be applied for the formation of future *PDLC* in proton conducting backbones. Finally, in chapter 6 a study of a new series of liquid crystal copolymers containing sulfonic groups is described. In these materials, the morphology is not dependent on the presence of the ionic groups, at least not entirely, and therefore this could be labelled as a semi-decoupled system.

The characterisation methods used in this thesis are intented to study the interactions between the components, the phase separation and the resulting morphology of the membranes and the thermal stability of the materials. With this in mind, one of the aims of this thesis is to establish a methodology for characterising new materials and to evaluate their potential to be used as controllable morphology membranes in *DMFC* (and also potentially in *DEFC*) This includes the use of physical and chemical analytical techniques as well as diffusion tests to study the selectivity of the polymers in alcohol and water mixtures.

The physical-chemical characterisation is carried out using Fourier Transform Infrared Spectroscopy (FTIR) and thermal analysis (Differential Scanning Calorimetry, DSC and Thermogravimetric Analysis - TGA). In some of the chapters additional techniques have been used (Polarised Light Microscopy, PLM and Nuclear Magnetic Resonance spectrsocopy, NMR). In order to study the diffusion properties in water and alcohol mixtures, swelling and diffusion tests have been performed. A new test module has been designed and constructed, which can measure the effect of morphological reorganisation on the diffusion properties (flux and selectivity) of externally controlled materials, such as liquid crystalline polymers, in real time. The methodology developed by combinating these techniques is explained in chapter 2.

This PhD thesis forms part of a research programme focused on the preparation of new electrolytes for *DMFC* and *DEFC*. The development of the characterisation methodology and the production of the first set of materials are part of a project to develop new electrolyte materials and to characterise them. To achieve the aims of the PhD studies it was necessary to design and set-up a laboratory for the preparation of the new polymeric materials. This included the acquisition of the laboratory instrumentation and chemicals for advanced organic synthesis, the development and implementation of safety instructions for the management and storage of dangerous and hazardous chemicals and for the proper management of solvents.

The future direction of the research involves the study of the dielectrical relaxations of the liquid crystalline polymers. With this aim, during the development of this thesis, a plant for measuring depolarisation processes has been set-up and built. This plant measures the polarisation and depolarisation phenomena which take place in low proton

conductive polymers, and provides a means of studying the reorientational processes of liquid crystalline materials in the presence of strong electrical fields.

Abbreviations

Ea	Activation Energy
ATR	Attenuated Total Reflectance
σ, σ_+	Proton Conductivity
DSC	Differential Scanning Calorimetry
DEFC	Direc Ethanol Fuel Cell
DMFC	Direct Methanol Fuel Cell
FTIR	Fourier Transform Infrared Spectroscopy
HD	Hydrolysis Degree
LCP	Liquid Crystal Polymers
MCLCP	Main-Chain Liquid-Crystalline Polymers
MW	Molecular Weight
NMR	Nuclear Magnetic Resosance Spectroscopy
PVA	Poly(vinyl alcohol)
PDLC	Polymer Dispersed Liquid Crystals
PEM	Polymer Electrolyte Membrane
PLM	Polarised Light Microscopy
PEMFC	Proton Exchange Membrane Fuel Cell
SCLCP	Side-Chain Liquid-Crystalline Polymers
TGA	Thermogravimetric Analysis

Contents

1

Introduction

1. Fuel Cells

1.1 Definition and basic features

Fuel cells (FCs) are electrochemical devices that convert the chemical energy of the reactants into electrical power [1, 2]. The fuel (*A*) is supplied to the anode where the oxidation reaction takes place with the consequent release of electrons. The electrons generated in the oxidation flow through an external circuit and are then consumed by the oxidation agent (*B*) at the cathode (reduction reaction):

Oxidation reaction	$A \rightarrow A^{+n} + ne^-$
Reduction reaction	$B + ne^- \rightarrow B^{-n}$

The electrodes (anode and cathode) are separated by an electrically isolating material (electrolyte) and the external flow of electrons produces direct current (*DC*). Some ionic species involved in the reactions must be transferred through the electrolyte to balance the ionic charge of the reaction. The generation of net electrical energy only happens if the electrochemical reactions take place at different sites of the cell.

Even though fuel cells and batteries have a similar electrochemical basis, there are several differences in their performance. Unlike batteries, fuel cells cannot be recharged. The energy is produced continuously as the fuel is supplied to the anode. The products of the reactions are removed from the cell together with the exhausted fuel stream. Therefore, it is necessary to have a system that continuously supplies the fuel and the oxidant to the electrodes. The absence of recharging cycles enhances the stability of the electrolyte and the other materials in the cell, which leads to higher life times (durability).

1.2 Brief history of fuel cells

The chemical basis of fuel cells was first discovered by Christian Friedrich Schönbeing in Switzerland in 1838. A few years later (1843) Sir William Grove manufactured the first fuel cell. The materials he used can still be found in current phosphoric acid fuel cells. In 1959 Francis Thomas Bacon, a British engineer, developed a stationary fuel

cell of 5 kW and a 15 kW fuel cell to supply electrical power to a soldering iron. At the same time, fuel cells started to be applied in some farming vehicles using potassium hydroxide in the electrolyte and compressed hydrogen and oxygen.

During the 1960s the patents developed by Bacon and his team were used in the NASA space programs. Alkaline fuel cells were used in the spaceships in the first missions. Proton exchange membrane fuel cells (designed by Pratt & Whitney Aircraft, General Electric) were first used in the Gemini program (1970s).

The first large scale stationary plant used for terrestrial applications was built and commercialized by *UTX* (*UTC Power Ltd*). The plant was used for co-generation in hospitals, universities and big company buildings. *UTC* still markets under the name of PureCell 200 (200 kW), which nowadays is the only fuel cell system used by the NASA. *UTC Ltd* is also developing fuel cell systems for vehicles, buses and mobile phone antennae, and was the first company to develop a fuel cell capable of working at low temperatures.

During recent years, fuel cells have undergone important improvements. The first fuel cells required high temperatures to achieve high performances, which required very resistant and expensive materials. Very pure reactants (hydrogen and oxygen) were also needed in order to avoid catalyst poisoning. Therefore, and despite their success in the NASA programs, their terrestrial applications were not realised until the end of the 1980s and beginning of the 1990s.

Nowadays there is a huge variety of fuel cells working in different application areas, including for example, stationary power supply on small and large scales, portable applications and military devices. The current research is focussed on improving their performance while reducing their cost, in order to broaden their potential application market.

1.3 Basic elements and materials

Fuel cells convert chemical energy into electrical energy by means of electrochemical reactions. In order to obtain a net flow of electrons, it is necessary to ensure that the

oxidation and the reduction reactions take place separately. The basic elements of a fuel cell using hydrogen are shown in *Figure 1.1*:

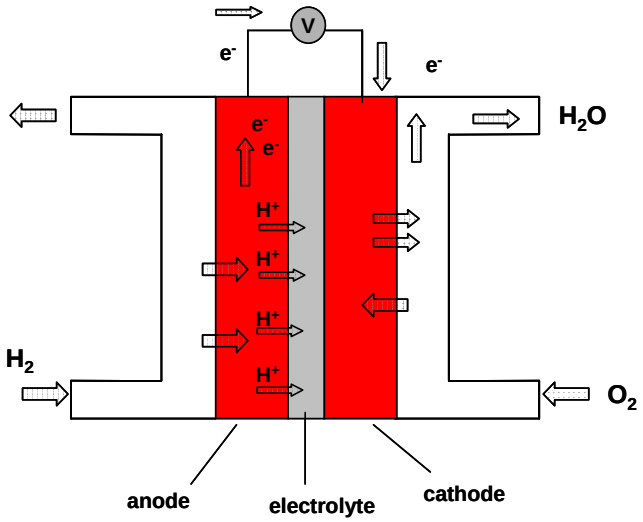

Figure 1.1 Schematic design of a fuel cell using hydrogen

Electrodes

The electrodes are the elements at which the electrochemical reactions take place. The fuel is oxidized at the anode and the oxidant (usually oxygen from the air) is reduced at the cathode. The electrodes are usually made of porous materials (graphite) in order to achieve high area-to-volume ratios. A catalyst (usually platinum or another metallic element) is then coated on the electrodes inner surface in order to reduce the activation energy of the electrochemical reactions. Due to the high costs of the catalysts (especially those used for low temperature fuel cells) the electrodes are usually the most expensive elements of a fuel cell.

The most important functions of the electrodes are:

-To provide physical sites for the electrochemical reactions to occur.

-To transport the ionic species in order to complete the reactions (mass and charge transport).

- To separate the gas phase (H_2 or O_2) from the electrolyte.

- To evacuate the spent fuel and oxidant and the products of the reaction.

The operation of the electrodes can be seriously affected by poisoning by impurities existing in the input streams. This fact is particularly critical at the anode of fuel cells operating at low temperatures. As a result, very restrictive cleaning and reforming of the fuel are required prior to its use.

Electrolyte

The electrolyte is the central part of the fuel cell and separates the anode from the cathode, so that the REDOX reactions take place at different sites of the cell. The electrolyte must therefore avoid the flow of the reactants from one side to the other of the cell. The electrolyte must also be impermeable to electrons since they must flow through an external circuit. However, in order to balance the electrochemical reactions, the electrolyte must transport some ionic species from the anode to the cathode, or vice versa (H^+, OH^-, etc).

The most important functions of the electrolyte can be summarised as follows:

- To separate the anode and the cathode.
- To avoid fuel crossover from the anode to the cathode.
- To avoid electrical conduction.
- To allow the ionic species involved in the reaction to be transferred from the anode to the cathode and vice versa.

Other common elements of fuel cells are:

Gas Diffusion Layers (*GDL*)

Gas Diffusion Layers (*GDL*) are used in low temperature fuel cells to supply and distribute the fuel and air to the surface of the electrodes. They are also used to remove the exhausted reactants and the reaction products and to connect the electrodes with the current collectors. Even though *GDL* are usually made of carbon cloth or carbon paper, they can be modified with Teflon sheets or other hydrophobic materials to increase their hydrophobic character and avoid water saturation

Bipolar field flow plates

One individual cell (one electrolyte sandwiched by two electrodes) provides low voltages (~1 V). In order to increase the electrical output power, single individual cells are connected in series or parallel configurations, in so-called fuel cells stacks. The bipolar plates are the elements used to separate adjacent fuel cell units.

The main functions of the bipolar plates are:

- To deliver the reactant gases to the electrodes.
-To remove waste heat (refrigeration).
- To conduct electrons within an internal circuit as part of the electrochemical reaction.

Bipolar plates are commonly made of graphite due to its high electrical conductivity and high resistance to corrosion. Alternatively, bipolar plates can be made of a metal to increase their conductivity and reduce their size.

Other auxiliary systems used in large scale fuel cells plants are:

Pre-treatment systems

Hydrogen is the most common fuel used in fuel cells. In high power generation, it is usually obtained from other commercial materials in previous stages. Natural gas (*NG*, methane) is the most common raw material for the production of H_2. Natural gas is cleaned and reformed to produce hydrogen (usually by steam reforming) and the resulting stream is further cleaned to obtain pure hydrogen. Cleaning and reforming operations are particularly important in low temperature fuel cells, since the catalysts used in the electrodes are very sensitive to the presence of particles or oxides.

Heat recovery systems

The electrochemical reaction occurring in a fuel cell is exothermic. The heat produced in the reaction can be used to improve the overall plant performance by using refrigerated bipolar plates. This energy can be then used in the fuel reforming reaction, which is highly endothermic.

Electrical current treatment

Fuel cells produce *DC* current. A power generation plant needs to attach a *DC* to alternative current (*AC)* converter prior to the electrical power distribution via the power grid.

1.4 Main characteristics of fuel cells

The following are some of the most remarkable properties of fuel cells:

High efficiencies

Since electrical power is directly obtained from the chemical reactions, the overall efficiency of the process is very high. Fuel cells do not require the existence of temperature differences or gradients to convert the energy. As a result, the performance of fuel cells is not restricted by the Carnot efficiency ($\eta_C = 1 - \frac{T_L}{T_H}$, where T_L and T_H are the low and high temperature of the reservoirs in a thermal machine). Instead, the maximum energy or electrical work available is defined by the Gibbs energy (ΔG) of the reactants and products:

$$\eta_{rev} = \frac{\Delta G}{\Delta H}$$

where η_{rev} is the reversible efficiency and ΔH is the enthalpy change of the electrochemical reaction.

The maximum efficiency of a fuel cell is around 83% when it works reversibly. This ideal value decreases when the fuel cells starts to generate electrical power. Despite this efficiency reduction, the actual performance of fuel cells ($\eta_{rev} = 40 - 55\%$) is still very high compared to thermal conversion systems.

Low environmental impact

Fuel cells have very low environmental impact, particularly when compared to other devices of power conversion. The only product of the electrochemical reactions is water or CO_2 at very low concentrations. Moreover, the use of low temperatures avoids other side reactions involving polluting by products (nitrogen and sulphur oxides, etc). Another important advantage is the use of bio-alcohols. Methanol and ethanol can be used in the so-called Direct Methanol Fuel Cells or Direct Ethanol Fuel Cells (*DMFC*, or *DEFC*, respectively). Since alcohols can be obtained from renewable sources, this process of energy conversion is sustainable.

Modularity

Individual cells can be arranged in parallel or in series in order to obtain higher electrical power. Fuel cell stacks can be designed and customized to provide different power supplies as required. Since the efficiency of the process does not vary much with the size of the pack, it is easy to use them on different scales.

Non-mobile elements

Fuel cells do not have mobile parts, leading to higher durability and longer life times than other thermal engines.

Despite these advantages of fuel cells, some negative aspects must be discussed:

Hydrogen sources and environmental impact

Even though hydrogen is one of the most abundant elements found on Earth, hydrogen gas (H_2) is very limited in the atmosphere. The methods and sources employed for the production of H_2 usually involves the use of fossil resources (natural gas) and other non-sustainable processes. Such methods demand high economical and technological efforts. Alternative methods to produce or store hydrogen are still under research. Interest has focused on the development of devices to produce hydrogen from renewable sources, using hydrogen as an energy vector.

Pre and post operations

The pre-treatment operations applied to the crude fuel (refining, reforming, cleaning, pressurizing) and post-treatment of the electrical signal obtained (*DC* to *AC* conversion) require energy and increase the cost of the overall operation. These facts are particularly critical in low temperature fuel cells.

Efficiency losses: polarisation

The reversible efficiency (η_{rev}) of a fuel cell is an ideal value that will never be achieved in real operations. As the fuel cell starts to generate electrical current, the voltage falls down due to a loss of efficiency. The efficiency loss in a fuel cell is called *polarisation*. There are three main polarisation sources:

- Activation polarisation, which is related to the activation energy necessary to initiate the electrochemical reactions.
- Ohmnic polarisation, which is the voltage loss related to the inherent electrical resistance of the physical elements between the anode and the cathode, mainly the electrolyte.
- Concentration polarisation. It occurs when the current density is very high and the reactants cannot be supplied to the electrodes at the same velocity (mass transport resistance).

The actual performance of a fuel cell will be controlled by the sum of these three contributions. Polarisation curves describe the actual performance of a fuel cell and relate the current density and the voltage of a cell. A typical polarisation curve of a fuel cell is shown in *Figure 1.2*:

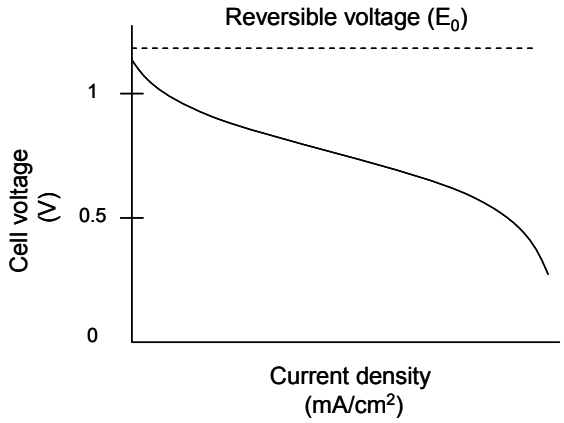

Figure 1.2 Example of a polarisation curve of a fuel cell

High installation costs

Even though the market for fuel cells has expanded in recent years, the technology is still not widely appreciated in the industrial sector. The costs related to their installation are still very high, and amortization times are very long. These factors will tend to decrease when the applications of fuel cells diversify into different sectors.

1. 5 Classification of fuel cells

There are many classifications of fuel cells based on different considerations, such as the operating temperature, the reactants used, the physical configuration, *etc*. However, fuel cells are most frequently classified considering the material used as the electrolyte.

The following is a brief description of the most representative types of fuel cells:

Proton Exchange Membrane Fuel Cells (*PEMFC*)

Proton Exchange Membrane Fuel Cells (*PEMFC*) use a polymeric electrolyte, usually a cationic exchange membrane, to provide high proton conductivities from the anode to the cathode. They operate at low temperatures (usually below 100°C) and have relatively high efficiencies and high current densities. The use of low temperatures and light electrolytes (usually polymers) make *PEMFC* suitable for portable applications in mobile phones, laptop computers, *etc.*

Alkaline Fuel Cells (*AFC*)

A concentrated KOH aqueous solution (85% by weight) usually supported in an asbestos matrix is used as the electrolyte in *AFC*. The electrolyte must be continuously refilled in order to compensate for evaporation as they operate in a temperature range between 65ºC and 220ºC. In *AFC* the ionic charge is compensated by the transport of OH^- groups from the cathode to the anode through the electrolyte.

Phosphoric Acid Fuel Cells (*PAFC*)

PAFC use a saturated phosphoric acid aqueous solution as the electrolyte which acts as a highly proton conducting medium. These fuel cells are the most used Worldwide, particularly in large scale plants for electrical power generation (5 MW). The usual working temperatures range of *PAFC* (150°C - 200°C) are slightly higher than those of *PEMFC* and *AFC*.

Molten Carbonate Fuel Cells (MCFC)

MCFC use molten carbonate solutions as the electrolyte contained inside a ceramic matrix, usually $LiAlO_2$. These fuel cells operate at high temperatures (*T*~650°C) and CO_3^{-2} is transferred from the cathode to the anode. *MCFC* consume CO_2 at the cathode at the same time that is produced at the anode. A recirculation system is used in *MFCF* to improve their performance.

Solid Oxide Fuel Cells (SOFC)

In *SOFC* solid oxides are used as electrolytes. *SOFC* usually work at very high temperatures (1000°C) and therefore very high efficiencies are achieved. However, cell materials must be thermally and chemically resistant in order to avoid degradation and corrosion problems. The performance of *SOFC* is based on the transport of O^{-2} ions from the cathode to the anode. Finally, several attempts have been made to lower the temperature of operation of *SOFC* to ~ 800ºC, in the so-called Intermediate Temperature Solid Oxide Fuel Cells (*ITSOFC*).

Table 1.1 summarises the different types of fuel cells and their most relevant characteristics.

Table 1.1 Classification of fuel cells and their main features

Fuel Cell Characteristics	PEMFC / DMFC*	AFC	PAFC	MCFC	TSOFC
Electrolyte	Cationic Exchange membranes	Potassium hydroxide	Phosphoric acid	Molten carbonate	Ceramics
Operation temperature	80ºC	65ºC–220ºC	205ºC	650ºC	800ºC–1000ºC
Charge carrier	H^+	OH^-	H^+	CO_3^{-2}	O^{-2}
NG reformer	Yes / No	Yes	Yes	No	No
Cell materials	Carbon	Carbon	Graphite	Iron steel	Ceramics
Water management	Evaporation	Evaporation	Evaporation	Gas	Gas
Catalyst	Platinum	Platinum	Platinum	Nickel	Nickel
Heat management	Gas processing Refrigerant	Gas processing Refrigerant	Gas processing Refrigerant	Internal reforming Gas processing	Internal reforming Gas processing

*Direct Methanol Fuel Cells (see paragraph 1.8)

1.6 Applications of fuel cells

Due to their flexibility and versatility, fuel cells can be used in a broad range of applications:

Space industry

Alkaline fuel cells were first used in spacecrafts in the 1960s and 1970s. They supplied not only electrical energy but also drinking water during the missions. Fuel cells were a very convenient alternative to the use of combustion engines (which would require very dense fuels) and batteries (which were too heavy). Fuel cells also fitted very well to the short times of the missions (usually less than one year) offering very reliable energy supply.

In the spacecraft launched during the Apollo program three fuel cells supplying 1.5 kW - 2.2 kW were used in a parallel configuration for over 10000 working hours in 18 missions. The fuel cells used cryogenic hydrogen and oxygen and weighed 114 kg. During the 1980s, *NASA* continued using 15 kW fuel cells in more than 100 missions for more than 80000 working hours.

Military applications

Different types of fuel cells are used as portable power generation plants in military missions. The high efficiencies, versatility, long operation times and silent performance make fuel cells a very useful power generation system for military purposes in terrestrial and marine operations. For example, *PEMFC* stacks (300 kW) have been used by the USA Navy in submarines providing a maximum speed of 145 km/h. The use of fuel cells reduces the amount of fuel used, as well as the number of auxiliary staff and equipment necessary in long-term operations.

Portable applications

The development of fuel cells has been applied in several portable electronic devices. Small fuel cells (mini-fuel cells) show longer operation times. Light prototypes of fuel cells are suitable for laptops (50 – 100 kW), mobile phones (10 W) or batteries chargers (<50 kW). The success of the performance of fuel cells in portable applications in the

future will depend on the operation temperature (usually below 100ºC), fuel availability and the achievement of short starting times.

Transport

Legislation surrounding environmental issues concerning the transport sector is becoming stricter, as a result of the impact of global warning. The use of fuel cells can reduce the CO_2 produced by internal combustion engines by up to 70%. However, fuel cells would not only address the environmental issues but also satisfy the features related to the starting times, fuel economy and power supply.

PEMFC are probably the most suitable fuel cells for vehicular applications. They work at low temperatures (around 80ºC) showing efficiency near 60% and high power densities. The use of solid electrolytes at low temperatures avoids corrosion problems. However, to date the use of *PEMFC* is restricted to the use of very pure hydrogen.

Different vehicle companies have developed prototypes of cars and buses using hydrogen and methanol fuel cells. *PEMFC* using hydrogen have been also proved successful in aerospace applications.

Low power stationary applications

Fuel cells are also used to supply electricity and heat in small buildings on a small scale. Fuel cells can be found in auxiliary and emergency supply systems (<10 kW), telecommunications and remote operations (100 W–1 kW) or in applications for the construction sector (< 10 kW).

Small scale *PAFC* and *PEMFC* are the most common fuel cells used to provide energy in buildings. In order to increase the use of these systems in cities, natural gas networks could be used together with individual reformers to obtain pure hydrogen for fuel cells. An alternative is to use different fuels, such as low molecular weight alcohols (see section 1.8).

High power stationary applications

Fuel cells are established in the markets of heat and electricity large scale generation. *PAFC*, *MCFC* and *SOFC* are used in stationary power plants providing a range of power from 1 to 5 MW. These fuel cells operate at very high temperatures and do not need metal based catalysts. This fact avoids strict pre-treatment operations of the fuel and reduces the cost of the operation.

Table 1.2 shows a summary of the different applications and the fuel cells used:

Table 1.2 Classification of fuel cells and their main application fields

Fuel Cell	Power supplied (kW)	Life time (hours)	Target capital costs (€/kW)	Potential or current applications / years
Polymeric electrolyte H_2, CH_3OH	1 – 1000	> 40000	> 140	Space 1960 - Transport 1996 - Stationary supply 1992 -
DMFC* **CH_3OH**	1 - 10000	> 10000	> 140	Transport 2010 – Remote supply 2000
AFC Alkaline H_2	10 – 100	> 10000	> 140	Space 1960 - Transport 1996 - Stationary supply 1966-
PAFC Phosphoric acid CH_4, CH_3OH	100 – 5000	> 40000	670 -	Stationary supply in integrated systems 1966
MCFC Molten carbonate CH_4 ,carbon	1000 – 100000	> 40000	670 -	Intermediate supply, cogeneration 1996 -
SOFC Solid oxide CH_4 ,carbon	100 - 100000	> 40000	1000 -	Intermediate supply, cogeneration 1996 – Regeneration 2010 – Spacel

*Direct Methanol Fuel Cells (see paragraph 1.8)

1.7 Proton exchange membranes fuel cells (*PEMFC*)

One of the most promising alternatives to the combustion engine in vehicular applications is the use of fuel cells operating at low temperatures. Proton exchange membranes fuel cells (*PEMFC*) use polymeric proton exchange membranes as electrolytes and operate at temperatures below 100°C and low pressure ranges (1 – 5 atm). Such mild conditions allow the use of a broad range of materials in cell design without the risk of corrosion. *PEMFC* have very simple configurations and need short starting times due to their low operation temperatures. *PEMFC* also show high efficiencies and high current densities compared to high temperature fuel cells. The use of low temperatures and pressures avoid problems related to leaks, corrosion and migration or recrystallisation of the electrolyte. All these features enhance the durability of *PEMFC*, which show life-times of up to 50000 hours.

PEMFC can be used in a wide range of applications, but they are particularly useful as low power generators in portable applications, and since they can also be configured into stacks, the power generated can be easily varied.

The core of *PEMFC* is the so-called Membrane Electrode Assembly (*MEA*). A small amount of catalyst is coated onto the two porous graphite layers, which have been previously covered with Teflon to prevent water absorption. The membrane is then placed between the two electrodes and sealed at high temperature and pressure (sinteration).

The other components of *PEMFC* are: bipolar plates, refrigerating plates and locking elements of the stack (see *Figure 1.3*).

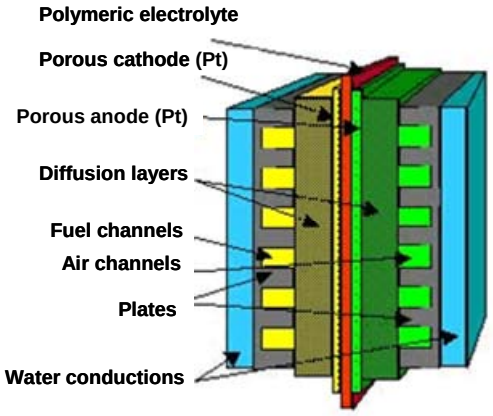

Figure 1.3 Schematic of a Membrane electrode assembly in a PEMFC

In *PEMFC* the hydrogen is supplied through the bipolar plates and diffused to the anode through the gas diffusion layer. The hydrogen molecules then diffuse through the porous structure of the anode to the catalytic active sites where the oxidation reaction takes place. The electrons released are then driven through the bipolar plates to the cathode by an external circuit while the protons are transported through the membrane. The oxygen from the air together with the electrons and the protons react at the cathode and water and heat are produced.

The overall reaction leads to the generation of electrical energy and water:

Oxidation reaction	$H_2(g) \rightarrow 2H^+(aq)+2e^-$
Reduction reaction	$2H^+(aq)+2e^-+½O_2(g) \rightarrow H_2O(l)$
Overall reaction	$\mathbf{H_2(g)+½O_2(g) \rightarrow H_2O(l)}$

PEFMC require very pure hydrogen input streams to avoid the poisoning of the catalysts. Even small amounts of nitrogen oxides, sulphur oxides or carbon monoxide can cause a decline in their performance. Therefore, very strict pre-treatment operations are required before the hydrogen stream enters the anode. All these operations increase the price of the fuel cell, the energy consumption and promote the formation of by-products.

One of the most important targets of *PEMFC* is to optimise the properties of the polymeric electrolyte. Even though perfluorinated polymers are the most common

materials used in *PEMFC*, in recent years a variety of new materials have been designed.

1.8 Direct Methanol and Direct Ethanol Fuel Cells

Low temperature fuel cells using hydrogen are a promising alternative to the use of fossil fuels in vehicular applications. Hydrogen has a high energy density and its oxidation leads to the formation of water as the only product. Hydrogen is a good energy vector, *i.e.*, it can be used as a carrier to store energy. If it is produced from renewable energy sources and then used in fuel cells, the whole process would be eventually sustainable and non- polluting.

Unfortunately, the use of hydrogen in portable applications presents several disadvantages. These problems represent a serious limitation to the use of *PEMFC* in vehicles on large scale. Hydrogen is found at very low concentrations in the atmosphere (H_2) and therefore it must be produced from other sources. This also implies the use of another energy source and the possible generation of undesirable by-products. Some processes involve electrolysis or thermo-chemical cycles by using different energy sources. However, the most important process for the production of hydrogen is steam reforming of natural gas (CH_4):

$$CH_4 + H_2O \rightarrow CO + 3H_2$$
$$CO + H_2O \rightarrow CO_2 + H_2$$

Steam reforming is widely used in stationary applications such as large scale power generation plants. However, steam reforming (as well as other kinds of reforming) uses fossil materials and other non-renewable energy sources.

In portable applications, *in situ* reforming of natural gas or other low molecular weight hydrocarbons is more complicated. The development of hydrogen gas pipeline networks similar to those used for natural gas distribution could be an alternative; however the costs and safety measures would be more restrictive. As an alternative, the hydrogen

can be stored as a liquid. Unfortunately, this involves high pressures and low temperatures with the consequent energetic and economic costs.

The use of hydrogen also implies strict safety restrictions due to its high flammability. Hydrogen forms explosive mixtures with the oxygen in the air and can diffuse rapidly due to its molecule size. In the case of on board storage, the tanks used for liquid hydrogen must accomplish a great variety of safety restrictions.

As a consequence of the problems related to the use of hydrogen, in recent years interest in other fuels for low temperature fuel cells has emerged. This is the case for the so-called Direct Methanol and Direct Ethanol Fuel Cells (*DMFCs* and *DEFCs*, respectively).

Direct Methanol and Ethanol Fuel Cells are based on the oxidation of methanol and ethanol in the anode of a *PEMFC*, according to the reactions:

DMFC:

Oxidation reaction	$CH_3OH + H_2O \rightarrow CO_2 + 6H^+ + 6e^-$
Reduction reaction	$3/2\ O_2 + 6H^+ + 6e^- \rightarrow 3H_2O$
Overall reaction	$\mathbf{CH_3OH + 3/2\ O_2 \rightarrow CO_2 + 2H_2O}$

DEFC:

Oxidation reaction	$CH_3CH_2OH + 3\ H_2O \rightarrow 2\ CO_2 + 12\ H^+ + 12e^-$
Reduction reaction	$3\ O_2 + 12H^+ + 12e^- \rightarrow 6H_2O$
Overall reaction	$\mathbf{CH_3CH_2OH + 3\ O_2 \rightarrow 2CO_2 + 3H_2O}$

Low concentration aqueous solutions of methanol and ethanol are supplied to the anode of *DMFC* and *DEFC*. The use of liquid mixtures instead of a gas makes the delivery and storage stages easier and avoids the use of reforming operations. This fact is paramount in portable applications. *DFMC* have already been used successfully in mobile phones, laptops and vehicles. In particular, several prototypes have been

developed by Toyota as well as other companies (Necar Prototypes). A fleet of different kinds of vehicles powered by *DMFC* have been designed and fabricated.

Another important advantage of *DMFC* and *DEFC* is the fact that methanol and particularly ethanol can be eventually produced on a large scale from renewable resources (bio-fuels). Bio-fuels are alcohols which have been produced using biomass or other sustainable processes. In some countries, bio-alcohols and their mixtures with gasoline have been successfully used to internal combustion engine vehicles. The infrastructure involved in the storage and delivery of bio-alcohols is very similar to that used for gasoline. Therefore, the cost necessary to set-up the delivery of alcohol for fuel cells would be minimized.

DMFC and *DEFC* still present some limitations compared to hydrogen fuel cells. The yield of the oxidation is lower mainly due to the lower energy densities of the methanol and ethanol. In addition, the reduction reaction generates CO_2, so *DMFC* and *DEFC* cannot be considered zero emission devices, but the CO_2 produced may have lower impact than combustion engines. The generation of CO_2 can also produce undesired mass transfer effects related to its removal.

Another important problem related to *DMFC* and *DEFC* is the so-called crossover phenomenon. Crossover consists of the flow of unreacted alcohol through the electrolyte and its reaction with oxygen at the cathode, leading to a normal combustion reaction. This effect represents a loss of efficiency of up to 30% in *DMFC* and *DEFC* [3].

Despite these problems and limitations, *DMFC* and *DEFC* represent a very attractive alternative to the use of hydrogen in low temperature fuel cells for portable applications. Before this potential can be used at industrial scale, however it is first necessary to solve some of these technological limitations which decrease their performance.

2. Polymer electrolytes for *DMFC* and *DEFC*

Fuel cells operating at low temperatures have emerged as a potential alternative electrical power generation source for portable applications due to their low cost, low weight and low corrosion problems. Low temperature fuel cells (T < 100°C) use polymeric proton exchange polymeric membranes (*PEM*) as electrolytes. The most relevant characteristics of Proton Exchange Membranes Fuel Cells (*PEMFC*) have been previously explained in section 1.7.

Even though hydrogen is the most common fuel used for *PEMFC*, some problems related to its production, delivery and storage conditions have promoted the development of the so-called Direct Methanol and Direct Ethanol Fuel Cells (*DMFC* and *DEFC*, respectively), as desribed in section 1.8. In *DMFC* and *DEFC* the direct oxidation of methanol or ethanol occurs at the anode of the cell [3]. Despite the several advantages losted of *DMFC* and *DEFC*, at present their performance is not competitive with other fuel cell systems. *DMFC* and *DEFC* present some problems related to poor oxidation of the alcohols in the anode and the occurrence of crossover, which is the flow of unreacted alcohol through the electrolyte. In order to reduce this effect, it is paramount to understand the transport mechanisms occurring in *PEMFC* and how these are related to the chemical structure of the membrane.

2.1 Transport through the electrolyte. Crossover

A schematic of a *PEMFC* was already shown in Figure 1.1. As previously mentioned, one of the functions of the electrolyte (a polymeric proton exchange membrane) is to separate the hydrogen (H_2) and oxygen (O_2) streams. The membrane must be also electrically isolating in order to drive the electrons to flow through an external circuit, and also must provide a pathway for the protons from the anode to the cathode, so that the electrochemical reactions can occur.

For Direct Methanol and Ethanol Fuel Cells the schematic representation is similar (*Figure 1.4*).

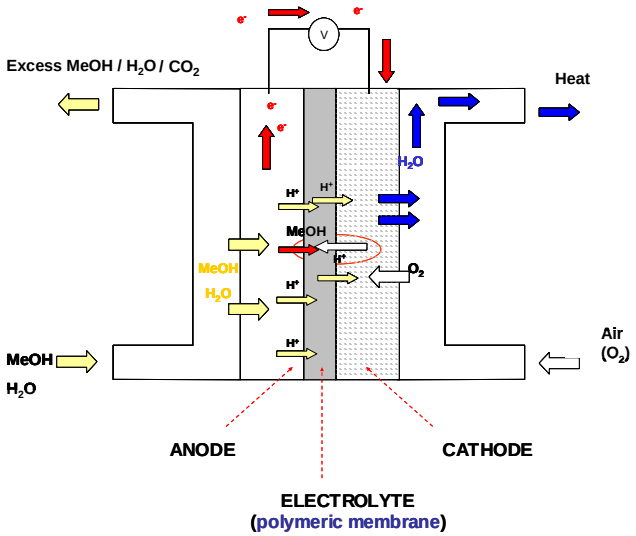

Figure 1.4 Schematic representation of transport and crossover in DMFC and DEFC

The performance of fuel cells depends not only on the yield of the reactions described earlier, but also on complex mass and energy transfer processes. Therefore, the proton transport through the electrolyte is crucial to the whole fuel cell performance. The transport of protons through a polymeric membrane is measured by its proton conductivity (σ_1 or σ_+), normally expressed in $S \cdot cm^{-1}$. Experiments performed to determine σ_+ usually imply the measurement of conductivity by frequency analysers in proton saturated conditions.

As mentioned earlier, one of the most important limitations of *DMFC* and *DEFC* is the so-called crossover phenomenon [4]. In membranes undergoing crossover the methanol and ethanol molecules flow from the anode to the cathode and react with the oxygen in a conventional combustion reaction (see *Figure 1.4*). Studies to reduce crossover must consider the transport mechanisms of the different compounds involved in *DMFC* (*DEFC*), namely, methanol (ethanol), water and protons.

Typically, transport of small molecules across a dense polymer follows a solution-diffusion mechanism [5]. Solutes are absorbed in the membrane, diffuse across the membrane and desorb out of the membrane. The transport rate is determined by a permeability coefficient (*P*) which includes the solubility (*S*) and the diffusion coefficients (*D*):

$$P = S \cdot D \qquad (1.1)$$

For transport phenomena in polymer electrolyte membranes (*PEM*) some other parameters must be considered, such as the ion transport or the ionic structure of the polymer. Moreover, the driving force is not only the concentration difference but also the electric potential difference.

Ideally, the transport of protons (desired) and methanol (undesired) can be described separately. The proton conductivity can be related to the diffusion coefficient [6] σ_1:

$$\sigma_1 = \frac{D_1 C_1 F^2}{RT} \qquad (1.2)$$

This is based on the Nernst-Planck equation, and relates the proton conductivity (σ_1) to the diffusion coefficient (D_1), the concentration (C_1) and charge of protons, the Faraday's constant (F) and the absolute temperature (T).

On the other hand, for methanol transport, and under certain circumstances, the steady – state flux can be described by the Fick's law:

$$j_2 = \frac{D_2 K_2 C_2}{L}$$

where K_2 is the partition coefficient (ratio of methanol concentration inside the membrane to that in the adjacent solution), D_2K_2 is the methanol permeability (P_2), and j_2 is the methanol flux.

From these equations, it is possible to define the selectivity for protons to methanol as:

$$\alpha_{1/2} = \frac{\sigma_1}{P_2} = \frac{D_1 C_1 F^2}{D_2 C_2 RT}$$

Conductivity and permeability are proportional to their respective diffusion coefficients, and can be separately measured in the development of *PEM* studies. For enhanced *DMFC* performance, high values of $\alpha_{1/2}$ are desired.

The factors that affect the membrane selectivity are interdependent and also depend on other parameters. D_2 is a function of water and methanol concentration and also of the free volume of the polymer. K_2 depends on C_1 and also on the water/methanol uptake and the solute–polymer interaction parameter. Finally, D_1 also depends on C_1 and on the water content and on the structure of the membrane. These interelationships makes the design of new membranes having enhanced selectivity ($\alpha_{1/2}$) a complex task. Furthermore, experiments with different membranes have shown that protons and methanol have similar molecular transport mechanisms in membranes containing sulfonic acid groups [7].

The transport of protons, water and methanol in *PEM* is very complicated, and occur simultaneously and over a wide length of scales. Furthermore, the influence of the voltage must also be considered. It is widely assumed that there are two main mechanisms for proton transport in *PEM*, namely, proton "hopping" [8] and the vehicular or electroosmotic drag [9] mechanisms. The hopping mechanism occurs when protons (H^+) hop from one hydrolysed site ($SO_3^-H_3O^+$) to another by the formation and destruction of hydrogen bonds (*Figure 1.5*):

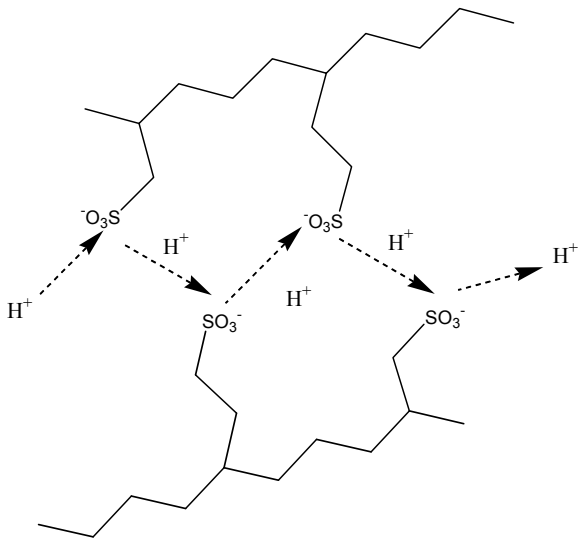

Figure 1.5 Schematic representation of the Grotthus (hopping) mechanism

On the other hand, protons transported by the vehicular mechanism are bound with water $(H^+(H_2O)_x)$ and drag one or more water molecules across the membrane, as seen in *Figure 1.6*:

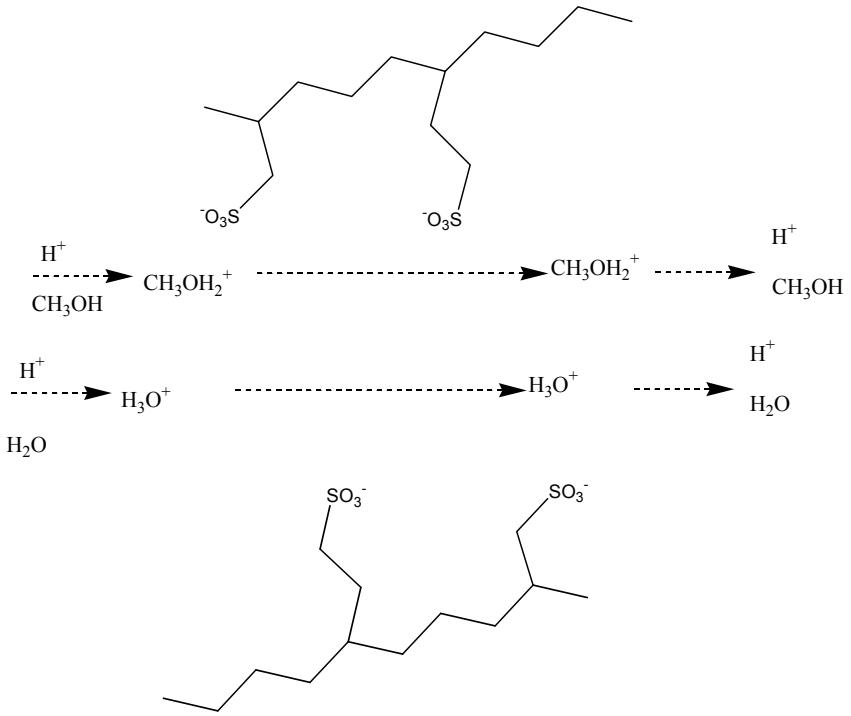

Figure 1.6 Schematic representation of the vehicular mechanism

The transport of water also occurs by two suggested mechanisms: electroosmotic drag and concentration gradient (as self-associated clusters), while the diffusion of methanol in water can be accounted for in a number of ways: as self-associated clusters $(CH_3OH)_\alpha$, as complex hydrogen-bonded to water $(CH_3OH)_m(H_2O)_n$ and also as a complex bound to protons $H^+(CH_3OH)_b$, which is similar to electroosmotic drag shown in *Figure 1.6*. The interconnection between the transport mechanisms is summarised in *Figure 1.7*:

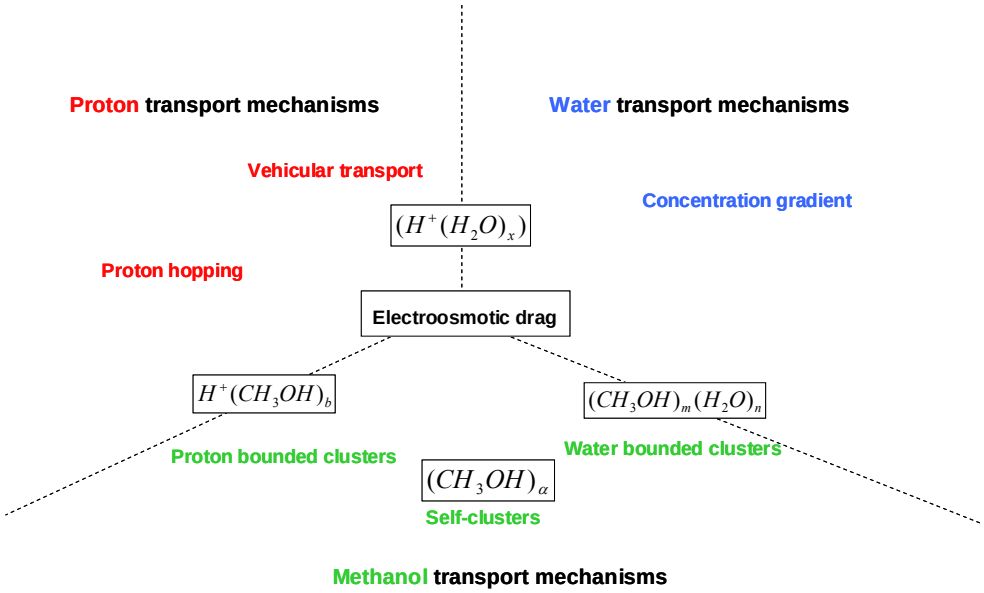

Figure 1.7 Schematic representation of different transport mechanisms in DMFC

The final transport mechanism must also include multicomponent diffusion, the interactions between the solutes and the polymer, and the electrostatic potential gradient for methanol and water. Therefore, all the transport equations should incorporate the Nernst-Planck and Stefan-Maxwell framework (considering electrostatic and multicomponent effects).

PEM must be designed to retain a certain degree of hydration in the membrane since water is involved in proton transport. Several experiments have shown that proton conductivity increases with increasing water content, ionic group concentration and temperature. In membranes with higher ionic group concentration there is an increase in the hydrophilic and ionic nature of the polymer which promotes higher conductivities and water levels [10]. However, when the water content reaches a certain value, the mechanical stability of the membrane suffers a drastic reduction. Moreover, high water content causes swelling of the membrane and promotes methanol crossover. Increasing temperature also promotes proton conductivity. However, over 80ºC there is a risk of membrane dehydration which leads to a reduction in the proton conductivity and poor water management [7, 11].

It is important to achieve a balance of the classes of water in the electrolyte. Two main types of water can be found in the membranes: free water and bound or structural water. The first can be readily removed from the membrane and is responsible for the vehicular

transport, while the latter remains in the structure of the polymer. The amount of water in the membrane will depend on the water present initially in the membrane, the water produced at the cathode, the water evaporated and the water dragged by the exhausted air at the cathode. The degree of humidity in the membrane can be also controlled by humidification of the fuel used (hydrogen, methanol, ethanol…) and by the temperature. The water balance in the cell should also consider the electro-osmotic drag of water from the anode to the cathode caused by the electrical potential drop through the membrane. The electro-osmotic drag coefficient (K_{drag}) can be calculated as the ratio of the water molecules and the protons transferred through the membrane.

2.2 Polymer electrolytes for *DMFC*

The most common electrolytes used in *PEMFC* are perfluorinated polymers containing proton conducting groups attached *via* side chains. In particular, DuPont‘s Nafion is the benchmark material in *PEMFC* [12], and its chemical structure can be seen in *Figure 1.8*:

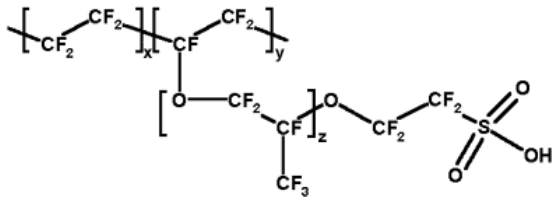

Figure 1.8 Chemical structure of Nafion

The substitution of the hydrogen atoms by fluorine in the main chain leads to a very stable and chemical resistant material while the presence of ionic groups gives high proton conductivity.

Even though there are numerous hypotheses about the detailed morphology of Nafion [13], it is widely accepted that microphase separation occurs. The ionic groups tend to form ion-rich aggregates (ionic clusters) the driving force being the electrostatic interactions between the ion pairs, while the most hydrophobic parts of the backbones form ion-poor domains [14]. It is thought that the ionic clusters are nanometer sized (diameter ϕ~5 nm) and are connected by small narrow ionic channels (ϕ~1 nm).

The proton conductivity depends on the ionic sites in the polymer. When the membrane is swollen in water, the ion clusters become interconnected and then the proton conductivity increases and an insulator-to-conductor transition or percolation threshold [13] is seen. The transport of molecules and ions is enhanced through this interconnected ionic network. Several investigations have shown that the diffusion of protons and water molecules is strongly affected by the ionic nanostructure. These showed that conductivity and diffusivity depend on the volume fraction and critical volume fraction of the hydrophilic phase, following a percolation model [15, 16, 17].

The combination of hydrophobic and hydrophilic regions gives Nafion its inherent properties:

- High cationic conductivity (necessary to achieve high proton conductivity).
- High chemical resistance (only some alkaline metals can damage the Nafion structure).
- High thermal resistance (Nafion can work at temperatures up to 190°C).
- Electrically isolating.

The proton conductivities of Nafion are in the range of $\sigma^{+} = 0.1$ mS·cm^{-1}, which is very high compared to other materials tested for *PEMFC*. Nafion is available commercialy in different forms depending on the composition (*x*, *y* and *z* in *Figure 1.8*) in emulsion or as a film. Some of its commercial trademarks are *101-IP, N111-IP, NE111F, NE101F, N112, NE1135, NE1035, N1110, N115* and *N117*. Materials commercialised by other companies include *Flemion*, *Dow*, *Aciplex* or *BAM3G*, and all of them have similar structure and properties to Nafion.

Even though Nafion shows excellent performance in hydrogen fuel cells, its application to *DMFC* and *DEFC* is more restricted due to its high methanol crossover [7]. As a consequence, in recent years the search for new polymeric materials for application in *DMFC* (and also *DEFC*) has increased enormously to obtain *PEM* with high proton conductivity and low methanol permeability.

The first strategy to improve the properties of commercial membranes is to modify Nafion or to prepare similar perfluorosulfonated acid (*PFSA*) polymer membranes. In commercial *PSFA* the carbon fluorine backbone provides high stability while the high acidity promotes high water uptakes and proton conductivity. However, *PFSA* membranes are expensive and suffer from several shortcomings, such as the high dependence on conductivity (among other properties) with water [13, 18]. The development of improved *PFSA* membranes has been carried out by reinforcement with *PTFE* [19], modification with hygroscopic oxides (SiO_2, TiO_2) [20] or addition of inorganic solid proton conductors (such as silica-phosphotungstic acid) [21].

Alternatively, sulfonated polymer membranes (hydrocarbon polymers) have been prepared as an attempt to obtain less expensive materials for low temperature *PEM*. In this case, the stability of the materials is a critical factor due to the introduction of tertiary carbon bonds in some of the polymer structures. For this reason, a wide range of different structures and compositions have been developed in an attempt to enhance mechanical and thermal stability, including crosslinked polymers [22], polymers with high glass transitions [23] or the addition of inorganic fillers and plasticizers.

Different strategies have been followed to obtain new hydrocarbon *PEM* exhibiting high proton conductivity and low methanol permeability. A set of ionic copolymers with sulfonate moieties in their structure have been prepared in the past, including:

Random copolymers:

- Sulfonated poly(styrene)-*SPS* [24, 25].
- Sulfonated poly(ether ethe ketone)-*SPEEK* [26, 27].
- Sulfonated poly(ether ethe ketone ketone)-*SPEEKK* [26, 27].
- Polyimides-PI [28, 29].
- Sulfonated poly(arylene ether sulfones)-*SPAES* [30, 31].

Graft copolymers:

- Sulfonated poly(styrenes) – *PSA* grafted on a variety of hydrophobic polymers, such as:
    - Poly(ethylene-tetrafluoroethlene)-*PETFE* [32].

- Poly(vilydene fluorine)-*PVDF* [33].
- Low density poly(ethylene)-*LDPE* [33].

Block copolymers

- Sulfonated poly(styrene-*b*-ethylene-r-butylene-b-styrene)- *S*-SEBS [34].
- Sulfonated poly(styrene-*b*-isobutylene-b-styrene) – *S-SIBS* [35]
- Sulfonated poly(styrene-*b*-ethylene) – *S-SE* [35].
- Sulfonated hydrogenated poly(styrene-*b*-butadiene)rubber – *HSBR* [36].
- Poly(arylene ether sulfone-*b*-polybutadiene) [37].

The use of block copolymers offers the possibility of obtaining microphase separation on a nanometer scale because of the thermodynamic incompatibility between the different blocks which may form a variety of self-assembled morphologies [38]. This separation provides the potential to obtain new and unique ordered morphologies, in which transport properties can be tailored [36]. A similar design potential can be found in liquid crystalline materials forming self-assembled mesomorphic morphologies [39] (see section 3 of this chapter).

Another strategy to obtain new materials for *DMFC* and *DEFC* electrolytes is the preparation of blends of different polymers. Polymer blends can combine the good characteristics of two components without their deficiencies, due to synergetic effects. This may be an effective low cost method for the preparation of new materials [41, 42].

In recent years, several *PEM* blends have been prepared to reduce methanol crossover. Poly(vinyl alcohol) (*PVA*) has been extensively used in polymer blends for its high selectivity in pervaporation separation of alcohol/water mixtures. Its chemical selectivity to water over ethanol and methanol suggests that these polymers may increase the proton/methanol selectivity [7] ($\alpha_{1/2}$). Some of the PVA blends investigated for *DMFC* and *DEFC* electrolytes are:

- With Nafion [42].
- With poly(styrene sulfonic acid) [43].
- *C*rosslinking with sulfo(succinid acid) – SSA [44].

- *PVA* - poly(2-acrylamido-2-methyl-1-propane sulfonic acid) – *PAMPS* [45, 46].

Other blends containing different polymers are:

- *PAMPS* with poly(2-hydroxyethyl methacrylate) – *PHEMA* [47].
- Sulfonated poly(etherketone) – *SPEK* with poly(benzimidazole) – *PBI* [48].
- Polysulfones with poly(ether sulfone) [36].
- Sulfonated poly(ether ether ketone ketone) – *SPEEK* with poly(ether sulfone) [36].
- *SPEEK* with *PE*I-poly(ether imide), *PAI*-poly(amide imide) and *PBI*-poly(benzimidazole) [49 - 51].

In general terms, blends used for *DMFC* and *DEFC* are based on acid – base polymers, in which the strong interactions between the blend components promote an ionic crosslinking. The presence of a basic backbone promotes the proton conductivity while the ionic crosslinking enhances the stability of the blends and reduces the methanol permeability [52, 53].

An alternative strategy to enhance the mechanical and chemical stability and also to reduce methanol diffusion is to carry out chemical crosslinking between the blend components, thus creating 3D networks [54, 55]. Crosslinked materials are easily prepared and the water contents and transport of proton and methanol can be adjusted by the crosslinking density.

Some interesting results have been obtained for PVA crosslinked materials, in which different crosslinkers have been used, such as SSA or glutaraldehyde [44, 55]. Some crosslinkers posses sulfonic groups to enhance the proton conductivity of the membrane [56, 57]. In this case, the studies have shown that there are two main factors affecting the transport of the solutes in the membranes. At low degrees of crosslinking, there is a considerable increase in the proton conductivity due to the presence of ionic conducting groups. However, at higher crosslinking densities the reduction of the free volume becomes limiting and the water swellability is drastically reduced, leading to a decrease in the proton conductivity. For such systems, it is paramount to establish an equilibrium

point between the number of sulfonic groups and the hydrophilicity. It is remarkable to note that the proton conductivity is dependent on the water content and also on the resulting morphology (coupled system).

Alternatively, several electrolytes have also been prepared by the impregnation of polymers using several techniques, such as in situ polymerisation and sorption within swollen and porous membranes. Some examples are:

- Poly(pyrrole) within a Nafion [58] matrix.
- *PAMPS*–co-1,6-hexanediol propylate diacrylate-co-ethyl methacrylate (crosslinked *PAMPS*) with Nafion [59].
- Poly(1-vinylimidazole) (*PVI*) with Nafion [60].
- Poly(furfuryl alcohol) with Nafion [61].
- Acid-doped *PBI* into a Nafion [62] matrix.
- Cosslinked styrene within a *PVDF* matrix and sulfonation of the impregnated polystyrene [63].
- Polymer-filled microporous membranes [64].

Another strategy to reduce crossover is to use composite membranes. Inorganic fillers act as blockers to methanol without causing a drastic drop in the proton conductivity. The incorporation of the inorganic phase also enhances thermal and mechanical stability [65, 66].

Several membranes have been prepared containing, for example, silica, zirconium phosphate, phosphotungstic acid, molybdophosphoric acid, Aerosil (silicon dioxide), *ORMOSILS* (organically modifed silicates), silane-based fillers, titanium oxide, hydroxyapatite, laponite, montmorillonite, zeolites and palladium [7]. A wide range of polymers have been used in this composites, such as Nafion [67], PVA/phosphotungstic acid (*PWA*) [66], polyethylene, glycol (*PEG*) membranes doped with 4-dodecylbenzene [65], crosslinked PVA/poly(acrylic acid) [68], sulfonated poly(phthalazinone ether sulfone ketone) (*SPPESK*) [69] and macroporous silica matrix [70]. Hybrid membranes also have some shortcomings, usually due to a poor water management and brittleness at high inorganic contents.

Several groups have prepared coated membranes with thin barrier layers using a variety of deposition techniques, such as immersion, radiation or multilayer coating techniques [64]. For example, Nafion has been coated with charged palladium [71], with PVA [72], with poly(1-methylpyrrole) [73], with *SPEEK* [74] and with poly(propylene)-grafted-*PSSA* [75].

In the membranes used in *DMFC*, the nature of the hydrophobic backbone and the hydrophilic groups play an important role in the resulting microphase structure. If the chemical nature of the hydrophobic and hydrophilic segments is very different, the resulting material will have a highly phase separated structure. This will lead to a material with large hydrophilic domains which are separated from each other. This structure will probably limit the proton conductivity. On the other hand, if the hydrophilic and hydrophobic segments are more similar, the phase separation will be less pronounced. In this case, the resulting microstructure will consist of narrower ionic channels but also with more interfacial regions. Examples of these possible structures can be seen in *Figure 1.9*.

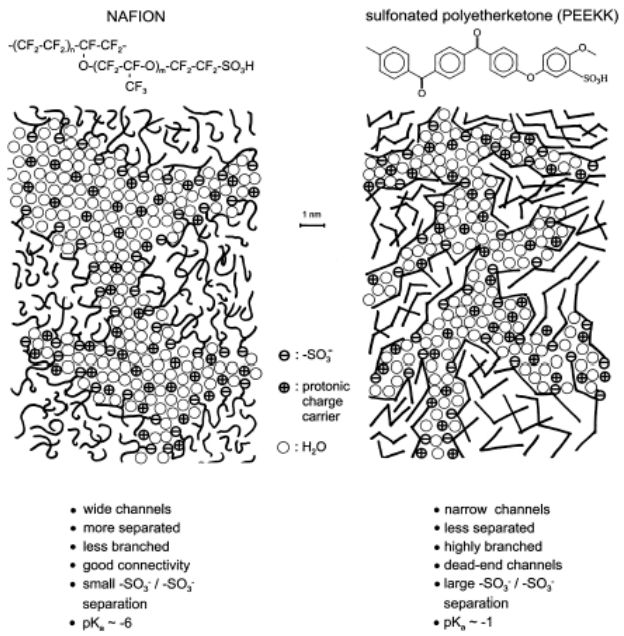

Figure 1.9 Phase separation in membranes for PEMFC: broader (left) and narrower (right) ionic channels for proton transport [76].

It has been shown that the existence of narrower and highly interconnected ionic channels promotes the proton conductivity, and at the same time reduces the methanol permeability [76]. Moreover, the use of narrower channels also reduces the water mobility, promoting structural diffusion (Grotthuss) mechanisms [77] instead of vehicular transport [78]. In general terms, it is necessary to obtain well dispersed and interconnected ionic channels to ensure high proton conductivity. This implies that not only the chemical composition but also the resulting morphology of the membranes plays an important role in the cell performance [77]. Therefore it is paramount to control the phase separation morphology in order to discriminate between the transport processes of protons, water and methanol through the membrane (see *Figure 1.8*) with the aim to optimize the use of *PEM* in *DMFC* and *DEFC*. *Figure 1.10* shows the proton conductivity (σ_+) and methanol permeability (P_{MeOH}) of some of the membranes used in *DMFC*.

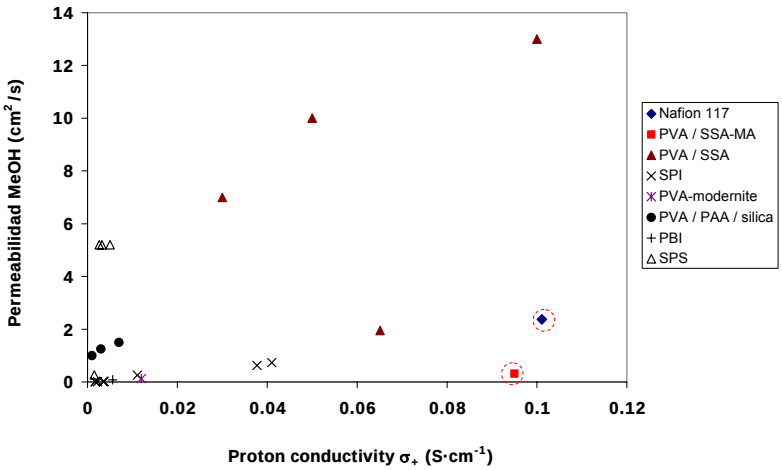

Figure 1.10 Methanol (MeOH) permeability and proton conductivity of different materials used as electrolytes in DMFC.

To date, Nafion remains the reference material, showing high proton conductivities ($\sigma_+ \sim 0.1$ Scm^{-1}) and relatively low methanol permeability ($P_{MeOH} \sim 2.4$ cm^2·s^{-1}). Other materials show low values of P_{MeOH} but also low σ_+ values. It is remarkable that only PVA based systems (with different compositions) achieve conductivity levels similar to those of Nafion, as seen in *Figure 1.10* (circled points).

3 Liquid crystals

Liquid crystals (*LC*) are substances that exhibit intermediate ordering states between solid crystals and isotropic liquids. They were first discovered in 1888 by the Austrian botanist Friedrich Reinitzer, who found that cholesteryl benzoate had two melting points. At a first transition, its crystals melted into a cloudy liquid which was then converted to a clear liquid at higher temperatures. The German scientist Otto Lehmann studied this compound through a polarised light microscope which he had invented and discovered that this intermediate state of matter was coloured under the microscope, unlike conventional liquids which were black. Thus, the cloudy liquid was birefringent like crystals but could flow like liquids. Substances undergoing similar transitions were called liquid crystals. Under certain conditions (temperature or concentration) such substances are capable of flow while still show anisotropic properties. The intermediate states that liquid crystals form are called mesophases [39, 79] (from the Greek *mesos* meaning "between").

Liquid crystals usually consist of either rod-shaped (calamitic liquid crystals) or disc-shaped (discotic liquid crystals) molecules. A substance showing liquid crystallinity undergoes at least two apparent melting transitions. The first one (assigned to the melting point, T_m) leads to the formation of an anisotropic cloudy liquid: the liquid crystalline phase or mesophase. In this phase, the molecules have enough thermal energy to move away from their crystal lattice positions, but they cannot rotate randomly. On increasing the temperature, the clearing point (T_{cl}) is reached. The molecules have sufficient thermal energy to move and rotate randomly and the liquid becomes an isotropic liquid phase.

3.1 Thermotropic liquid crystals and mesophases

The formation of liquid crystal mesophases depends either on the concentration of the compound or on temperature. When the formation of the mesophases depends on concentration, the liquid crystals are called lyotropic. This type of liquid crystal can be found in nature, for example, in cell membranes. On the other hand, when the formation of the liquid crystalline phases depends on temperature, the materials are called

thermotropic liquid crystals. Moreover, thermotropic liquid crystals which exhibit mesomorphism on heating and cooling are classified as enantiotropic, while if the mesophase is only observed on cooling, the liquid crystals are classified as being monotropic.

All the liquid crystals used in this thesis are calamitic thermotropic liquid crystals (except when stated otherwise). This type of liquid crystal consists of long rod-like molecules with a rigid core (mesogenic unit) and flexible terminal groups. The mesogenic unit confers rigidity to the molecule and, in some cases, also contains functional groups that promote intermolecular interactions. The presence of the mesogenic unit facilitates ordering between the different molecules. At the same time, the flexible terminal groups reduce the temperature of the transitions and allow the liquid crystal phases to be observed at accessible temperatures. This may be understood either entropically or enthalpically.

Some examples of calamitic liquid crystals molecules include:

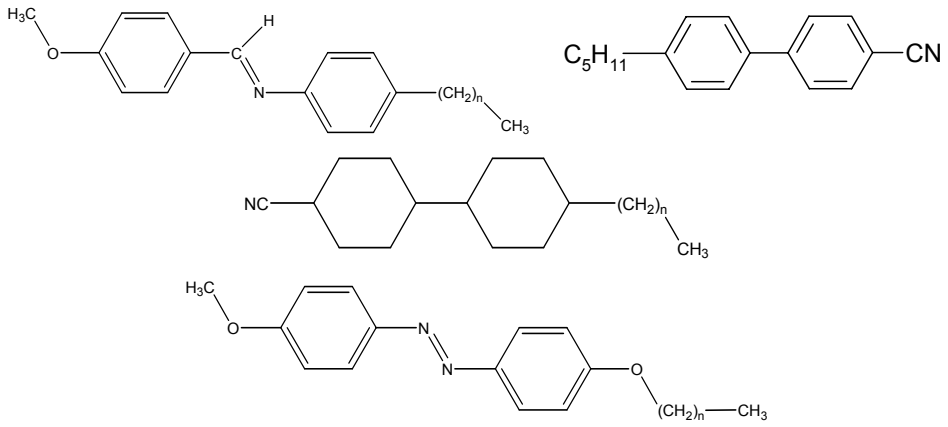

There are many different types of liquid crystalline phases. The simplest and commonest mesophase is the nematic phase (*N*). In a nematic phase, the centres of mass of the molecules are randomly arranged but the molecules are aligned along a preferred average direction. This average direction is known as the director $\bar{n}$.

Another common group of liquid crystalline phases are the smectic phases (*Sm*). Molecules in a smectic phase have their centres of mass arranged in layers and have their symmetry axes aligned along a preferred average direction ($\bar{n}$). There are several

types of smectic phases depending on the degree of positional order of the molecules. In a *smectic A* phase (*SmA*), the director is perpendicular to the plane of the layers and the molecules are randomly arranged within each layer. In a *smectic C* phase (*SmC*) the molecules are tilted to the perpendicular layer. In a *smectic B* phase (*SmB*) the molecules in each layer are on a hexagonal lattice, but with no correlation between layers. If there are correlations between layers leading to a 3D order, the phases are classified as disordered crystals rather than liquid crystals.

A schematic representation of nematic and smectic phases can be seen in *Figure 1.11* and *Table 1.3* summarises the most common thermotropic mesophases.

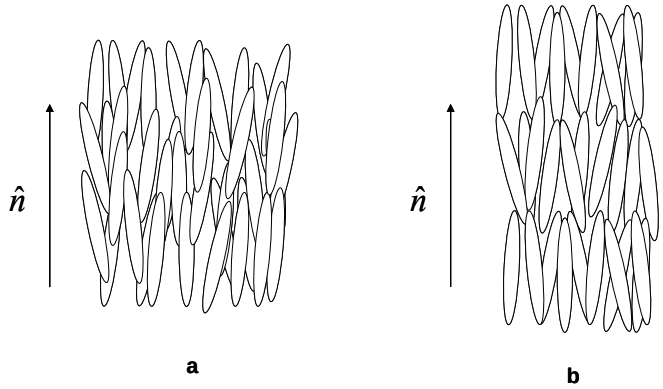

Figure 1.11 Examples of nematic (a) and smectic A (b) phases

Table 1.3 Structures of the most common thermotropic mesophases

Phase	Description	Subtypes
Nematic	Orientation of the axis in an average direction ($\hat{n}$) and centres of molecules random	Nematic *(N)*
Smectic	Orientation of the axis in an average direction ($\hat{n}$) The molecules are grouped into layers. The direction $\hat{n}$ can vary from one layer to the other.	Smectic A *(SmA)* Smectic C *(SmC)* Smectic B *(SmB)* Smectic I *(SmI)* Smectic F *(SmF)*
Columnar	Axis are oriented so that the molecules can be packed into columns	Columnar ordered *(D_{xo})* Columnar disordered *(D_{xd})* Columnar hexagonal *(D_{hy})* Columnar rectangular *(D_{ry})* Columnar oblique *(D_{ob})*
Crystal	Mesophases show order and orientation. They are not strictly liquid crystalline phases, but they still show some intermediate ordering states.	Crystalline *B (B)* Crystalline *E (E)* Crystalline *G (G)* Crystalline *K (K)* Crystalline *J (J)* Crystalline *H (H)*

Not all liquid crystals show all the mesophases. Depending on the nature of the molecule, a liquid crystal can exhibit one, two or several mesophases.

3.2 Side Chain Liquid Crystal Polymers (*SCLCP*)

LCP are polymers containing mesogenic groups in either their backbone or their side chains. This difference leads to the so-called main-chain liquid crystalline polymers (*MCLCP*) and side-chain liquid crystalline polymers (*SCLCP*), respectively [39]. Schematic representations of both sorts of *LCP* can be seen in *Figures 1.12* and *1.13*:

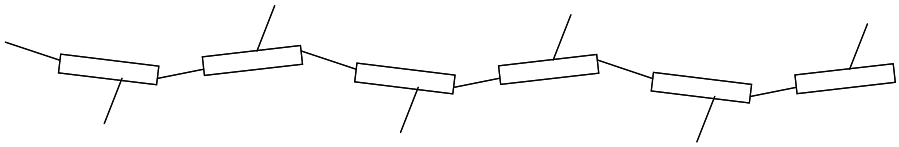

Figure 1.12 Schematic representation of a main-chain liquid-crystalline polymer (MCLCP)

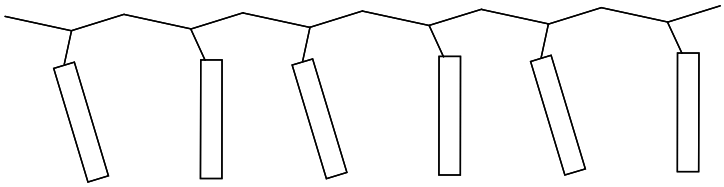

Figure 1.13 Schematic representation of a side-chain liquid-crystal polymer (SCLCP)

In *MCLCP* the mesogenic units form the backbone and if the linking units are long and flexible, semi-flexible polymers are obtained. Instead, if the mesogenic groups are directly linked, then the polymer will be very rigid. Both the flexibility of the chain and the structural composition of the polymer determine the mesomorphic properties of *MCLCP*.

All the liquid crystal polymers prepared and studied in this thesis are side-chain liquid crystal polymers (*SCLCP*). There are three main components of a *SCLCP*: the polymeric backbone, the mesogenic group and a spacer which connects them. All the *SCLCP* studied in this PhD thesis contain calamitic groups (see *Figure 1.14*):

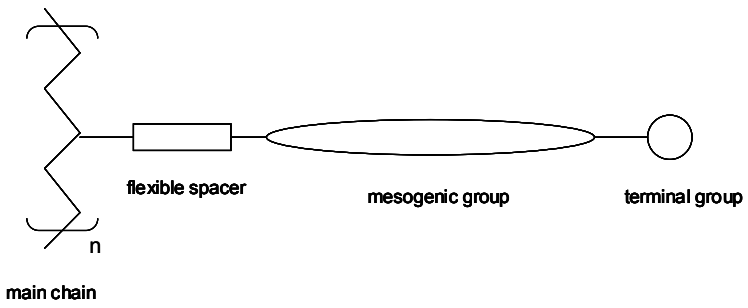

Figure 1.14 Components of a SCLCP

The properties of *SCLCP* depend on structural factors such as the spacer length, the backbone flexibility and the distance between the side chains (*i.e.*, the repeating unit

length). The molecular weight (*MW*) of the polymer also affects its thermal properties. The transition temperatures of the polymers are higher than those of the corresponding monomers. The transition temperatures show a rapid increase initially on increasing the molecular weight and then a plateau value is reached when the *MW* is sufficiently high. At this point the polymer properties are independent of the degree of polymerisation. On the other hand, if the polydispersity of the polymer is high, then their transitions will broaden. In general terms, polymerisation stabilises the mesophase thus producing an increase in the clearing temperature and the enantiotropic character of the materials.

The molecular motions of the backbone and the mesogenic unit are coupled through the flexible spacer. The degree of decoupling can be increased by increasing the flexibility of the backbone, by increasing the distance between the side chains or by increasing the length of the spacer. Decoupling promotes a decrease in the glass transition temperature (T_g) and an increase in the clearing temperature (T_c). This leads to more ordered phases. However, X-ray studies have shown that the polymer backbone is deformed in the systems, without a strong dependence of the mesophase rather than showing an isotropic conformation. Therefore, it is impossible to completely decouple the motions of the main chain from those of the side chain.

SCLCP show complex phase behaviour. The most common mesophase observed in *SCLCP* is the *smectic A* phase (*SmA*) although some polymers also show nematic phases (*N*). In all cases, the deformation of the backbone to accommodate the mesogenic group is important in understanding the mesomorphic behaviour of the polymer. In the nematic phase no phase separation is involved and the distortion of the backbones to accommodate the mesogenic groups in the average direction ($\hat{n}$) is a facile process (*Figure 1.15*):

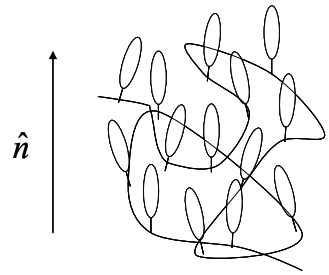

Figure 1.15 Nematic phase in a SCLCP

On the other hand, at least six possible types of smectic *A* phases have been shown to exist in *SCLCP* [80 - 82]. Such structures depend on the role of the polymer backbone in the structure and also on the ratio between the layer spacing (*d*) and the molecular length (*l*) of the side-chain (see *Figure 1.16*):

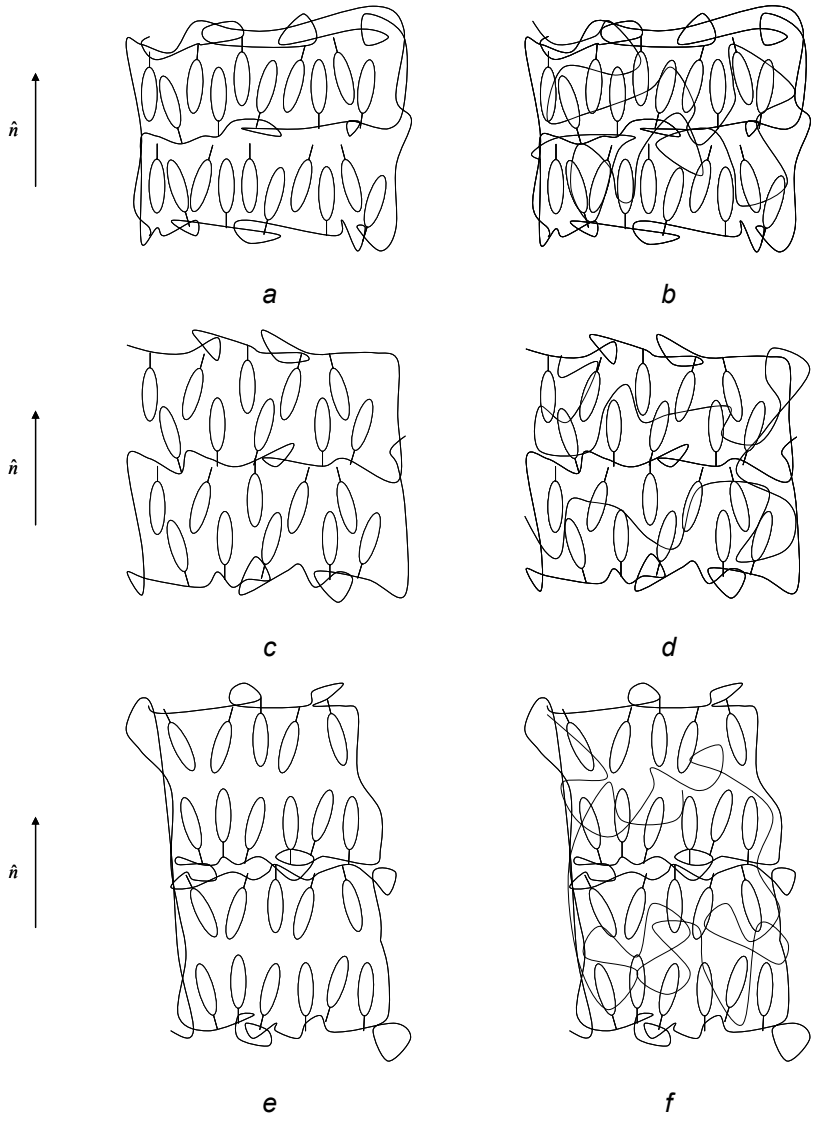

Figure 1.18 Smectic phases in a SCLCP showing possible backbone configurations

In the first set of structures in *Figure 1.18* (*a, c* and *e*) the backbone is confined by the smectic field and lies between the layers. This arrangement has been explained in terms of microphase separation. In the second set of structures (*b, d* and *f*) the conformation of the backbone is largely unaffected by the smectic field and possesses a three-dimensional structure.

Each set shows three structural variations of the *smectic* phase with regard to the *d/l* ratio. In the first of them (*a* and *b*) the side chains overlap fully and the *d/l* ratio approaches unity (*SmA1*). The other extreme is the *SmA* phase, in which the side chains exhibit no interdigitation and thus *d/l* is 2 (*e* and *f*). Between these extremes, a range of partially interidigitated phases termed *SmAd*, ($1 < d < 2l$) can be found (*c* and *d*).

There is a very wide range of possible *SCLCP* if we consider the nature of the backbone, the spacer and the mesogenic unit. The first synthesised *SCLCP* were poly(siloxane)s, poly(methacrylate)s and poly(acrylate)s. During the last 20 years a wide range of backbones have been used to prepare different *SCLCP*, such as poly(vinyl ether)s, poly(phosphazene)s, poly(tartrate)s and poly(styrene)s. Many different mesogenic groups are used in *SCLPC*, including azobenzenes and biphenyls. The effect of the terminal group, the nature of the spacer (more flexible or rigid) and its length determine to some extent the thermal properties of the resulting polymers [80, 83 - 90].

In order to achieve tailored properties, it is common to combine two different monomers to form a side-chain liquid crystal copolymer (*SCLCcP*). The temperature range of liquid crystallinity as well as all other thermal properties is then varied along with composition. Indeed, it is very common to copolymerise a mesogenic monomer with a non-mesogenic monomer. In this case, it is very important to study the effect of the concentration of the non-mesogenic unit for the copolymer to undergo liquid crystallinty phases.

The introduction of the non-mesogenic group can also affect the type of mesomorphism of the copolymer. Some studies regarding poly(methacrylate)s copolymers showed that the smectic phase observed for the pure copolymer was rapidly depressed even at low concentrations of the non-mesogenic group. The introduction of non-mesogenic units can also affect the glass transition and clearing temperatures of the polymer. The use of such copolymers is then an interesting way to vary the properties of *SCLCcP* or to introduce new functional groups.

3.3 Polymer Dispersed Liquid Crystals (*PDLC*)

As an alternative to liquid crystal polymers (*LCP*), low molecular mass liquid crystals can also be dispersed into a polymer network. These are the so-called Polymer Dispersed Liquid Crystals (*PDLC*). In ideal *PDLC* the polymer matrix supports the liquid crystals aggregates which still maintain their mesomorphic behaviour, resulting in a phase separation micro-structure [91].

However, real *PDLC* systems can show strong interactions between the polymeric matrix and the liquid crystals and then the thermal properties of the polymer as well as the mesomorphism of the *LC* can be seriously altered. The actual behaviour of the *PDLC* will depend on the degree of phase separation and the size of the liquid crystal aggregates. All these facts will strongly depend on the nature of the components, but also on the preparation of the dispersions [92].

PDLC are an interesting alternative to the use of low molecular liquid crystals in the field of information storage, but also to the use of *LCP* in other advanced applications. The use of *PDLC* reduces the price of the materials and at the same time avoids the use of additional substrates because are self-supporting.

3.4 Liquid Crystal in external controlled operations

One of the most interesting features of liquid crystals is their anisotropic properties. When a liquid crystal exhibits a mesophase, the molecules have at least one preferential orientation and anisotropic behaviour with respect to light or electrical and magnetic fields [39].

Considering a physical property ε, the response $\vec{R}$ to an external force $\vec{F}$ can be expressed as follows in a 3D space:

$$\vec{R} = \varepsilon \cdot \vec{F}$$

For an isotropic material, ε is represented by a number, since it has the same value in any of the three directions of the space. For an anisotropic material, the value of ε depends on the direction, and therefore a 3x3 matrix must be used:

$$\vec{R} = \begin{pmatrix} \varepsilon_{11} & \varepsilon_{12} & \varepsilon_{13} \\ \varepsilon_{21} & \varepsilon_{22} & \varepsilon_{23} \\ \varepsilon_{31} & \varepsilon_{32} & \varepsilon_{33} \end{pmatrix} \cdot \vec{F}$$

This is applicable to light, mechanical, electrical and magnetic response. The optical anisotropy leads to the birefringence that is observed thought the polarised light microscopy. On the other hand, the magnetic and electrical anisotropy provides liquid crystals the capability to be aligned in the presence of external magnetic and electrical fields. These are the basis of their applications in liquid crystals displays [79].

In the case of electric polarisation an electrical field ($\vec{E}$) causes polarisation ($\vec{P}$) in the liquid crystalline material. Polarisation depends linearly on the electrical field, but the anisotropy of the liquid crystal causes $\vec{P}$ and $\vec{E}$ to have different directions in general. The polarisation and the electrical field are related by the tensor $\vec{\vec{\chi}}$ (electric susceptibility) by the following expression:

$$\vec{P} = \varepsilon_0 \vec{\vec{\chi}} \cdot \vec{E}$$

where ε_0 is the permittivity of free space ($8.85 \cdot 10^{-12}$ C^2/Nm^2).

Considering the liquid crystal director vector $\hat{n}$ to be aligned along the *z*-axis, the polarisation $\vec{P}$ can be expressed as follows:

$$\begin{pmatrix} P_x \\ P_y \\ P_z \end{pmatrix} = \varepsilon_0 \begin{pmatrix} \chi_{e_\perp} & 0 & 0 \\ 0 & \chi_{e_\perp} & 0 \\ 0 & 0 & \chi_{e_\parallel} \end{pmatrix} \cdot \begin{pmatrix} E_x \\ E_y \\ E_z \end{pmatrix}$$

The electric field and the polarisation define the electric displacement ($\vec{D}$):

$$\vec{D} = \varepsilon_0 \cdot \vec{E} + \vec{P} = \vec{\varepsilon}\vec{E}$$

with

$$\vec{\varepsilon} = \varepsilon_0(\vec{\vec{1}} + \vec{\vec{\chi}}_e)$$

and $\vec{\vec{1}}$ the unit matrix:

$$\vec{\vec{1}} = \begin{pmatrix} 1 & 0 & 0 \\ 0 & 1 & 0 \\ 0 & 0 & 1 \end{pmatrix}$$

The anisotropy in the conductivity can be calculated as:

$$\Delta\varepsilon = \varepsilon_0 - \varepsilon_\perp$$

When an electrical field ($\vec{E}$) is applied across a liquid crystalline material, the director will align in the direction of the electrical field $\vec{E}$ in order to minimize their energy (*Figure 1.19*):

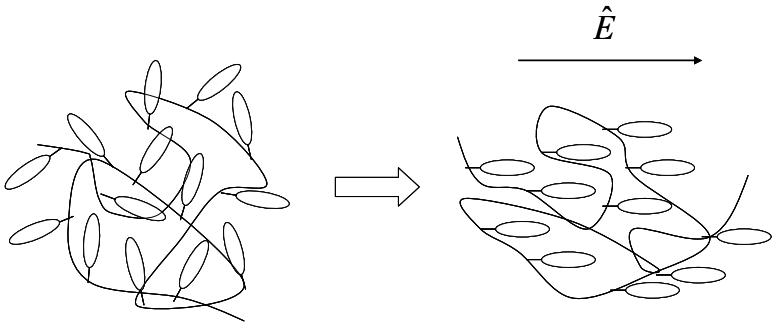

Figure 1.19 Rearrangement of a SCLCP in an electrical field.

Considering the energy involved in an electrical field ($\vec{E}$) through a liquid crystal per unit volume U_e:

$$U_e = \frac{1}{2}\vec{D} \cdot \vec{E}$$

it is then possible to relate the energy involved in the process of alignment:

$$dU_e = -\frac{1}{2}\varepsilon_0 \Delta\chi_e \left(\vec{E}\cdot d\hat{n}\right)\left(\vec{E}\cdot\hat{n}\right) - \frac{1}{2}\varepsilon_0 \Delta\chi_e \left(\vec{E}\cdot\hat{n}\right)\left(\vec{E}\cdot d\hat{n}\right)$$

If the director is described by the angle θ between $\hat{n}$ and a plane perpendicular to $\vec{E}$, then:

$$\vec{E}\cdot\hat{n} = E\sin\theta \qquad \text{and} \qquad \vec{E}\cdot d\hat{n} = E\cos\theta d\theta$$

and so:

$$dU_e = -\varepsilon_0 \Delta\chi_e E^2 \sin\theta\cos\theta d\theta$$

Considering $U_e = 0$ at $\theta = 0$, then the electric energy (per volume of liquid crystal) is:

$$U_e = -\varepsilon_0 \Delta\chi_e E^2 \int_0^{\theta} \sin\theta' \cos\theta' d\theta' = -\frac{1}{2}\varepsilon_0 \Delta\chi_e E^2 \sin^2\theta = -\frac{1}{2}\varepsilon_0 \Delta\chi_e \left(\hat{n}\cdot\vec{E}\right)^2$$

The capability of *LC* to be aligned can be used to design materials which could be externally regulated by electrical or magnetic fields. A change in the orientation of liquid crystals could also lead to a change in the morphology of the materials.

REFERENCES CHAPTER 1

1. Blomen, L. *Fuel Cell Systems*, Ed. Plenum Press, New York, (1993), G. Hoogers, Fuel Cell Technology Handbook, CRC Press, Nueva York, (2003)

2. U.S. Department of Energy, *Handbook of Fuel Cells*, Fifth Edition, EG&G Services, 2000

3. DeLuca, N.W.; Elabd, Y.A. J. Polym. Sci. Part B: Polym. Phys. 44 (2006) 2201

4. Pivovar, B.S.; Wang, Y.; Cussler, E. L. J. Membr. Sci. 154 (1999) 155

5. Comyn., J. *Polymer Permeability*; Springer: New York, 1985

6. Newman, J.; Thomas, K.E. *Electrochemical Systems*, 3rd ed.; Wiley-Interscience: New York, 2004

7. Elmér, A.M.;. Jannasch, P. J Polym. Sci. Part B: Polym. Phys. 44 (2006) 2205

8. DeGrotthus, C. I. T. Ann. Chim. 58 (1806) 54

9. K.D. Kreuer, W. Weppner, A. Rabenau, Angew. Chem. In. Ed. Engl. 21 (1982) 208

10. Y. A. Elabd, E. Napadensky, C. W. Walker, K. I. Winey, Macromolecules 39 (2006) 399

11. C. Yang, P. Costamagnab, S. Srinivasanb, J. Benzigerc, A. B. Bocarsly J. Power Sources 103 (2001) 1

12. Grot, W.G. Macromol. Symp. 82 (1994) 161

13. Mauritz K.A.; Moore, R.B. Chem. Rev. 104 (2004) 4535

14. Eisenberg, A.; King, M. *Ion Containing Polymers: Physical Properties and Structure*; Academic Press: New York, 1997

15. Elabd, Y.A.; Napadensky, E.; Sloan, J.M.; Crawford, D. M.; Walker, C. W. J. Membr. Sci. 217 (2003) 227

16. Hsu, W.Y.; Barkley, J. R.; Meakin, P. Macromolecules 13 (1980) 198

17. Gronowski, A.A.; Jiang, M.; Yeager, H.L.; Wu, G.; Eisenberg, A. J. Membr. Sci. 82 (1993) 83

18. Costamagna, P.; Srinivasan, S. J. Power Sources 102 (2001) 242

19. U.S. Patent application 0026883A1, EP1139472 (2001)

20. Watanabe, M.; Uchida, H.; Seki, Y.; Emori, M.; Stonehart, P. J. Electrochem. Soc. 143 (1996) 3847

21. Staiti, P.; Aricò, A. S; Baglio, V.; Lufrano, F.; Passalacqua, E.; Antonucci, V.; Solid State Ionics 145 (2001) 101

22. Tanaka, R.; Yamamoto, H.; Shono, A.; Kubo, K.; Sakurai, M. Electrochim. Acta 45 (2000) 1385

23. Amutha, R.; Subbarayan, A.; Sathyamoorthy, R.; Natarajan, K; Velumani, S. J. New Mater. Electrochem. Syst. 10 (2002) 27

24. Carretta, N.; Tricoli, V.; Picchioni, F.; Costamagna, P.; Srinivasan, S.;J. Membr. Sci. 166 (2000) 189

25. Jung, B.; Kim, B.; Mok Yang, J.M. J. Membr. Sci. 245 (2004) 61

26. Ravi, P.; Sin, S.L.; Gan, L.H.; Gan, Y.Y.; Tam, K.C.; Xia, X.L.; Hu, X. Polymer 46 (2005) 237

27. Gil, M.; Ji, X.; Li, X.; Na, H.; Hampsey, J.E.; Lu, Y. J. Membr. Sci. 234 (2004) 75

28. Okamoto, K.; Yin, Y.; Yamada, O.; Islam, Md.N.; Honda, T.; Mishima, T.; Suto, Y.; Tanaka, K.; Kita, H. J. Membr. Sci. 258 (2005) 115

29. Einsla, B.R.; Kim, Y.S.; Hickner, M.A.; Hong, Y.; Hill, M.L.; Pivovar, B.S.; McGrath, J.E. J Membr Sci 255 (2005) 141

30. Sumner, M.J.; Harrison, W.L.; Weyers, R.M.; Kim, Y.S.; McGrath, J.E.; Riffle, J.S.; Brink, A.; Brink, M.H. J. Membr. Sci. 239 (2004) 199

31. Kim, Y.S.; Sumner, M.J.; Harrison, W.L.; Riffle, J.S.; McGrath, J.E.; Pivovar, B.S. J Electrochem. Soc. 151 (2004) A2150

32. Hatanaka, T.; Hasegawa, N.; Kamiya, A.; Kawasumi, M.; Morimoto, Y.; Kawahara, K. Fuel 81 (2002) 2173

33. Shen, M.; Roy, S.; Kuhlmann, J.W.; Scott, K.; Lovell, K.; Horsfall, J.A. J. Membr. Sci. 251 (2005) 121

34. Kim, B.; Kim, J.; Jung, B. J. Membr. Sci. 250 (2005) 175

35. Lee, J.C; Tomita, I.; Endo, T. Macromolecules 31 (2002) 5916

36. Nácher, A.; Escribano, P.; Del Río, C.; Rodríguez, A.; Acosta, J.L. J. Polym. Sci., Part A: Polym. Chem. 41 (2003) 2809

37. Zhang, X.; Liu, S.; Liu, L.; J. Yin Polymer 46 (2005) 1719

38. Hamley, I.W. *The Physics of Block Copolymers*, Oxford University Press: New York, 1998

39. Collings, P.J.; Hird, M. *Introduction to liquid crystals. Chemistry and physic*s; Ed. Taylor & Francis: New York, 1997

40. Manea, C.; Mulder, M. J. Membr. Sci. 206 (2002) 443

41. Park, J.S.; Park, J.W. E. Ruckenstein, Polymer 42 (2001) 4271

42. Shao, Z.G.; Wang, X.; Hsing, I.M. J Membr Sci 210 (2002) 147

43. Banerjee, S.; Curtin, D.E. J. Fluorine Chem. 125 (2004) 1211

44. Rhim, J.W.; Bum Park, H.; Lee,C.S.; Jun,J.; Kim, D.S.; Lee,Y.M. J. Membr. Sci. 238 (2004) 143

45. Kang, M.S.; Kim, J. H.; Won, J.; Moon, S.H.; Kang, Y.S. J. Membr. Sci. 247 (2005) 127

46. Qiao, J.; Hamaya, T.; Okada, T. Chem. Mater. 17 (2005) 2413

47. Walker Jr, C. W. J. Power Sources 110 (2002) 144

48. Hasiotis, C.; Deimede, V.; Kontoyannis, C. Electrochim. Acta 46 (2001) 2401

49. Kerres, J.; Ullrich, A.; Meier, F.; Häring, T. Solid State Ionics 125 (1999) 243

50. Wu, H.L; Ma, C.C.M.; Li, C.H.; Lee, T.M.; Chen, C.Y.; Chiang, C.L; Wu, C. J. Membr. Sci. 280 (2006) 501

51. Javaid Zaidi, S.M. Electrochim. Acta 50 (2005) 4771

52. Walker, M.; Baumgärtner, K.M.; Kaiser, M.; Kerres, J.; Ullrich, A.; Räuchle, E. J. Appl. Polym. Sci. 74 (1999) 67

53. Kerres, J. A. J. Membr. Sci. 185 (2001) 3

54. Qiao, J.; Hamaya, T.; Okada, T. Polymer 46 (2005) 10809

55. Shen, C.C; J. Joseph, Lin, Y.C.; Lin, S.H.; Lin, C.W.; Hwang, B.J. Desalination 233 (2008) 82

56. Yang, C.C.; Chiu, S.J.; Chien, W.C. J. Power Sources 162 (2006) 21

57. Rhim, J.W.; Yeom, C.K.; Kim, S.W. J. Appl. Polym. Sci. 68 (1998) 1717

58. Smit, M. A.; Ocampo, L.; Espinosa-Medina, M.A.; Sebastián, P.J. J. Power Sources 124 (2003)

59. Walker, C.W. J. Electrochem. Soc. 151 (2004) A1797

60. Bae, B.; Ha, H.Y.; Kim, D. J Electrochem Soc 152 (2005) A1366

61. Liu, J.; Wang, H.; Cheng, S.; Chan, K.Y. J. Membr. Sci. 246 (2005) 95

62. Hobson, L. J.; Nakano, Y.; Ozu, H.; Hayase, S. J. Power Sources 104 (2004) 79

63. Surya Prakash, G.K.; Smart, M.C.; Wang, Q.J.; Atti, A.; Pleynet, V.; Yang, B.; McGrath, K.; Olah, G.A.; Narayanan, S.R.; Chun, W.; Valdez, T.; Surampudi, S.J. Fluorine Chem. 125, (2004) 1217

64. Yamaguchi, T.; Nakao, S.I.; Kimura, S. J. Polym. Sci. Part B: Polym. Phys. 35 (1997) 469

65. Thangamuthu, R.; Lin, C.W. Solid State Ionics 176 (2005) 531

66. Xu, W.; Liu, C.; Xue, X.; Su, Y.; Lv, Y.; Xing, W.; Lu, T. Solid State Ionics 171 (2004) 121

67. Xu, W.; Lu, T.; Liu, C.; Xing, W. Electrochim. Acta 50 (2005) 3280

68. Kim, D.S.; Park, H. B.; Rhim, J.W.; Lee, Y.M. Solid State Ionics 176 (2005) 117

69. Kim, D.S.; Shin, K.H.; Park, H.B.; Lee, Y.M. Macromol. Res. 12 (2004) 413

70. Munakata, H.; Yamamoto, D.; Kanamura, K.Chem. Commun. 31 (2005) 3986

71. Tang, H.; Pan, M.; Jiang, S; Wan, Z.; Yuan, R. Colloids Surf. A 262 (2005) 65

72. Lee, K.H; Kim, K.H.; Lim, H.S J. Electrochem. Soc. 148 (2001) A1185

73. Kadirgan, F.; Savadogo, O. Russ. J. Electrochem. 40 (2004) 1141

74. Ren, S.; Li, C.; Zhao, X.; Wu, Z.; Wang, S.; Sun, G.; Xin, Q.; Yang, X. J. Membr. Sci. 247 (2005) 59

75. Saun, J.; Byun, J.; Kang, Y.; Kim, H. Korean J. Chem. Eng. 22 (2005) 605

76. Kreuer, K.D. J. Membr. Sci. 185 (2001) 29

77. Kreuer, K.D Chem. Mater. 8 (1996) 610

78. Kreuer, K.D. Solid State Ionics 97 (1997) 1

79. Demus, D.; Goodby, J.; Gray, G.W.; Spiess, H.W.; Vill, V. *Handbook of Liquid Crystals. Fundamentals*, Ed. Wiley-VCH: New York, 1998

80. Percec, V.; Hahn, B.; Ebert, M.; Wendorff, J.H. Macromolecules 23 (1990) 2092

81. Diele, S.; Oelsner, S.; Kuschel, F.; Hisgen, B.; Ringsdorf, H.; Zentel, R. Makromol. Chem. 188 (1987) 1993

82. Westphal, S.; Diele, S.; Mädicke, A.; Kuschel, F.; Scheim, U.; Rühlmann, K.; Hisgen, B.; Ringsdorf, H. Makromol. Chem. Rapid Commun. 9 (1988) 489

83. Percec, V.; Lee, M. J. Mater. Chem. 2 (1992) 617

84. Ringsdorf, H.; Schneller, A. Makromol. Chem. Commun. 3 (1982) 557

85. Starnes Jr., W.H. Pure Appl. Chem 57 (1985) 1009

86. Gray, G.W. *In Side Chain Liquid Crystal Polymers*, C.B. McArdle, Ed., Blackie and Sons, Glasgow, 1989

87. Percec, V.; Hahn, B.; Macromolecules 22 (1989) 1588

88. Percec, V.; Hahn, B.; Ebert, M.; Wendorff, J.H. Macromolecules 23 (1990) 2092

89. Neumann, H.J; Hellmann, G.P. Makromol. Chem. 194 (1993) 2349

90. Neumann, H.J.; Jarek, M.; Hellmann, G.P.Macromolecules 26 (1993) 2489

91. Mucha, M. Prog. Polym. Sci. 28 (2003) 837

92. G.P. Crawford, S. Zumer, Ed. Taylor and Francis: New York, 1996

2

Characterisation methodology

The techniques used to characterise the materials studied in this thesis were: Fourier Transform Infrared Spectroscopy (FTIR), Thermogravimetric Analysis (TGA), Differential Scanning Calorimetry (DSC) and Polarised Light Microscopy (PLM). The diffusivity of some of the membranes prepared in this PhD thesis was studied by means of swelling and diffusion tests. The diffusion tests were performed in a in-house designed module which also permits the evaluation of the effect of the electrical field on the diffusion properties of the membranes.

The scope of this chapter is to describe the characterisation techniques, including: the basic and theoretical background, the description of the instrumental equipment, relevant information about the experiments and also features of the methodology of the analysis carried out. This corresponds to one of the aims of this PhD thesis, which was to establish of a methodology for the characterisation of new materials for *DMFC* and *DEFC*. Some of the aspects are illustrated with examples.

INSTRUMENTAL TECHNIQUES

1. Fourier Transform Infrared Spectroscopy (FTIR)

1.1 Fundamentals

Infrared Spectroscopy (IR) is based on measuring the energy absorbed by the molecules when they are irradiated with energy in the infrared range [1, 2]. The energy of an IR source cannot promote electronic transitions but it is high enough to promote molecular vibrations. A signal in the IR spectrum will be observed when the energy provided is coincident to that of a vibrational transition of a molecule or functional group in the sample. As a result, the intensity of the radiation reaching the detector will decrease and will be then recorded. The different peaks in a spectrum represent absorptions corresponding to vibrational transitions with different energy. In particular, FTIR spectrometers use the Fourier transform to process the information mathematically.

The main vibrationsof a molecule can be classified as either stretching or bending:

In plane stretching:

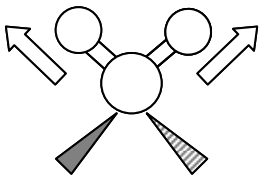

Symmetric

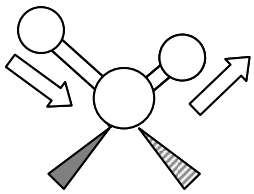

Antisymmetric

In plane bending:

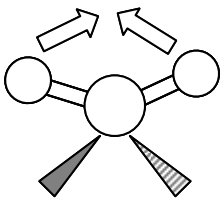

Scissoring

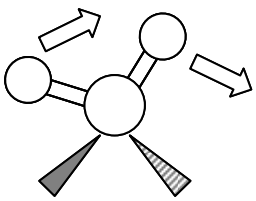

Rocking

Out of plane bending:

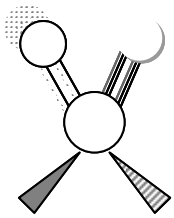

Twisting

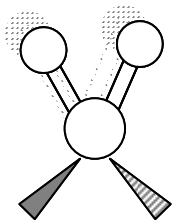

Wagging

Only those vibrations promoting the formation of a net dipole moment in the molecule will be visible in FTIR spectroscopy.

Infrared spectra are usually recorded in wavenumber units (cm^{-1}), a frequency measurement which is the inverse of the wavelength (λ) in centimetres. The energy related to a wavelength and frequency is (*Equation 2.1*):

$$E = h\nu = h\frac{c}{\lambda} \qquad (2.1)$$

A common FTIR spectrum ranges from 400 to 4000 cm^{-1}. Higher numbers are to the left of the actual spectrum because it is wavelength that is being scanned. Some of the most common functional groups and the wavenumbers associated to their vibration transitions are shown in *Table 2.1*.

Table 2.1 Functional groups and wavenumbers in an FTIR spectrum

Wavenumber (cm^{-1})				
4000	**3000**	**2000**	**1500**	**1000**
Bonds to hydrogen O – H N – H C – H	Triple bonds C ≡ C C ≡ N		Double bonds C = C C = O	Single bonds C – O C – F C - F

The wavenumber associated to the vibrational transition of a group depends not only on the chemical nature of the group but also on its environment. It is possible to relate the signals in the IR spectra to the chemical structure and the chemical environment of the groups and molecules.

FTIR spectrometers use fixed and movable mirrors to generate and record the signals. An example is shown in *Figure 2.1*.

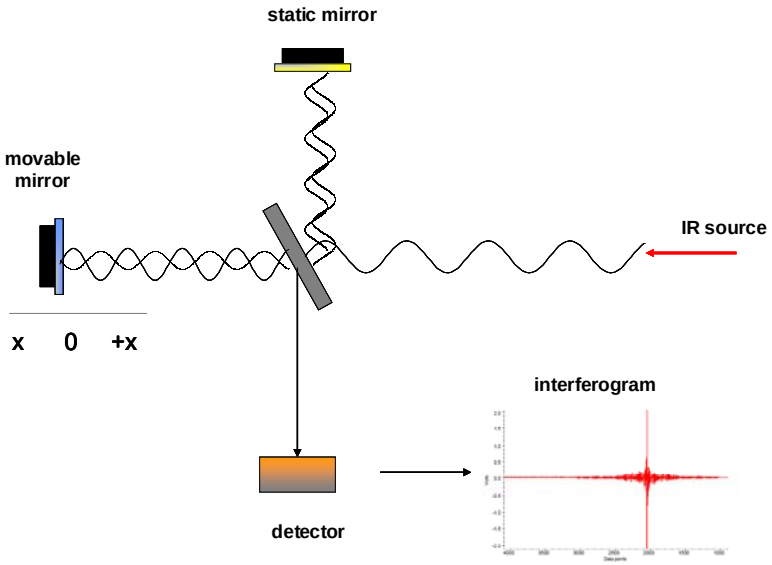

Figure 2.1 Schematic diagram of a generic FTIR spectrometer.

The IR beam is generated with E_0 energy by an IR source in a frequency range and is then reflected by the static and movable mirrors. The beam is then passed through the sample (or the reference) and a detector measures the amount of energy which the sample has absorbed ($E_{abs} = E_0 - E$). The resulting interferogram is then converted into the frequency domain (*Figure* 2.2). The final spectrum can be expressed in terms of absorbance (*Abs*, %) or transmittance (*Tran*, %), considering either the energy absorbed by or passed through the sample, respectively.

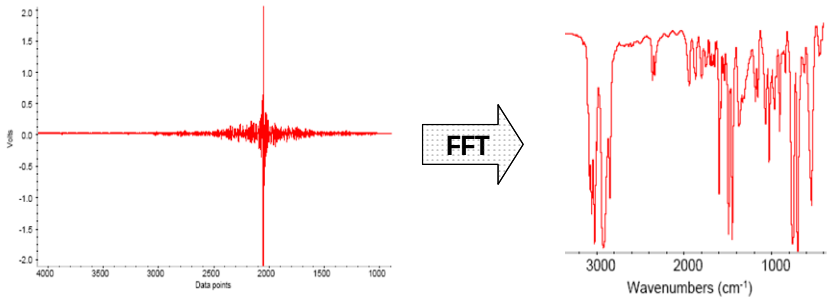

Figure 2.2 Signal conversion to the frequency domain

1.2 Types of FTIR experiments

There are several possible configurations of FTIR experiments. Even though they are all related to the chemical structure of the sample, some of them may be more convenient considering the physical properties of the sample (physical state, concentration, etc). All the FTIR experiments require a reference sample to subtract the effect of the blank (ambient CO_2, H_2O or other materials). The absorption bands of a FTIR spectrum should be sufficient intense not to be overlapped by noise, but not too strong to avoid saturation (E_{abs}< 1.6 % of absorption, *Abs*)

1.2.1 KBr disc experiments

Potassium bromide (KBr) experiments are suitable for solid powders with high IR absorbance. The sample is mixed with dry KBr and ground to obtain a very small grain. After the appliance of high pressure during some minutes a thin disc is obtained. The reference sample consists of a pure KBr disc, prepared following a similar procedure.

The concentration of the sample in the KBr disc can be varied to optimize the FTIR signal, but typical values of concentration are between 1 and 2% by weight of the sample. It is very important to use dry components (KBr, samples, discs, etc) since the presence of moisture can seriously affect the process of the disc formation.

A background spectrum is subtracted from that of the sample. The most relevant peaks of KBr (background) are those corresponding to the absorption of water (3000 cm^{-1} and 1630 cm^{-1} regions) and of carbon dioxide (2300 cm^{-1} region). Since the H_2O and CO_2 contents in the environment can vary, it is important to perform the background and the sample measurements as close as possible in time.

1.2.2 ATR experiments

Attenuated Total Reflectance (FTIR - ATR) is a technique usually applied to characterise films or liquids by Infrared Spectroscopy. It is particularly suitable to samples which would saturate the FTIR signal in typical absorbance experiments or when a KBr disc cannot be prepared [3].

In ATR experiments the sample (with a refractive index n_1) is placed between a crystal (with a high refractive index n_2) and a clamp, as seen in *Figure* 2.3.

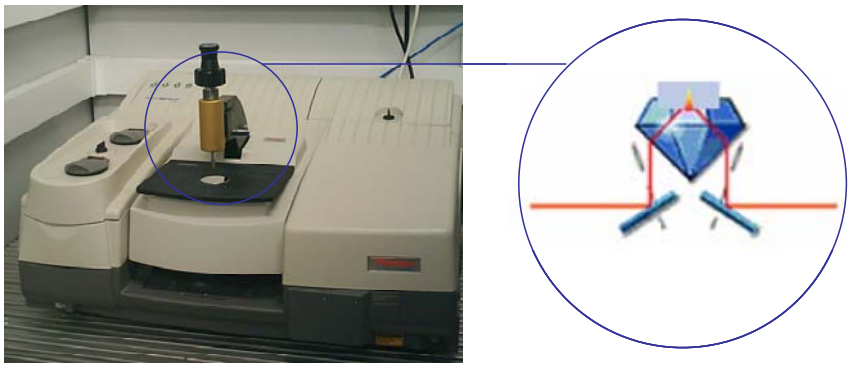

Figure 2.3 ATR modulus in an FTIR spectrometer.

The IR beam is transmitted through the crystal which is in contact with the sample. The beam is then partially reflected by the crystal and partially absorbed by the sample, generating the so-called evanescent wave. A scheme of the pathway of the IR beam in an ATR experiment can be seen in *Figure 2.4*.

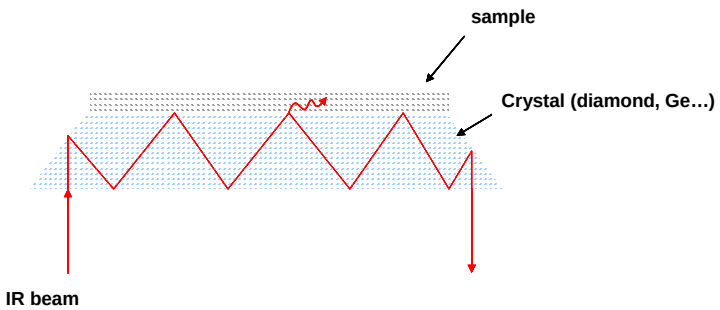

Figure 2.4 Beam reflexion and evanescence wave in an ATR experiment

Different crystals can be used in ATR experiments, such as ZnSe, Ge or diamond. In order to obtain internal reflectance the incident angle must exceed a minimum value: the so-called critical angle (θ). This angle depends on the real parts of the refractive indices of the sample and the ATR crystal, as *Equation 2.2* shows:

$$\theta = \sin^{-1}\left(\frac{n_2}{n_1}\right) \qquad (2.2)$$

The distance the evanescent wave penetrates the sample before attenuating to the 33.33 % of its original value is called the depth of penetration *d* (see *Figure* 2.5) and can be calculated by:

$$d = \frac{\lambda}{2\pi \cdot n_1 \left(\sin 2\pi - \left(\frac{n_2}{n_1}\right)^2\right)^{1/2}} \qquad (2.3)$$

where λ is the wavelength of the IR radiation.

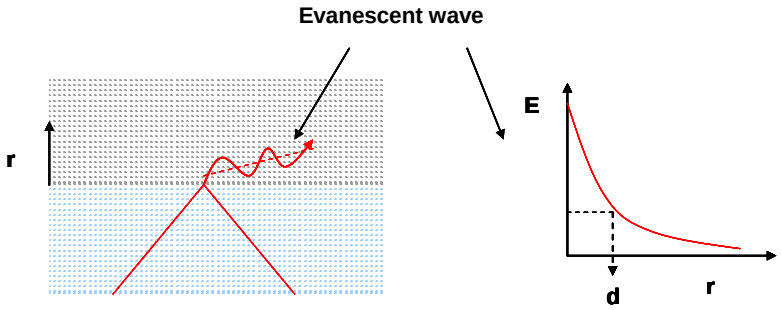

Figure 2.5 Calculation of d (depth of penetration)

The information obtained from an ATR experiment is similar to that using KBr discs. A background must be performed before the sample is analysed. The effect of water and CO_2 in the atmosphere as well as the crystal structure is then subtracted from the sample spectrum. Further corrections to the original spectra such as baseline, refractive index and incident angle might be also done depending on the experimental conditions.

1.3 Equipment

All the FTIR experiments were performed using a Thermo Nicolet 5700 module (Thermo electron), as shown in *Figure 2.6*.

Figure 2.6 Picture of the FTIR spectrometer

The FTIR experiments were carried out in the Thermal Analysis Laboratory in the School of Industrial Design Engineering of the Univesitat Politècnica de València. FTIR-ATR was used for the characterisation of the films and KBr discs were prepared for the characterisation of the liquid crystal polymers.

2. Differential Scanning Calorimetry (DSC)

2.1 Fundamentals

Differential Scanning Calorimetry (DSC) is a technique used to study the thermal transitions of a sample by measuring the absorbed or evolved energy by this sample in relation to a reference when it is submitted to a controlled temperature program [4-6].

There are two main types of calorimeters. In the calorimeters that use the "null balance of temperature" principle or power compensated, the sample and reference are placed in different ovens. When they are submitted to the temperature program and the sample undergoes a thermal transition, the sensors placed in the oven detect a difference in the temperatures, and then the entrance power is adjusted to exceed this difference. The temperatures are kept equal by continuous and automatic adjustments of the heating power, and the difference between the entrance heat in the sample and in the reference is sent to a recorder (*dH/dt*).

On the other hand, calorimeters that are based on the measurement of temperature difference have only one oven for both the sample and the reference. The thermal transitions in the sample promote temperature differences respect to the reference which are measured by thermocouples, and the heat flux that should be provided or absorbed is calculated.

The thermal flow rate can be calculated by:

$$\frac{dH}{dt} = mC_P \frac{dT}{dt} \qquad (2.4)$$

Where *m* is the sample mass, *Cp* is the specific heat and *dT/dt* is the heating or cooling rate.

A schematical representation of the two types of calorimeters is shown in *Figure 2.7*.

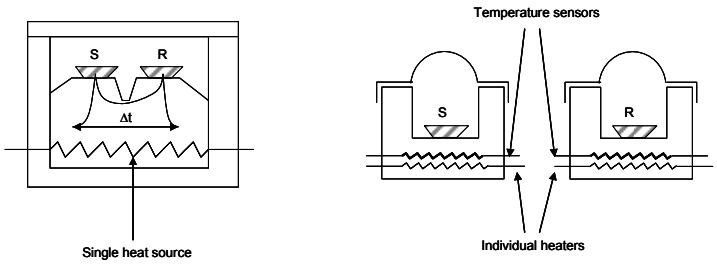

Figure 2.7 Single and separated chambers for the sample and reference.

Calorimeters also include a set of auxiliary systems to ensure controlled atmosphere in the cell and to regulate the temperature when heating (electrical resistances) and when cooling down (using coolers or liquid nitrogen). The data corresponding to the temperature, time and heat released or consumed are recorded into a computer. The evaluation of the experimental curves can usually be performed by using the equipment software.

DSC experiments can be isothermal or dynamic. In isothermal experiments the temperature is kept constant and then the power released or consumed by the sample is recorded as a function of the time. This type of experiments is very useful to study kinetic phenomena, crosslinking reactions, isothermal crystallisations or the thermal stability of materials. On the other hand, dynamic experiments consist on heating or cooling the samples by following temperature scans at a determined rate.

DSC curves (calorimetric curves or thermograms) give valuable information about first order transitions, pseudo-first order transitions, crystallinity or the morphology of the samples. It is possible to calculate parameters related to first order transitions such as melting, crystallisations or annealing processes. Depending on the sign convention, the exothermic and endothermic transitions will appear as either positive or negative peaks in the thermogram. The enthalpy involved in a transition can be calculated from the integral of the curve

$$\Delta H = \int \frac{dH}{dT} dT \qquad (2.5)$$

The calorimetric data of the dynamic experiments are usually expressed as heat flux per mass unit versus time or temperature. Therefore, it is necessary to consider the heating (or cooling) rate (β) for the calculation of ΔH in dynamic experiments.

DSC is also used to measure the glass transition of polymers (T_g). The change in the free volume associated to the glass to rubber transition can be observed by a change in the C_p values, and this change appears in the thermograms as an inflexion point. There are several methods for the calculation of the T_g considering the onset of the transitions (T_{onset}), the mid point of the inflexion of the curve (T_{inf}) or other geometrical or mathematical values.

In the field of liquid crystals, DSC is commonly used to study the mesophases ranges and their transitions by analysing the different transitions between crystal phases, mesophases or the clearing temperature. The enthalpies of the transitions are calculated providing important information about the mesomorphism.

DSC is also very useful to study polymer mixtures or blends, by comparing the thermal properties of the starting materials with that of the final mixtures. DSC is also used to detect phase separation morphologies, copolymerisation yields and other effects in complex systems.

2.2 Equipment

All the calorimetries in this thesis were performed using a Mettler Toledo DSC 822 module. The DSC experiments were carried out at the Thermal Analysis Laboratory in the School of Industrial Design Engineering of the Universidad Politécnica de Valencia (see *Figure 2.8*).

Figure 2.8 Picture of the DSC Modulus

3. Thermogravimetric Analysis (TGA)

3.1 Fundamentals

Thermogravimetric anaylsis (TGA) is a technique used in this PhD thesis to analyse the thermal stability of the materials. Small amounts of a sample (usually between 1 and 10 mg) are introduced into a high precision balance inside an oven and submitted to a temperature controlled program. When the material undergoes a decomposition process, a mass loss is detected by the balance. The result of a TGA experiment is the thermogravimetrivc curve (TG curve): a plot of the sample mass as a function of the temperature or the time [4-6].

The thermobalances used in TGA experiments are very high precision balances that measure the mass of a sample under study and the mass of a reference sample versus the time and temperature. The sample and the reference masses are measured inside aluminium oxide pans which have a small aperture to evacuate possible outlet gases generated in the reactions. The balances are placed inside a high temperature oven (reaching up to 1400°C) which heats the sample and the reference according to the temperature program.

The oven chamber is flushed with a gas to provide a controlled environment during the decomposition reactions. TGA measurements can be carried out under inert (N_2, argon, etc) or oxidising (O_2) atmospheres. Experiments performed using inert atmospheres display information about the pyrolisis of the material, while those performed under O_2 usually involve the oxidation of the sample. Another possibility is to use a nitrogen atmosphere and then use O_2 to oxidize the material which cannot be pyrolised at low temperatures.

The TGA balances can have either a vertical or a horizontal configuration, but the majority of the current TGA modules use horizontal balances because they avoid problems related to gas expansion in the chamber. In horizontal balances it is necessary to subtract a blank curve in order to eliminate the effect of thermal expansion of the balance itself (*Figure 2.9*).

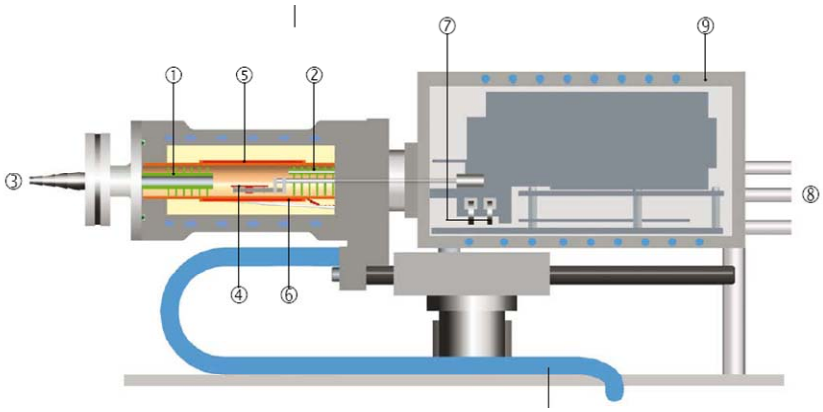

Figure 2.9 Horizontal TGA balance. 1) baffles, 2) Reactive gas capillarity, 3) Gas outlet, 4) Temperature sensor, 5) Furnace header, 6) Furnace temperature sensor, 7) Adjustment ring weights, 8) Protective and purge gas connector, 9) Thermostated balance chamber

TGA experiments can be isothermal or dynamic. In isothermal experiments the thermal stability of the sample is measured as a function of the time. On the other hand, dynamic experiments consist of temperature scans at a heating rate β. As the temperature increases, the different decomposition processes occur and the mass losses associated with them are recorded. The TGA signal is usually monitored as the mass percentage of the initial mass w_0 (in order to normalise the results) as a function of the time or temperature. A typical TG curve of a polymer is shown in *Figure 2.10*.

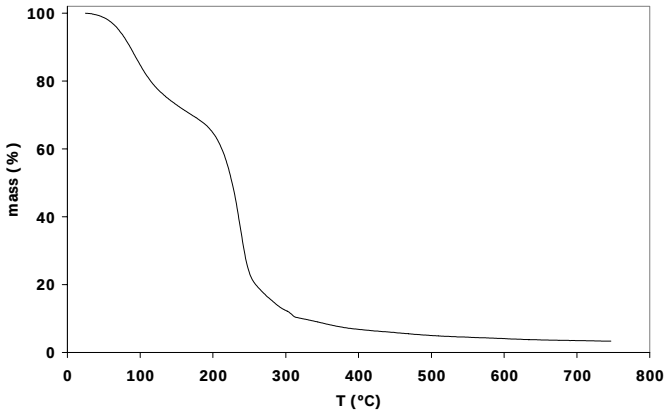

Figure 2.10 Example of a TG curve

A typical TG signal of the decomposition of a polymeric material consists of a sigmoidal curve like that shown in *Figure 2.10*. At low temperatures (T~100°C) a mass loss process related to the loss of water and other solvents in the sample can be observed. At higher temperatures (200 – 400ºC) some intramolecular bonded water and

other side groups with low thermal stability are released. The main decomposition process takes place usually at higher temperatures (400ºC – 600ºC) and involves the degradation of the polymer backbone. Finally, a fraction of the polymer mass remains in the pan after the experiment is finished (residual).

It is very common to obtain the derivative curve (DTG curve) of the thermogravimetric curve as a function of the temperature in order to analyse the different decomposition processes with more accuracy. The different steps in the TG curve appear as peaks in the DTG curve (*Figure 2.11*).

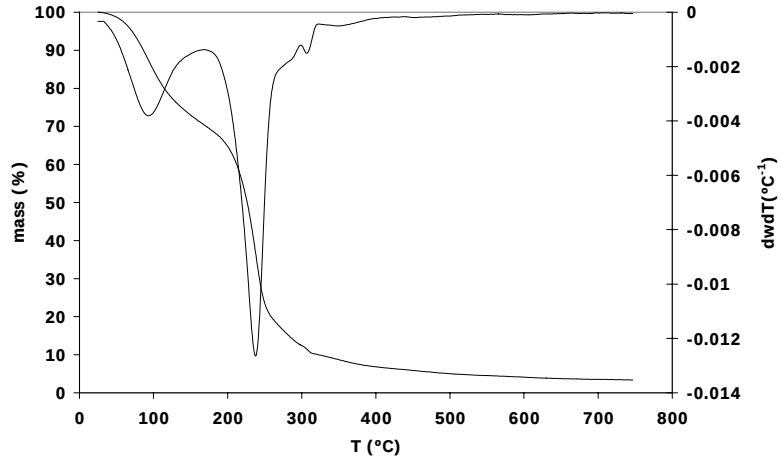

Figure 2.11 Typical TG and DTG curves of a polymer decomposition

TGA has been largely applied to the characterisation of polymeric and inorganic materials as a useful tool to study their thermal stability. It provides useful information about for example interactions at high temperatures, solvents contents, and degradation reactions. It can also be used in combination with other techniques such as mass spectroscopy (*MS*) or infrared spectroscopy (FTIR) in order to analyse the products of decomposition as a function of the temperature.

2.2 Equipment

All the thermogravimetric experiments were performed using a Mettler Toledo TGA/SDTA 851 modulus. Some TGA experiments concerning the synthesis of materials (chapters 5 and 6) where carried out at the Thermal Analysis Laboratory in the Department of Chemistry of the University of Aberdeen. On the other hand, the

experiments performed using commercial materials (chapter 3), the polymeric dispersions (chapter 4), the PVA films (chapter 5), and the liquid crystal polymers (*LCP*) (chapter 6) were carried out at the Thermal Analysis Laboratory in the School of Industrial Design Engineering of the Univesidad Politecnica de Valencia. A picture of the TGA module used in this PhD thesis is showin in *Figure 2.12*.

Figure 2.12 Picture of the TGA Modulus

4. Polarised Light Microscopy (PLM)

4.1 Fundamentals

Polarised Light Microscopy (PLM) is a very useful technique to study liquid crystals due to their birefringence (see chapter 1). The first polarised light microscope was invented by Otto Lehmann and was crucial in the discovery of liquid crystals [7].

In its wave form, light can be expressed as the sum of an electric field ($\vec{E}$) and an orthogonal magnetic field ($\vec{M}$) which depend on the propagation (z) and time (t), as seen in *Equation 2.6*:

$$\vec{L} = \vec{E}(z,t) + M(z,t) \qquad (2.6)$$

with:

$$\vec{E}(z,t) = E_0 \cdot \cos(kz - wt) \quad \text{and} \quad \vec{M}(z,t) = M_0 \cdot \cos(kz - wt + \delta)$$

In the most general case, there is a damping angle δ between both components. A representation of the electromagnetic wave can be seen in *Figure 2.13*.

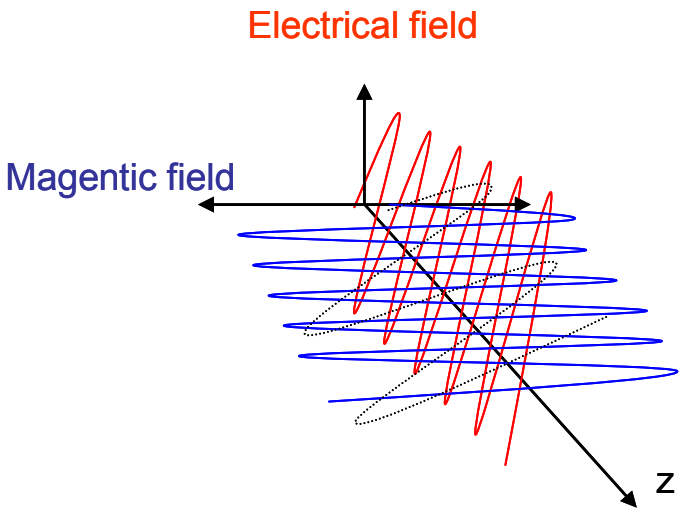

Figure 2.13 Scheme of electromagenic wave (light)

For some δ values, $\vec{E}$ and $\vec{M}$ are somehow related and the form of the resulting wave has specific features: the light is then polarised.

When δ equals 0, i.e. both waves are in phase, the projection of the different points of the wave at different times onto an orthogonal plane ($z = 0$) would lead to a straight line, like the one shown in *Figure 2.14*.

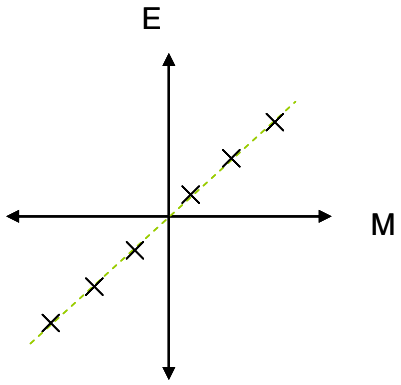

Figure 2.14 Linearly polarised light, projection onto the z = 0 plane.

In this case, the light is linearly polarised, because the values of the wave align into a line in the $z = 0$ plane.

If $\delta = 90$ºC, the resulting plot would be a circle and then the light is circular polarised, as seen in *Figure 2.15*.

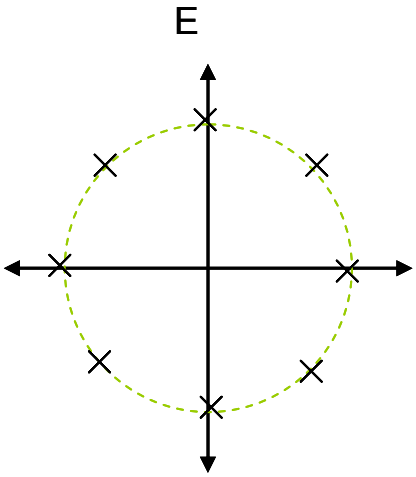

Figure 2.15 Circular polarised light, projection onto the z = 0 plane.

For the most general case, different values of E_0, M_0 and δ would lead to elliptical plots in the $z = 0$ projection (non-polarised light).

A polarised light microscope is capable of detecting the polarised light passing through a sample. It consists of a set of two polarisers (filters) with perpendicular directions ($d_{\parallel}$ and $d_{\perp}$) between which the sample is placed, as seen in *Figure 2.16*.

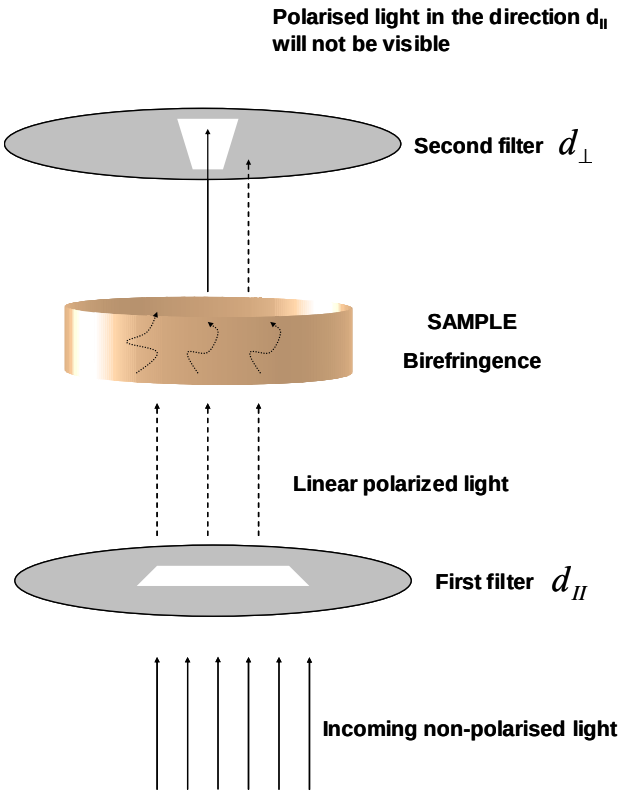

Figure 2.16 Schematic representation of a polarised light microscope.

When observing an isotropic sample through a polarised light microscopy, then the light polarised in the $d_{\parallel}$ direction will pass through it at the same speed, and independently of the direction of propagation. As a result, no change in the polarisation will occur. When the wave arrives to the second filter $d_{\perp}$, it will still be linearly polarised as $d_{\parallel}$. Since the filters are perpendicular, the result will be that no light will pass through the second filter, and the material will appear black under the microscope.

However, the speed of light traversing an anisotropic material (such as a liquid crystal) depends on the direction, due to its birefringence. A liquid crystal can show two different refractive indexes: $n_{\|}$ (for the direction of the director $\hat{n}$) and $n_{\perp}$ (for the orthogonal of $\hat{n}$). This means that the speed of the light propagation inside a liquid crystal can be expressed as a contribution of both components, as *Equation 2.7* indicates:

$$\vec{V} = V_{\|}\hat{i} + V_{\perp}\hat{j} = c(\frac{1}{n_{\|}}\hat{i} + \frac{1}{n_{\perp}}\hat{j}) \qquad (2.7)$$

When light passes through a *LC*, the two components of the light propagate at different speeds causing retardation in one of the two components. If retardation is that of 1 or a whole number, the polarisation will still be the same when reaching out the material. If the light experiences retardation of the slow wave by whole wavelengths plus one half (0.5, 1.5, 2.5…) then the polarisation of the outcoming light will be perpendicular to the incoming light, as the following *Figure 2.17* shows.

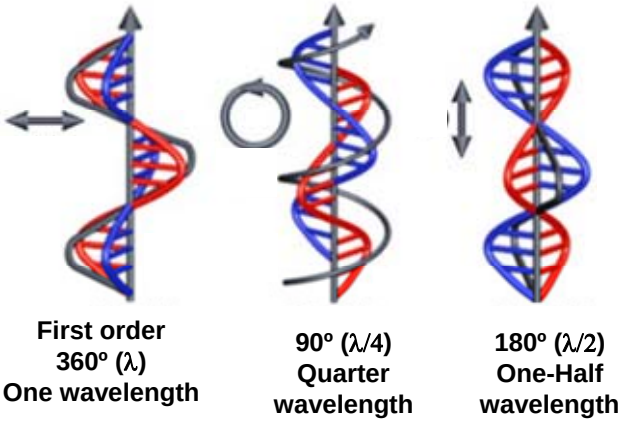

Figure 2.17 Polarisation and retardation.

Since the filters of a polarised light microscope are perpendicular, for liquid crystals showing certain values of retardation the light will come out to the viewer. The result is a mixture of kaleidoscopic colours caused by the interference of the outcoming waves.

Liquid crystals show different appearances under PLM depending on their mesomorphism. Since it is possible to relate the different textures with the mesomorphism, PLM is used to determine the mesophases that a liquid crystal undergoes. Some examples of liquid crystals textures under PLM are shown in *Figure 2.18*.

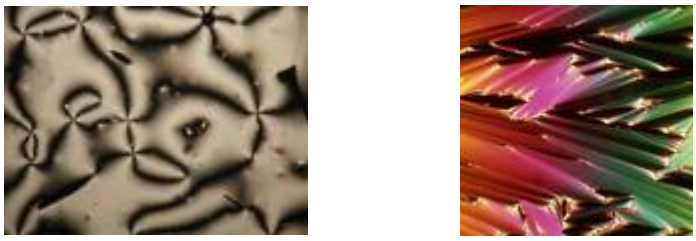

Nematic phase *Smectic phase*

Figure 2.18 Textures and mesophases

Polarised light microscopes usually have attached a temperature controller, so that it is possible to study the range of mesophases of thermotropic liquid crystals. Samples are placed on glass slides to avoid interferences with the optical signal. Changing the sample state can induce sample melting and even sublimation, and sometimes it is necessary to cover the sample once melted to avoid contamination of the lens and obtain a thin sample. In order to observe properly the textures of some mesophases it is necessary to anneal the sample for long times at high temperatures.

4.2 Equipment and experiment conditions

All the polarised light microscopy observations were performed in the Thermal Analysis Laboratory in the Department of Chemistry of the University of Aberdeen using using an Olympus BH-2 optical microscope equipped with a Linkam THMS 600 heating stage and TMS 91 control unit.

An example of a PLM image corresponding to a liquid crystal is shown in *Figure 2.19*.

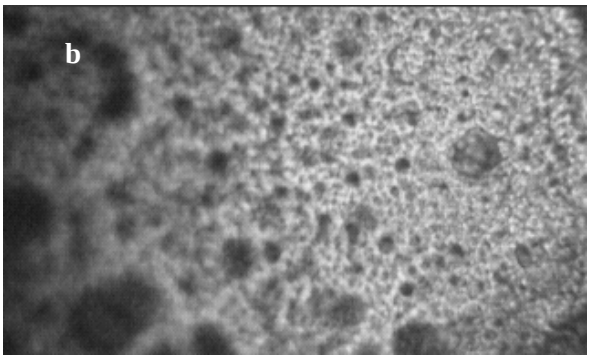

Figure 2.19 Example of a PLM image showing a cholesteryl phase

A picture of the microscope used in this PhD thesis is shown in *Figure 2.20.*

Figure 2.20 Picture of the Polarised Light Microscope, Olympus BH-2

DIFFUSIVITY PROPERTIES OF THE MEMBRANES

5. Swelling tests

5.1 Fundamentals

The performance of polymeric materials can be seriously affected by water absorption, since some of their properties may be changed (plasticisation, biodegradability, etc). Moreover, as was discussed in chapter 1, water content plays a very important role in Polymer Electrolyte Membranes as it affects the proton conductivity. Commercial polymeric electrolytes used in *PEMFC* show a biphasic structure consisting of a hydrophobic backbone with hydrophilic channels. The hydrophilic domains usually contain sulfonic groups which provide high proton conductivity.

The role of water absorption is also crucial in polyelectrolyte materials used in *DMFC*. The water contents in the membranes depend on different factors such as the concentration of anionic groups, the degree of phase separation or the interconnection between the ionic channels [8]. Moreover, water and methanol contents in such membranes are strongly interrelated, and efforts to decrease the methanol in the membrane usually promote a decrease in water content and also in proton conductivity [9].

Swelling tests are a very valuable technique to determine the solubility of solvents in polymers. A typical swelling test consists on submerging a polymer sample (usually a film) into a solution and studying the solvent absorption as a function of the time. The absorption of the solvent into the polymer is monitored gravimetrically and can be calculated as the swelling percentage, as in *Equation 2.8*:

$$M_t(\%) = S_w(\%) = \left(\frac{w_t - w_0}{w_0} \right) \cdot 100 \qquad (2.8)$$

where w_t and w_0 are the mass of the sample at time t and at time $t = 0$, respectively.

A typical curve obtained from a swelling experiment is shown in *Figure 2.21*.

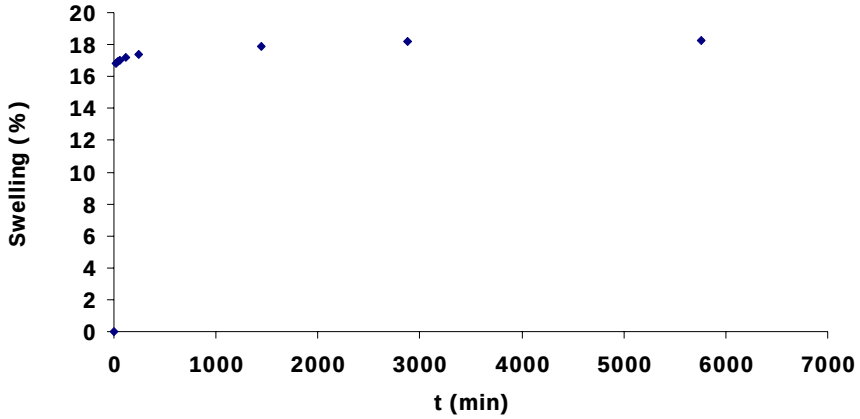

Figure 2.21 Typical curve of a swelling experiment.

The rate of absorption is high during the first moments of the test (usually following a linear pattern) and reaches equilibrium after some time (saturation). It is possible to graphically determine the swollen equilibrium mass w_∞ (the maximum amount of mass in the sample at $t \rightarrow \infty$) and the "relaxation time" τ (the time at which the amount of mass absorbed corresponds to the 66.67 % of w_∞)

The absorption process in polymers can be classified considering the relative mobility of the solvent and the polymeric segments. There are three well-known cases of solvent absorption in polymers [10]:

Case I. Fickian Diffusion

The rate of diffusion is much less than that of the polymer segment mobility. In this case, the equilibrium inside the polymer is rapidly reached and maintained independent of time.

Case II and Supercase II

The penetrant mobility is much greater than other relaxation processes. The diffusion is then characterised by the development of a boundary between the swollen part and the inner glassy core of the polymer. The boundary advances at a constant rate and the core decreases until an equilibrium penetrant concentration is reached in the whole polymer.

Non-Fickian – anomalous diffusion.

This case occurs when the penetrant mobility and the polymer segments relaxation rate are comparable. This case represents an intermediate behavior between Case I and Case II.

The three cases can be distinguished by analysing the sorption curve (*Equation 2.9*):

$$\frac{w_t}{w_\infty} = kt^n \qquad (2.9)$$

where k and n are two constants. Coefficient n shows typical values: n = ½ for Fickian diffusion, n = 1 for Case II (n > 1 for Super Case II) and intermediate values (½ < n < 1) for anomalous diffusion.

In the case of composite materials showing a phase separated morphology, other mechanisms can occur on solvent exposure. The solvent molecules can flow by capillary action between the interface of the components and also through cracks, pores or small channels in the polymer structure.

The values of n and k can be estimated by fitting the experimental data to *Equation 2.10*:

$$\log(\frac{w_t}{w_\infty}) = \log(k) + n\log(t) \qquad (2.10)$$

n can be calculated from the slope and k from the ordinate in the origin if $\log(\frac{w_t}{w_\infty})$ is plotted against log*(t)*, for small values of w_t / w_∞.

For a polymer following a Fickian behaviour, the diffusivity (D) of the membrane can be calculated from *Equation 2.11*:

$$\frac{w_t}{w_\infty} = \frac{4}{L}\left(\frac{D}{\pi}\right)^{0.5} t^{0.5} \qquad (2.11)$$

where L is a shape factor of the sample (the thickness of the sample) and t the experiment time. The representation of w_t/w_∞ versus $t^{0.5}$ gives a straight line for small values of w_t/w_∞ (usually less than 0.5, i.e. at short experiment times).

In order to study possible differences between the swelling curves, it is also common to display the values of the fractional mass uptake (w_t/w_{eq}) as a function of the square root of time, following the standard procedure used by other authors [11]. The shape of the fraction mass curve then provides useful information about possible deviations from the Fickian behaviour. *Figure 2.22* shows four examples of absorption patters in polymers, considering the Fickian or classical (a), the so-called sigmoidal (b), the two-step (c) and Case II described above (d).

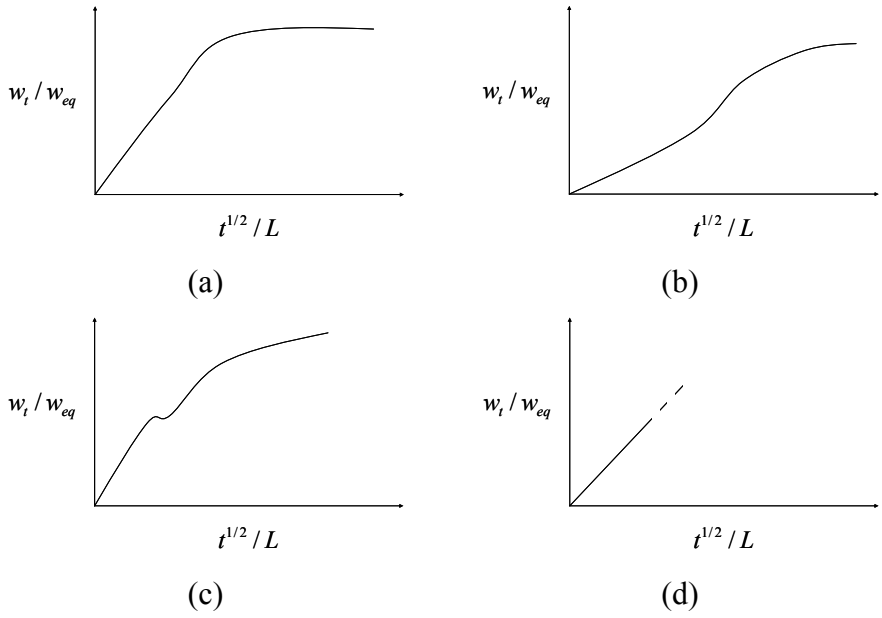

Figure 2.22 Different diffusion patterns in polymers

The representation of the parameter w_t/w_{eq} describes the diffusion of the solvents, and therefore possible deviations of the experimental data from the Fickian behaviour.

5.2 Experimental procedures and instrumentation

Swelling tests are a very sensitive technique. Therefore, in order to obtain reproducible and reliable data, it is very important to follow the same procedure with high accuracy in the different measurements. The general procedure adpted is now described.

The membranes under study were cut into rectangular films of 4x1 cm^2 size and were weighed (t = 0, w_0). Then, they were submerged in test tubes containing the solutions which will diffuse into the polymer. The test tubes were submerged in isothermal SELECTA Ultrasonic baths ($T \pm 0.1$ºC) to control the temperature.

The absorption of solvent was measured gravimetrically several times during the swelling experiment, according to the following standard procedure:

1 First, the tubes were removed from the bath, and the membranes were taken out from the tubes.

2. Then, the excess liquid was removed from the samples with two tissues.

3. The membranes were then weighed using a Mettler Toledo balance (w=0.1 mg accuracy).

4. After the mass was measured (w_t), the membranes were placed back into the test tubes and the tubes were resubmerged in the isothermal bath again.

The membranes were immersed in the solutions for one week. After the last measurement was complete, the samples were covered and stored for further analysis. All the experiments were performed three times using different membranes in order to obtain average values.

5.3 Analysis of the experimental results

The values of S_w (also M_t) were calculated as the average value of three experiments. The representation of the results provided typical absorption curves similar to those shown in *Figure 2.23*.

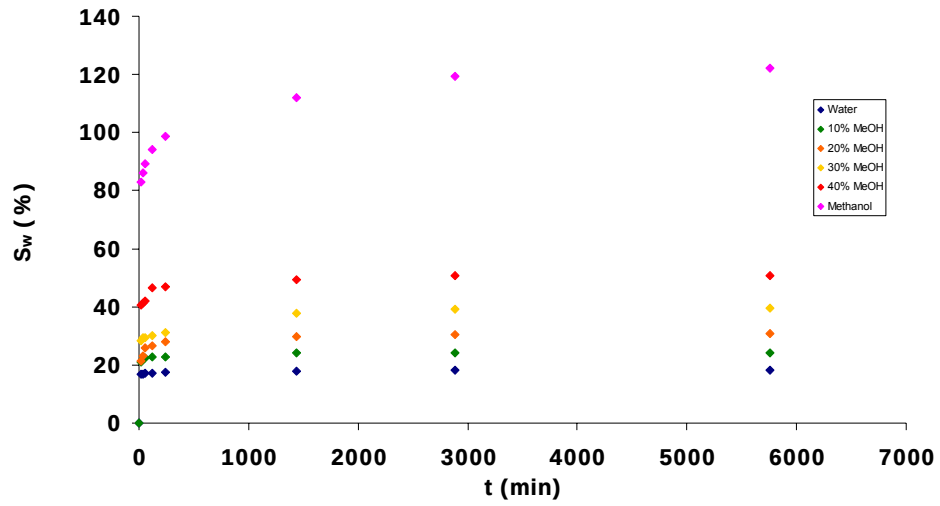

Figure 2.23 Swelling curves corresponding to the membranes submerged in binary aqueous solutions of methanol (MeOH) and water at 35ºC

The values of the solvent absorbed at the equilibrium point (S_{eq} *or* M_{eq}) and the time to reach half of the equilibrium swelling value ($t_{1/2}$) were estimated from the experimental swelling curves. The mass flux at the beginning stages of absorption (J) was also estimated considering the mass absorbed at $t_{1/2}$ ($w_{1/2}$) and the surface of mass transfer (S), as seen in *Equation 2.12*:

$$J = \frac{w_{1/2} / t_{1/2}}{S} \qquad (2.12)$$

For the calculation of J, the convection effects were neglected ($S^{1/2} >> L$) and the dynamics was considered one-dimensional [10].

The values of M_{eq}, J and $t_{1/2}$ provided valuable information about the effect of the solvent composition on its absorption in the membranes, as seen in *Table 2.2* and *Figure 2.24*.

Table 2.2 Parameters of the swelling tests performed in binary mixtures of water and methanol

Sample	S_{eq} (%)	$t_{½}$ (min)	J (kg / sec·cm^2·10^5)
Water	18.3	10.7	2.16
10% MeOH	24.3	11.9	2.76
20% MeOH	32.9	12.6	2.87
30% MeOH	39.5	12.8	3.57
40% MeOH	50.9	17.6	3.41
Methanol	122.1	18.2	10.74

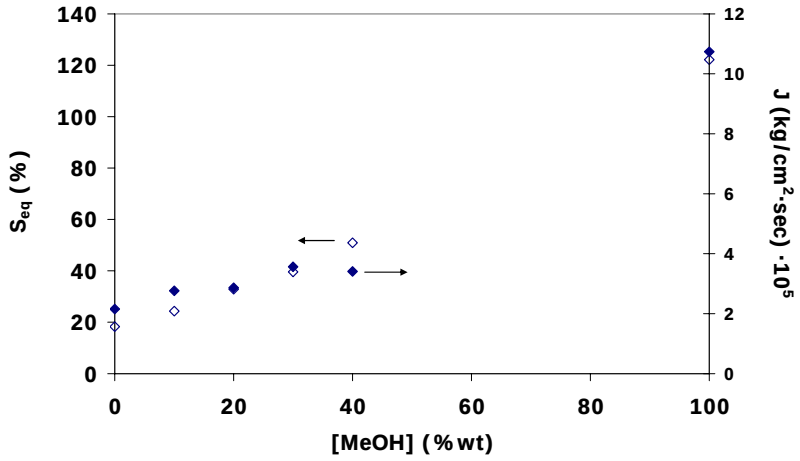

Figure 2.24 Values of the mass of solvent absorbed at equilibrium (S_{eq}, ◇) and mass flux (J, ◆) corresponding to the membranes submerged in binary aqueous solutions of methanol (MeOH) and water at 35ºC

Another interesting parameter to describe the solubility of a solute in a polymer is the number of molecules of solvent absorbed per equivalent, λ, which can be calculated using:

$$\lambda = \frac{w_{solvent} / MW_{solvent}}{w_0 / EW_{polymer}} \qquad (2.13)$$

Where $w_{solvent}$ and w_0 are the mass of solvent absorbed and the mass of dry polymer membranes, respectively, and $MW_{solvent}$ and $EW_{polymer}$ are the molecular and equivalent weights of the solvent and the polymer, respectively. $EW_{polymer}$ corresponds to the weight of the elemental repetition unit of Nafion, which in Nafion 117 equals 1100 eq/mol, considering the weight of the repeating unit.

The values of the fractional mass uptake (w_t/w_{eq}) were calculated and plotted as a function of the square root of time ($t^{1/2}/L$), where L is the thickness of the membranes. An example of a set of fractional curves is shown in *Figure 2.25*.

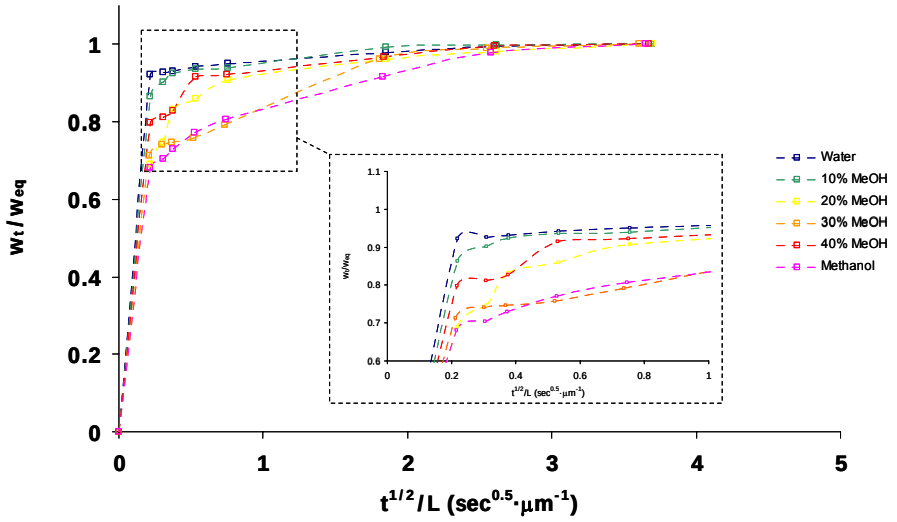

Figure 2.25 Fractional mass uptake for the membranes submerged in the water and methanol binary mixtures

The changes in the shape of the curves provided relevant information about the diffusion stages in the membranes, by observing possible deviations from Fickian behaviour (see *Figure* 2.22).

6. Time resolved FTIR – ATR desorption tests

6.1 General features

Desorption tests are used in order to complete the study of the transport properties of solutes through membranes used as electrolytes in *DMFC*. In general terms, the absorption and desorption tests through the membranes are related but do not provide the same information. The study of the diffusion of the solutes from the polymer structure can provide important information about the state of the solvents inside the membranes, such as their aggregation state or the existence of interactions with the polymer groups. In the case of the absorption of mixtures of solvents, it is very important to study the selectivity of the membranes with respect to each of the components.

These experiments are particularly suitable for studying controlled release phenomena in which where a compound must be released from a solid at a determined rate. This is broadly applied in the controlled release of drugs, pesticides or fragrances at prescribed rates [11, 12]. In general terms, the release of a solute from a substrate can be modelled according to several mechanisms. Some of the simplest models are shown in *Figure 2.26*.

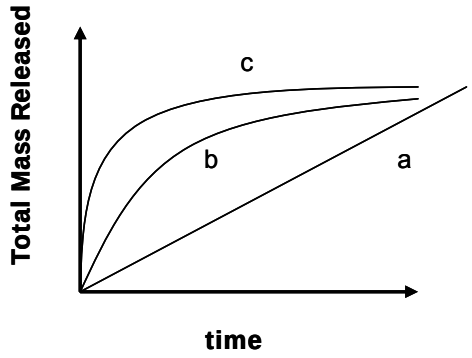

Figure 2.26 Mass of solute released by different mechanisms: (a) Zero order diffusion, (b) $t^{1/2}$ diffusion, (c) First order diffusion

Solvent diffusion is usually a complex phenomenon involving complex solvent-polymer interactions. In general terms, the desorption rate of solvents from a swollen material decreases with the square root of time, thus following a profile such as that shown in

Figure 2.26b. However, this profile can change under some conditions. The diffusion can depend on the rate of relaxation of the polymer chains of the membranes. Such relaxation-controlled diffusion commonly involves glassy polymers that are very soluble in water. In this case, the diffusion can be described as Case-II transport or non-Fickian diffusion, as shown in *Figure 2.22d*, and the rate of diffusion is constant (zero order in time, *Figure 2.26a*) [13].

6.2 Experimental procedures and instrumentation

Time resolved FTIR - ATR was used to perform the desorption tests of solvents from some of the materials prepared here. The general scheme of the experiments is shown in *Figure 2.27*.

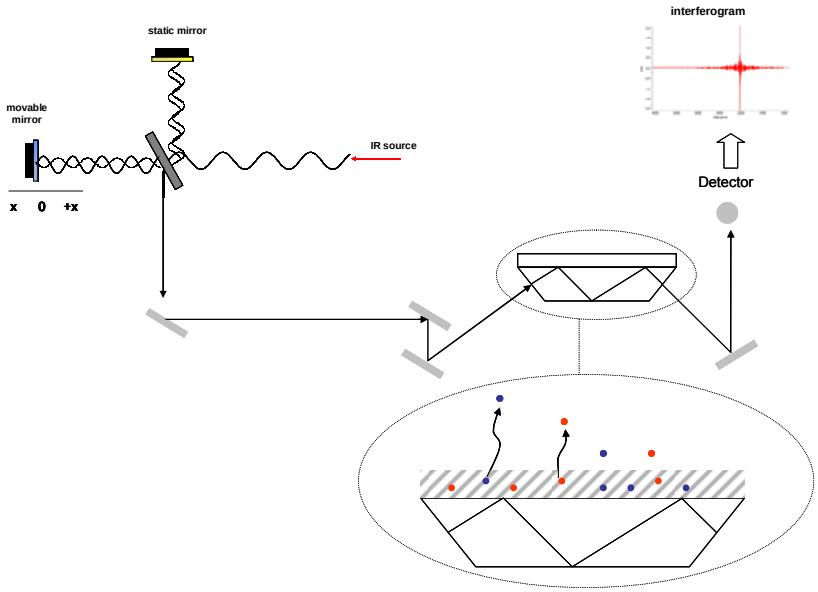

Figure 2.27 Schematic of the FTIR-ATR apparatus

The membrane under study is placed on the ATR diamond crystal and then the clamp is attached over the membrane to apply pressure over the sample. The experiment is then launched and the FTIR spectra are obtained as a function of time.

The diffusion experiments were performed using a Thermo Nicolet 5700 modulus with an ATR attachment. The spectra were obtained continuously for 30 minutes, with 32 scans per spectrum at a resolution of 4 cm^{-1}. All spectra were corrected using a background subtraction on the ATR element spectrum.

6.3 Analysis of the experimental results

The analysis of the experimental results was carried out according to the following standard procedure:

1. The results were recorded as a *SRS* file, containing all the spectra acquired during the 30 minutes. A general view of the results as a function of the wavenumber (cm^{-1}) and the time of experiment (minutes) is shown in *Figure 2.28*.

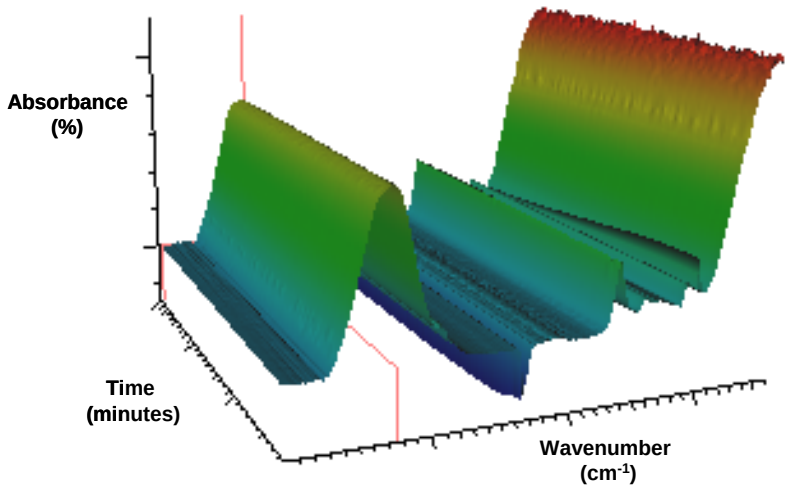

Figure 2.28. An example of time resolved FTIR-ATR spectra

2. The study was focused on particular IR bands in the spectra and specifically. In particular on the regions related to the IR bands corresponding to the hydroxyl stretching band (ν=3600-3000 cm^{-1}), to water bending (ν=1650 cm^{-1}) and to methanol (ν=1016 cm^{-1} for the C-O stretching band).

3. The IR absorption (*I*) and frequency (ν) of these bands, and also of other bands related to functional groups of the materials, were obtained using the *Omnic* software (*Find Peaks*) at time *t*=0. The values obtained in this way were considered as the initial values.

4. The values of IR absorption (*I*) of the three bands were plotted as a function of the time by exporting the corresponding curves for each band of interest.

5. The absorption of the bands with time were normalised by the initial absorption (I/I_0) and plotted as a function of time for the different samples, in order to compare the diffusion of the solvents and also to study the effect on the transport properties. Some examples of the diffusion curves can be seen in *Figure 2.29*.

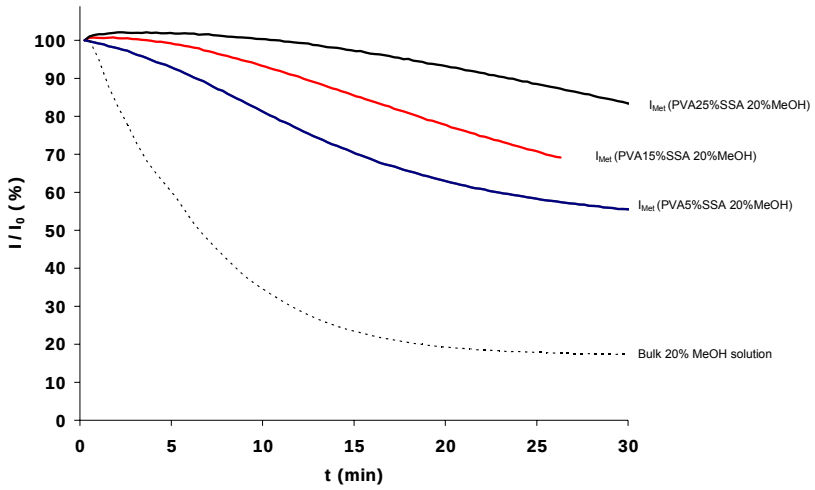

Figure 2.29 Normalised diffusion curves (I/I_0) obtained from the FTIR-ATR experiments. C-O stretching band at 1016 cm^{-1} corresponding to methanol.

These curves can be very useful in assessing the mechanism of diffusion.

6. In addition, the derivative of the absorption curves $d(I/I_0)/dt$ were obtained to compare parameters related to the maximum rate of diffusion, or to better determine the mechanism of transport. In *Figure 2.30* some examples corresponding to the derivative curves of different samples have been plotted as a function of time.

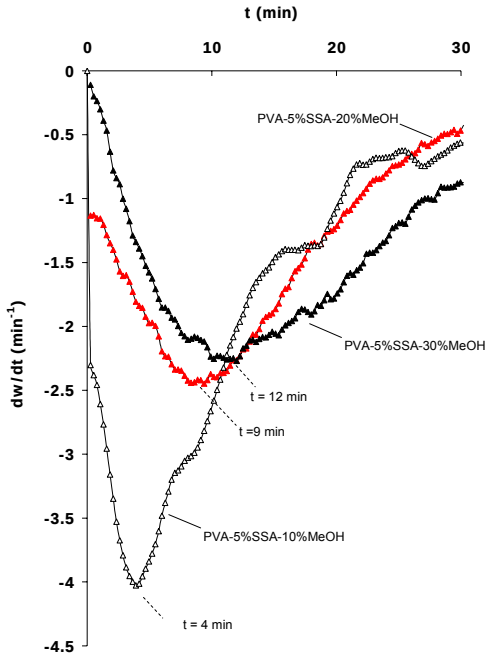

Figure 2.30 Diffusion rate curves obtained from the FTIR-ATR experiments. C-O stretching band at 1016 cm^{-1} corresponding to methanol.

7. Diffusion tests

7.1 General features

In order to test the diffusion properties of the membranes in solutions of water and alcohols, a separation plant has been designed, built and set-up. Even though the plant has been used for testing the selectivity of the membranes against water and methanol, it could also be used for the evaluation of other perm-selective membranes with other solvents.

If we consider a diffusion experiment in which methanol is transferred from a solution (*A*) to a less concentrated solution (*B*) through a membrane, the diffusivity can be calculated as shown in *Equation 2.14*:

$$C_B(t) = \frac{A}{V_B}\frac{DK}{L}C_A(t-t_0) \qquad (2.14)$$

where C_B and C_A are the two methanol concentrations in the tanks, and A and L are the membrane area and thickness, respectively. D is the methanol diffusivity of the membrane, and K the partition coefficient between the membrane and the adjacent solution. Assuming that D is homogeneous inside the membrane and K independent of the concentration of methanol, the permeability P can be calculated as $P = DK$ using *Equation 2.15*:

$$P = DK = \frac{C_B(t)}{C_A(t-t_0)}\frac{LV_B}{A} \qquad (2.15)$$

In diffusion tests the value of C_B is measured several times during the experiment obtaining plots of the concentration with time. The permeability (*P*) can be calculated from the gradient of the lines.

The results of the diffusion experiments complement those obtained from the swelling tests (see section 5). Therefore a set of diffusion data obtained in different conditions depending of the sample geometry, temperature, concentration and pressure is obtained.

This approach provides a more complete picture about the preferential diffusion of water and alcohols in the membranes.

7.2 Description of the plant used in the diffusion tests

A schematic of the plant used in the diffusion tests is shown in *Figure 2.31*.

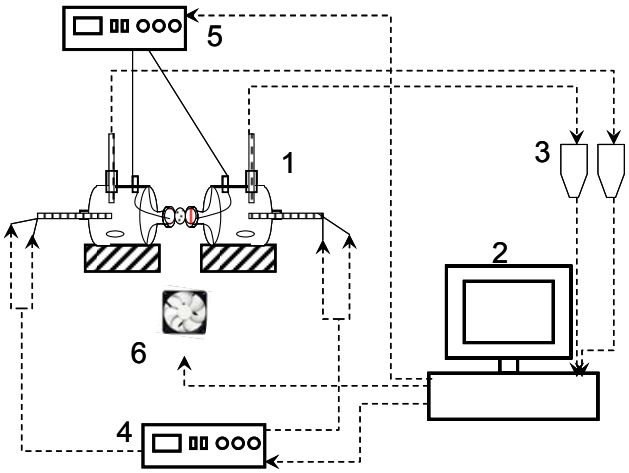

Figure 2.31 Schemeatic of the plant used in the diffusion tests. (1) Tanks with the solutions and membrane, (2) Personal Computer (PC), (3) Conductimeters, (4) Power supply (temperature control), (5) Power supply for the electrical field control.

A more detailed picture and a scheme of the main module (*1*) are shown in *Figures 2.32* and *2.33*, respectively.

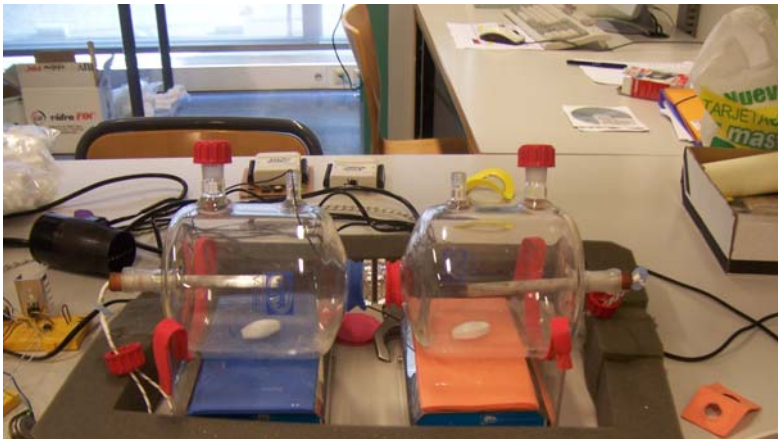

Figure 2.32 Picture of the modulus.

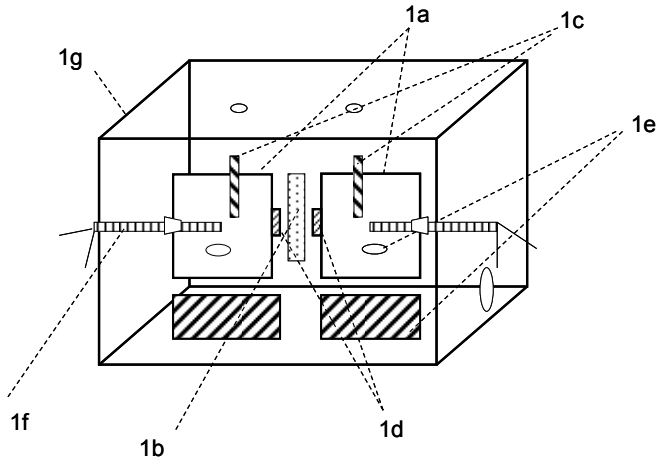

Figure 2.33 Detail of the modulus. (1a) tanks, (1b) membrane under test, (1c) Conductimeters probes, (1d) Electrodes, (1e) Stirrers, (1f) Heaters, (1g) Methacrylate cover.

The core of the plant (*1*) consists on two rounded glass tanks of 1 liter capacity (*1a*) between which the membrane is placed (*1b*). The tanks were designed in-house and supplied by *Afora*. One of the flasks contains the water/alcohol solution (simulating the anode fuel stream) while the other contains pure water (simulating the cathode conditions). Two iron mesh electrodes (*1d*) are located on both sides of the membrane to apply an electrical field. The temperature is controlled by two cylindrical resistors protected by silicon tubes and placed inside the tanks (*1f*). The concentration in the tanks is monitored by means of conductivity by using two conductimeter probes (*1c*) submerged into the solutions, which are homogenised by continuous stirring (*1e*). The plant is isolated by a methacrylate cover (1g).

In the previous description, one of the tanks (*A*) contains a methanol and water solution, simulating the behaviour of the anode in *DMFC*, and the other one contains pure water (*B*). When the experiment starts, methanol diffuses from *A* to *B* through the membrane due to the difference in concentration. The methanol concentration in the tanks is measured in real time by conductivity. The module performs experiments at controlled temperatures and the two electrodes can be used to simulate the electro-osmotic effect in *DMFC* and also to test the external response of liquid crystalline materials to an

applied field. The system is controlled by a Personal Computer (*PC*) by means of a Data Acquisition Card (*DAC*).

An Acer personal computer (*PC*) with an acquisition card (*PCI 9112*) is used to collect the data and control the plant (*2*). The computer is equipped with an Intel Core™ 2 CPU, at 2.13 GHz with a 2 GB RAM memory. The PC has one COM gate (*COM1*), and a second one was enabled (*COM2*). Two conductimeters CON110 provided by Eutech Instruments are used to measure conductivity and temperature (*3*). The cell constant for the experiments is $K = 1$, and the temperature accuracy $T \pm 0.1$ºC. The conductimers are connected to *COM1* and *COM2*.

The resistors (*1f*) and the electrodes (*1d*) were powered by two *Grelco 6VD305SF* power supplies (*4, 5*) in a voltage range of 0 – 30 V and an intensity range of 0 - 5 A.

In order to improve the temperature control of the system, the tanks are isolated by a methacrylate box. A heating fan (Braun Cosmo 1000, *6*) works additionally to improve the thermal response by supplying warm air into the plant.

Control system

The control of the plant is carried out by a PC using *LabView*. The scheme of the control system is shown in *Figure 2.34*.

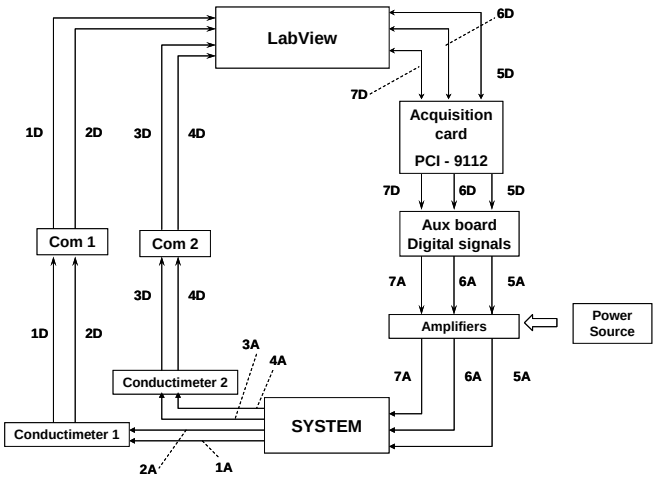

Figure 2.34 Scheme of the control system. Variables: 1, 3) Temperature of the solutions 2, 4) Conductivity of the solutions, 5) Temperature control signal, 6) Fan trigger signal, 7) Electrical field control signal. A and D after the number indicate Analogical and Digital respectively.

The conductivity (streams *2A* and *4A*) and temperature (streams *1A* and *3A*) analog signals are read from the solutions and are driven by the probes to the conductimeters. The signals are converted into digital (streams *1D, 2D, 3D* and *4D*) and printed to the PC every 5 seconds through *COM1* and *COM2*. The signals of *COM1* and *COM2* were desynchronised to avoid overlapping in the LabView program.

A *PCI-9112* acquisition board (*DAC*) was installed into the computer to control the system. The *PCI – 9112* board comprises a 32-bit bus and a 12-bit accuracy *A/D* conversion. The board has 16 analog inputs, 2 analog outputs and 16/16 digital inputs/outputs. The digital signals corresponding to the temperature and electrical field control (streams *5D*, *6D* and *7D*) in *Figure 2.35* are driven to the acquisition card through an auxiliary board. The corresponding analog signals are corrected by amplifiers and then lead to the system, as shown in *Figure 2.35*. Magnetic stirring is kept constant during all the experiments and is not considered a control variable.

Software specifications

LabView 8 was used as the interface between the PC and the acquisition board using Windows 2000 operating system. A similar scheme to *Figure* 2.35 was programmed. The program has the following information streams in real time:

Input signals

- Conductivity of the two solutions
- Temperature of the two solutions

Output signals

- Temperature control signal
- Electrical field control signal

A text file with the corresponding temperature, conductivity and other internal parameters is obtained after every experiment.

Temperature and Electrical Field Control

The temperature inside the tanks was controlled by two iron 15 Ω resistors and a heating fan. The resistors were prepared inside quartz tubes and were sealed with silicone. The fan injects hot air by an aperture into the methacrylate box in order to increase the speed of the temperature response.

A diagram of the temperature control is shown in *Figure 2.35*.

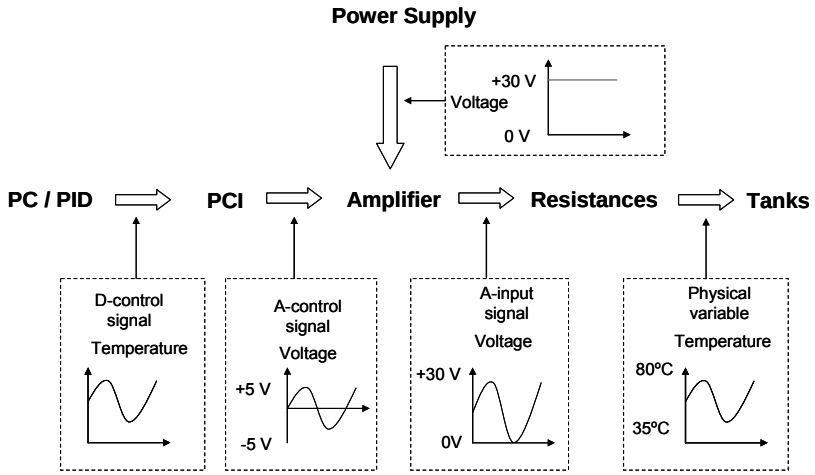

Figure 2.35 Representation of the temperature control by the LabView program (PC, PID)

A proportional-integral-differential controller (*PID*) was designed and programmed with *LabView*. Pulse Width Modulation (*PWM*) is used to control the temperature through the PCI-card. A set of transistors in Darlington configuration and several resistors were designed and sealed in a board (*Figure 2.37*). The control signal from the PCI card (±5 V) was led to an amplifier circuit to modulate the electrical signal from the Grelco power supply source (30 V and 1.98 A). The schematic and a picture of the circuit are shown in *Figure 2.36*.

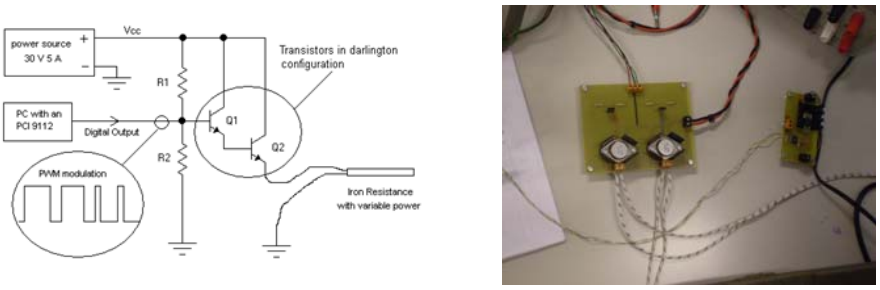

Figure 2.36 PWM circuit for the temperature control

7.4.3 Plant set-up

Temperature control set-up

The temperature control was adjusted by varying the *PID* parameters from different response curves at different temperatures. The temperature control range was kept between 35 ºC and 70ºC. Lower temperatures led to long stabilization times and at temperatures over 70ºC the formation of bubbles in the conductimeter probes prevented reliable temperature measurements.

The response curve for T = 35°C is shown in *Figures 2.37* and *2.38*. The values of the *PID* internal signal are also displayed.

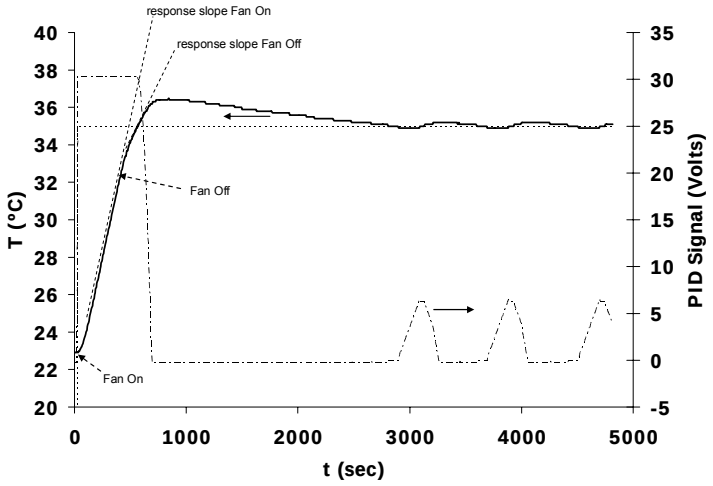

Figure 2.37 Temperature response curve (T_{Offset} = 35ºC)

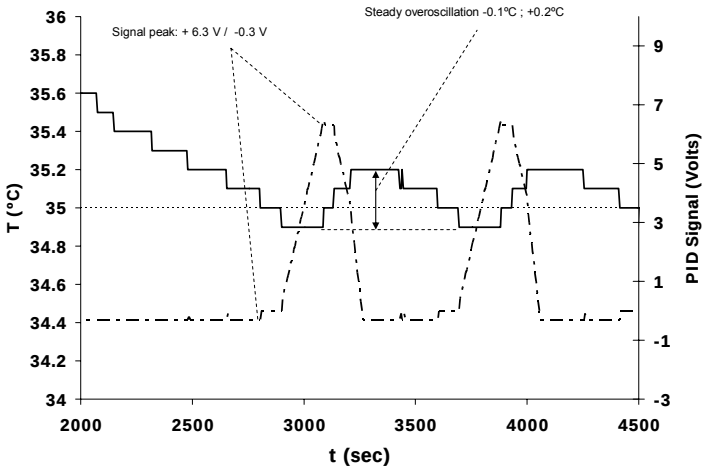

Figure 2.38 Detail of the response curve (T_{Offset} = 35ºC)

The solutions reached the temperature offset (35ºC) after 10 seconds, but it did not stabilize for 45 minutes. The system had a maximum over oscillation of 1.4 ºC and a steady over oscillation of 0.3 ºC. The *PID* signal varied from 0 (-0.3 V to ensure complete disconnection) to 6.3 V. The fan was triggered to increase the initial warming and switched off after 7 minutes. The use of the fan increased the heating rate by a factor of 10 (from 0.0107 to 0.1143 ºC/sec) as can be seen from the different slopes in *Figure* 2.37. All these results were considered within specification for the temperature control purpose.

The response curves for T = 35, 45, 55 and 65ºC can be seen in *Figure 2.39*. The summary of the control parameter is displayed in *Table 2.3*, and an example of the PID scheme in the *LabView* program in *Figure 2.40*.

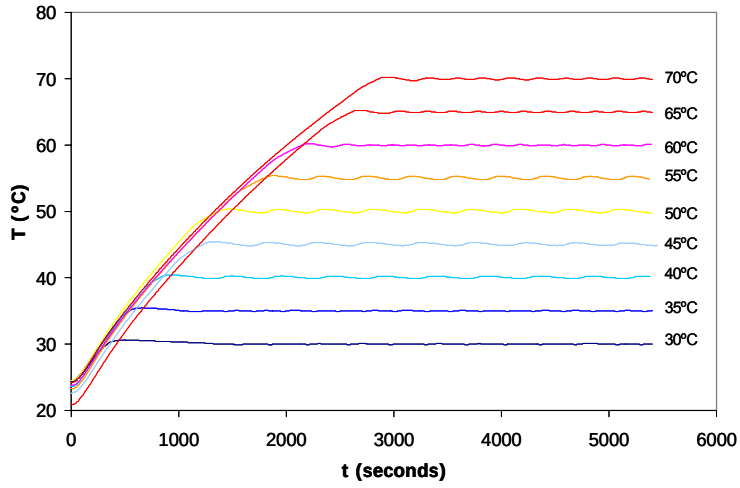

Figure 2.39 Temperature step curves for temperatures 30ºC < T < 70ºC

Table 2.3. PID parameters

K_P	K_D	K_I
10	5	2

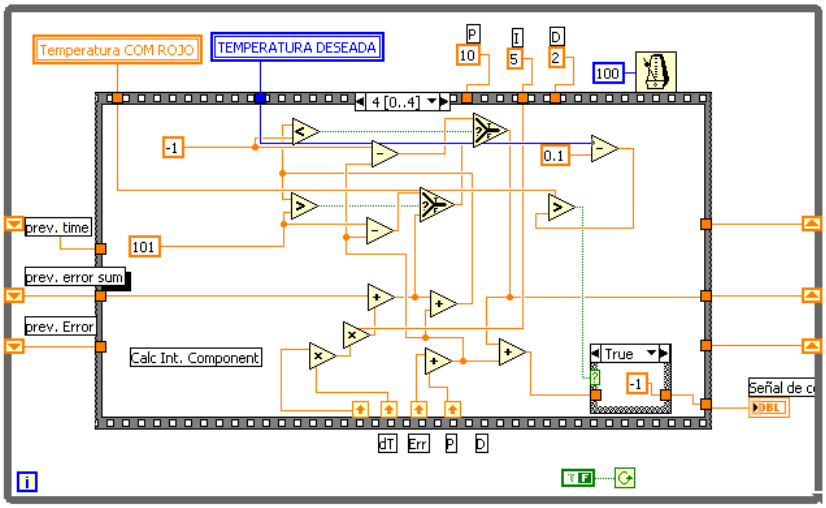

Figure 2.40 Section of the LabView program corresponding to the PID

Conductivity control set-up

The conductimeters were internally calibrated prior to their use in the plant. Once the internal calibration was successfully completed, calibration curves were obtained in order to relate the conductivity of each probe to the alcohol concentration.

With this aim, the conductivity of different water solutions of 5%, 10%, 15%, 20%, 25% and 30% by weight of methanol and ethanol were measured inside the tanks. The experiments were carried out in both tanks in order to correct possible drift effects of the conductimeters. The conductivity was measured while the temperature was varied in steps of 5ºC, from 35ºC to 70°C in order to consider the effect of the temperature on the conductivity.

The conductivity curves at different temperatures are shown in *Figure 2.41*.

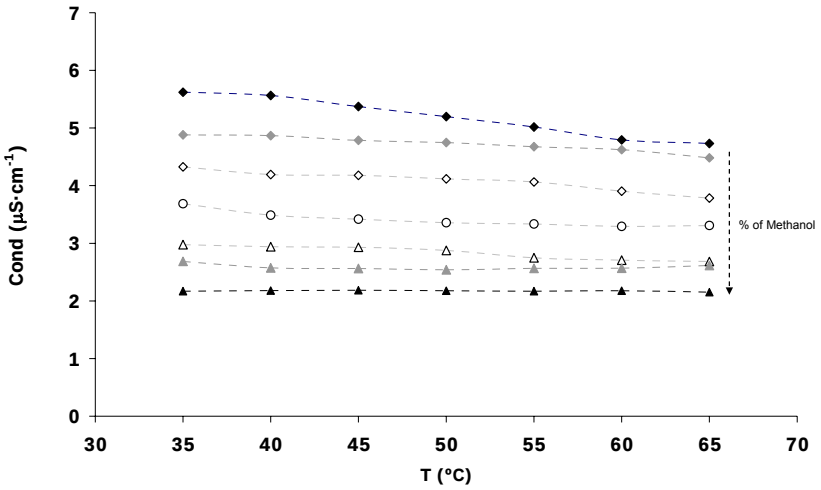

Figure 2.41 Conductivity curves and temperature at different methanol concentrations. ◆ water, ◆ 5% methanol, ◇ 10% methanol, ○ 15% methanol, △ 20% methanol, ▲ 25% methanol, ▲ 30% methanol.

The curves were then implemented in the *LabView* program for the direct conversion of the conductivity into alcohol concentration, and allowing for considering the temperature effect.

METHODS OF ANALYSIS

The previous techniques are used to characterise the physical-chemical and diffusion properties of the materials studied in this PhD thesis. Although the following chapters are focused on particular issues regarding the materials, there are common aspects which have necessitated the development of a standard methodology for data analysis. The method of analysis provides tools to analyse the possible interactions between the components in the materials, and their effect on morphology and other properties (see *Figure 2.42*).

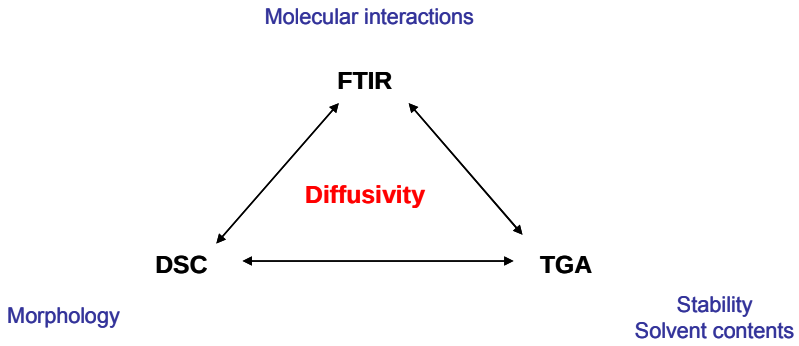

Figure 2.42 Techniques and their appliance to the studies

This PhD thesis is focused on the study of complex materials, containing different degrees of order. Polymeric Electrolyte Membranes (*PEM*) materials usually posses a phase separated structure arising from the inclusion of polar groups which enhance the proton conductivity. This makes the study of the interactions between the components a very important factor in understanding the observed morphology. As shown in *Figure* 2.42, the combination of the techniques used here provides complementary information about the different materials.

Specifically, in chapter 3 the techniques are focused on the study of interactions between solvents and the functional groups in Nafion, which is the reference polymer electrolyte in Fuel Cells. In chapters 4, 5 and 6, the techniques are applied to evaluate the preparation processes of membranes consisting of different materials prepared in this PhD thesis and their effects on the final structures. In each case the physical properties of interest are the same, it is possible therefore to establish a general

methodology. The scope of the next section is to describe this methodology which is then used in the following chapters.

8. Analysis of the FTIR experimental results

All the results of the different FTIR experiments were analysed following a similar methodology. The detail of the methodology depended on the regions of interest in the FTIR spectra. The general steps for the analysis of the results obtained in the FTIR experiments are described now, although some specific aspects of the procedures will be described where relevant in subsequent chapters.

The FTIR curves were obtained using 128 scans with an accuracy of 4 cm^{-1} in the 400-4000 cm^{-1} range. The use of higher accuracy (2 or 1 cm^{-1}) increased the noise in the spectra to unacceptable levels for a reliable study of some of the FTIR regions. For the ATR experiments, the *Automatic ATR correction* option was used. *Automatic baseline correction* was also applied to all the FTIR curves. All the spectra were obtained after subtracting a background curve to the single beam signal. The background was performed before each series of experiments to allow for variations in the water ($\nu \sim 3000\ cm^{-1}$ and $1630\ cm^{-1}$) and CO_2 ($\nu \sim 2300\ cm^{-1}$) absorption bands .The intensity of all the curves (*Y*-axis) were obtained in absorbance units (*Abs, %*) as a function of the frequency (*X*–axis) of the beam in wavenumber (ν, cm^{-1}). An example of FTIR curves obtained in this thesis is shown in *Figure 2.43*. When more than one FTIR curve is displayed, the curves are displaced along the *Y*-axis.

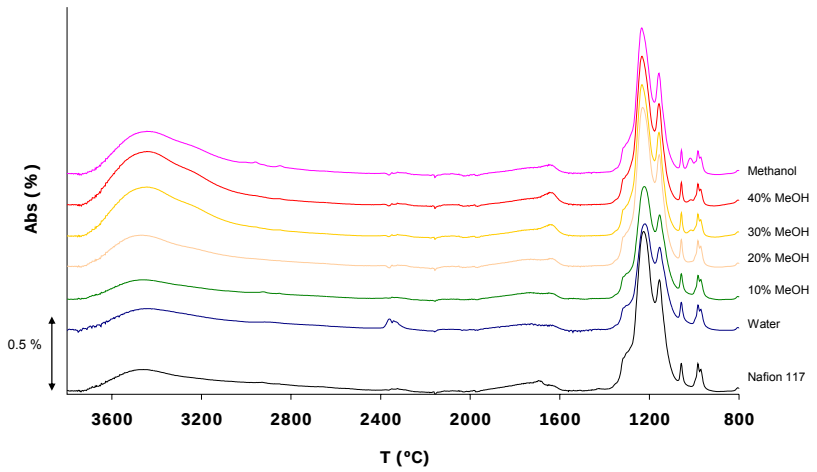

Figure 2.43 FTIR spectra corresponding to membranes submitted to a swelling test at 35ºC.

The maximum absorbance (Abs_{max}) and the associated frequency (ν_{max}) of the most characteristic absorption bands of the FTIR spectra were estimated using the *OMNIC* Software (*Find Peaks*) considering the baseline of the spectra in the 4000-400 cm^{-1} range. *Table 2.4* shows an example of the information obtained.

Table 2.4 Parameters of the most characteristic absorption bands in the FTIR spectra corresponding to the membranes submitted to the swelling test

	ν_{max} (cm^{-1})	Abs_{max} (%)	ν_{max} (cm^{-1})	Abs_{max} (%)	ν_{max} (cm^{-1})	Abs_{max} (%)
Nafion	3460	0.16	1225	1.05	1155	0.74
Water	3435	0.15	1220	0.70	1154	0.55
MeOH 10%	3466	0.14	1222	0.74	1154	0.56
MeOH 20%	3479	0.23	1229	1.05	1156	0.75
MeOH 30%	3445	0.34	1233	1.00	1157	0.70
MeOH 40%	3445	0.37	1233	0.99	1157	0.68
Methanol	3445	0.30	1234	0.97	1158	0.67

Further analysis of the curves was carried out using either the *OMNIC* Software or the *Origin* Lab software. In the latter case, the experimental data were exported using *CSV* format.

The FTIR regions of particular interest were analysed in further detail. In some cases, and with the aim to discriminate the presence of overlapping features, the FTIR curves were deconvoluted considering the different absorption bands. The individual peaks represented particular contributions and their study provided relevant information about the chemical environment of the groups in the samples. The deconvolution was performed using either the *Advanced Fit Tool* of the *Origin* Lab Software or the *Peak Resolve* option of the *OMNIC* Software.

When the *Origin* Lab Software was used, the curves were fitted to two main kinds of curves, or the combination of both:

Amplified Gaussian curves (*Equation 2.16*):

$$y = \sum_{i=1}^{n} A_i \cdot \exp(-0.5 \cdot \frac{(x - xc_i)^2}{w_i^2}) \qquad (2.16)$$

Asymmetric peak functions (*Equation 2.17*):

$$y = \sum_{i=1}^{n} A_3 \cdot (\frac{1}{1 + \exp(\frac{-(x - x_{c3} + 0.5)}{w_{23}})}) + (1 - \frac{1}{1 + \exp(\frac{-(x - x_{c3} - 0.5)}{w_{33}})}) \qquad (2.17)$$

Examples of Gaussian and Asymmetrical peaks used to fit experimental FTIR curves are shown in the following *Figures 2.44* and *2.45*.

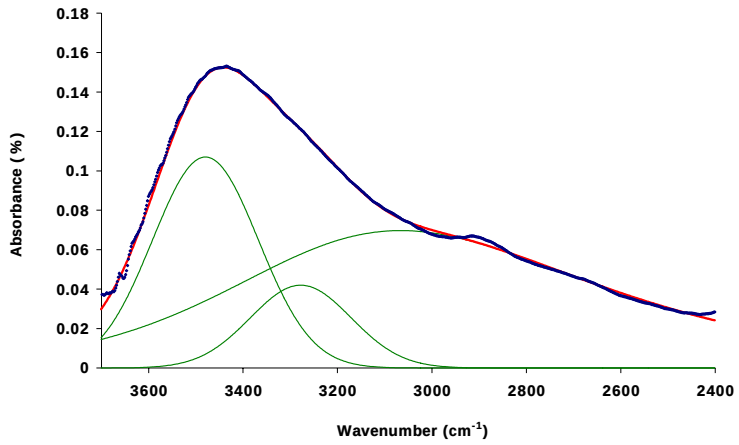

Figure 2.44 Experimental (blue points) and fitted curve (red line) in the O-H vibration region (3000 cm^{-1}). Sample submerged in water. Green lines indicate individual contributions of OH regions.

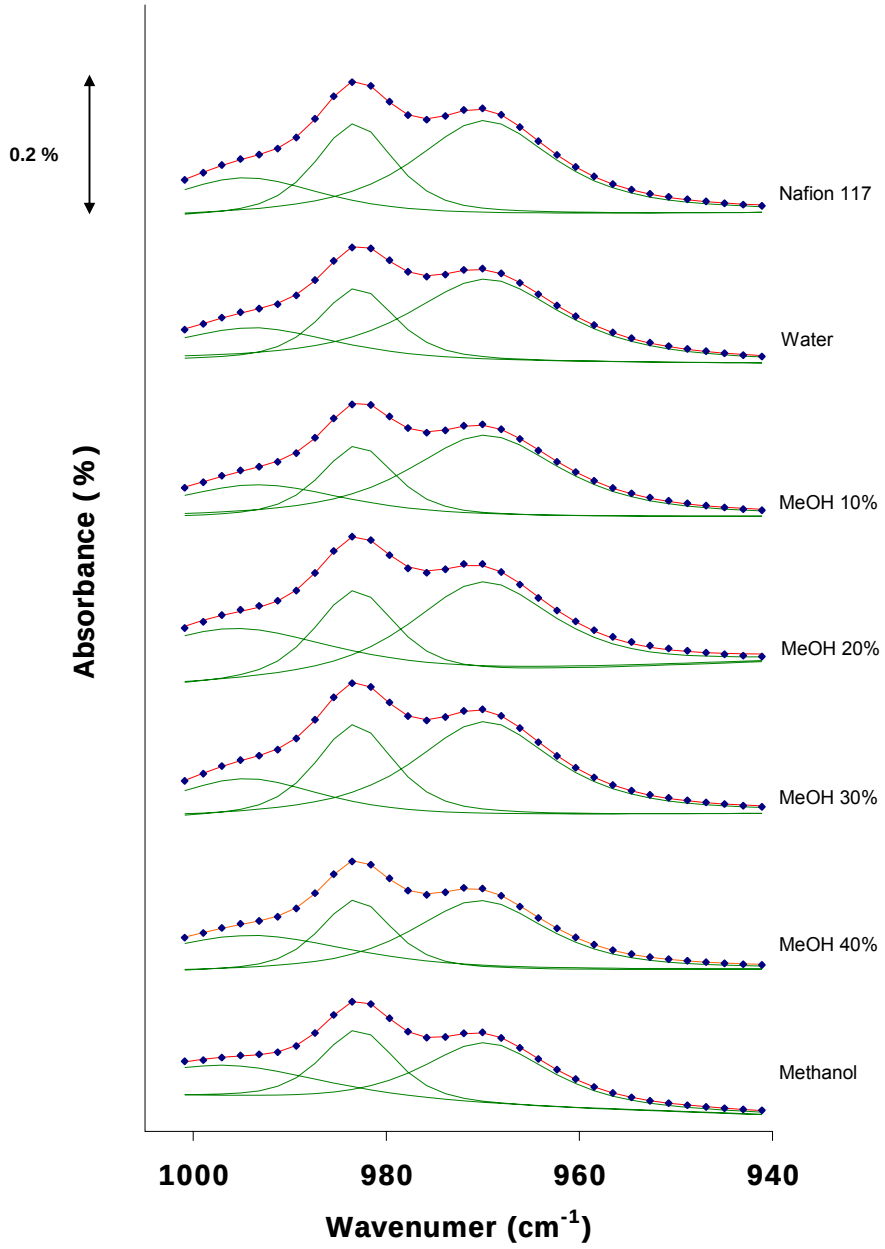

Figure 2.45. Ether vibrational region (C-O-C) in the Nafion samples immersed in methanol and water mixtures. Green curves indicate individual contributions of groups with different chemical environments.

When the *OMNIC* Software was used, then the curves were fitted to a sum of Gaussian peaks (*Equation* 2.18):

$$y = \sum_{i=1}^{n} A_i \cdot \exp(-0.5 \cdot \frac{(x - xc_i)^2}{w_i^2}) \qquad (2.18)$$

An example of deconvolution using the *OMNIC* Software is shown in *Figure 2.46.*

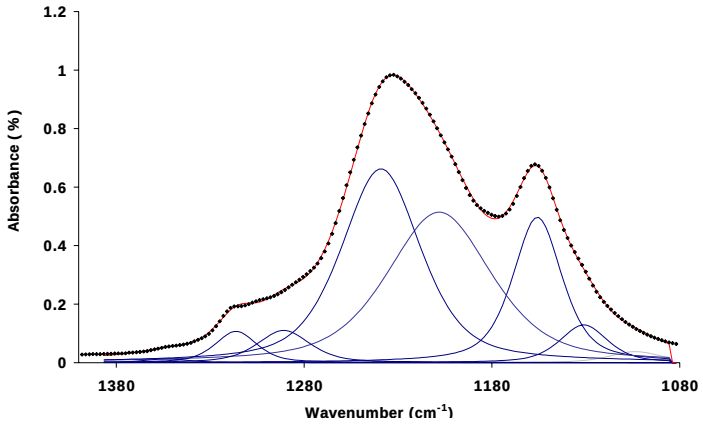

Figure 2.46 Deconvolution of the 1050 – 1400 cm^{-1}region. Membrane submitted to the swelling test in a binary mixture with 40% of methanol. Experimental (black points) and fitted curve (red line). Blue curves correspond to the contributions of the different functional groups.

In Equations *2.16* to *2.18*, *n* indicates the number of individual peaks used to fit the experimental FTIR curve. Only fits with high values of R^2 were accepted ($R^2 > 0.999$). The effect of the local baseline was subtracted before carrying out the deconvolution.

The individual peaks obtained by deconvolution were assigned to different contributions according to the literature. Examples of these assignments are shown in *Tables 2.5* and *2.6*.

Table 2.5 FTIR results. Assignments of the OH vibration bands

Region (cm^{-1})	Subregion (cm^{-1})	Assignment	References
3800 – 2400 OH Stretching	3800 – 3600	• OH groups forming weak H-bonds between the solvent molecules and the hydrophobic regions through the hydrophobic-hydrophilic interface	[15, 16]
	3600 – 3400	• OH groups of solvent molecules forming strong H-bonds with the polar groups of the polymer	[15, 16]
		• OH groups of solvent molecules forming ether complexes	[17, 18] [19, 20]
	3400 – 3000	• Bulk-like water and methanol molecules	[21]
		• Solvation and external OH groups in the solvent clusters	
	3000 –	• H_3O^+, $H_2O_5^+$, $CH_3OH_2^+$ grouping species forming clusters in the membranes by dissociation of SO_2OH*	[17, 18, 21]
		• Internal OH groups in the solvent clusters	
2000 – 1400 OH bending	~ 1688	• Structural vibrations	
	~ 1630	• External OH in solvent clusters	[22, 21]

Table 2.6 FTIR results. Assignments of the vibration bands of the polymer groups

Assignment	Wavenumber (cm^{-1})
$\nu_{as}(CF_2)$	1240
	1153
ν_{as}(C-C)	1317
	1294
$\nu_{as}(SO_3^-)$	1130
ν_s (SO_3^-)	1057
ν_s (COC)	940 – 1010
δ (CF_2)	525
t (CF_2)	558
ω (CF_2)	636
$\nu_s(CF_2)$	718
ν (C-S)	805

The individual peaks obtained by deconvolution were analysed separately. The area (%·cm^{-1}), maximum intensity (Abs_{max},, %), wavenumber for Abs_{max} (ν_{max},, cm^{-1}) and width at half the maximum intensity (*FWHH,* cm^{-1}) of the peaks were obtained by using the integration tool in the *Origin* Lab *Software*. The results were displayed in tables and/or figures to highlight possible effects in the individual processes, as shown in *Table 2.7* and *Figure 2.47*.

Table 2.7 Results of the deconvolution of the O-H vibration region (3000 cm^{-1}). Peak at high wavenumbers (peak #1)

	Area (%· cm^{-1})	ν_{max} (cm^{-1})	Width (cm^{-1})	Abs_{max} (%)
Nafion	24	3502	241	0.09
Water	30	3479	264	0.11
MeOH 10	29	3500	278	0.10
MeOH 20	45	3508	262	0.17
MeOH 30	60	3504	253	0.23
MeOH 40	66	3502	255	0.25
MeOH 100	50	3496	251	0.19

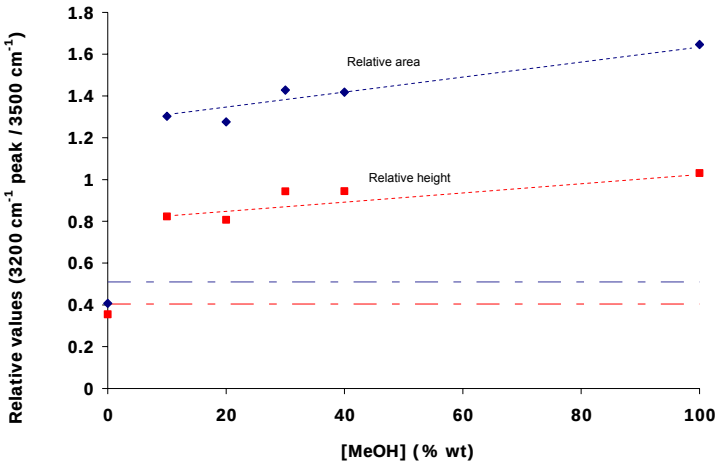

Figure 2.47 FTIR results corresponding to the Nafion membranes. Deconvolution of the 3000 cm^{-1} region. Relative area and height of the peak at low wavenumbers respect to the peak at high wavenumbers.

The analysis of the individual peaks and the comparison with the rest of the bands provided valuable information about the chemical environment of the molecular groups, such as the interactions involving the solvent molecules (OH stretching band) and those of the different polymer groups with the solvents, as seen in *Figure 2.48*.

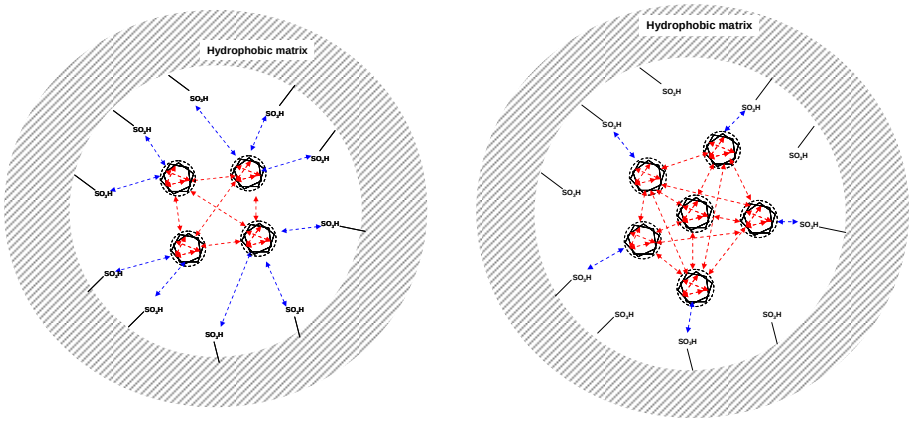

a) Interactions at low methanol concentration solutions

b) Interactions at high methanol concentration solutions

Figure 2.48. Diagram of water and methanol clusters. Interactions within the clusters (red arrows) and between the clusters and the Nafion structure (blue arrows)

9. Analysis of the TGA experimental results

All the Thermogravimetric curves (TG curves) were obtained in heating scans from 25ºC to 750ºC at a heating rate of 10ºC/min under an inert atmosphere, of 80 ml/min flux of argon (Ar). A blank was used preceding each series of experiments. The results of percentage of mass loss as a function of temperature were obtained. Typical TG curves obtained in this PhD thesis are shown in *Figure 2.49*.

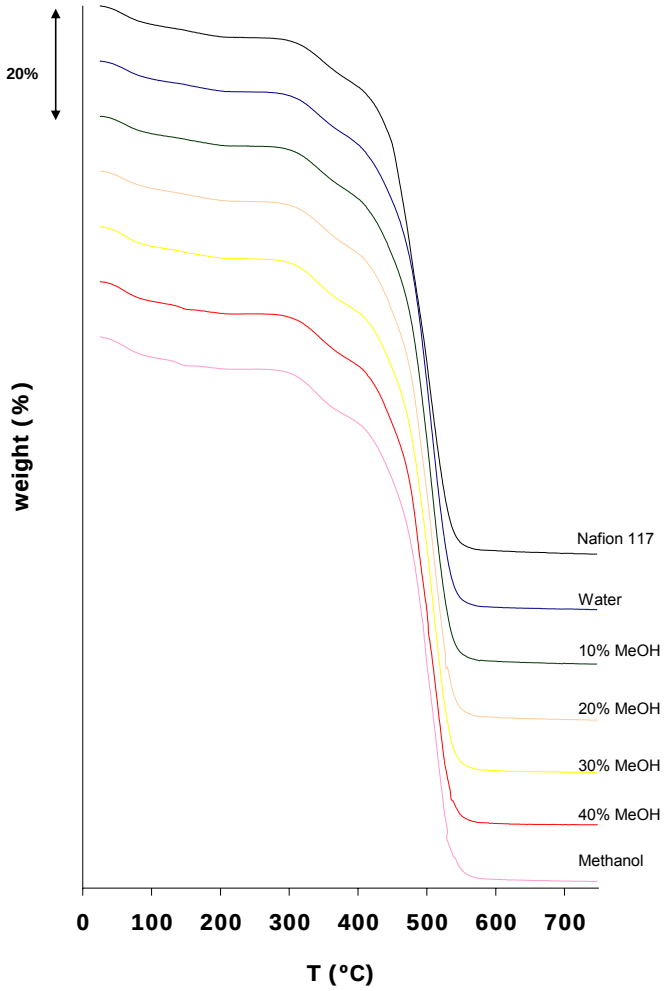

Figure 2.49 Thermogravimetric (TG) curves of the Nafion membranes submerged in water and methanol binary mixtures at 35ºC

When more than one curve was displayed, the curves were displaced arbitrarily along the *Y*-axis and non-absolute scales were used.

In order to better distinguish the different degradation processes, the Derivative Thermogravimetric (DTG) curves were obtained by the derivation of the corresponding TG curves, using the *STAR* Software. *Figure 2.50* shows a set of DTG curves.

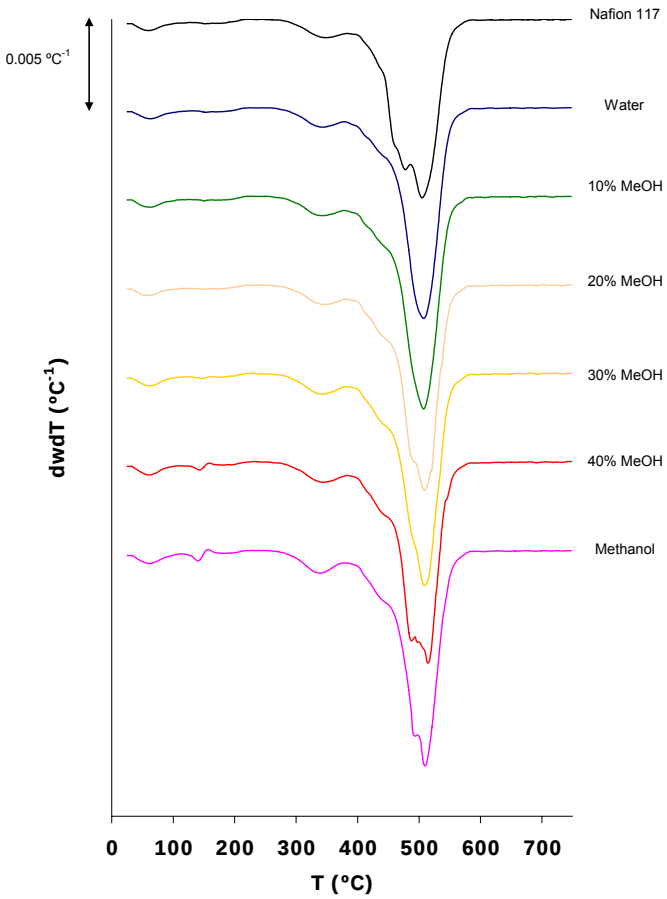

Figure 2.50 DTG curves of the Nafion membranes submerged in water and methanol binary mixtures at 35ºC

Relevant information about the different stages of mass loss observed in the DTG curves was obtained using the *STAR* Evaluation Software, including:

- The onset temperature (T_{onset}). This parameter indicates when a degradation step starts and is considered as a descriptor of the thermal stability.
- The temperature of the maximum decomposition rate (T_{max}). This corresponds to the inflexion point of the TG curve. If the peak is symmetric, it will also be the mid point of the degradation step.

- The endset temperature (T_{endset}). The temperature at which the process is considered finished.
- The mass loss (Δw). The amount of sample (or percentage) that is degraded in the step.
- The residual percentage. The fraction of sample mass which remains in the pan after the experiment finishes.

For further analysis and presentation, the TG and DTG curves were exported to a text file (*.txt)* using 1000 points. In composite materials, it is common practice to compare the experimental DTG curves (DTG_{exp}) with the ideal DTG curve (DTG_{id}) which is the weight averaged sum of the curves corresponding to the pure components:

$$DTG_{id} = \%_{\ compoundA} \cdot DTG_{\ compoundA} + \%_{compoundB} \cdot DTG_{compoundB}$$

The differences between DTG_{exp} and DTG_{id} can imply the existence of interactions between the groups of the components affecting their thermal degradation. An example of such a comparison of experimental and ideal DTG curves is shown in *Figure 2.51*.

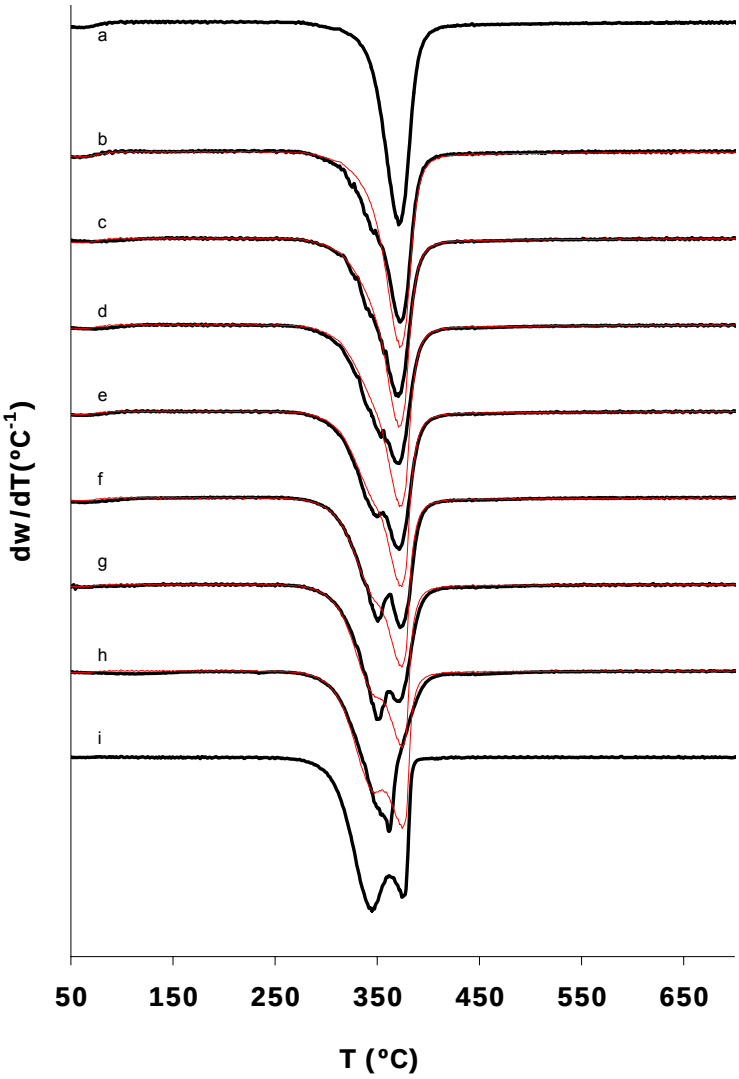

Figure 2.51 DTG curves of the membranes containing CA and COC: (a) 0%, (b) 10%, (c) 20%, (d) 30%, (e) 40%, (f) 50%, (g) 60%, (h) 70% and (i) 100% COC. Red lines indicate ideal curves

In the temperature regions of interest, when more than one process was observed, the DTG curve was fitted to a sum of contributions, using the *Advanced Fitting Tool* of the *Origin* Lab Software (as for the FTIR results). The experimental DTG curves were converted into positive values, and the results were fitted to the following expression (*Equation 2.19*):

$$y = \sum_{i=1}^{n} A_i \cdot \left[\left(\frac{1}{1 + \exp\left(\frac{-(x - x_{ci} + 0.5)}{w_{2i}} \right)} \right) + \left(1 - \frac{1}{1 + \exp\left(\frac{-(x - x_{ci} - 0.5)}{w_{3i}} \right)} \right) \right] \qquad (2.19)$$

where n indicates the number of individual peaks used to fit the experimental DTG curve. Only fits with high values of R^2 were accepted ($R^2 > 0.999$). The effect of the local baseline was subtracted before carrying out the deconvolution. Examples of the deconvolutions are shown in *Figures 2.52* and *2.53*.

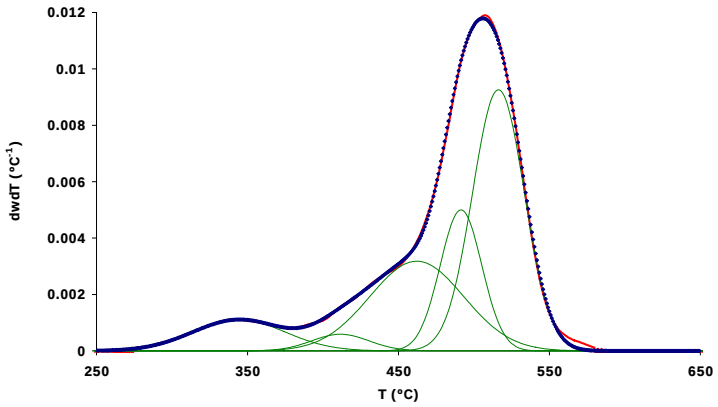

Figure 2.52 Deconvolution of the DTG curve (membrane absorbed in water). Blue points correspond to the experimental values and the red line to the fitted curve. Green lines indicate individual contributions to the thermal degradation.

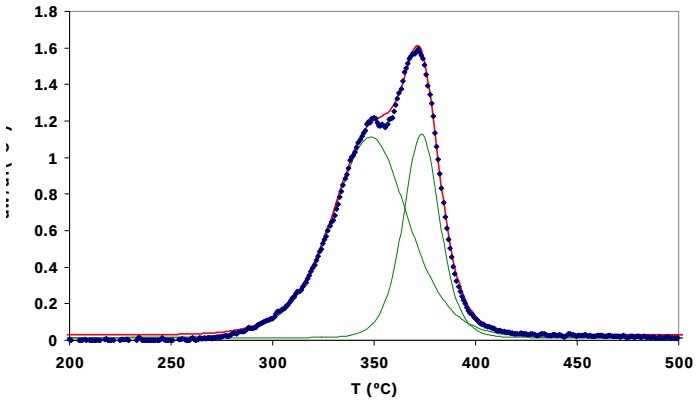

Figure 2.53 Deconvolution of the DTG curve of the membrane containing CA and COC (40% wt of COC). Blue points correspond to the experimental values and the red line to the fitted curve. Green lines indicate individual contributions to the thermal degradation.

The individual peaks obtained by deconvolution were analysed separately. The area (%), maximum degradation rate (dw/dT_{max},, %·ºC^{-1}), temperature for dw/dT_{max} (T_{max},,

ºC) and width at half the maximum intensity (*FFHW*, %) of the peaks were obtained by using the integration tool in the Origin Lab Software. The results were displayed in tables and/or figures in order to highlight possible effects in the individual processes, as shown in *Table 2.8*.

Table 2.8 Deconvolution of the DTG curves.
Individual peaks. Desulfonation process

Sample	Area (%)	T_{max} (ºC)	Width (ºC)	dw/dT_{max} 10^3 (%·ºC^{-1})
Nafion	8.19	348	75	1.03
Water	8.48	344	72	1.11
10% MeOH	8.25	343	71	1.09
20% MeOH	8.70	346	74	1.12
30% MeOH	8.99	344	73	1.16
40% MeOH	7.60	341	65	1.10
Methanol	8.01	340	62	1.22

The representation of the individual peaks gave relevant information about the decomposition process by turning complex and overlapped degradation stages into individual contributions (see *Figures 2.54* and *2.55*).

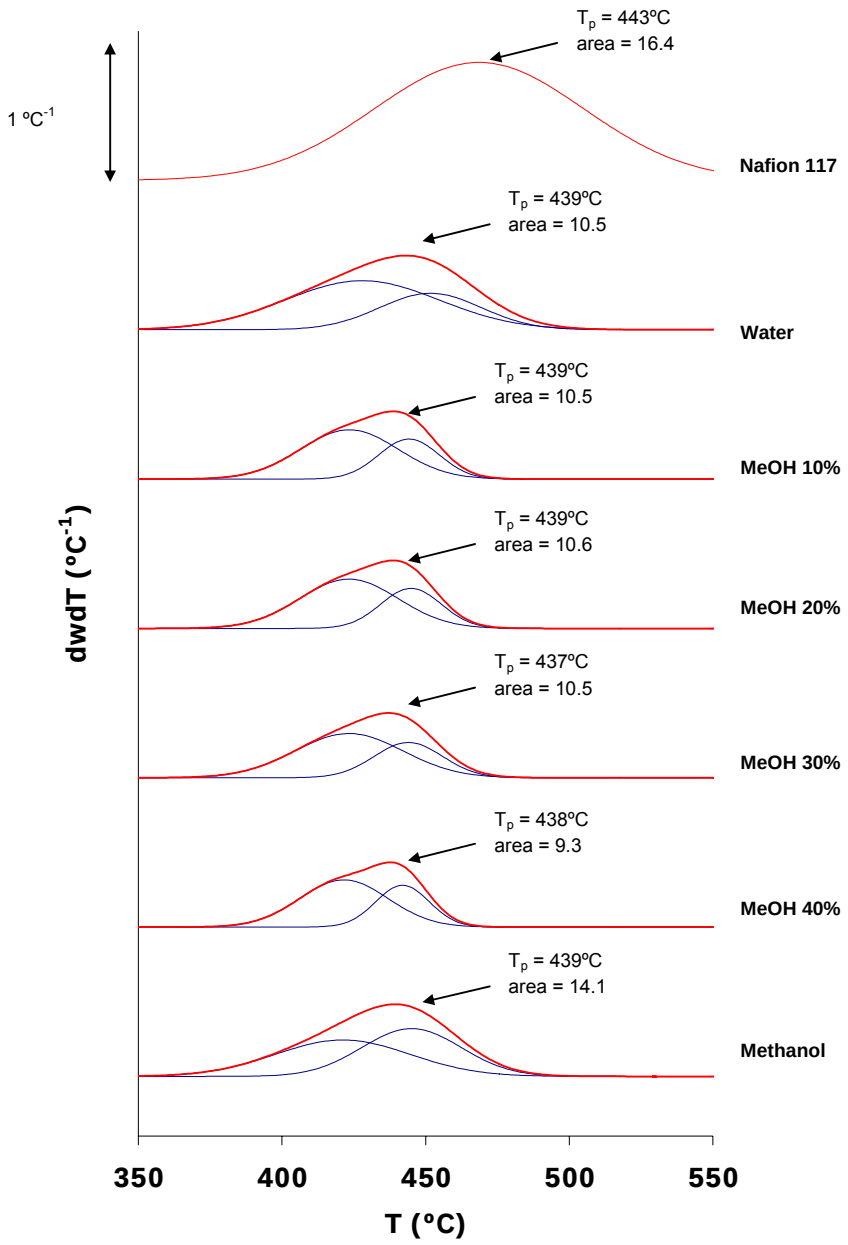

Figure 2.54 Fitted curve (red line) and individual contributions (blue dotted lines) in the region of decomposition of side-chains of the Nafion membranes

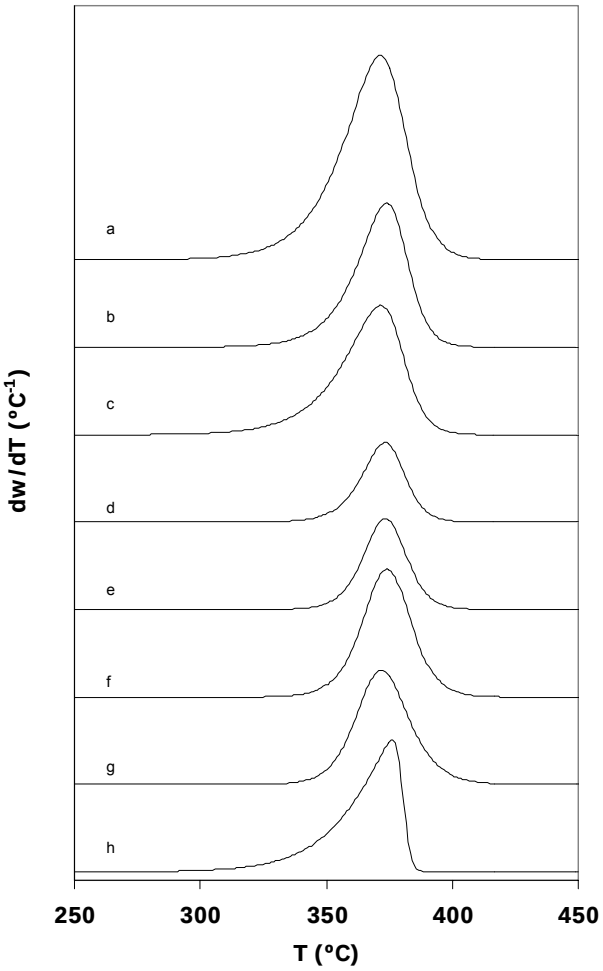

Figure 2.55 Individual curves corresponding to the deconvolution of the DTG curves of the films containing CA and COC: (a) 0%, (b) 10%, (c) 20%, (d) 30%, (e) 40%, (f) 50%, (g) 60%, (h) 100.

Kinetic Analysis of the thermal decomposition process

The mechanisms of degradation of the individual decomposition processes can be studied by kinetic analysis [23]. The decomposition process of a solid material can be expressed as follows:

$$A_{solid} \rightarrow B_{solid} + C_{gas}$$

It is possible to study the kinetics of decomposition considering two main contributions: the reaction rate depending on the concentration of reactants and the dependence of the rate constants with the temperature. Therefore, the rate law expression must describe the

chemical changes in a system through an equation which depends on the concentration and the temperature. All the reactions are considered irreversible. The general form of a rate law expression is:

$$\frac{d\alpha}{dt} = f(\alpha)\cdot k(T) \qquad (2.20)$$

The dependence of the conversion rate with the reaction time is expressed by two separate contributions. The first term expresses the dependence with the concentration of reactants in terms of the conversion degree (α). The second term involves the dependence on the absolute temperature (T).

The conversion degree or reacted fraction (α) is defined as the mass fraction that a sample has lost after a time t, respect to the overall mass lost at the end of the experiment (*Equation 2.21*):

$$\alpha = \frac{w_0 - w}{w_0 - w_\infty} \qquad (2.21)$$

On the other hand, the temperature dependence of $k(T)$ can be expressed in terms of an Arrhenius model:

$$k(T) = k_0 \cdot \exp(\frac{-E_a}{R\cdot T}) \qquad (2.22)$$

where k_0 is the pre-exponential parameter, E_a is the activation energy, R is the gas constant and T the absolute temperature.

Considering *Equations 2.20* and *2.21*, the rate expression may be expressed by *Equation 2.23*:

$$\frac{d\alpha}{dt} = f(\alpha)\cdot k_0 \cdot \exp(\frac{-E_a}{R\cdot T}) \qquad (2.23)$$

Modeling the rate law expression. Analysis methods

When the decomposition of the material is controlled by the chemical reaction, the kinetic equation has the following expression (*Equation 2.24*):

$$f(\alpha) = (1-\alpha)^n \qquad (2.24)$$

where *n* is the reaction order.

Applying (*2.24*) to the rate law expression, gives *Equation 2.25*:

$$\frac{d\alpha}{dt} = (1-\alpha)^n \cdot k_0 \cdot \exp(\frac{-E_a}{R \cdot T}) \qquad (2.25)$$

Although *Equation 2.25* has been successfully used to describe the decomposition of many polymeric systems, for some complex systems it is necessary to consider other kinetic models. This is the case of mixtures or blends where the interactions between the components can change the expected decomposition process.

In *Table 2.9* some of the most common models applied to the decomposition of polymers are listed. *Table 2.9* also shows the corresponding values of $g(\alpha) = \int_0^\alpha \frac{d\alpha}{f(\alpha)}$, which is an important function for the integration of *Equation 2.25*.

Table 2.9 Most common models used in the description of the thermal degradation of polymers

Model	f(α)	g(α)
Chemical reaction control		
n=0	1	α
n=0.75	$(1-\alpha)^{0.75}$	$(1/0.25)\cdot(1-(1-\alpha)^{0.25})$
n=1	$(1-\alpha)$	$-\ln(1-\alpha)$
n=1.5	$(1-\alpha)^{1.5}$	$2(-1+(1-\alpha)^{-1/2})$
n=2	$(1-\alpha)^{2}$	$-1+(1-\alpha)^{-1}$
n=3	$(1-\alpha)^{3}$	$½(-1+(1-\alpha)^{-2})$
Diffusion control		
D1	$½(1-\alpha)-1$	α^{2}
D2	$-\ln(1-\alpha)$	$(1-\alpha)\ln(1-\alpha)+\alpha$
D3J	$3/2(1-\alpha)^{2/3}(1-(1-\alpha)^{1/3})^{-1}$	$(1-(1-\alpha)^{1/3})^{2}$
D4=D36	$3/2(1-\alpha)^{1/3}(1-(1-\alpha)^{1/3})^{-1}$	$(1-2/3\ \alpha)(1-\alpha)^{2/3}$
Nucleation models		
n=1.5 ; m=0.5	$\alpha^{0.5}(1-\alpha)^{1.5}$	$((1-\alpha)/\alpha)^{-0.5}(0.5^{-1})$
n=1.9 ; m=0.5	$\alpha^{0.1}(1-\alpha)^{1.9}$	$((1-\alpha)/\alpha)^{-0.9}(0.9^{-1})$
Other		
R2	$2(1-\alpha)^{1/2}$	$1-(1-\alpha)^{1/2}$
R3	$3(1-\alpha)^{2/3}$	$1-(1-\alpha)^{1/3}$
A2	$2(1-\alpha)(-\ln(1-\alpha))^{1/2}$	$(-\ln(1-\alpha))^{1/2}$
A3	$3(1-\alpha)(-\ln(1-a))^{2/3}$	$(-\ln(1-\alpha))^{1/3}$
F1	$1-\alpha$	$-\ln(1-\alpha)$
Power 2	$2\ \alpha^{1/2}$	$\alpha^{½}$

By fitting the experimental TGA data to the previous expressions it is possible to calculate the kinetic parameters related to the degradation of a sample. Since *Equation 2.25* cannot be directly integrated, it is necessary to use numerical approximations. The resulting models allow the parameters that describe the thermal degradation of the material to be estimated.

The mathematical methods can be classified according to different criteria:

- The model used. One important group of methods is the so-called *Free Model Kinetic Methods* (*FMKM*). Such methods do not assume any model for the calculation of the kinetic parameters. In contrast, some other methods need the assumption of a model to fit the data to the corresponding expression.

- Number of heating rates. Some models require information of experiments performed at different heating rates (β) to calculate the kinetic parameters. Some others obtain the information only from one single experiment.

- Whether the rate expression is integrated or derived. Leading to integral or derivative methods.

The methods and expressions used in this thesis are listed in displayed in *Table 2.10*.

Table 2.10 Methods used for the kinetic analysis

Method	Expression	Parameters
Criado [24] *	$\frac{z(\alpha)}{z(0.5)} = \frac{f(\alpha)g(\alpha)}{f(0.5)g(0.5)}$ Master curves (Theoretical) $\frac{z(\alpha)}{z(0.5)} = \left(\frac{T_\alpha}{T_{0.5}}\right)^2 \cdot \frac{(d\alpha/dt)_\alpha}{(d\alpha/dt)_{0.5}}$ Master curves (Experimental)	$f(\alpha)$
Coats-Redfern [25]	$\int_0^\alpha \frac{d\alpha}{f(\alpha)} = \ln\left[\frac{g(\alpha)-g(0)}{T^2}\right] = \ln\left(\frac{k_0 \cdot R}{b \cdot E_{CR}}\right) - \frac{E_{CR}}{R \cdot T}$	E_{CR}
Chang [25]	$\ln\left[\frac{d\alpha/dt}{(1-\alpha)^n}\right] = \ln Z - \frac{E_{Ch}}{R \cdot T}$	n, E_{Ch}
Kissinger [26]	$S = \frac{\left[d^2\alpha/dt^2\right]_l}{\left[d^2\alpha/dt^2\right]_r}$ $n_K = 1.88 \times S$	n_K

* $g(\alpha) = \int_0^\alpha \frac{1}{f(\alpha)} d\alpha$

α is the degree of conversion of the individual process.

The graphical representations of some of the methods shown in *Table 2.10* are shown in *Figure 2.56.*

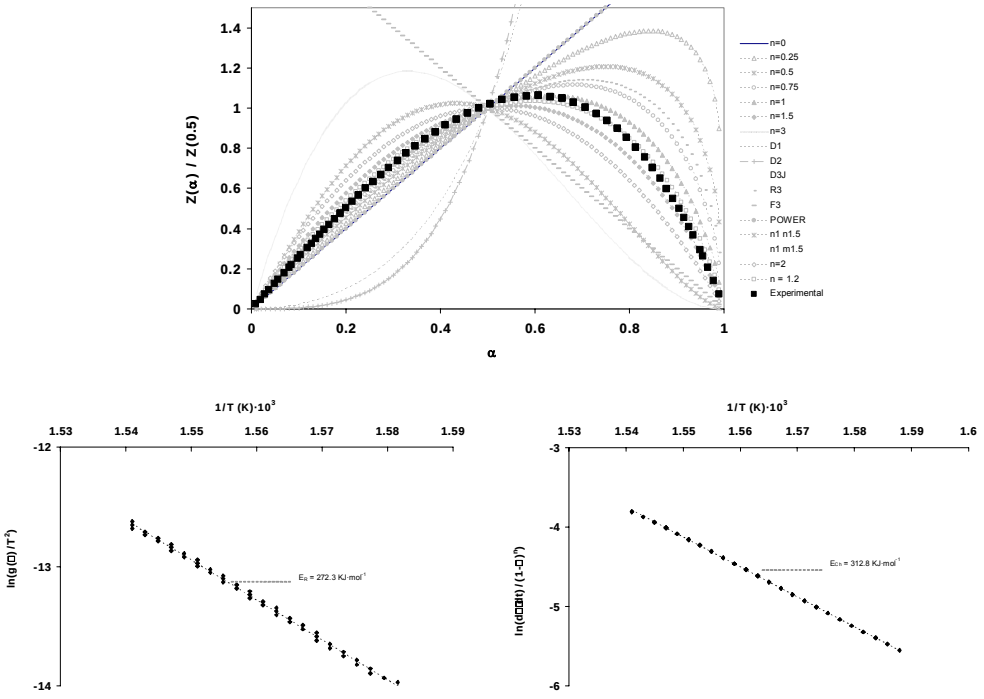

Figure 2.56 Results of the kinetic analysis applied to the DTG curve of cellulose acetate (CA): (a) Criado method, (b) Coat-Redfern method, (c) Chang method

10. Analysis of the DSC experimental results

The DSC curves (DSC thermograms) were obtained in heating and cooling scans at 10ºC/min in an inert atmosphere, using 80 ml/min flux of Nitrogen (N_2). The temperature intervals varied depending on the samples. The exact conditions of the experiments are explained in the corresponding chapters. A blank run was acquired performed preceding the each series of experiments. The normalised heat flow (per gram of sample, W/g) was obtained as a function of the temperature of the sample and the time of experiment.

The analysis of the DSC curves was carried out using the STAR Evaluation Software, including the study of solvent loss, first-order transitions (such as phase transitions) and pseudo-first order transitions (such as the glass transition).

The first heating scan has been used to remove the thermal history of the material and to study the loss of solvents from the samples. Some examples of series of DSC curves in the first heating scan are shown in *Figures 2.57* and *2.58*.

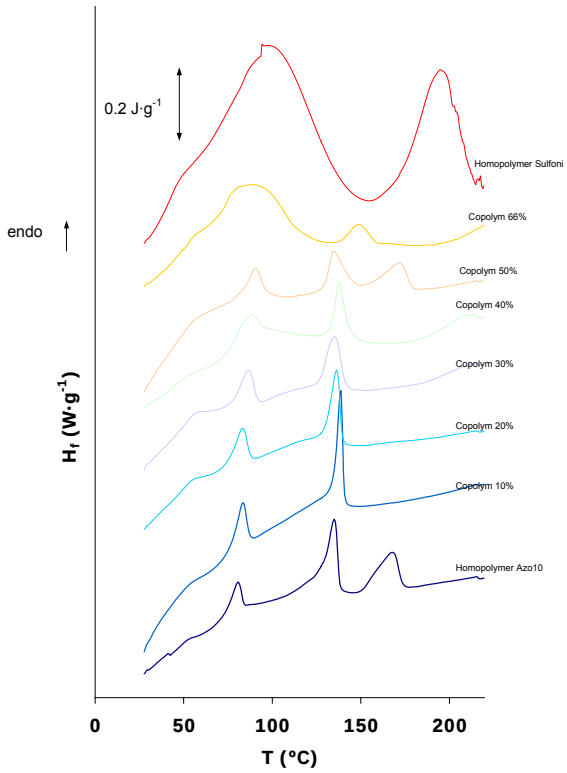

Figure 2.57 First heating scans of the Azo10-copolymers

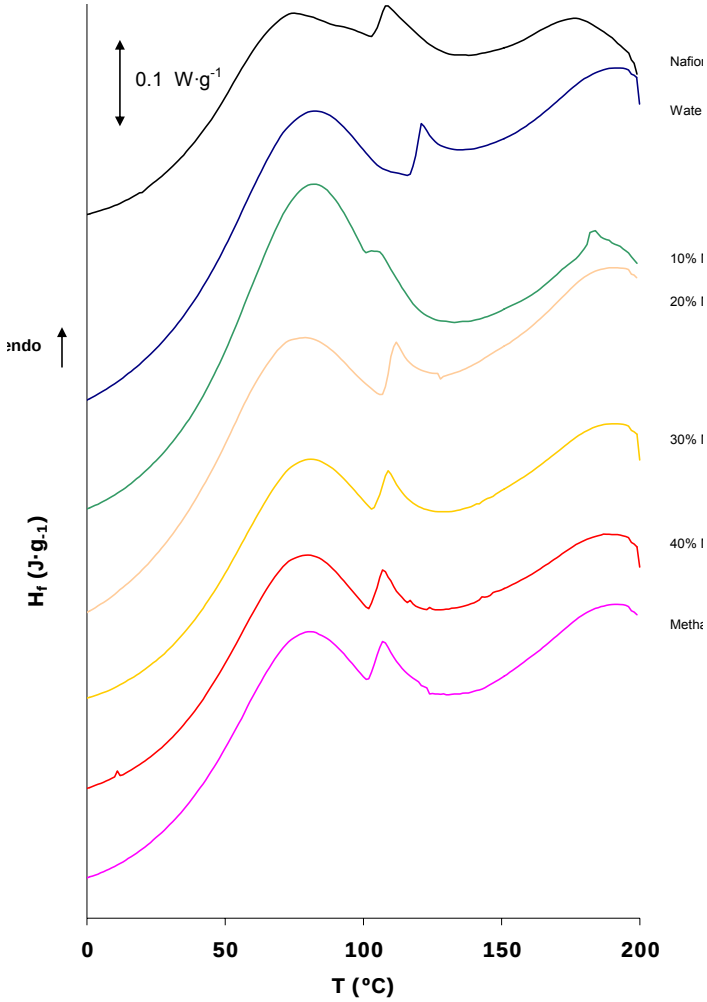

Figure 2.58 First heating scan corresponding to the Nafion membranes inmersed in the water and methanol binary mixtures

In the second heating scan the thermal history and the loss of solvents are not present, which facilitates the study of other thermal processes which could be obscured or overlapped with those effects. An example of a series of DSC curves in a second heating scan is shown in *Figure 2.59*.

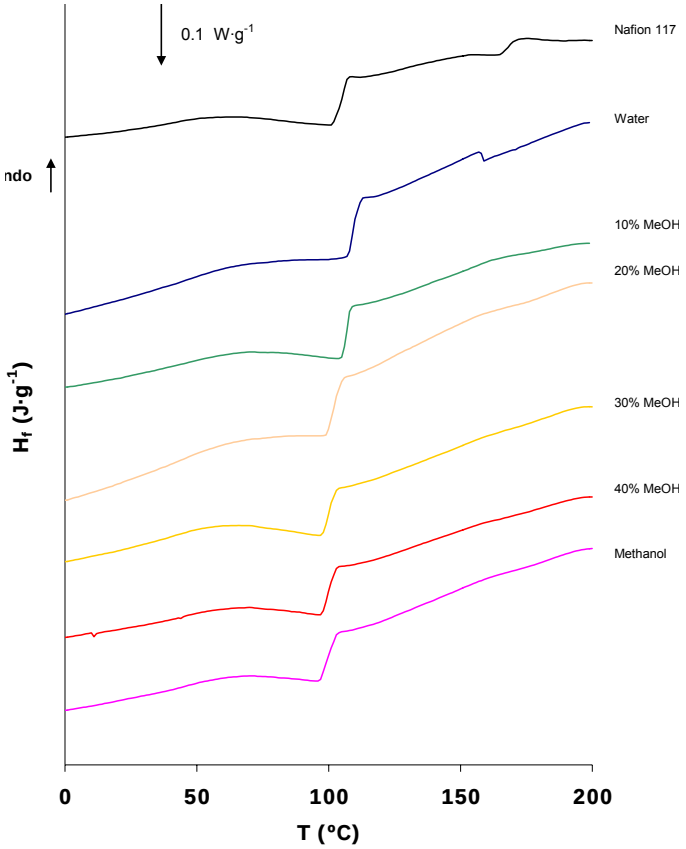

Figure 2.59 Second heating scan corresponding to the Nafion membranes submerged in water and methanol binary mixtures (first heating scan shown in Figure 2.58)

The enthalpy involved in first order transitions or a solvent desorption process was calculated from the area existing between the DSC curve and a baseline. The baseline was calculated for the temperature range where the transition was studied. The enthalpy calculations were carried out using the *STAR* Software in the *Evaluation* option. The type of baseline can be fitted to the shape of the curve, but only linear and spline baselines were used.

The glass transitions were calculated using the *STAR* Software in the *Evaluation* option for the second heating scans or the cooling scans of the DSC curves. The inflexion point and the onset of the transition were considered as representative values of T_g. The values of the change in the heat capacity (ΔC_p) were also calculated. An example of the

calculation of the T_g in DSC calorimetries and the results are shown in *Figure 2.60* and *Table 2.11*.

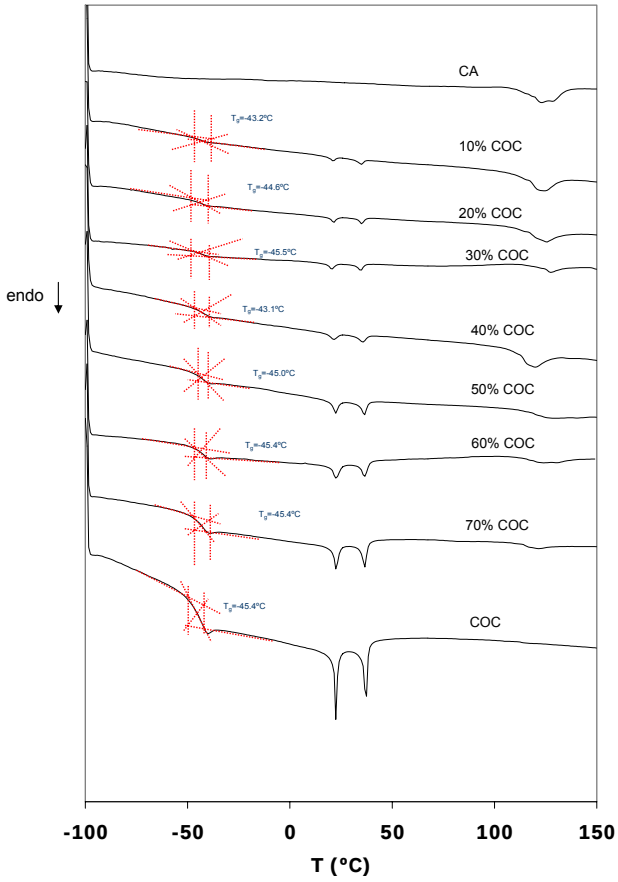

Figure 2.60. Calculation of T_g for the second heating scan corresponding to the films containing CA and COC (chapter 5)

Table 2.11 Calorimetric results corresponding to the second heating scan of Nafion samples submerged in water and methanol mixtures at 35ºC

Sample	T_{peak} (ºC)	ΔH_3 (J·g^{-1})	Δc_p (J·K^{-1}·g^{-1}) ·10^3
Nafion	105	-9.67	0.045
Water	109	-43.18	0.337
10% MeOH	107	-13.18	0.334
20% MeOH	102	-9.19	0.030
30% MeOH	100	-8.30	0.114
40% MeOH	100	-9.67	0.009
Methanol	98	-8.19	0.123

REFERENCES CHAPTER 2

1. Griffiths,P.R.; de Haseth,J.A. *Fourier Transform Infrared Spectrometry*, Wiley-Interscience, (2007)

2. Garton, A. *Infrared Spectroscopy of polymer blends, composites and surfaces*, Munich; New York : Hanser Publishers, New York :Distributed in the U.S.A. and Canada by Oxford University Press (1992)

3. Urban, W., *Attenuated Total Reflectance Spectroscopy of Polymers, theory and Practice*, 1996, American Chemical Society, Washington, DC

4. Turi, E. *Thermal characterization of polymeric materials*, Academic Press: New York, 1997

5. Mathot, V.B.F. *Calorimetry and Thermal Analysis of Polymers,* Hanser, New York, 1994

6. Groenewoud, W.M. *Characterisation of Polymers by Thermal Analysis*, Elsevier Science B.V., Amsterdam (2001)

7. Collings, P.J.; Hird, M. *Introduction to liquid crystals. Chemistry and physics*, Ed. Taylor & Francis: New York (1997)

8. Elmér, A.M.; Jannasch, P.; Mauritz, A.K.; Moore, R. B. Chem. Rev. 104 (2004) 4535

9. DeLuca, N.W.; A. Elabd, Y.A. J. Polym. Sci. Part B: Polym. Phys. 44 (2006) 2201

10. Vieth, W. *Diffusion in and through polymers, principles and applications*, Hanser Publishers, New York (1991)

11. Neogi, P. *Diffusion in Polymers* Marcel Dekker, Inc, New York, (1996)

12. Langer, R S.; Wise, D.L. *Medical Applications of Controlled Release*", Boca Raton: CRC Press (1984)

13. Kost, J. *Pulsed and Self-Regulated Drug Delivery*, Boca Raton: CRC Press, (1990)

14. Tarcha, P.J. *Polymers for Controlled Drug Delivery*, Boca Raton: CRC Press (1990)

15. Falk, M. Can. J. Chem. 58 (1980) 1495

16. Quezado, S.; Kwak, J.C.T.; Malk, M. Can. J. Chem. 62 (1984) 958

17. Ostrowska, J.; Narebska, A. Colloid Polym. Sci. 261 (1983) 93

18. Buzzoni, R.; Bordiga, S.; Ricchiardi, G.; Spoto, G.; Zecchina, A. J. Phys. Chem. 99 (1995) 11937

19. Zundel, G. *Easily Polarizable Hydrogen Bonds-Their Interaction with the Environment-IR Continuum and Anomalous Large Proton Conductivity*, *Hydrogen Bond-Recent Developments in Theory and Experiments*, Vol II, pp683 ff. Schuster, P.; Zundel, G.; Sandorfy, C. Eds., North Holland Publ. Co., Amsterdam (1976)

20. Mohr, S.C.; Wilk, W.D. Gordon; Barrow, M. J. Am. Chem. Soc. 87 (1965) 3048

21. Zundel, G. *The Hydrogen Bond*; Schuster, P.; Zundel, G.; Sandorfy, C. Eds.; Amsterdam, (1979)

22. Hallinan, D.T.; Elabd, Y.A. J. Phys. Chem. B. 111 (2007) 13221

23. Brown, M.E.; Gallagher, P.K. *Recent advances, Techniques and applications, Handbook of Thermal Analysis And Calorimetry: Recent Advances, Techniques And Applications* Vol. 5 (2008)

24. Criado, J.M.; Thermochim. Acta 24 (1978) 186

25. Chang, W.L. J Appl. Polym. Sci. 53 (1994) 1759

26. Huang, M.R.; Li, X.G. J. Appl. Polym. Sci., 68 (1998) 293

3

Spectroscopic and thermal characterisation of the absorbance of water and methanol mixtures in Nafion membranes

1 SUMMARY

Nafion is the benchmark material used in low temperature fuel cells. Its structure, which is described in chapter 1, consists of a perfluorinated backbone with side chains containing pendant sulfonic acid groups. The C-F bonds give Nafion its high chemical and mechanical integrity while the sulfonic acid groups promote high proton conductivity.

The proton conductivity of Nafion has been linked to the presence of water in the polymer. When water is absorbed in Nafion the sulfonate groups tend to reorganize to form ionic clusters. As the amount of water increases the ionic domains tend to become more interconnected at a disconnected-connected transition or percolation thereshold [1-3]. The sulfonic acid groups dissociate and the proton is transferred to water molecules to form hydroxonium ions (H_3O^+). Protons can flow easily through the ionic dispersed phase and the proton conductivity is greatly increased, while the hydrophobic backbone gives the polymer mechanical strength. This phase-separation morphology gives Nafion its unique properties. Although more detailed models of its morphology have been proposed by different authors, for example Gierke [4], Fujiyama [1, 5], Dreyfus [6] Lift [2], Houbold [7] or Rubalat [8] all of them emphasize the importance of the ionic cluster structure and the interconnection of the ionic domains (*Figure 3.1*).

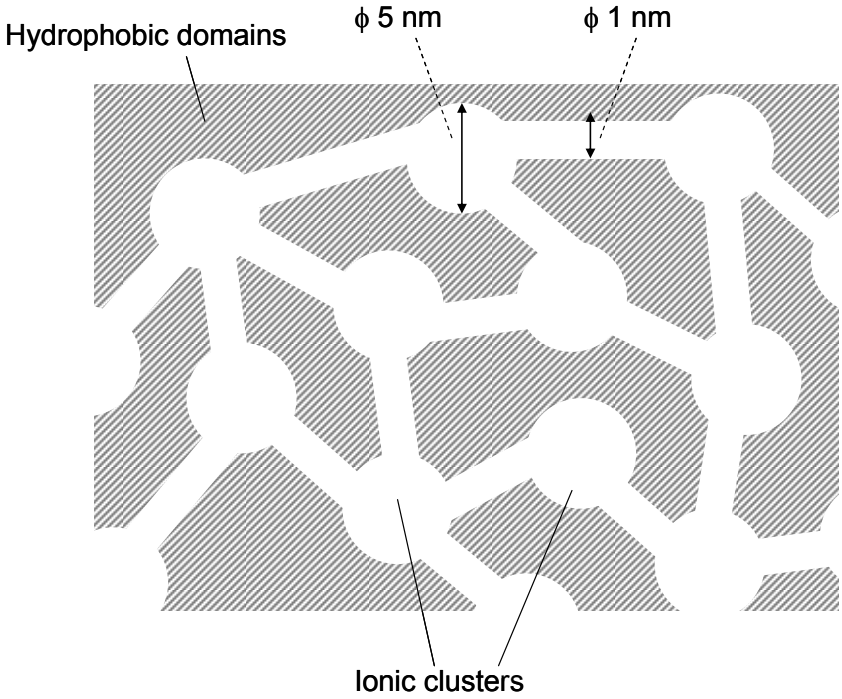

Figure 3.1 Schematic representation of the structure of Nafion.

Although Nafion membranes have been used extensively in hydrogen *PEMFC*, their application in Direct Methanol and Direct Ethanol Fuel Cells (*DMFC* and *DEFC*, respectively) has not been very successful, mainly due to the occurrence of crossover of unspent fuel (see chapter 1). The transport mechanisms of protons, water and methanol are interconnected, since proton conductivity can occur by the formation of complexes with water and methanol (vehicular mechanism). A reduction in the methanol solubility usually implies the reduction of water content and this causes a decrease in proton conductivity.

The mechanisms of absorption change when methanol and ethanol molecules (CH_3-OH or CH_3CH_2-OH) are absorbed, as it occurs in *DMFC*. It has been stated that methanol can interact with the tetrafluoroethylene chains (*TFE*) and then solubilise easier in the non-polar phase [10]. This probably involves not only the amorphous regions of the non-polar phase (*TFE*) but also the interfaces with the ionic domains [10]. Since the side chains are connecting the polar and non-polar regions, it is expected that they play an important role in the absorption of solvents in Nafion, and in particular the ether groups may act as polar sites. When binary mixtures of solvents are absorbed in the membranes the mechanisms are likely to be more complex, since the interactions between the solvents themselves must also be taken into account.

This chapter studies the absorption of methanol and water mixtures in Nafion membranes at 35ºC over the period of one week. The main aims of the chapter are:

1. To study the absorption of water, methanol and their binary mixtures in Nafion membranes.
2. To characterise the membranes after reaching equilibrium (saturated).

The study of the solvents' absorption is carried out by swelling tests, in which the solvent uptake is measured gravimetrically. Further details about the method and the analysis methodology have been given in chapter 2. Two main aspects have been studied:

- The kinetics of solvent absorption

  These membranes have shown very quick absorption of water in the early stages of inmersion leading to stabilization after a few hours. Two parameters were calculated from the curves: the apparent flux (J) and the maximum mass uptake at equilibrium (S_{eq}).

- The effect of the presence of methanol in the absorption of solvents

  As expected, there are noticeable changes in the values of J and S_{eq} when binary mixtures are absorbed. The results show a clear increase in the values of the solvent uptake at higher methanol concentrations. Differences in the shapes of the absorption curves have also been found. All these changes suggest that the absorption of methanol and water is a complex process and depending on the feed solution concentration.

The characterisation of the materials at equilibrium was performed using Fourier Transform Infrared Spectroscopy (FTIR), Thermogravimetric Analysis (TGA) and Differential Scanning Calorimetry (DSC).

Fourier Transform Infrared Spectroscopy (FTIR) has been used to investigate the interactions existing between the different groups of the polymer backbone and side chains and the solvents (water and methanol).

The study has focused on the following regions:

- OH – stretching and bending regions (3800 – 2400 cm^{-1} and 1600 cm^{-1})

  Different OH groups contribute to this region, including the water and methanol molecules and the OH sulfonic groups. The different contributions are studied separately considering that high frequencies correspond to weak hydrogen bonds while lower frequencies to stronger interactions. The results are compared with the work of other authors who associated the higher wavenumber region ($\nu > 3600$ cm^{-1}) to interactions of solvents with the hydrophobic regions of Nafion and at lower wavenumbers ($\nu < 3600$ cm^{-1}) to interactions between the solvents and the polar regions [11]. The interactions between water and methanol were also studied. The

low frequency band ($\nu < 3000$ cm^{-1}) was related to the dissociation of sulfonic acid groups and was also considered in the discussion of the results.

- Region corresponding to SO_3 and C-F groups (1050 - 1400 cm^{-1} region)
  The different stretching vibrations of the main groups of Nafion were studied in the 1050 – 1400 cm^{-1} region. The results are separated into the contributions of the hydrophilic ($\nu_{as}(SO_3^-)$) and hydrophobic ($\nu_{as}(CF_2)$) groups. Notable differences have been found in the behaviour of the bands as the composition of the solutions varied, suggesting that the solvent-polymer interactions are strongly dependent on the presence of methanol.

- Ether region (940 – 1010 cm^{-1})
  The ether region has been studied in detail by several authors. The role of this group may be important in the phase separation morphology since they form part of the side chains of the polymer and structurally close to the hydrophobic and hydrophilic (sulfonic groups) regions. The results are focused on several contributions which have been previously attributed to the presence of ether groups in different chemical environments in the polymer. The changes observed for the previous regions discussed (3800 – 2400 cm^{-1} and 1050 - 1400 cm^{-1}) are also visible in the ether region, suggesting that methanol has an effect on the polar C-O bond, and not only in the non-polar regions, as suggested by other authors.

The study of the thermal stability of the membranes and the state of the solvent was carried out by Thermogravimetric Analysis (TGA). The thermogravimetric curves (TG) and derivative thermogravimetric curves (DTG) of the membranes before and after being submitted to swelling tests were obtained. The curves show differences in the thermal degradation of the samples with the composition of solvent.

Two main temperature regions have been studied. At low temperatures (T< 250ºC) several processes in the DTG curves are indicative of solvent desorption occurring in different stages. It is possible to observe the loss of free solvent in the vicinity of 100ºC and some additional processes at higher temperatures (T> 100ºC) which are related to the loss of tightly bound solvent. It is remarkable that the amount of tightly absorbed

water increased rapidly with the methanol concentration in the solutions, while the increase in the free solvent was more moderate. This fact is indicative of a preferential tightly bounded solvent uptake at high methanol concentrations.

The decomposition of the polymer has also been studied by analysing the DTG curves at higher temperatures (T> 250ºC). Thermal degradation proceeds in several stages including the desulfonation process (T~350ºC), the decomposition of the side-chains of Nafion (T~450ºC) and the decomposition of the main-chains (T~500ºC). The different regions were fitted by several individual peaks by a deconvolution procedure. While the desulfonation process is not greatly changed by the presence of solvent, there is a decrease in the thermal stability of the side chains in the samples submerged in pure methanol and water.

Finally, DSC has been used to study possible changes in the morphology arising from solvent absorption. Different thermal transitions have been observed in the DSC curves corresponding to the first and second heating scans at $10ºC \cdot min^{-1}$. In the first heating scan a large and broad endothermic transition is observed in the vicinity of 100ºC overlapped with a secondary process. This transition is attributed to the loss of solvent from the membranes, and the secondary process to a glass transition of the polar phase of Nafion.

In the second heating scan, the loss of solvent does not appear in the DSC curves and so the remaining transitions can be studied in further detail. The glass transition attributed to the polar phase can be clearly observed in all the samples. This indicates that the cluster morphology is maintained in the Nafion membranes after the solvent is removed. However, the results suggest that the methanol and water concentration of the solutions can affect the characterisitics of the polar phase in the Nafion membranes.

2 COMMUNICATION

Spectroscopic and thermal characterisation of the swelling behaviour of Nafion membranes in water and methanol mixtures.

SPECTROSCOPIC AND THERMAL CHARACTERISATION OF THE SWELLING BEHAVIOUR OF NAFION MEMBRANES IN WATER AND METHANOL MIXTURES.

[1]A. Martínez-Felipe, C.T. Imrie[2], [1]A. Ribes-Greus

[1]Institute of Materials Technology, Universidad Politécnica de Valencia,
Camino de Vera s/n, 46022, Valencia, Spain

[2]Department of Chemistry, University of Aberdeen, Meston Walk, Aberdeen, Scotland, United Kingdom

Keywords: Nafion, crossover, thermal stability, FTIR

Abstract

Nafion membranes were submitted to swelling tests in water, methanol and their binary mixtures. The swelling curves showed deviations from Fickian behaviour as the methanol concentration in the solutions increases. The interactions between the solvent molecules and the polymer groups have been investigated using Fourier Transform Infrared Spectroscopy (FTIR). The results showed variations in the interactions between the solvent and the polar and non-polar groups of the polymer as a function of the methanol composition. Moreover, the increase of the mass flux suggests the existence of chain dynamic processes probably located in the non-polar phase of the polymer which were also solvent composition dependent. The presence of tightly bound solvent in the samples submerged in methanol rich solutions was detected by thermogravimetric analysis (TGA). A decrease in the thermal stability of the side-chains was also observed. Finally, Differential Scanning Calorimetry (DSC) was used to study the thermal transitions of the membranes. The results suggested a change in the morphology

of the polar phase in the polymers in the presence of methanol even at low methanol concentrations.

Introduction

Nafion has become the reference benchmark polymeric electrolyte material used in low temperature hydrogen fuel cells [1]. Its chemical structure consists of a perfluorinated backbone (PTFE, polytetrafluoroethylene groups) with perfluoroalkyl ether side chains (PFEA) which contain pendant SO_3X residues, where *X* denotes an alkaline metal such as sodium or lithium, or hydrogen. In some conditions the salt or the acid is dissociated, yielding ionic groups (ionomers). The perfluorinated chains provide high mechanical and chemical stability while the ionic groups act as sites for polar absorption or proton exchange processes [2]. However, when Nafion membranes are used in Direct Methanol Fuel Cells (*DMFC*) the performance of the electrolyte decreases drastically, mainly due to activation and mass transfer effects [3]. Among the different reasons affecting the behaviour of Nafion membranes in *DMFC*, particular attention has focussed on the so-called "crossover" phenomenon. Crossover consists of the flux of unreacted methanol through the electrolyte and its reaction with oxygen at the cathode. This reaction does not contribute to electrical power generation and as a result the efficiency of the cell drops by up to a 30% [4, 5].

The appearance of crossover in Nafion membranes has been related to the different mechanisms of transport of water, methanol and the protonic species through its structure. The absorption of solvents is also influenced by the morphology of the membrane. Different models describing the morphology of Nafion have been proposed in recent years, such as those suggested by Gierke [6], Fujiyama [7. 8], Dreyfus [9], Litt [10], Houbold [11] and Rubalat [12]. Despite differences between these models, all include the existence of ionic group aggregates in a perfluororinated polymer matrix. The ionic aggregates form a network of clusters that promote swelling by polar solvents and support ionic transport. In general terms, it is assumed that water (as other polar solvents) is absorbed through the ionic sites by filling these clusters. These clusters pools together with the significant morphological variations seen in Nafion membranes on swelling have been discussed extensively and different models have been proposed to rasionalise the observations [8, 10, 13]. However, the mechanisms of absorption

change when less polar molecules are absorbed, as, for example, in DMFCs. It has been stated that methanol can interact with the tetrafluoroethylene chains (*TFE*) and therefore be bound in the hydrophobic domains [4]. This probably involves not only the amorphous regions of the non-polar phase (*TFE*) but also the interfaces with the ionic domains [14]. Since the side chains are effectively the link connections between the polar and non-polar regions, they are expected to play an important role in the absorption of solvents in Nafion. Specifically the ether groups may act as polar sites. When binary mixtures of solvents are absorbed, the mechanisms are even more complex, since the interactions between the solvents themselves must also be taken into account.

In this paper we present a study of the absorption of water and methanol binary mixtures in Nafion membranes. The absorption of the solvents was measured gravimetrically for various absortion times until reaching the equilibrium in order to study the mechanisms of the diffusion in the polymer. After the membranes were submitted to the swelling tests, they were characterised by several techniques in order to study the behaviour of the solvent molecules inside the structure of the polymer. Fourier Transform Infrared Spectroscopy (FTIR) was used to study the short-range interactions of the polar and non-polar groups of the polymers [15], Thermogravimetric Analysis (TGA) was performed to investigate their thermal stability, and finally Differential Scanning Calorimetry (DSC) was carried out to detect possible changes in their morphology after the swelling tests are performed [16]. These techniques provide highly complementary insights into improving our understanding of the crossover phenomenon in *DMFC*.

Experimental procedure

Nafion 117 was purchased from Fuelcellscientific and used as-received (equivalent weight EW = 1100). The methanol-water binary mixtures were prepared using 99.9 % methanol (purchased from Sigma-Aldrich) and distilled water (prepared in our laboratory). The Nafion membranes were submitted to swelling tests at 35ºC for a maximum inmersion time of one week, and were then analysed by Fourier Transform Infrared Spectroscopy (FTIR), Thermogravimetric Analysis (TGA) and Differential Scanning Calorimetry (DSC). The thickness of the membranes was measured by a clock Comparator Stand (Mitutoyo) with ±1 μm accuracy. The thickness was calculated as the mean of triplicate measurements across different parts of the membranes.

Swelling tests

The commercial membranes were cut into rectangular films measuring 4x1 cm^2, weighed ($t = 0$, w_0) and submerged in test tubes containing binary solutions of water and methanol. Solutions of 10%, 20%, 30% and 40% by weight of methanol were prepared, corresponding to methanol molar fractions of 0.06, 0.12, 0.19 and 0.27, respectively. The samples were also submerged in tubes containing pure water and pure methanol. The test tubes containing the water and methanol solutions at different concentrations and the membranes were submerged in a thermostatic SELECTA Ultrasonic bath (accuracy 0.1ºC) at 35ºC, in order to simulate the behaviour of the materials at low temperatures.

The absorption of solvent was measured gravimetrically several times during the swelling experiment, according to the following standard procedure. The samples were removed from the test tubes and the excess liquid was drained with a tissue. The samples were then weighed using a Mettler Toledo balance (0.1 mg accuracy, w_t). The membranes were then placed back into the tests tubes and re-submerged in the isotherm bath. Membranes were inmersed into the solutions for a maximum time of one week. After the last measurement was performed, the samples were covered and stored for further analysis. All the experiments were performed three times with different membranes in order to obtain average values.

The samples were labelled in accordance with the % weight methanol in the solution in which they were submerged (see *Table 1*).

Table 1. Designation of the samples.

Sample name	Weight percentage of methanol in the solution (%)
Water	0
10% MeOH	10
20% MeOH	20
30% MeOH	30
40% MeOH	40
Methanol	100

Attenuated Total Reflectance - Fourier Transform Infrared Spectroscopy (ATR-FTIR)

The FTIR experiments were performed using a Thermo Nicolet 5700 spectrometer (MA, Walthman) equipped with an ATR attachment. The samples were placed on a diamond crystal, and the experiments were performed using 1 bounce and an incident angle of 45ºC. The spectra were collected after 128 scans with an accuracy of 4 cm^{-1}. Backgrounds were collected before each series of experiments. All the experiments were performed seven times and the average calculated.

Thermogravimetric Analysis (TGA)

TGA experiments were carried out using a Mettler Toledo TGA/SDTA 851 analyser (OH, Columbus). Measurements were performed following a dynamic program from 25ºC to 750ºC at a heating rate of 10ºC/min under inert Argon (Ar) atmosphere with a flow rate of 200 ml/min. Sample masses were around 5 mg.

Differential Scanning Calorimetry (DSC)

The DSC thermograms were obtained using a Mettler Toledo DSC 822 analyser (OH, Columbus). The samples containing around 5 mg were heated up from -50ºC to 200ºC, held at 200ºC for 3 minutes, cooled to -50ºC, held for 3 minutes, and re-heated to

200ºC. All the scans were performed at 10ºC/min in a nitrogen atmosphere and using liquid nitrogen as the coolant.

Results and discussion

Swelling tests

The amount of solvent absorbed by the membranes during the swelling tests was calculated as the mass difference between the samples exposed to the solvent and the dry sample. The results were normalised respect to the mass of the dried sample by calculating the swelling percentage of the solvent absorption as shown in *Equation 1*:

$$S_w(\%) = \frac{w_t - w_0}{w_0} \cdot 100 \qquad (1)$$

where w_t and w_0 are the masses of the membrane after a time of absorption *t* and the value of the dry sample, respectively.

The swelling curves of the membranes submerged in different binary mixtures of water and methanol at 35ºC are shown in *Figure 1*.

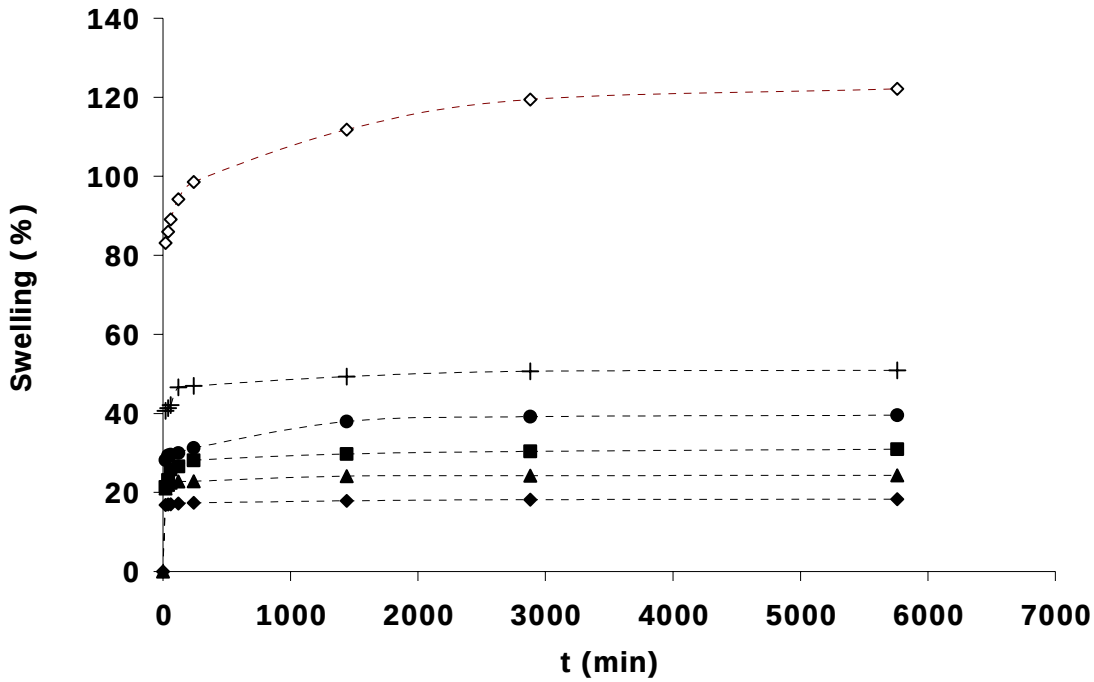

Figure 1. Swelling curves corresponding to the membranes submerged in binary aqueous solutions of methanol and water at 35ºC. ◆ Water, ▲ MeOH10%, ■ MeOH20%, ● MeOH30%, + MeOH40%, ◇ Methanol.

All the samples show a rapid absorption process during the first moments of the experiment before stabilizing to an equilibrium value. The values of the solvent absorbed at the equilibrium (S_{eq}) and the time to reach half of the equilibrium swelling value ($t_{1/2}$) were estimated from the experimental swelling curves. The mass flux at the beginning stages of absorption (J) was also estimated considering the mass absorbed at half-time of the equilibrium ($w_{1/2}$) and the surface of mass transfer (S), as seen in *Equation.2*:

$$J = \frac{w_{1/2} / t_{1/2}}{S} \qquad (2)$$

For the calculation of J the convection effects were neglected ($S^{1/2} >> L$) and the dynamics was considered one-dimensional [17].

The results of S_{eq}, $t_{1/2}$ and J for all the samples are summarized in *Table 2*.

Table 2. Parameters of the swelling tests performed in binary mixtures of water and methanol

Sample	S_∞ (%)	$t_{½}$ (min)	J (kg / sec·cm^2 10^5)
Water	18.3	10.7	2.2
10% MeOH	24.3	11.9	2.8
20% MeOH	32.9	12.6	2.9
30% MeOH	39.5	12.8	3.6
40% MeOH	50.9	17.6	3.4
Methanol	122.1	18.2	10.7

The amount of solvent absorbed by the membranes at equilibrium increases for increasing methanol concentrations in the solutions. This behaviour was previously studied by other authors who showed that the absorption of solvent in water and methanol mixtures was favoured at high methanol concentrations [18, 19, 20]. The number of molecules of water absorbed per sulfonic acid group was calculated considering the initial mass of the membranes, the equivalent weight of Nafion (1100)

as the repeating sulfonic unit and the amount of solvent absorbed at the equilibrium, as seen in *Equation 3*:

$$\lambda = \frac{w_{solvent} / MW_{solvent}}{w_{Nafion} / EW_{Nafion}} \qquad (3)$$

Where $w_{solvent}$ and w_{Nafion} are the masses of the water or methanol absorbed and the dry Nafion membranes (w_0) and $MW_{solvent}$ and EW_{Nafion} are the molecular weight of the solvent (18 g·mol^{-1} for water and 32 g·mol^{-1} for methanol) and the equivalent weight of Nafion (1100 g·eq^{-1}), respectively.

A value of $\lambda = 11.56$ was obtained for the membrane submerged in pure water and $\lambda = 44.31$ for the membrane submerged in pure methanol. These values are in good agreement with those in the literature [20]. The values of mass flux (*J*) also increase with the methanol concentration.

In order to study possible differences between the swelling curves, the values of the fractional mass uptake (w_t/w_{eq}) were calculated and plotted as a function of the square root of time, following the standard procedure used elsewhere [21, 22]. The results of w_t/w_{eq} versus $t^{1/2}/L$ are shown in *Figure 2*, where *L* is the thickness of the membranes. The shape of the curves varies with the concentration of the solution.

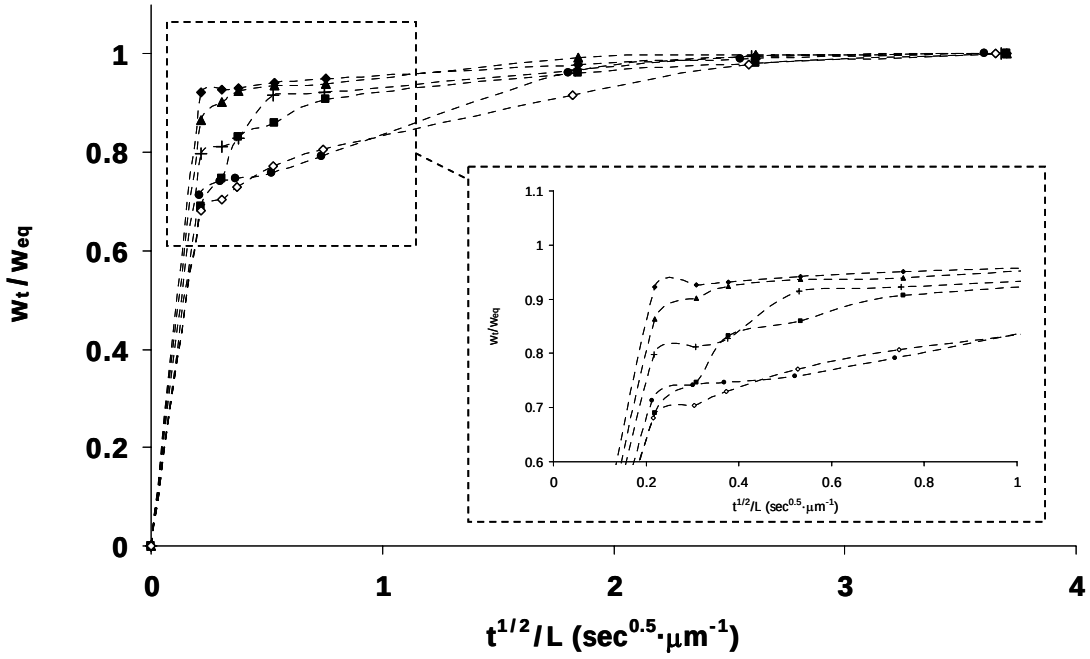

Figure 2. Fractional mass uptake for the membranes submerged in the water and methanol binary mixtures at 35ºC, ◆ Water, ▲ MeOH10%, ■ MeOH20%, ● MeOH30%, + MeOH40%, ◇ Methanol.

While the curve corresponding to the pure water uptake fits very well to a typical Fickian diffusion process [21], the curve corresponding to the mixtures show some deviations from such behaviour. The absorption of solvent in the membranes submerged in methanol and its mixtures seems to occur in, at least, two different steps: a quick linear solvent uptake followed by a second and slower absorption process [22]. The deviation from Fickian behaviour is greatest for the membrane submerged in pure methanol, which undergoes a more gradual mass absorption during the second step than the other samples.

Although there is not a consensus of opinion as to why, it is accepted that the concentration influences the diffusivity of methanol in aqueous mixtures in Nafion membranes [23]. Some authors have previously reported similar results and suggest that the swelling process at high methanol concentrations produces an increase in the values of mass flux, probably due to an increase in the free volume of the chains which enhances the dynamic process of polymeric chains [22, 24].

Characterisation of the membranes after the swelling tests

Fourier Transform Infrared Spectroscopy (FTIR)

The FTIR spectra of the Nafion membranes previously submerged in water and methanol binary mixtures at 35°C until obtaining equilibrium conditions are shown in *Figure 3*. The characteristic bands corresponding to the OH groups of the solvent molecules and to the chemical groups in Nafion are visible in the FTIR spectra of all the membranes studied.

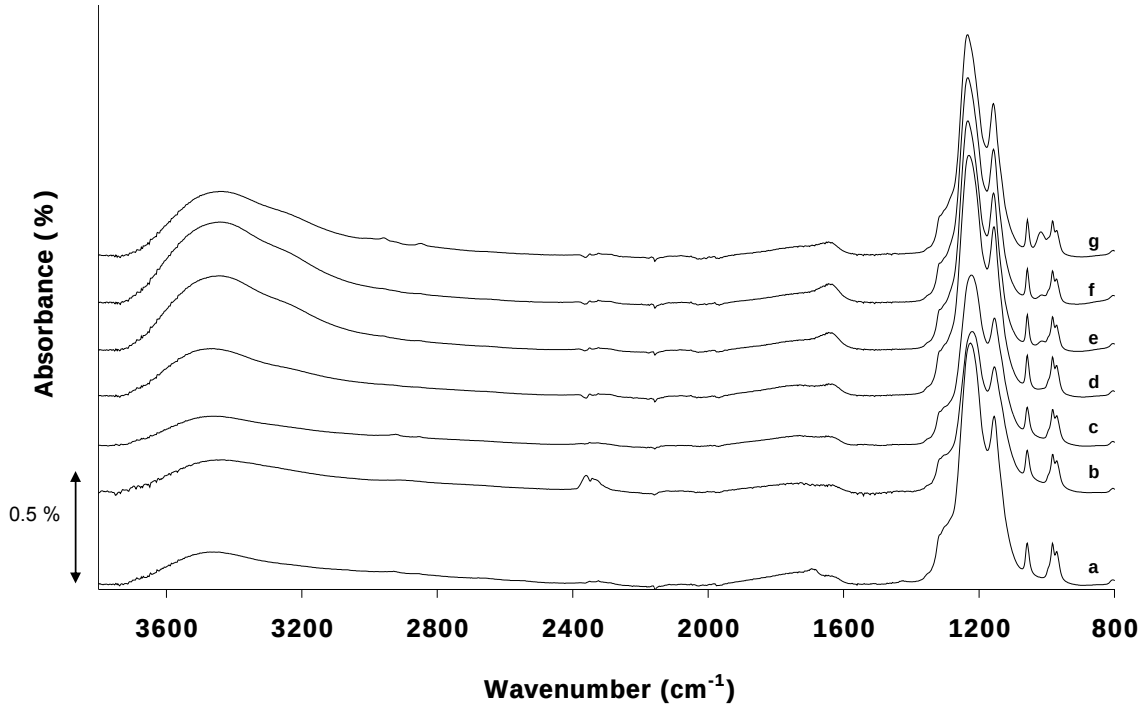

Figure 3 FTIR-ATR curves of the Nafion membranes submerged in water and methanol binary mixtures at 35ºC: (a) Nafion, (b) Water, (c) MeOH 10%, (d) MeOH 20%, (e) MeOH 30%, (f) MeOH 40%, (g) Methanol.

The assignment of the different bands corresponding to the OH vibration modes are summarised in *Table 3*. As expected, Figure 3 shows an increase in the OH vibration regions of the membranes after swelling, due to the absorption of solvent. The high frequencies region in the FTIR spectra ($\nu > 3600$ cm^{-1}) has been plotted with more detail in *Figure 4*. It is possible to observe that the FTIR curves of the samples submerged in water and *10%MeOH* show the lowest absorption values, while the curves corresponding to the samples submerged in solutions with high methanol concentrations are higher. The increase observed in the region suggests that the formation of H-bonds

by the OH groups at the hydrophobic/hydrophilic interface is promoted by the presence of methanol in the solutions.

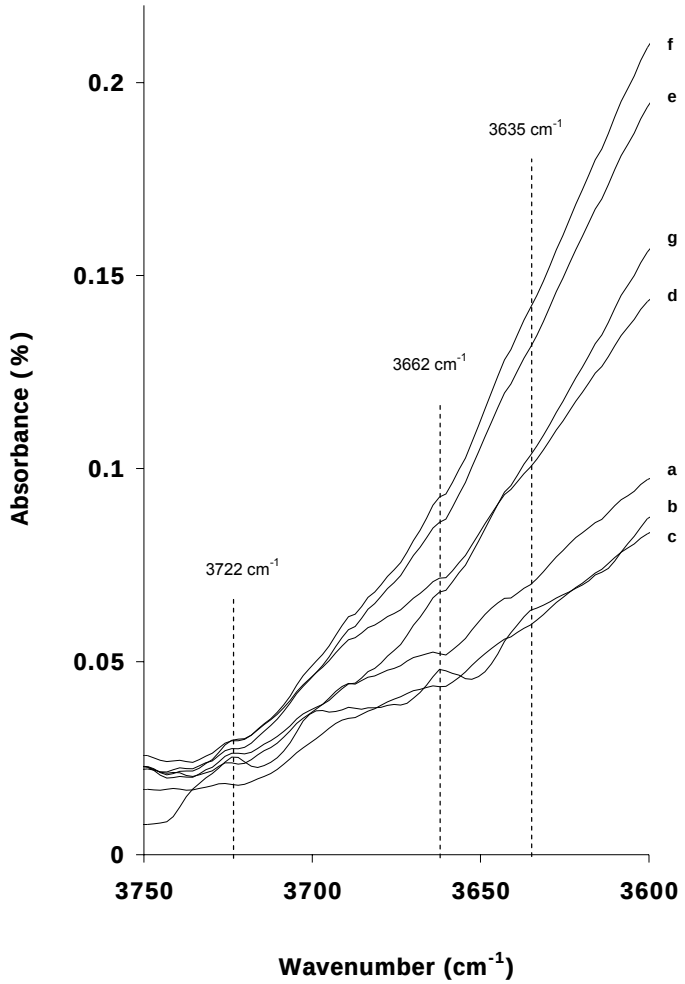

Figure 4 Detail of the ν > 3600 cm^{-1} region (FTIR curves) (a) Nafion, (b) Water, (c) MeOH 10%, (d) MeOH 20%, (e) MeOH 30%, (f) MeOH 40%, (g) Methanol.

The changes in the region at lower frequencies (ν < 3600 cm^{-1}) seem to be more marked. In order to study some of the effects of the concentration of the solvent in this region, a deconvolution procedure was performed. The FTIR experimental curves were fitted to a sum of two Gaussian peaks and one asymmetric peak, considering the different contributions shown in *Table 3*. The region is shown with more detail in *Figure 5* and the expression in *Equation 4*:

$$y = \sum_{i=1}^{2} A_i \cdot \exp(-0.5 \cdot \frac{(x - x_{ci})^2}{w_i^2}) + A_3 \cdot (\frac{1}{1 + \exp(\frac{-(x - x_{c3} + 0.5)}{w_{23}})}) + (1 - \frac{1}{1 + \exp(\frac{-(x - x_{c3} - 0.5)}{w_{33}})}) \quad (4)$$

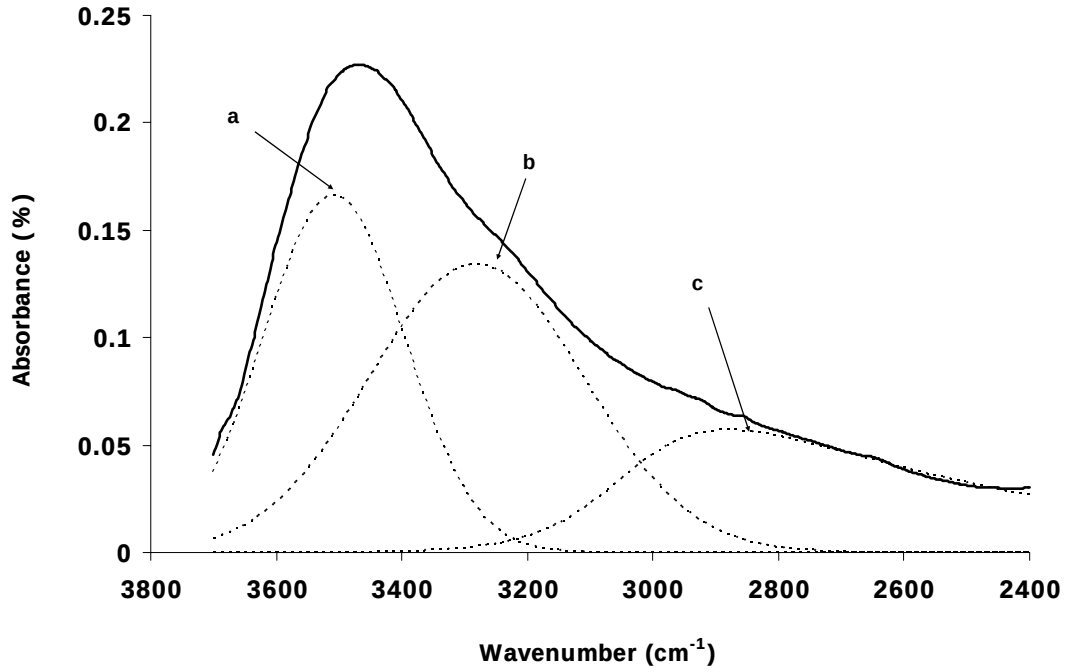

Figure 5 Deconvolution of the ν < 3600 cm^{-1} region (MeOH 20%): (a) Peak #1, (b) Peak #2 (c) Peak #3.

where the parameters A_i indicate the intensity of the curves, x_{ci} is the frequency of the maximum absorbance, w_i describes the width of the Gaussian curves and w_{23} and w_{33} the dispersion and shape of the asymmetric curve.

Table 3. FTIR results. Assignation of the OH vibration bands.

Region (cm^{-1})	Subregion (cm^{-1})	Assigment	References
3800 – 2400 OH Stretching	3800 – 3600	• OH forming weak H-bonds between the solvent molecules and the hydrophobic regions of Nafion through the hydrophobic-hydrophilic interface	[25, 26]
	3600 – 3400	• OH groups of solvent molecules forming strong H-bonds with the polar groups of the polymer	[25, 26]
		• OH groups of solvent molecules forming ether complexes	[27, 28, 29, 30]
	3400 – 3000	• Bulk-like water and methanol molecules	[31]
		• Solvation and external OH groups in the solvent clusters	
	3000 –	• H_3O+, $H_2O_5^+$, $CH_3OH_2^+$ grouping species forming clusters in the membranes by dissociation of SO_2OH*	[27, 28, 31]
		• Internal OH groups in the solvent clusters	
2000 – 1400 OH bending	~ 1688	• Structural vibrations	
	~ 1630	• External OH in solvent clusters	[24, 31]

* The dissociation of the SO_2OH (into SO_3^-) is confirmed by the absence of the stretching asymmetric vibration of the S=O bond (ν_{as} (S=O) ~ 1425 cm^{-1}) and the single S-O bond (ν_s (S-O) ~ 920 cm^{-1}) in the FTIR spectra of all the samples.

The values of position, area and width (at half of the maximum absorbance) of the three peaks were calculated. The results are shown in *Table 4*.

Table 4. Deconvolution of the FTIR curves in the OH stretching region. Values of the individual peaks.

	Peak #1		
Sample	**Centre (cm^{-1})**	**Area (%· cm^{-1})**	**Width (cm^{-1})**
Nafion	3502	23.5	241
Water	3479	29.4	264
10% MeOH	3500	28.8	278
20% MeOH	3508	44.5	262
30% MeOH	3504	59.9	253
40% MeOH	3502	65.5	255
Methanol	3496	50.2	251

	Peak #2		
Sample	**Centre (cm^{-1})**	**Area (%· cm^{-1})**	**Width (cm^{-1})**
Nafion	3340	11.9	297
Water	3278	11.2	251
10% MeOH	3253	37.6	422
20% MeOH	3280	56.8	401
30% MeOH	3298	85.6	372
40% MeOH	3296	92.9	372
Methanol	3286	82.6	392

	Peak #3		
Sample	**Centre (cm^{-1})**	**Area (%· cm^{-1})**	**Width (cm^{-1})**
Nafion	3107	71.6	935
Water	3066	60.9	914
10% MeOH	2872	21.9	540
20% MeOH	2879	32.1	640
30% MeOH	2926	30.2	530
40% MeOH	2922	29.9	536
Methanol	2922	31.4	497

For the sample submerged in water the high values of the 3500 cm^{-1} peak, together with the decrease in the ν>3600 cm^{-1} region described earlier, suggests that the water OH groups tend to form strong hydrogen bonds with the polar groups, rather than with the non-polar regions. This is in agreement with the mechanisms of absorption of water molecules through the ionic clusters of Nafion [3].

On the other hand, it is possible to observe some changes in the values of the peaks in the samples inmersed in solutions containing methanol. At higher methanol concentrations, the two peaks at high frequencies (peak #1, centred at $\nu \sim 3500 cm^{-1}$ and peak #2, centred at $\nu \sim 3300 cm^{-1}$) increase in both maximum absorbance and intensity respect to the low frequencies peak (peak #3, $\nu < 3000 cm^{-1}$). This suggests a promotion of less energetic hydrogen bonds in the samples submerged in methanol. The relative area values of peak #2 respect to peak #1 were also calculated and the results have been plotted in *Figure 6*.

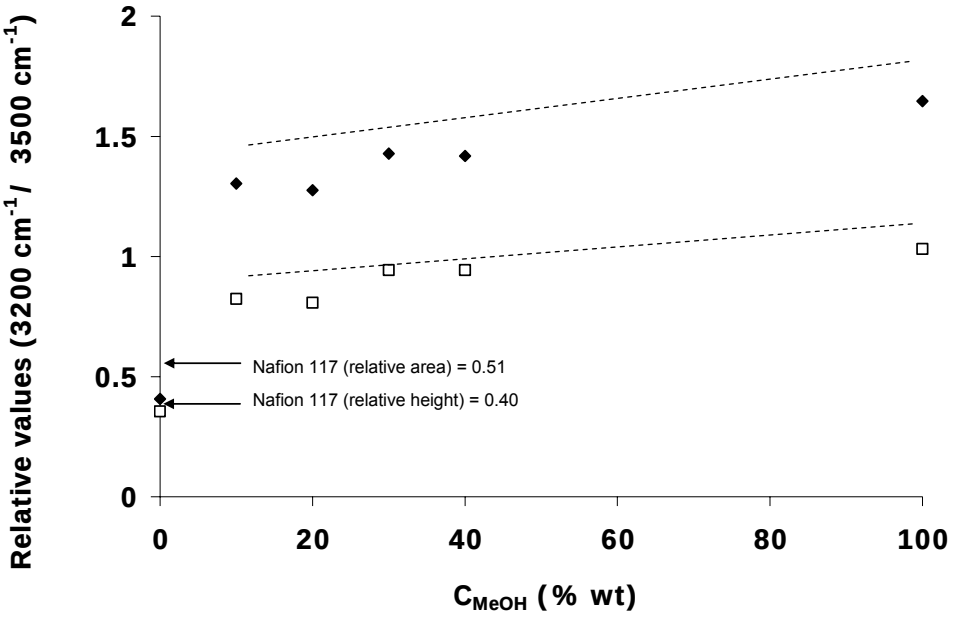

Figure 6 Relative values of area and absorbance of the peak at 3300 cm^{-1} respect to the peak at 3500 cm^{-1} (deconvolution results). (◆) relative area and (□) relative height

The increase of the relative area of the peak at 3330 cm^{-1} (peak #2) indicates a preferential absorption of bulk-like methanol (3344 cm^{-1}) and the presence of solvation or external molecules of solvent in the clusters (see *Figure 7*). The absorption of

methanol molecules in the solutions is confirmed by the appearance and growth of the absorption band at 1016 cm^{-1} (methanol C–O stretching) even at low MeOH concentrations [24]. Moreover, the gradual increase in peak #1 indicates that the formation of H-bonds between the solvent molecules and polar groups is also taking place, although to a minor extent.

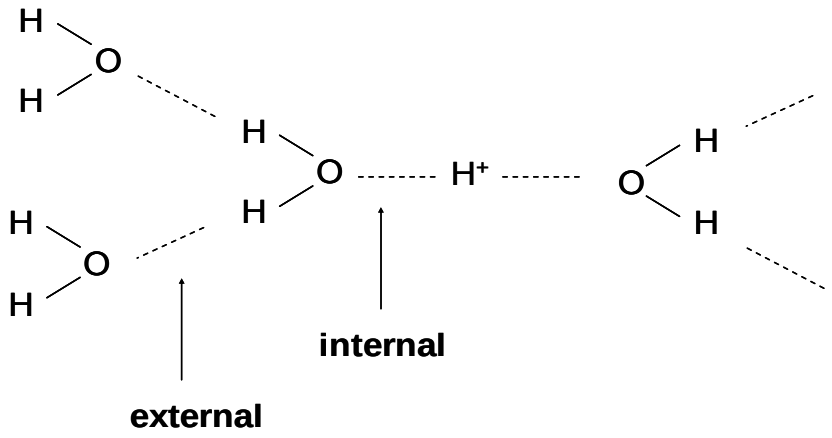

Figure 7 Cluster model proposed by Zundel [31]

The results in *Table 4* also indicate a red-shift of the peak #2 at 3300 cm^{-1} that suggests that the H-bonds formed between the OH groups of the solvent and the polar groups of the polymer are weaker as the concentration of methanol in the solutions increases [32]. Moreover, it is possible to observe a slight blue-shift of the peak #2 at 3500 cm^{-1} on increasing methanol concentrations which indicates that the methanol molecules are very sensitive to the chemical environment. The values of wavenumber found for peak #1 (3200 cm^{-1}) are lower than those expected for the water (3404 cm^{-1}) or methanol (3344 cm^{-1}) in the bulk liquid phase, which suggests the existence of intermolecular forces between methanol and water.

The increase of the OH stretching region is accompanied by an increase in the OH bending vibration bands, as shown in *Figure 8*. This remarkably sharp increase in the peak at 1630 cm^{-1} can be related to the OH groups in the solvent clusters [24].

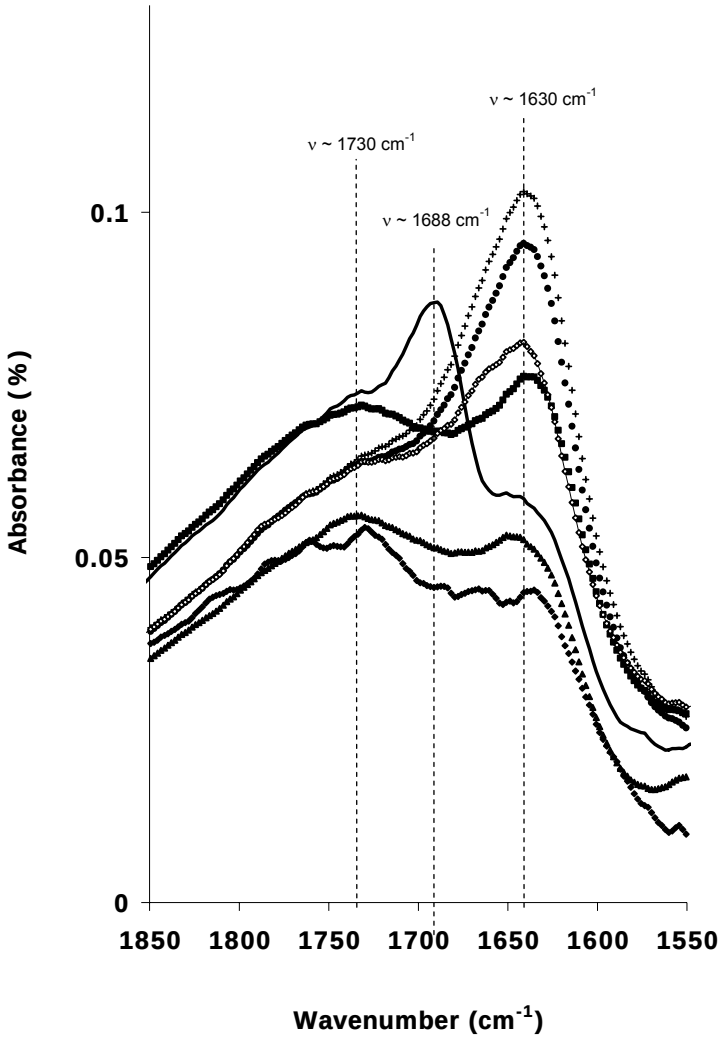

Figure 8 FTIR curves in the 1800 – 1600 cm^{-1} region: ◆ Water, ▲ MeOH10%, ■ MeOH20%, ● MeOH30%, + MeOH40%, ◇ Methanol. Solid line corresponds to Nafion 117.

The FTIR curves in the 1400 – 1000 cm^{-1} absorption region show several contributions from the polymer functional groups, which have been summarised in *Table 5*. It is possible to observe some changes in this region with the composition of the solutions (*Figure 3*). In order to probe the influence of the methanol concentration on this region, the FTIR curves of all the samples were fitted to a sum of eight Gaussian peaks (n = 8). The FTIR curve corresponding to the Nafion membrane in the region and the individual peaks are shown in *Figure 9*. The position, area and width of the individual peaks were calculated. The results corresponding to the area of the peaks are shown in *Figure 10*. The results corresponding to the 1057 cm^{-1} region ($\nu_s(SO_3^-)$) have also been included.

Table 5. FTIR results. Assignation of the vibration bands of the polymeric groups.

Assignment	Wavenumber (cm^{-1})
$\nu_{as}(CF_2)$	1240
	1153
ν_{as} (C-C)	1317
	1294
$\nu_{as}(SO_3^-)$	1130
$\nu_s(SO_3^-)$	1057
ν_s (COC)	940 – 1010
$\delta(CF_2)$	525
t (CF_2)	558
$\omega(CF_2)$	636
$\nu_s(CF_2)$	718
ν (C - S)	805

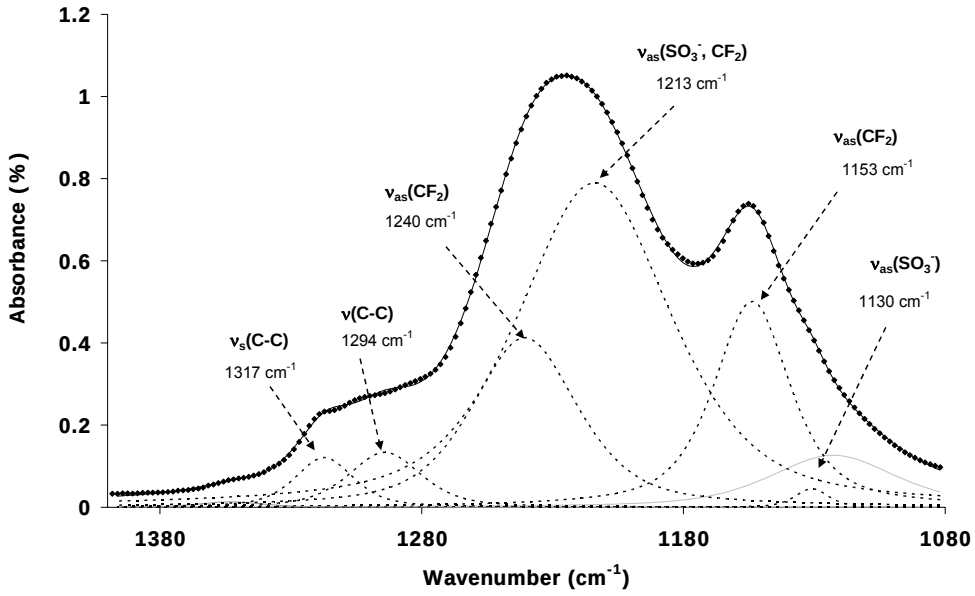

Figure 9 Deconvolution of the FTIR curve of Nafion in the 1000 – 1400 cm^{-1} region. ◆ corresponds to the experimental points, solid line to the fitted curve and dotted lines to the individual Gaussian contributions. Peak in grey have not been assigned to a particular vibration.

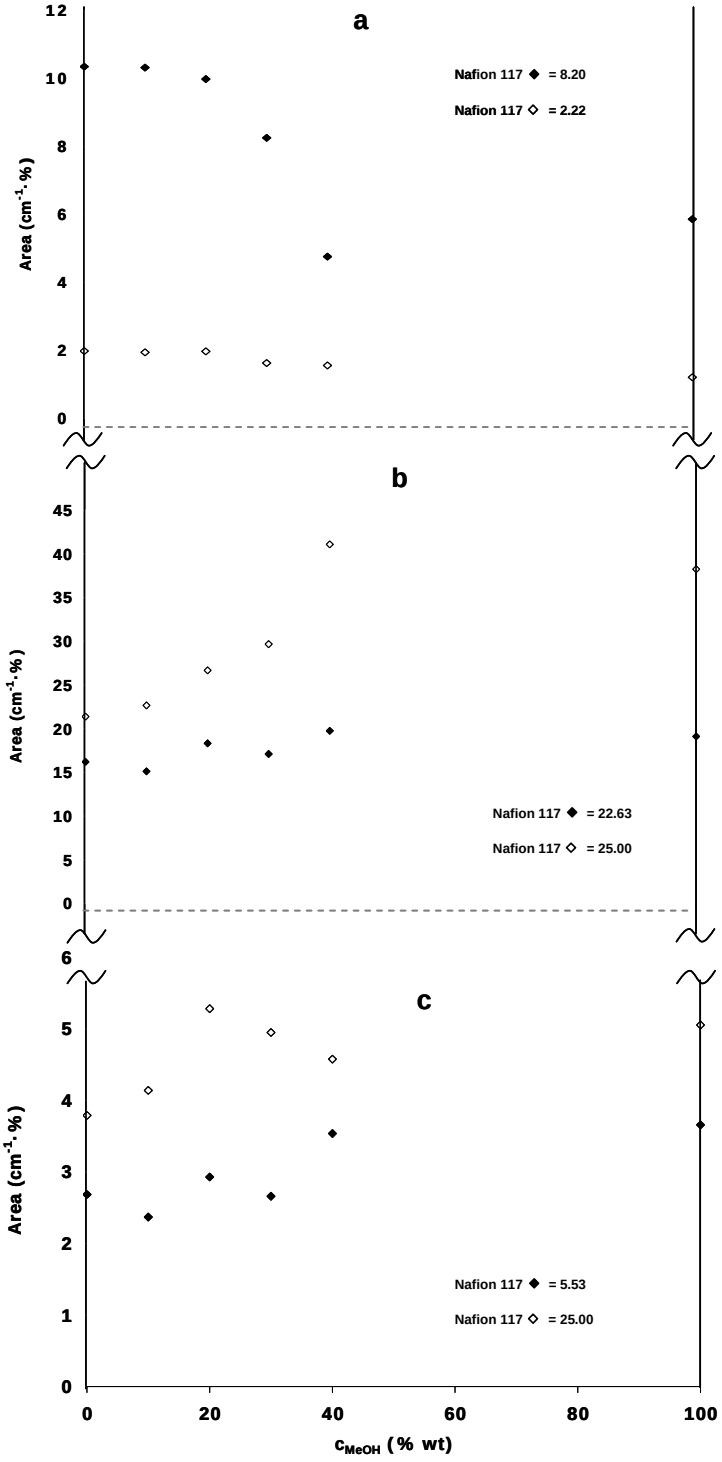

Figure 10 Values of area corresponding to the individual peaks in the 1000 – 1400 cm^{-1} region: (a) SO_3^- bands at ◆ 1127 cm^{-1} , ◇ 1057 cm^{-1} (b) CF_2 bands at ◆ 1153 cm^{-1} , ◇ 1240 cm^{-1} (c) C-C bands at ◆ 1317 cm^{-1}, ◇ 1294 cm^{-1}.

The results in *Figure 10* show different tendencies for the peaks corresponding to the different polymer groups on solvent composition. The peaks related to the sulfonate

groups (*Figure 10a*) decrease at high methanol concentrations and shift to higher wavenumbers, while those corresponding to the perfluorinated matrix (*Figure 10b* and *10c*) increase and appeared at lower frequencies. These facts suggest that the interactions of the solvent with the SO_3^- groups are promoted in the presence of water, but are then weakened as the methanol concentration increases, *i.e.* in opposite sense to what happens to the interactions with the hydrophobic groups. These results are in good agreement with those observed by other authors in absorption tests of water/methanol mixtures and also with our own results observed in the OH stretching and bending regions [33, 34]. Indeed, this change in the nature of the interactions of the solvent might be one of the main reasons for the appearance of crossover in *DMFC*.

The ether vibration region corresponding to the Nafion membrane has been plotted in more detail in *Figure 11* (a). It is worth noting the presence of distinct bands in the 1010 – 940 cm^{-1} region corresponding to the absorption envelope for the symmetric C-O-C stretching vibration [35, 36]. The experimental curves corresponding to the samples following the swelling tests (and that corresponding to the Nafion membrane) were fitted to a sum of Gaussian/Lorentzial peaks. Three bands were used to fit the different contributions at 970 cm^{-1}, 983 cm^{-1} and 993 cm^{-1}. The resulting individual and fitted curves are also shown in *Figure 11 (b)*.

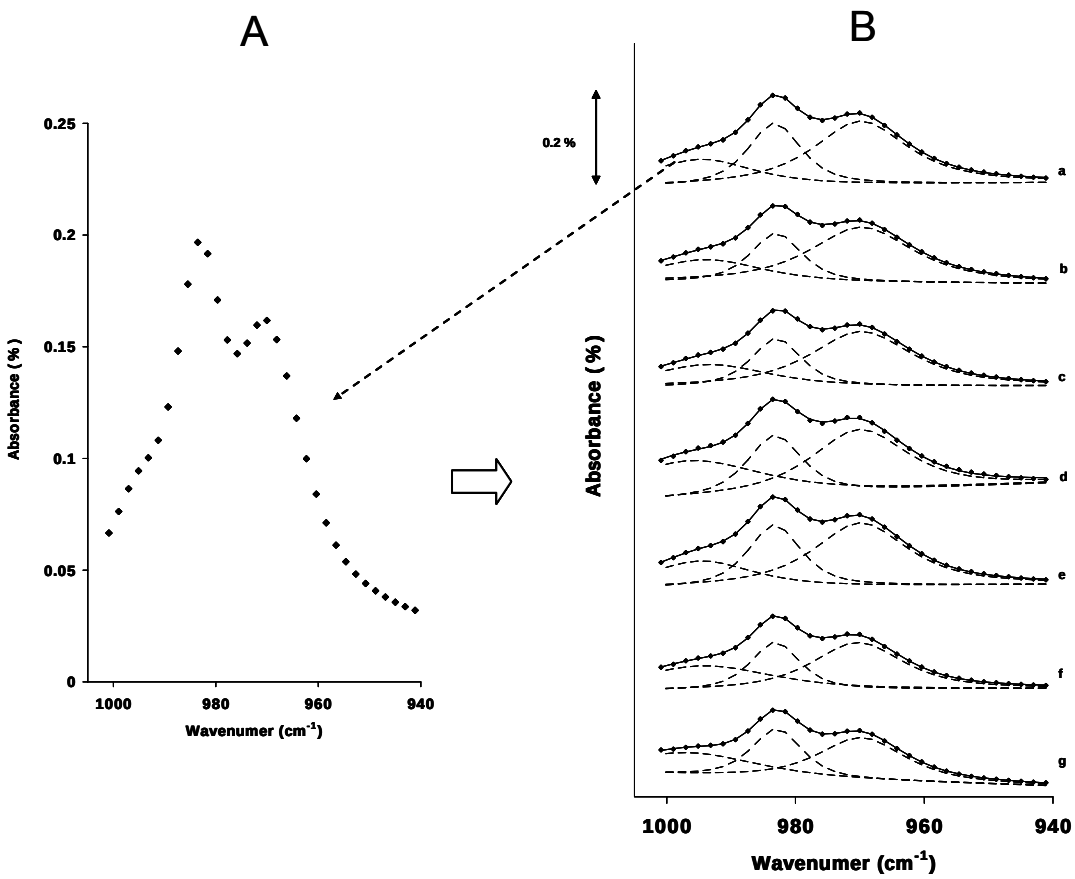

Figure 11 FTIR curves in the ether (COC) vibration region (940 – 1100 cm^{-1}). (A): Nafion 117 curve. (B): deconvolution of the envelope for all the samples. (a) Nafion, (b) Water, (c) MeOH 10%, (d) MeOH 20%, (e) MeOH 30%, (f) MeOH 40%, (g) Methanol. ◆ corresponds to the experimental points, solid line to the fitted curve and dotted lines to the individual Gaussian contributions.

The normalised areas of the individual peaks were calculated by simple integration and are shown in *Figure 12*. The contribution of the peaks at lower wavenumbers (970 cm^{-1} and 983 cm^{-1}) decreases and the value corresponding to the peak at higher wavenumbers (993 cm^{-1}) increases for higher methanol concentrations in the solutions. Such changes denote variations in the chemical environment of the ether groups in the polymer, which suggests that the side chains of the polymer are also involved and affected by the absorption of the solvents.

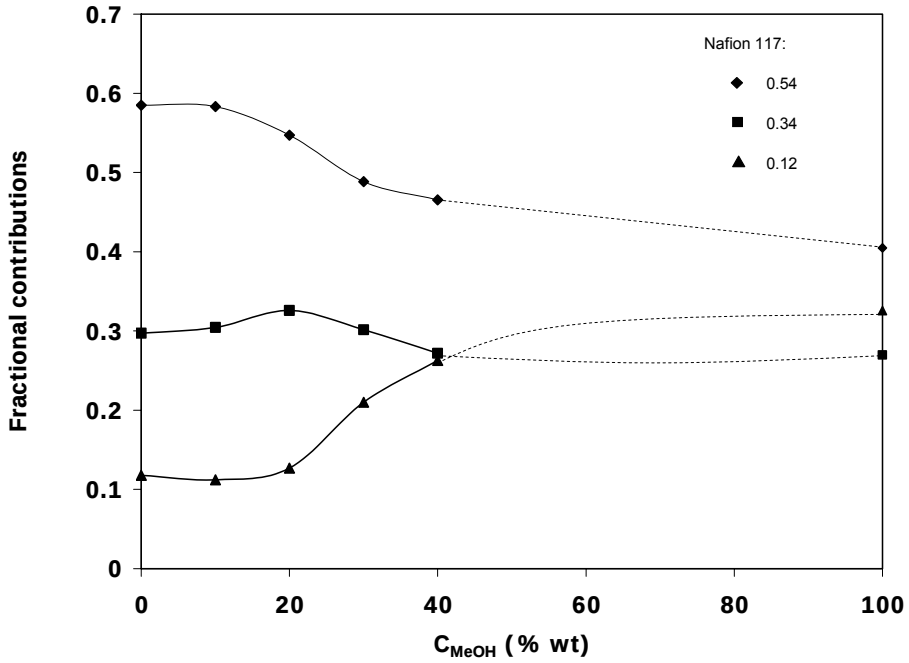

Figure 12 Values of area corresponding to the individual peaks in the ether vibration region (1010 – 940 cm^{-1}). Bands at ◆ 970 cm^{-1} , 983 cm^{-1} , ▲ 993 cm^{-1}.

Although there is no clear consensus concerning the assignments of some of the processes in the ether region [3], Cable and Falk associated the band at 970 cm^{-1} to the formation of clusters and the 980 cm^{-1} band to structural vibrations of ether bonds which were already present in the PTFE predecessor of Nafion [37, 38]. The decrease in the 970 cm^{-1} band can be then interpreted as a decrease in the number of perfluorether side chains interdigated in the ionic clusters when methanol is absorbed in the membrane. The increase in the band at high frequencies (993 cm^{-1}) can be assigned to ether bonds weakly perturbed by the state of the ion par, and therefore to side chains more shielded from the ionic regions. The growth of this band at high methanol concentrations indicates an increase in the interactions between solvent molecules and C-O-C groups more shielded from the clusters, *i.e.* more related to the non-polar phase. Such interactions can be based on the formation of complexes between the ether groups and the methanol molecules, which is in accord with the growth of the band at 3500cm^{-1} in the OH stretching region, and would also explain the increase in the permeation of methanol through the membranes and the occurrence of crossover.

Thermogravimetric Analysis (TGA)

Figure 13 shows the derivative thermogravimetric (DTG) curves of the Nafion membranes after the absorption tests were performed. The decomposition of Nafion (*Figure 13a*) occurs following a complex degradation process in several steps, corresponding to the different peaks of the DTG curve. The gradual mass loss observed at low temperatures (25ºC – 250ºC) can be attributed to the volatilization of water or other solvents from the membrane (Δw = 5.70 %). The existence of several peaks in the 100ºC – 250ºC region suggests that a fraction of the solvent may be tightly bound to the polymer structure, as already inferred by FTIR [39, 40].

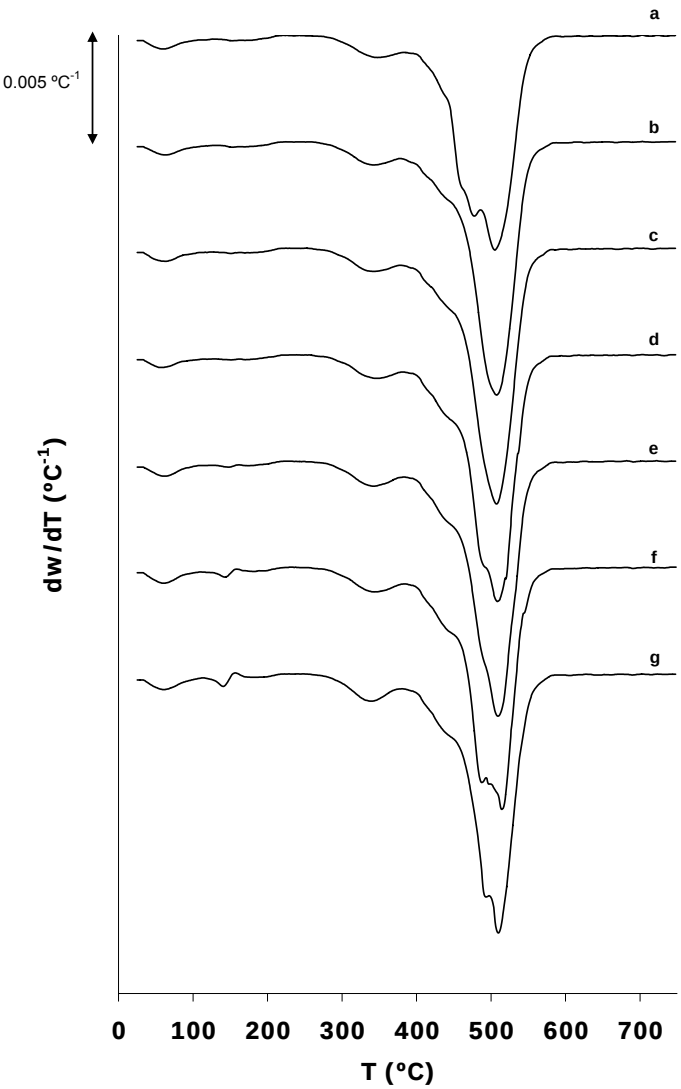

Figure 13 DTG curves of the Nafion membranes submerged in water and methanol binary mixtures at 35ºC: (a) Nafion, (b) Water, (c) MeOH 10%, (d) MeOH 20%, (e) MeOH 30%, (f) MeOH 40%, (g) Methanol.

The degradation of the polymer starts around 250ºC. A low intensity process can be observed in the 250ºC – 390ºC region associated to the desulfonation of the side chains of the polymer [39, 41] with a maximum mass loss rate at T_{peak} = 348ºC. Several peaks with low intensity can be observed between 390ºC and 470ºC. According to previous TGA studies, these peaks can be attributed to the degradation of the side chains of the polymer [39, 41, 42, 43]. Finally, two processes (T_{peak}=475ºC and T_{peak}=501ºC) with high intensities can be observed at high temperatures. These processes can be related to the PFTE backbone decomposition [44]. The residual polymer fraction at 750ºC was 0.63 % of the initial mass. All these results are consistent with the values given by other authors [45, 46, 39].

The swelling tests promote changes in the DTG curves in the regions related to the loss of solvent (T<250ºC) and also in regions related to the thermal degradation of the membranes.

The DTG curves in the low temperatures region are plotted in more detail in Figure 14. All the peaks in the DTG curves in the 25ºC – 250ºC region tend to increase at higher methanol concentrations in the solutions. This result is consistent with the increase of solvent absorption which was reported in the swelling tests (see *Figure 2*). However, the peaks in the 100ºC – 250ºC region increase more rapidly than those appearing in the vicinity of 100ºC and the temperature at the maximum degradation rate of this process decreases on increasing methanol concentrations. These results suggest that the absorption of solvent tightly bound to the polymer is promoted by the presence of methanol [39, 47].

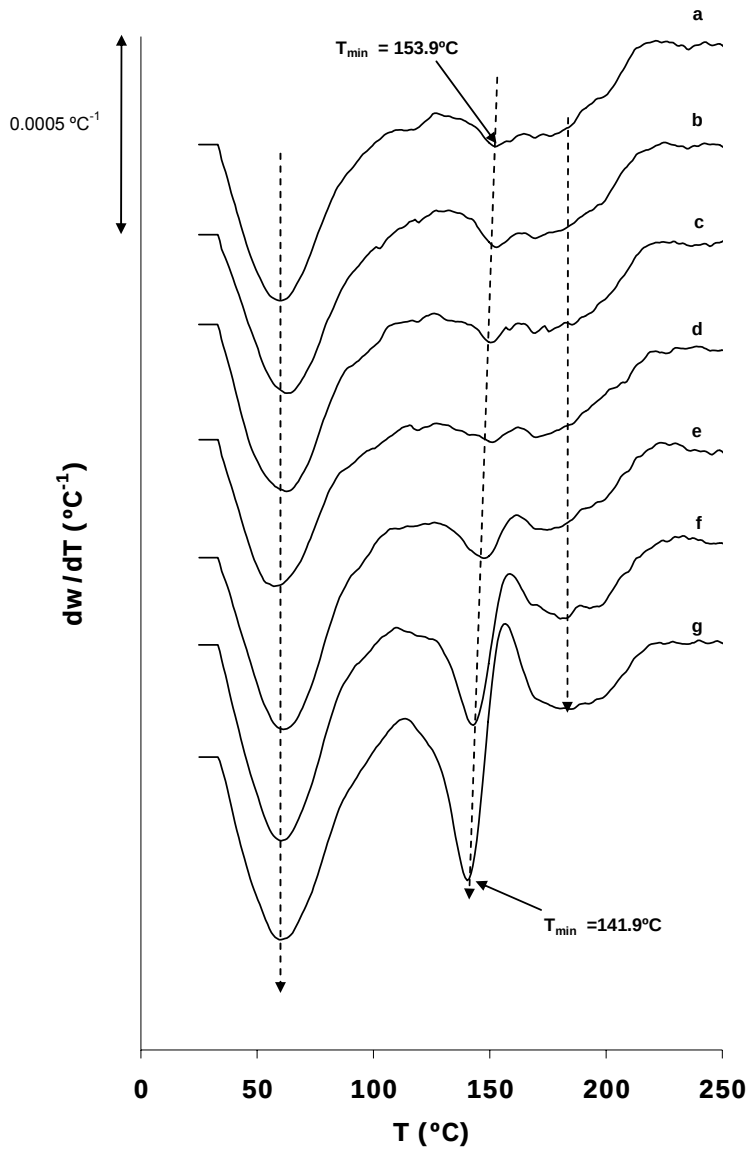

Figure 14 DTG curves of the Nafion membranes submerged in water and methanol binary mixtures at 35ºC. Low temperatures region (T < 250ºC): (a) Nafion, (b) Water, (c) MeOH 10%, (d) MeOH 20%, (e) MeOH 30%, (f) MeOH 40%, (g) Methanol.

The swelling tests also have effects on the thermal degradation of the polymeric groups of Nafion (region 250ºC – 650ºC). In order to study this region in more detail, and due to the presence of several processes overlapping, the DTG curves were fit to five Gaussian peaks. An example of the deconvolution in the region corresponding to the membrane submerged in water is shown in *Figure 15*. The use of five peaks gave a satisfactory fitting in the region (R^2 >0.9990). The values of area, temperature at the maximum intensity (T_{max}), width and maximum intensity ($dw/dT|_{max}$) corresponding to

the individual peaks were calculated. The results of area and T_{max} of the peaks are shown in *Table 6*.

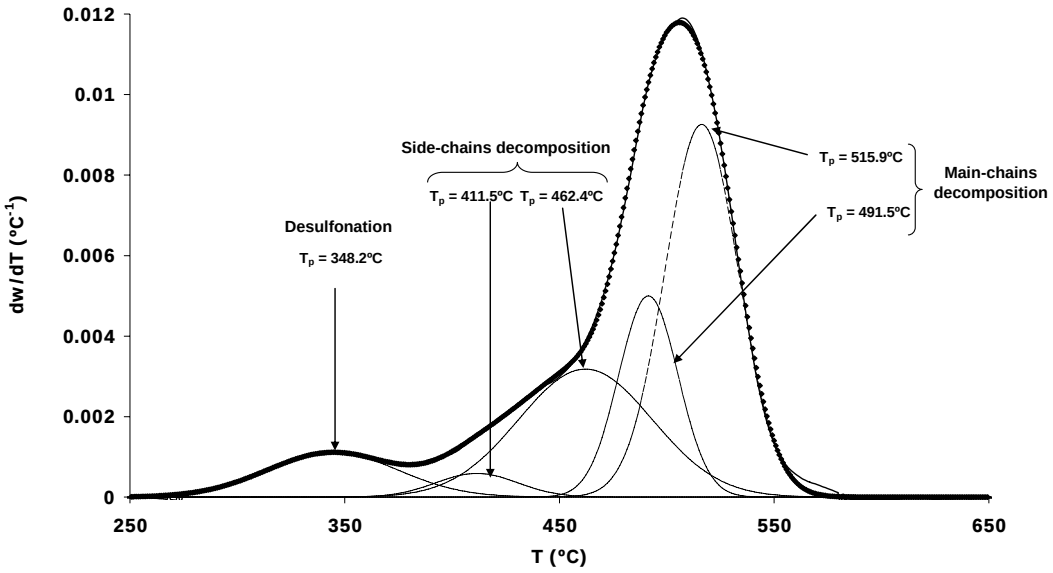

Figure 15 Deconvolution of the DTG curve in the 250º C – 650ºC region (membrane absorbed in water). ◆ corresponds to the experimental points, solid line to the fitted curve and dotted lines to the individual Gaussian contributions.

Table 6. Parameters of the individual peaks corresponding to the deconvolution of the 250ºC – 650ºC degradation region

Sample	Desulfonation process		Side-chains decomposition (low temperatures)	
	T_{peak} (ºC)	Area (%)	T_{peak} (ºC)	Area (%)
Nafion	348	8.17	457	3.24
Water	344	8.48	412	2.81
10% MeOH	343	8.25	412	2.98
20% MeOH	346	8.70	424	2.59
30% MeOH	344	8.98	427	4.60
40% MeOH	341	7.60	448	5.07
Methanol	340	8.01	472	38.74

Sample	Main-chains decomposition (low temperatures)		Main-chains decomposition (high temperatures)	
	T_{peak} (ºC)	Area (%)	T_{peak} (ºC)	Area (%)
Nafion	473	7.05	473	7.05
Water	492	17.34	492	17.34
10% MeOH	492	17.21	492	17.21
20% MeOH	484	6.96	484	6.96
30% MeOH	483	4.66	483	4.66
40% MeOH	486	15.05	486	15.05
Methanol	491	1.98	491	1.98

The desulfonation process (250ºC – 400ºC) and the values of T_{peak} corresponding to the low temperature degradation of the side chains of the membranes submerged in the solutions slightly shift to lower temperatures. These results indicate that the absorption of solvent seems to promote a decrease in the thermal stability of the side chains of Nafion. Moreover in *Table 6* it is also possible to observe an increase in the temperatures corresponding to the maximum degradation rate of the main chains in the swollen membranes. These facts suggest that the degradation of the main chains is somehow retarded after the membranes are submitted to the swelling tests.

Differential Scanning Calorimetry (DSC)

The DSC curves corresponding to the first heating scan of the Nafion membranes submitted to the swelling tests are shown in *Figure 16*. The curves show that the membranes undergo several thermal transitions in the -50ºC - 200ºC temperature region. A broad main endothermic peak can be observed between 20ºC and 120ºC and a secondary thermal process can be detected overlapped at T_2~108ºC.

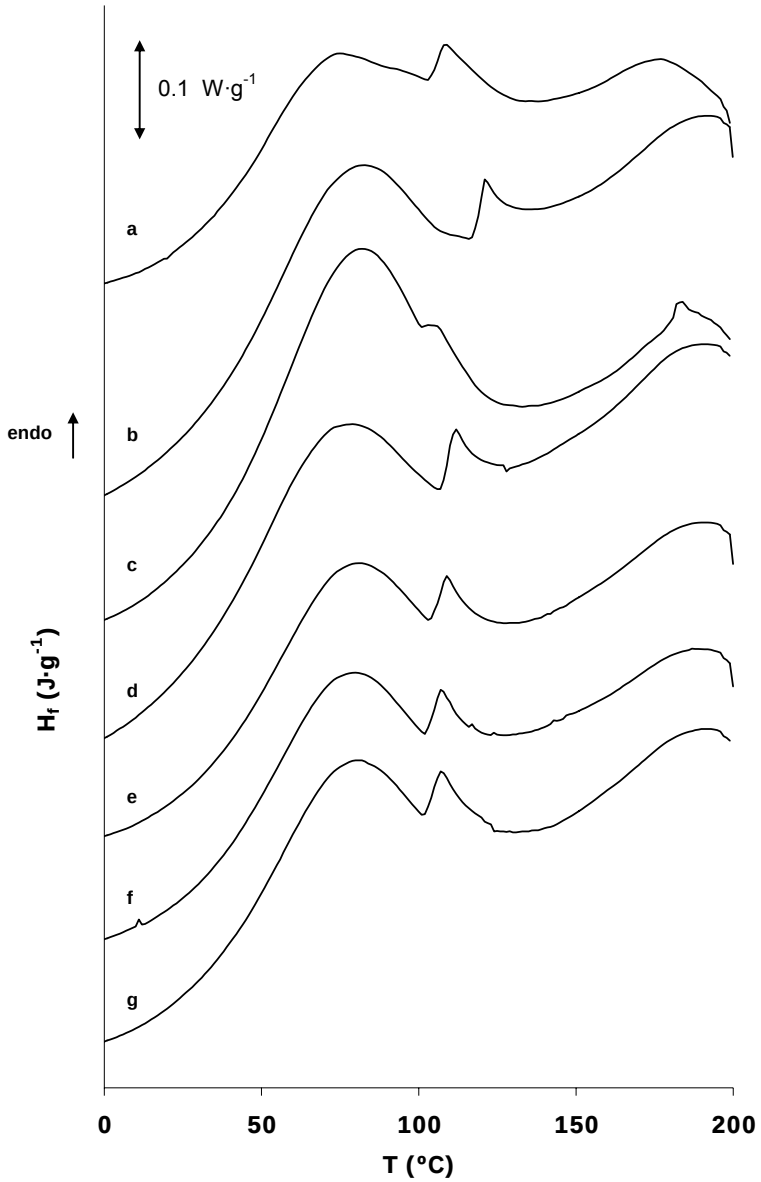

Figure 16 Calorimetric curves corresponding to the membranes submitted to the swelling tests. First heating scan: (a) Nafion, (b) Water, (c) MeOH 10%, (d) MeOH 20%, (e) MeOH 30%, (f) MeOH 40%, (g) Methanol.

Since the main peak cannot be found in the cooling or the second heating scans, it can be attributed to the loss of water or other solvents from the membranes [41]. The maximum of this peak was observed at T_1 = 73ºC for the Nafion membrane. The enthalpy of the process was calculated by using spline baselines in the 0ºC to 150ºC region, obtaining a value of ΔH_1 = 30 J·g^{-1} for the Nafion membrane. The values of ΔH_1 and T_1 corresponding to the swollen samples were also calculated and the results are shown in *Table 7*. As expected, there is an increase in the values of ΔH_1 as the

membranes are submitted to the swelling tests. Neither the values of the enthalpies (ΔH_1) nor the values of the temperature peak (T_1) follow a clear tendency within the series.

Table 7. Summary of calorimetric results. Membranes submitted to the swelling tests.

Sample	T_1 (ºC)	ΔH_1 ($J \cdot g^{-1}$)	T_g (ºC)	ΔC_p ($J \cdot g^{-1} \cdot K^{-1}$) $\cdot 10^2$
Nafion	73	29.9	105	7.06
Water	77	76.9	109	9.32
10% MeOH	80	79.6	107	8.18
20% MeOH	73	72.8	102	8.26
30% MeOH	75	75.3	100	7.06
40% MeOH	74	73.9	100	6.92
Methanol	75	75.3	98	6.26

Finally, a third endothermic process can be detected in the 100ºC – 200ºC region, centred at T_3~178ºC, suggesting that more than one process would appear overlapped in this temperature region. Other authors reported some thermal transitions related to the perflourinated matrix of Nafion at the same range of temperatures (around 200ºC), including the melting of the crystalline PTFE regions [45] or an apparent glass transition of the polymer backbone (T_g ~ 179ºC) [48]. However, since this process also appears at the same temperature region as one of the degradation steps in the TG and DTG curves (see *Figure 14*), it could also be related to the desorption of solvent tightly bound from the polymer structure [40, 41].

There are not noticeable thermal transitions or changes in the curves corresponding to the cooling scan of the membranes, which is in good agreement with other previous studies performed in the region [49].

Figure 17 shows the DSC thermograms corresponding to the second heating scans of the Nafion membranes. All the thermograms show similar shapes to the curve corresponding to Nafion. A process is visible in the 100ºC region which other authors

previously attributed to a glass transition of the polar phase of Nafion [39, 45, 50]. The appearance of this transition in all the samples indicates that the membranes maintain their cluster morphology after being submitted to the swelling tests within all the composition range studied.

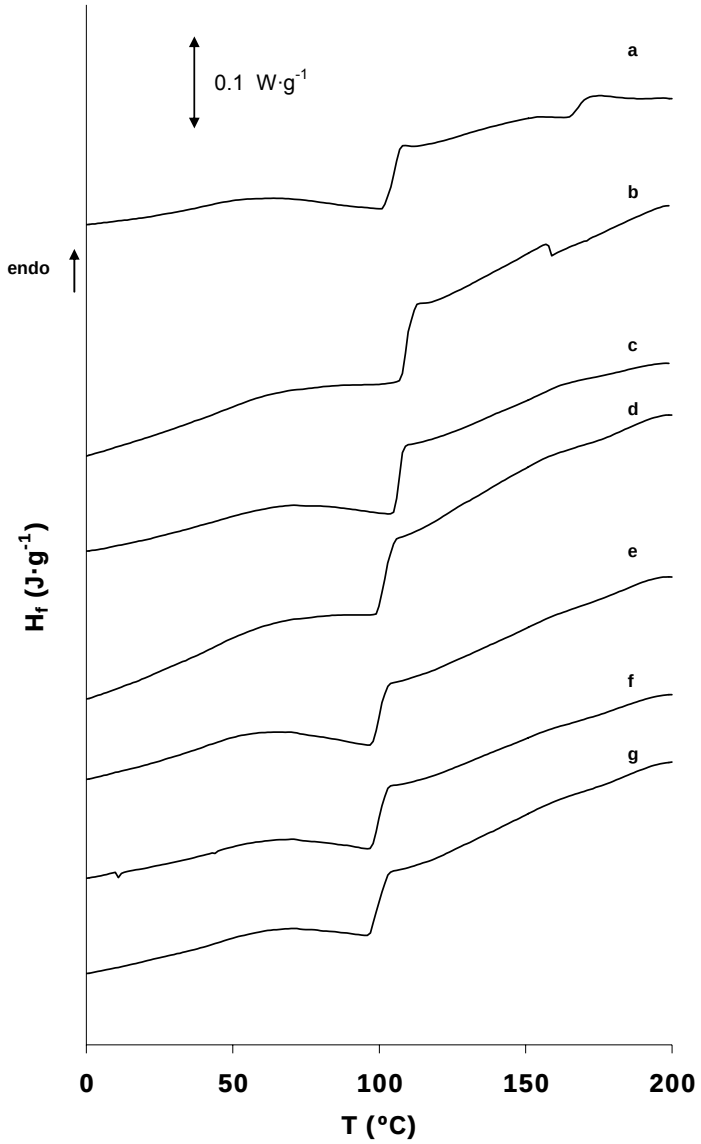

Figure 17 Calorimetric curves corresponding to the membranes submitted to the swelling tests. Second heating scan: (a) Nafion, (b) Water, (c) MeOH 10%, (d) MeOH 20%, (e) MeOH 30%, (f) MeOH 40%, (g) Methanol.

The values of the glass transition temperature (T_g) and of the change of the specific heat coeffient (ΔC_p) were calculated and are shown in *Table 7*. The values of T_g have been

also plotted in *Figure 18*. The samples submerged in pure water and in the 10%MeOH solution show higher T_g values than the Nafion membrane. However, the values of T_g decrease at higher methanol concentration with a certain asymptotic tendency to the value of the sample submerged in pure methanol (T_g = 105ºC). On the other hand, the values of ΔC_p tend to decrease with the concentration of methanol in the binary mixtures. Since Nafion consists of a phase separated system comprising polar and non-polar regions, it is expected that the size and distribution of the clusters tend to minimize the interfacial force between these regions [45, 51]. In the sample submerged in pure water, the increase in the magnitudes of the thermal transitions associated to the polar phase suggests that the absorption of water molecules through the Nafion membranes promotes an increase in the clusters size following a coalescence process. On the other hand, the reduction in the values of T_g and ΔC_p observed for the samples submerged in the binary mixtures with higher methanol concentrations suggest that the coalescence of ionic domains are somehow inhibited in the presence of methanol.

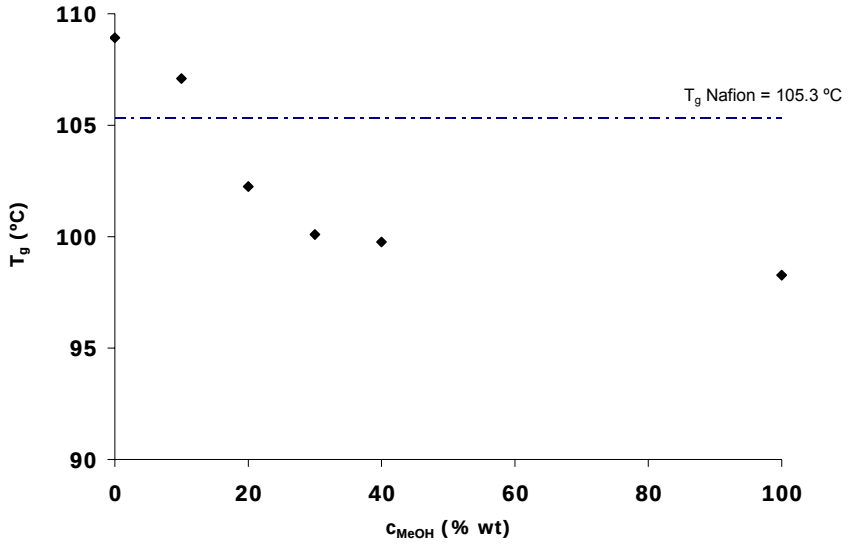

Figure 18 Values of T_g corresponding to the second heating scan curves of the membranes submitted to the swelling tests.

Conclusions

Commercial samples of Nafion membranes submitted to absorption tests in water exhibited a typical Fickian behaviour. However, the absorption of methanol and its binary mixtures with water showed a more complex behaviour. The values of mass flux indicated that the absorption of solvent was faster in the solutions containing methanol than in pure water.

In the swollen membranes the IR stretching and bending vibration regions of the OH groups (3000 cm^{-1} and 1650 cm^{-1}, respectively) changed with the composition of the solutions. The strength of the interactions between the solvent and the hydrophobic groups of Nafion increased on increasing methanol concentrations, while the opposite effect was observed for the interactions between the solvent and the polar regions. The variations in these bands illustrated the effect of the solvent composition in the molecular environment of the polymer groups of the membranes. Therefore, these bands can be used as reference to study the effect of the polymer groups in the transport mechanisms of the solvents through the membranes and thus to study crossover.

A decrease in the thermal stability of the degradation of the side chains corresponding to the samples submitted to the swelling tests was observed. Moreover, two sorts of solvent were found absorbed in the membranes: free or loosely absorbed solvent in the membranes and tightly bound solvent. The results indicate that the amount of bound solvent increased gradually with the methanol concentration in the binary mixtures.

The cluster morphology of the polymers was maintained in the membranes submitted to the swelling tests. However, some variations observed in the transitions related to the polar phase suggest that the composition of the solvent could change the morphology of the clusters in Nafion. This change of morphology could be responsible for the difference in the mechanisms observed for the absorption of methanol and water through Nafion and could explain the high degree of crossover observed for these membranes operating in DMFC.

References

1. Blomen, L. *Fuel Cell Systems*, Ed. Plenum Press, New York, (1993)
2. Grot, W.G. Macromol. Symposia 82 (1994), 161
3. Mauritz, K.A.; Moore, R.B. Chem. Rev. 104 (2004) 4535
4. Elmér, A.M.; Jannasch, P. J. Polym. Sci. Part B: Polym. Phys. 44 (2006) 2201
5. Larminie, J.; Dicks, A. *Fuel Cell Systems Explained*, 2nd Ed., Wiley: New York, 2003
6. William Y. Hsu and Timothy D. Gierke J. Memb Sci 13 (1983) 307
7. Fujimura, M.; Hashimoto, T.; Kawai, H Macromolecules 14 (1981) 1309
8. Horkay, F.; Zrinyi, M. Macromolecules 15 (1982) 1309
9. Dreyfus, B.;Gebel, G.;Aldebert, P.;Pineri, M.;Escoubes, M J.Phys (Paris) 51(1990) 1341
10. Litt, M.H. Polym Prepr. 38 (1997) 80
11. Haubold, H.G.; Vad, Th.; Jungbluth, H.; Hiller, P. Electrochim. Acta 46 (2001) 1559
12. Rubatat, L.; Rollet, A.L.; Gebel, G.; Diat, O. Macromolecules 35 (2002) 4050
13. Kumar, S.; Pineri, M. J. Polym. Sci. Part B: Polym. Phys. 24 (1986) 1767
14. Yeager, H.L.; Steck, A. J. Electrochem. Soc. 128 (1981) 1880
15. Urban, W. *Attenuated Total Reflectance Spectroscopy of Polymers, theory and Practice*, , American Chemical Society, Washington, DC (1996)
16. Tury, A. *Thermal Characterization of Polymeric Materials* Vol 1, Academic Press, San Diego (1997)
17. Vieth, W. *Diffusion in and through polymers, principles and applications* Hanser Publishers (1991)
18. Venturi, M.T. J. Mol. Struct. 14 (1972) 293
19. Hietala, S.; Maunu, S.L.; Sundholm, F. J. Polym. Sci. Part B: Polym. Phys 38 (2000) 3277
20. Saarinen, V.; Kreuer, K.D.; Schuster, M.; Merkle, R.; Maier, J. Solid States Ionics 178 (2007) 533
21. Comyn, J. *Polymer Permeability*; Springer: New York, (1985)
22. Neogi, P. *Diffusion in Polymers* Marcel Dekker, Inc, New York, (1996) p 186
23. Ren, X.; Springer, T.E.; Zawodzinski, T.A.; Gottesfeld, S. J. Electrochemical society 147 (2000) 466
24. Daniel T. Hallinan Jr, D.T.; Elabd Y.A. J. Phys. Chem. B. 111 (2007) 13221
25. Falk, M. Can. J. Chem. 58 (1980) 1495
26 Quezado, S.; Kwak, J.C. T.; Malk, M. Can. J. Chem. 62 (1984) 958
27. Ostrowska1, J.; Narebska, A. Colloid. Polym. Sci. 261 (1983) 93
28. Buzzoni, R.; Bordiga, S.; Ricchiardi, G.; Spoto, G.; Zecchina, A. J. Phys. Chem. 99 (1995) 11937
29. Zundel, G. *Easily Polarizable Hydrogen Bonds-Their Interaction with the Environment-IR Continuum and Anomalous Large Proton Conductivity*, in: the Hydrogen Bond-Recent Developments in Theory and Experiments, Vol II, pp683 ff., P.Schuster, G. Zundel and C. Sandorfy, Eds., North Holland Publ. Co., Amsterdam (1976)
30. Mohr, S.C.; Wilk, W.D.; Barrow, G.M. J. Am. Chem. Soc. 87 (1965) 3048

31. Zundel, G. *The Hydrogen Bond* Schister, P. Zundel, G. Sandorf, C.,Eds.; Amsterdam, (1979) pp 683

32. *The hydrogen bond*, Freeman and Company, (1960) p. 83

33. Dimitrova, P.; Friedrich, K.A.; Vogt, B.; Stimming, U. J. Electroanal. Chem. Interfac. Electrochem. 532 (2002) 75

34. Luan, Y.; Zhang, Y.; Zhang, H.; Li, L.; Li, H; Liu, Y. J. Appl. Polym. Sci. 107 (2008) 396

35. Heitner-Wirguin, C. Polymer 20 (1979) 371

36. Eisenberg, A. *In perfluorinated Ionomer Membranes*, American Chemical Society, Washington DC (1982) p 139

37. Cable, K.M.; Mauritz, K.A.; Moore, R.B. J. Polym. Sci. Part. B: Polym. Phys. 33 (1995) 1065

38. Falk, M. *In. Perfluorinated Ionomer membranes*, Eisenberg, A., Yeager, H.L., Eds.; ACS Symposium Series 180: Americal Chemical Society: Washington, DC, (1982) p 139

39. de Almeida, S.H.; Kawano, Y. J. Therm. Anal. Calorim. 58 (1999) 569

40. Duplessix, R.; Escoubes, M.M M. Rodmacq, B.; Volino, F.; Roche E.; Eisenberg, A. M Pineri M. *Water in Polymers*, Rowlands ACS Symposium Series 127; ACS Washington DC (1980) p 469

41. Sun, L.; Thrasher, J.S. Polym. Degrad. Stab 89 (2005) 43

42. Shao, Z.G.; Joghee, P; Hsing, I.M. J. Memb. Sci. 229 (2004) 43

43. Wilkie, C.A.; Thomsen, J.R.; Mittleman, M.L. J. Appl. Polym. Sci., 42 (1991) 901

44. Tiwari, S.K.;. Nema, S.K.; Agarwal, Y.K. Thermochim. Acta 317 (1998) 175

45. Stefanithis, I.D.; Mauritz, K.A. Macromolecules 23 (1990) 2397

46. Feldheim, D.L.; Lawson, D.R.; Martin, C.R. J. Polym. Sci. Polym. Phys. 31 (1993) 953

47. Young, S.K.; Trevino, S.F; Beck Tan, N.C. J. Polym. Sci. Part B: Polym. Phys. 40 (2002) 387

48. Moore III, R.B.; Martin, C.R.; Macromolecules 22 (1989) 3594

49. Corti, H.R.; Nores-Pondal, F.; Buera, M.P. J. Power Sources 161 (2006) 799

50. Yeo, S.C.; Eisenberg, A. J. Appl. Polym. Sci. 21 (1997) 875

51. Gebel, G. Polymer 41 (2000) 5829

3 CONCLUDING REMARKS

The methods used in this chapter have been useful in obtaining information about the effect of the absorption of water and methanol mixtures in commercial Nafion membranes.

The swelling tests have revealed information about the absorption of the solvents in the membranes. The sampling frequency is sufficiently high at the beginning of the test to study the linear stage of absorption, and the experiment duration (one week) ensures the materials reach equilibrium , but without an excessive investment of time. However, it may be interesting to monitor the first stages of absorption in further detail, particularly due to the high values of diffusivity shown by the materials. With this in this mind, some experiments have been proposed which will study the absorption of solvent continuously by using gravimetric and FTIR measurements.

The combination of FTIR, TGA and DSC techniques has provided information about the state of the solvent, the phase separated morphology and the interactions between the polymer groups and solvent molecules. As mentioned elsewhere in this thesis, all these data are extremely important in understanding and reducing the crossover phenomenon in *DMFC*.

The study of the FTIR band at 3000 cm^{-1} provided important information about the interactions between solvent and the polymer, and also between the solvent molecules. The different regions inside the band can be associated with the cluster structure. This information will be useful in understanding similar materials. The variations in the OH band (position and intensity) have been related to variations in the FTIR bands of ionic and non-ionic groups.

The TGA results have provided relevant information about the state of solvent from the desorption temperatures ($T \leq 100ºC$) and ($T > 100ºC$). The methodology based on the study of the DTG curves and their deconvolution is readily applicable to similar polymeric systems. The differentiation of the different regions, desulfonation, degradation of side-chains and degradation of main chains is reproducible in other materials used as Polymeric Electrolytes Membranes (*PEM*), due to two main reasons:

- The main chains are most usually coupled with the side chains (or with the crosslinkers) by an ester bond.

- Most of the *PEM* materials use sulfonic acid groups as the proton conductive sites, which means that it is possible to compare the stability of the system (and to some extent the interactions of this group) by studying the onset of the decomposition of this group.

The cluster transition and the phase separated morphology have been studied by means of DSC. The influence of the absorption of water, methanol and their binary mixtures in the commercial materials has provided a model for future studies on self-made membranes.

The four techniques used in this chapter have been combined to provide detailed description of a commercial membrane and the effect of the absorption of solvent and its composition on its structure. The techniques require low cost and time, and the methodology of analysis can be applied in further investigations.

REFERENCES CHAPTER 3

1. Horkay, F.; Zrinyi, M. Macromolecules 15 (1982) 1306

2. Litt, M.H. Polym Prepr. 38 (1997) 80

3. Kumar, S.; Pineri, M. J. Pol. Sci. Part B: Polym. Phys. 24 (1986) 1767

4. Hsu, W.Y.; Gierke, T.D. J. Memb. Sci 13 (1983) 307

5. Fujimura, M.; Hashimoto, T.; Kawai, H. Macromolecules 14 (1981) 1309

6. Dreyfus, B.; Gebel, G.; Aldebert, P.; Pineri, M.; Escoubes, M. J.Phys (Paris) 51(1990) 1341

7. Haubold, H.G.; Vad, Th.; Jungbluth, H.; Hiller, P. Electrochim. Acta 46 (2001) 1559

8. Rubatat, L.; Rollet, A.L.; Gebel, G; Diat, O. Macromolecules 35 (2002) 4050

9. DeLuca, N.W; Elabd, Y.A. J. Polym. Sci. Part B: Polym. Phys. 44 (2006) 2201

10. Yeager, H.L.; Steck, A. J. Electrochem. Soc. 128 (1981) 1880

11. Falk, M. Can. J. Chem. 58 (1980) 1495

4

Preparation and Thermal Characterisation of Liquid Crystals Dispersed on a Cellulose Acetate substrate

1 SUMMARY

In Polymer Dispersed Liquid Crystals (*PDLC*) low molecular weight liquid crystals are dispersed in a polymer matrix [1]. *PDLC* are easily prepared and the use of a polymeric matrix reduces the cost of the final material. In theory, the polymer substrate is used simply to provide mechanical stability and obtain self-standing films, while the liquid crystal provides functionality. In a *PDLC*, phase separation occurs and the liquid crystal acts as a dispersed phase in the polymer matrix, and is some respects may be considered analogous to the clusters structure of Nafion.

However, in real *PDLC* the presence of interactions between the components leads to deviations from the expected behaviour [2, 3]. Examples of such interactions are shown in *Figure 4.1*.

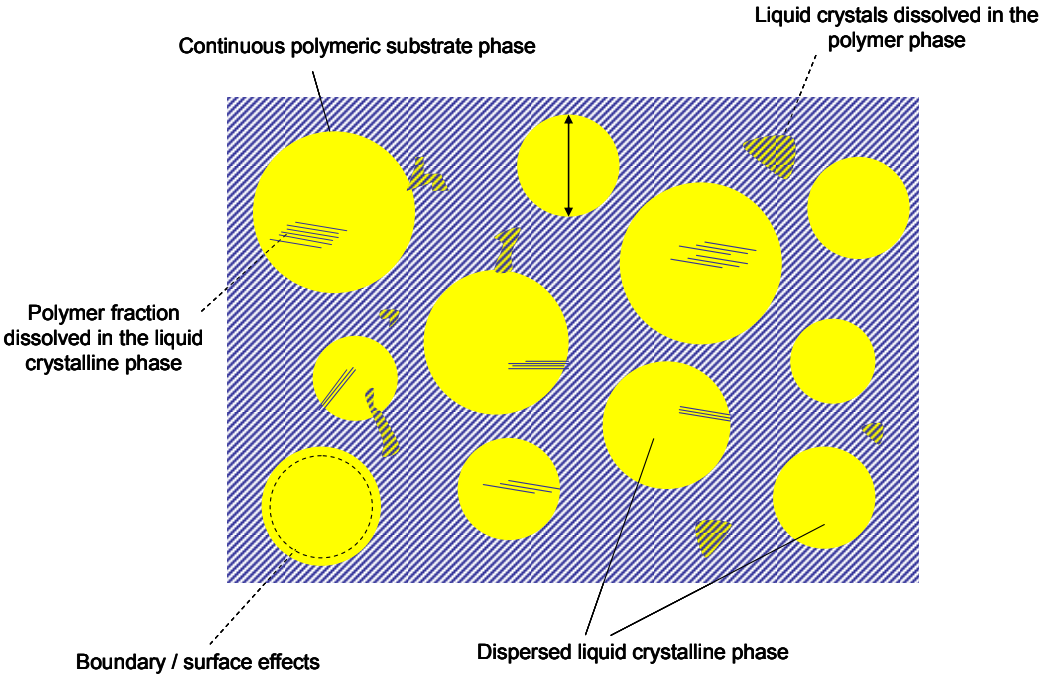

Figure 4.1 Phase morphology of a real PDLC

In *Figure 4.1* it can be seen that the different components may be solubilised in the other phase, depending on their miscibility. The existence of multicomponent phases can cause deviations from the expected behaviour of the individual components. The mobility of the liquid crystals dissolved in the polymer substrate may be strongly restricted, due to the existence of interactions with the polymer groups or for steric

reasons. For this reason, it is expected that a fraction of the liquid crystal will not contribute to the liquid crystalline behaviour of the material. Similar effects can be found for the liquid crystal at the boundary with the polymeric substrate (dotted lines in *Figure 4.1*). Several studies have shown that the molecules close to the interface may suffer from anchoring or surface effects by the existence of interactions with the neighbouring polymer groups [4, 5]. Moreover, if some of the polymer chains are dissolved in the liquid crystalline phase, the behaviour of the liquid crystal can be seriously affected. The interactions with the polymer can cause differences or and even inhibit the liquid crystal behaviour.

The substrate can also be affected by liquid crystals which dissolve in the polymer. The glass transition temperature, the crystallinity, and the stability are among the physical-chemical parameters of the polymer which can be significantly changed by the presence of liquid crystal [6].

Thus it is very important to study the physical properties of *PDLC* prior to their use. In this chapter new polymer dispersions of commercial liquid crystals have been prepared for their potential use as electrolytes in Direct Methanol Fuel Cells (*DMFC*). The materials were characterised by Differential Scanning Calorimetry (DSC) and Thermogravimetric Analysis (TGA).

Two different liquid crystals, cholesteryl oleyl carbonate (*COC*) and (4-methoxybenzylidine)-4-*n*-butylaniline (*MBBA*), were dispersed in a cellulose acetate (*CA*) substrate. The chemical structures of the three components are shown in *Figure 4.2*.

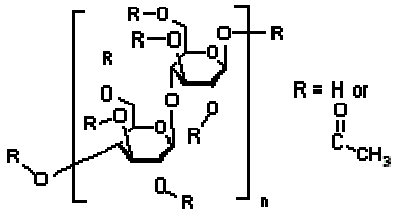

(a) Cellulose Acetate

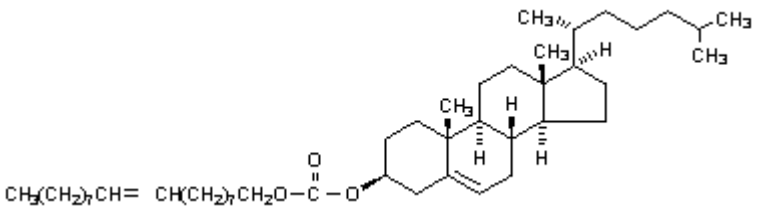

(b) Cholesteryl oleyl carbonate (COC)

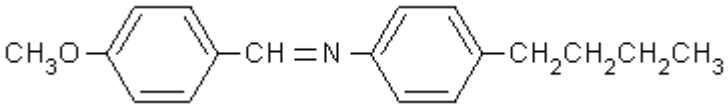

(c) n-(4-methoxybenzylidine)-4-butylaniline (MBBA)

Figure 4.2 Chemical structures of the PDLC components

The main aims of this chapter are:

1. To prepare and characterise new *PDLC* based on *CA* as the polymeric substrate as models for future electrolytes to be used in fuel cells
2. To determine a methodology to study two-phase systems based on thermal analysis.

The preparation of the dispersions was carried out by the solvent evaporation method. The use of this method is advantageous due to its simplicity. However, it is paramount to control the experimental conditions to obtain reproducible results. Two series of *PLDC* have been prepared using *CA* as the polymeric substrate. *COC* and *MBBA* have been used as the commercial liquid crystals. First, *CA* was mixed with acetone and stirred for 1 day at room temperature to form the collodion with a polymer weight concentration of 12%. Then, the liquid crystal was added to the collodion and further stirred during 1 day at room temperature. The amount of liquid crystal was varied to obtain dry films containing concentrations of liquid crystal in the 10 – 70% by weight. The solution containing the collodion and the liquid crystal was then casted on a glass plate for solvent evaporation during several days at ambient conditions.

The characterisation of the films has been carried out by two techniques of thermal analysis: Differential Scanning Calorimetry (DSC) and Thermogravimetric Analysis (TGA).

The DSC curves were obtained following a standard program including one heating ramp, one cooling scan, and a second heating scan, all of them at $10ºC \cdot min^{-1}$. The study of the *PDLC* morphology has been based on the thermal transitions observed in the DSC curves. The pure components have been also characterised. All the thermal transitions observed in the dispersions can be related to those of the pure components. As explained in chapter 2, the DSC and TGA results of the pure components provide a basis to identify possible interactions between the components from deviations between the experimental and what may be considered ideal behaviour.

In the first DSC scans corresponding to the two *PDLC* series it is possible to observe a broad and intense process at low temperatures (T~100ºC) overlapping other transitions. This process has been assigned to the desorption of solvent initially present in the *CA* substrate, due to its highly hygroscopic character (OH groups). Due to the high dispersion of the peak, the study of the solvent content in the membranes was based on the TGA results.

Several transitions are observed in the DSC second heating scan, after the solvent was removed. Thus, the most remarkable differences between the two series are found in the second heating DSC scans. The results show an inhibition of the mesomorphic behaviour in the *MBBA* containing films, while *COC* still maintains its liquid crystalline transitions in the dispersions. It is also seen that in the films containing *COC*, there is little or no modification of the transitions temperatures of the components (liquid crystals and polymer) implying that a clear phase separation has occurred.

Further study using DSC of the liquid crystal transitions revealed that some of the *COC* dissolved into the matrix. The results are interpreted in terms of a certain degree of mixing within the phase separated structure caused by the existence of interactions between the components (see *Figure 4.1*). As expected, the degree of phase separation is found to be concentration dependent.

TGA has been used to study the thermal stability of the films. Heating ramps from 25ºC to 700ºC have been performed at a heating rate of 10ºC·min^{-1} in an Argon atmosphere.

The TGA results also reveal differing behaviours for the two series of films. In general terms the results of the films containing *CA* and *MBBA* deviate greatly from ideal behaviour. Specifically, a dramatic decrease in the thermal stability has been found even at low *MBBA* concentrations. This fact, together with some additional analysis made by NMR spectroscopy, suggests that reactions between the two components occur promoting the decomposition of the liquid crystal.

On the other hand, although the temperature range of the degradation of the *COC – CA* films does not differ with respect to the expected values, there is evidence of some deviations from ideal behaviour. These deviations suggest the existence of interactions at high temperatures which promote a certain increase in the non-degraded fraction of the polymer.

A more detailed study of the polymer decomposition in the *COC – CA* films has been performed. The curves have been deconvoluted in order to separate out the individual contributions, following the methodology described in chapter 2. The DTG peak corresponding to polymer decomposition has been studied through the application of several kinetic methods. The results confirm a change in the polymer decomposition mechanism to a more energetic process. The analysis also suggests that the mechanism of polymer decomposition differs from the random decomposition reaction typically observed for the degradation of long linear polymers.

2 COMMUNICATION

Preparation and thermal characterisation of films containing liquid crystals in a cellulose acetate substrate for externally regulated applications

Preparation and Thermal Characterization of Films Containing Liquid Crystals in a Cellulose Acetate Substrate for Externally Regulated Applications

AQ1 **Alfonso Martínez-Felipe,[1] Enrique Ballester-Sarrias,[1] C. T. Imrie,[2] Amparo Ribes-Greus[1]**

[1]*Instituto de Tecnología de Materiales, Escuela Técnica Superior de Ingeniería del Diseño, Polytechnic University of Valencia, Camino de Vera S/N, Valencia 46022, Spain*
[2]*Department of Chemistry, University of Aberdeen, Meston Walk, Aberdeen Scotland, United Kingdom*

Received 7 May 2009; accepted 15 August 2009
DOI 10.1002/app.31376
Published online 00 Month 2009 in Wiley InterScience (www.interscience.wiley.com).

ABSTRACT: Two different series of polymer dispersed liquid crystal (PDLC) films were prepared for their future use as externally controlled electrolytes in direct methanol fuel cells (DMFC). The liquid crystals used in this work were commercial cholesteryl oleyl carbonate (COC) and *n*-(4-methoxybencylidine)-4-butylanilyne (MBBA); cellulose acetate (CA) was used as the polymer substrate. All the films were characterized by differential scanning calorimetry (DSC) and Thermogravimetric analysis (TGA) to analyze the existence of interactions between the components, the modification of the liquid crystal behavior and the thermal stability of the films. The two series of films exhibited very different behaviors. While the films containing CA and COC maintained most of the properties characteristic of the pure components, including the COC mesomorphism, the analysis of films containing CA and MBBA revealed the existence of strong interactions between the components that promoted the inhibition of the MBBA mesomorphic behavior. © 2009 Wiley Periodicals, Inc. J Appl Polym Sci 000: 000–000, 2009

Key words: differential scanning calorimetry (DSC); thermogravimetric analysis (TGA)

INTRODUCTION

During the last years, direct methanol fuel cells (DMFC) have attracted the interest of many researchers and companies because of their advantages with respect to hydrogen fuel cells.[1,2] Since methanol (MeOH) is liquid at room temperature, fuel storage and transport are less complicated than in hydrogen fuel cells. Furthermore, methanol can also be obtained from renewable sources (bio-alcohols). However, DMFC still present several drawbacks, and their technology is not competitive with other fuel cells or energy conversion devices. One of the most important problems of DMFC is the phenomenon known as crossover. Crossover consists on the transfer of unreacted methanol from the anode to the cathode through the electrolyte and occurs when the polymers used in hydrogen fuel cells are applied to DMFC.[1] This phenomenon causes cell efficiency loss of up the 30%, as the MeOH reacts with the oxygen in the cathode in a conventional combustion reaction, and does not contribute to electrical power generation.

Research in DMFC has been focused in the preparation of new polymer electrolytes that suppress crossover of MeOH to the cathode.[1] However, the transport mechanisms of MeOH are strongly related to the proton conductivity through water in the electrolyte, and the morphology of the polymer constitutes a key factor to control the cell performance. Although a great variety of materials has been tested in DMFC, the results are not improving to a great extent those of the commercial materials used in hydrogen fuel cells.[3–5]

In this work we propose the use of polymer dispersed liquid crystals (PDLC) as electrolytes in DMFC. Liquid crystals (LC) are low molecular compounds that exhibit intermediate states between crystalline solids and isotropic liquids. LC can be oriented in the presence of external stimuli such as electrical and magnetic fields[6,7] and therefore can be externally regulated. In PDLCs, LC form a disperse phase in a polymeric substrate, which allows lowering their cost and increasing some of their mechanical properties. Although the polymer is supposed to act as a mere matrix for the liquid crystal aggregates,[8] most of the PDLC show physical and chemical interactions between LC and the polymers. Such interactions can influence the formation of mesophases[9] and also modify the stability of the

AQ1 *Correspondence to:* A. Ribes-Greus (aribes@ter.upv.es).
Contract grant sponsor: Spanish Ministry of Science and Innovation; contract grant number: ENE2007-67584-C03-01.

J_ID: Z8E Customer A_ID: APP31376 Date: 13-October-09 Stage: Page: 2

polymeric substrate.[10] Therefore it is important to study the effect of mixing on the resulting morphology before their use, since it can lead to the appearance of interactions and to a change in the individual properties of the components.

In this work we used the solvent evaporation method to prepare two different series of PDLCs films containing cholesteryl oleyl carbonate (COC) and *n*-(4-methoxybencylidine)-4-butylanilyne (MBBA) as the LC and cellulose acetate (CA) as the polymer substrate. Thermal analysis was used to determine the materials properties after their preparation. Differential scanning calorimetry (DSC) was performed on the samples to study the thermal transitions of the components in the mixtures. Thermogravimetric analysis (TGA) was carried out to evaluate the influence of mixing on the thermal decomposition of the components and their stability.

EXPERIMENTAL PROCEDURE

Materials

Two series of films were prepared using the same polymeric substrate with two different commercial LC. CA (powder with $M_r \sim 61{,}000$, 40% acetyl groups, provided by Fluka™) was used as the polymer substrate as it is widely used as a component in membranes for separation purposes.[11,12] On the other hand the LC used in the study were COC (98% purity) and MBBA (98% purity) provided by Sigma-Aldrich™, since both compounds exhibit mesomorphism at low temperatures.[13,14] Acetone was used as the solvent in the preparation of the films.

Films preparation

The solvent evaporation method was used to prepare the films containing 10, 20, 30, 40, 50, 60, and 70% in weight percentage of liquid crystal.[15,16] Initially the CA and the acetone were mixed and stirred during 24 hr to obtain the collodion. Then, the liquid crystal was added to the collodion in the corresponding amounts and stirred again. Finally, the solution containing the liquid crystal, the polymer and the solvent were cast onto a glass plate. The samples were dried slowly at room temperature during several days until constant weight was determined. In both series, macroscopic phase separation was observed in the solutions with contents higher than 70% weight in liquid crystal percentage, thus the corresponding films could not be prepared.

Differential scanning calorimetry (DSC)

The DSC thermograms were performed with a Mettler Toledo DSC 822e (supplied by Mettler Toledo, OH, Columbus) analyser. Around 5 mg of the samples were placed into a sealed aluminum pan, and then heated from −100°C to 150°C (first heating scan). Then the samples were held at 150°C for 3 min and cooled to −100°C (cooling scan). Finally, the samples were held for further 3 min at that temperature again, and then reheated to 150°C (second heating scan). All the scans were performed at a heating rate of 10°C/min under nitrogen atmosphere with a flow rate of 50 mL/min.

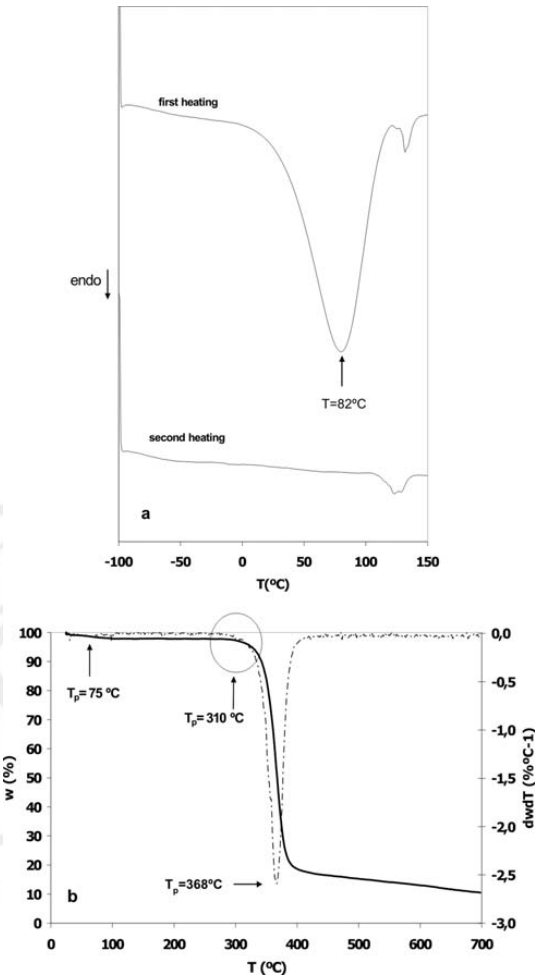

Figure 1 (a) DSC and (b) TG-DTG curves of pure CA. ED1

Thermogravimetric analysis (TGA)

The TGA thermograms were carried out by a Mettler Toledo TGA/SDTA 851 analyser (supplied by Mettler Toledo OH, Columbus). Measurements were performed following a dynamic program from 25 to 700°C at a linear heating rate of 10°C/min under

ID: srinivasanv | Black Lining: [ON] | Time: 16:40 | Path: N:/Wiley/3b2/APP#/Vol00000/091972/APPFile/C2APP#091972

J_ID: Z8E Customer A_ID: APP31376 Date: 13-October-09 Stage: Page: 3

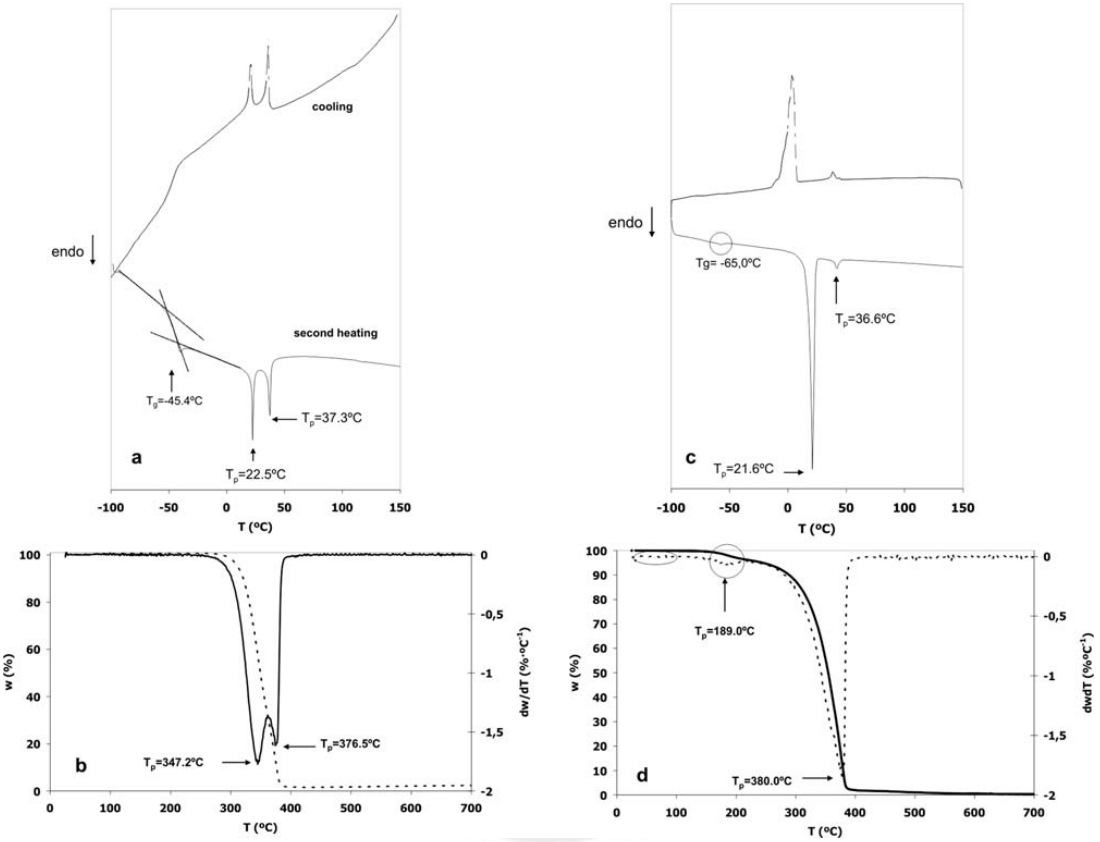

Figure 2 (a) DSC curves of pure COC; (b) TG-DTG curves of pure COC; (c) DSC curves of pure MBBA; (d) TG-DTG curves of pure MBBA.

inert Argon (Ar) atmosphere with a flow rate of 50 mL/min. Sample masses were around 5 mg.

RESULTS AND DISCUSSION

Pure CA

F1 Figure 1(a) shows the DSC thermograms corresponding to the heating scans of the pure CA. The first heating scan shows a broad endothermic process centered at $T = 81.6°C$. The enthalpy associated to this transition was calculated by integration of the DSC curve using a baseline, obtaining a value of $\Delta H = 87.1 \pm 0.1$ J g^{-1}. Since this process does not appear in the second heating scan, other authors associated it to the loss of water initially present in the CA.[17,18] A small endothermic peak is observed in the 130°C region with a very low enthalpy change. Since this peak is visible in the two heating scans with similar enthalpy values, it can be related to a reversible process occurring within the structure of the polymer.

The thermogravimetric (TG) and derivative thermogravimetric (DTG) curves of CA are shown in Figure 1(b). The DTG curve shows a main process centered at $T = 376°C$, corresponding to the pyrolysis of the polymer skeleton backbone, and a secondary process centered at $T = 311°C$ that other authors assigned to deacetylation of CA.[18–20] Furthermore, a low weight-loss region appears around 100°C. This peak can be associated to the moisture content in the CA already observed by DSC. The mass loss calculated for this process was $\Delta w = 3.27\%$. The residual fraction of the polymer at 700°C was 10.53%, which is in good agreement with the literature.[18,21,22,23]

Pure COC

The first heating and cooling DSC scans corresponding to the pure COC are shown in Figure 2(a). The F2 glass transition of the liquid crystal is visible at $T_g = -45.4°C$, the smectic to cholesteric transition at $T_{COC\_SC} = 22.5°C$ with $\Delta H_{COC\_SC} = 1.29 \pm 0.1$ J g^{-1},

ID: srinivasanv | Black Lining: [ON] | Time: 16:40 | Path: N:/Wiley/3b2/APP#/Vol00000/091972/APPFile/C2APP#091972

J_ID: Z8E Customer A_ID: APP31376 Date: 13-October-09 Stage: Page: 4

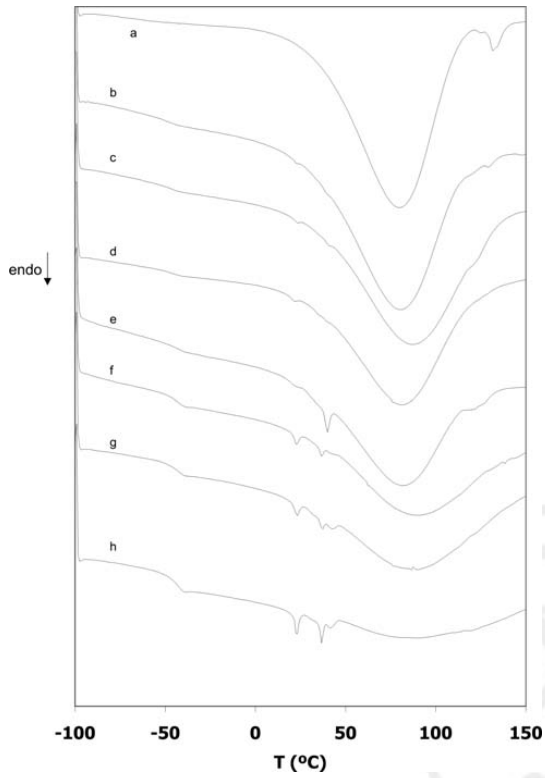

Figure 3 DSC thermograms corresponding to the first heating scan of the samples containing CA and COC: (a) 0, (b) 10, (c) 20, (d) 30, (e) 40, (f) 50, (g) 60, and (h) 70% in weight percentage of COC.

and the cholesteric to isotropic transition at $T_{COC\_CI} = 37.3°C$ with $\Delta H_{COC\_CI} = 1.30 \pm 0.1$ J g^{-1}. The type of mesomorphism was assessed by polarized light microscopy and appraised with literature records.[13]

On the other hand, the TG and DTG curves of COC [Fig. 2(b)] show two processes of decomposition located at $T_{COC\_1} = 345°C$ and $T_{COC\_2} = 376°C$. No significant loss weight in the 100°C region can be observed in the TG curve, which indicates that no moisture or other solvents can be detected in the pure COC sample. The residual fraction of the COC at 700°C was $\Delta w = 2.56\%$.

Pure MBBA

Figure 2(c) displays the DSC thermograms corresponding to the pure MBBA. A small glass transition can be distinguished near $T_g = -65.5°C$. The thermograms also show the phase transitions of the MBBA: the crystalline to nematic transition at $T_{MBBA\_CN} = 21.6°C$ with $\Delta H_{MBBA\_CN} = 46.2 \pm 0.1$ J g^{-1} and the nematic to isotropic transition at $T_{MBBA\_NI} = 36.6°C$ with $\Delta H_{MBBA\_NI} = 1.7 \pm 0.1$ J g^{-1}. The mesomorphism was also assessed by polarized Light Microscopy. The results are in good agreement with the literature.[14]

The TG and DTG curves of MBBA [Fig. 2(d)] show a main asymmetric thermal decomposition process with a maximum at $T_{MBBA\_1} = 380°C$ and a secondary process appearing in the proximity of 189°C (T_{MBBA_2}). A small peak in the 100°C region of the DTG curve indicates the presence of little amounts of solvent in MBBA ($\Delta w = 0.08\%$). The residual fraction of the sample at 700°C was also very low (0.34%).

Films containing CA and COC

Figure 3 shows the DSC thermograms corresponding to the first heating scan of CA, COC, and the CA-COC films containing between 10% and 70% in weight percentage of COC. The thermograms of all the CA-COC films reveal the presence of the endothermic process in the 100°C region, which was previously attributed to the water absorbed in the pure CA. The thermograms also show the process in the

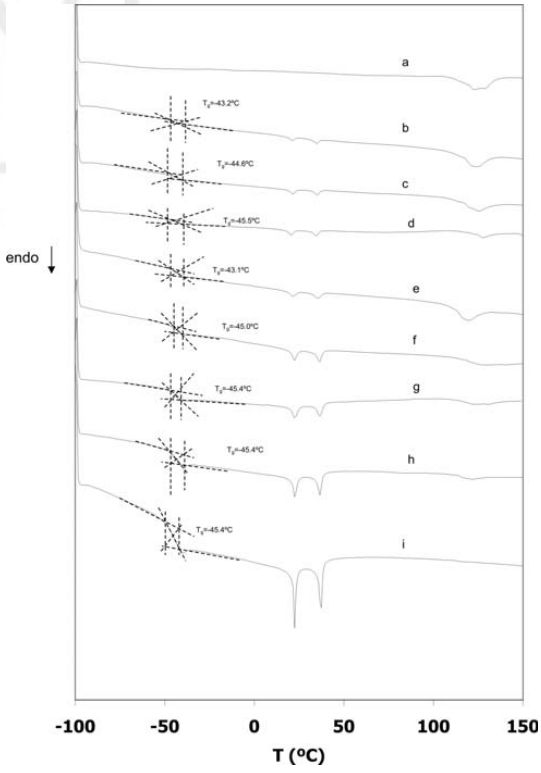

Figure 4 DSC thermograms corresponding to the second heating scan of the samples containing CA and COC: (a) 0%, (b) 10%, (c) 20%, (d) 30%, (e) 40%, (f) 50%, (g) 60%, and (h) 70% in weight percentage of COC.

ID: srinivasanv | Black Lining: [ON] | Time: 16:40 | Path: N:/Wiley/3b2/APP#/Vol00000/091972/APPFile/C2APP#091972

J_ID: Z8E Customer A_ID: APP31376 Date: 13-October-09 Stage: Page: 5

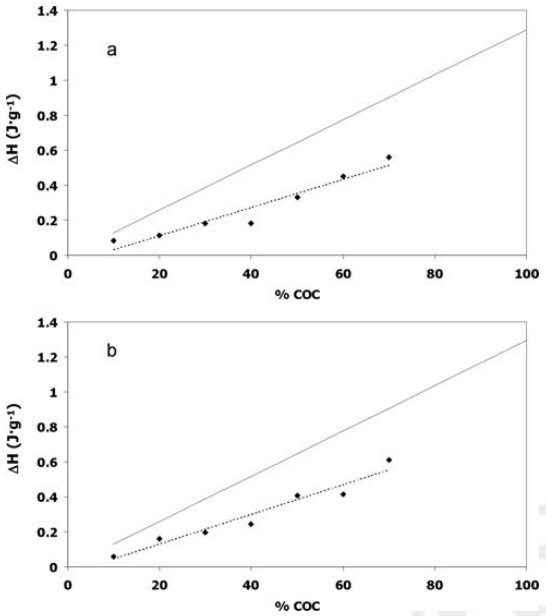

Figure 5 Experimental enthalpies of the COC transitions (◆). The solid lines represent the values considering all the COC contributes to the transition: (a) C→S, (b) S→I transition.

130°C region previously ascribed to CA and discussed above. As expected, the enthalpies corresponding to this process decrease with lower CA percentages in the films, while their T_{max} scarcely changes.

In the same Figure 3 it is also possible to observe two endothermic shoulders at 24°C and 39°C attributed to the COC phase transitions. The study of these transitions in the first heating thermograms can not be carried out as they are overlapped by the endothermic process at 100°C. The glass transition of the liquid crystal is also observed around $T_g = -45$°C in all the composition range. The appearance of all these transitions indicates separation of the components in the films.[24]

F4 Figure 4 shows the curves corresponding to the second heating scan of the films containing CA and COC. The endothermic process related to the water or solvent desorption does not appear, allowing a better observation of the rest of thermal transitions. On the other hand, all the thermograms in Figure 4 show the two phase transitions of COC at $T_{COC\_SC} = 24$°C and $T_{COC\_CI} = 39$°C as well as the glass transition $T_g = -45.4$°C in all the composition range. The appearance of these transitions indicates that the COC maintained its mesomorphic behavior in the films.[17] The mesomorphism of the films was confirmed by polarized light microscopy.

TABLE I
Distribution Coefficient (α), Calculated Using the Enthalpy of the Smectic to Cholesteric (S→C) and Cholesteric to Isotropic (C→I) Transitions in the CA−COC Films

% COC	α (S→C)	α (C→I)
10	0.64	0.46
20	0.43	0.62
30	0.47	0.51
40	0.35	0.47
50	0.51	0.63
60	0.58	0.53
70	0.62	0.67

The enthalpies corresponding to the phase transitions (ΔH_{SC} and ΔH_{CI}) were obtained from the areas of the endothermic peaks in the thermograms in Figure 4. The expected enthalpy values of the transitions ($\Delta H_{exp\_SC} = \Delta H_{COC\_SC} \cdot \frac{\chi}{100}$ for the Smectic to Cholesteric transition SC and $\Delta H_{exp\_CI} = \Delta H_{COC\_CI} \cdot \frac{\chi}{100}$ for the cholesteric to isotropic transition CI) were also calculated based on the enthalpies of the phase transitions observed for the pure COC (ΔH_{COC_SC} and

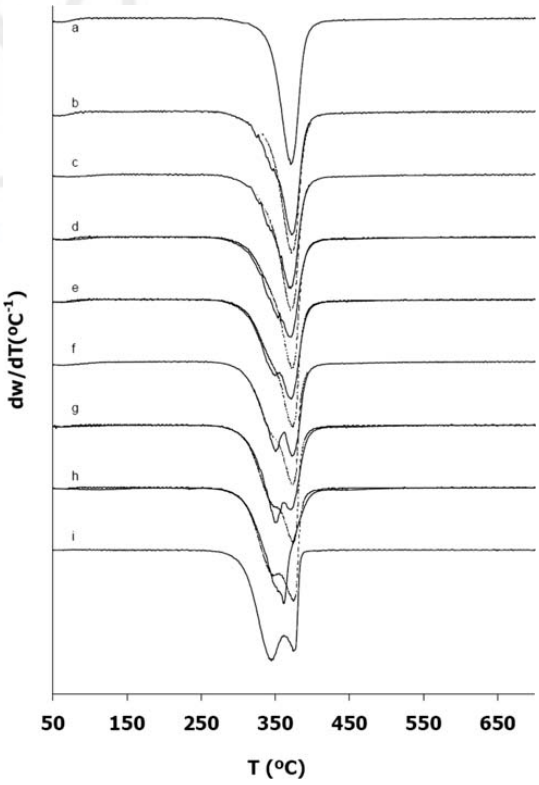

Figure 6 DTG curves of the membranes containing CA and COC: (a) 0, (b) 10, (c) 20, (d) 30, (e) 40, (f) 50, (g) 60, (h) 70, and (i) 100% COC. Dotted lines indicate ideal curves.

ID: srinivasanv | Black Lining: [ON] | Time: 16:41 | Path: N:/Wiley/3b2/APP#/Vol00000/091972/APPFile/C2APP#091972

J_ID: Z8E Customer A_ID: APP31376 Date: 13-October-09 Stage: Page: 6

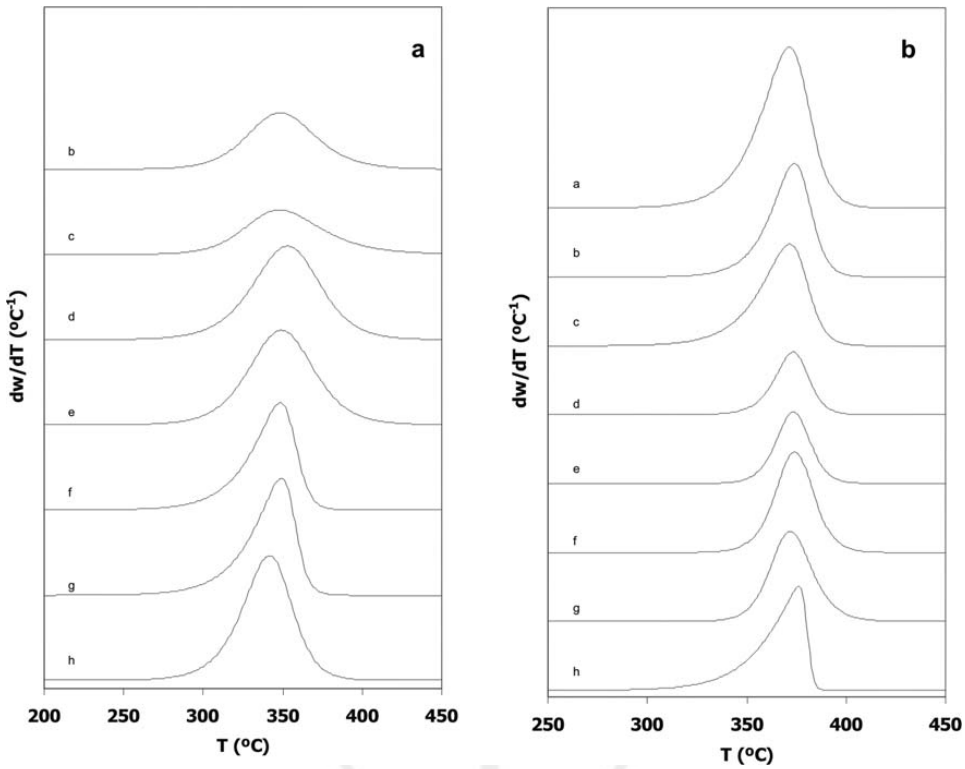

Figure 7 Individual curves corresponding to the deconvolution of the DTG curves of the films containing CA and COC: (a) 0, (b) 10, (c) 20, (d) 30, (e) 40, (f) 50, (g) 60, (h) 100% in COC weight percentage. Figure 7(a) corresponds to the low temperatures peak (peak *b*); and Figure 7(b) to the high temperatures peak (peak *a*).

ΔH_{COC_CI}), where X is the liquid crystal mass percentage in the films ΔH_{exp_SC} and ΔH_{exp_CI} represent the theoretical enthalpy values of the smectic to cholesteric and cholesteric to isotropic transitions in absence of interactions between the components, respectively.

The comparison between the experimental (ΔH_{SC}, ΔH_{CI}) and the expected (ΔH_{exp}) entalphies corresponding to the films containing COC and CA is shown in Figure 5(a,b). As it was expected, ΔH_{SC} and ΔH_{CI} increase at higher COC percentages in the films. However, Figure 5(a,b) evidence differences between the experimental and the expected enthalpies. The deviations between both values in the two transitions indicate that part of the COC does not contribute to the mesomorphism of the films. This behavior was previously reported in other PDLCs and can be attributed to the dissolution of some amount of liquid crystal into the polymer structure.[25,26]

Based on the results of ΔH_{SC}, ΔH_{CI}, and ΔH_{exp}, it is possible to calculate the distribution coefficient

TABLE II
Summary of the Values Corresponding to the Individual Peaks Obtained by Deconvolution of the DTG Curves (CA-COC Films)

	Peak 1/low temperatures				Peak 2/high temperatures			
	Area (%)	T_{peak} (°C)	Width (°C)	Height (°C^{-1})	Area (%)	T_{peak} (°C)	Width (°C)	Height (°C^{-1})
CA					76.94	371.6	28.3	2.331
COC 10%	37.59	348.1	49.2	0.662	44.16	374.0	23.4	1.648
COC 20%	33.43	348.1	55.9	0.524	47.23	371.5	26.7	1.479
COC 30%	61.11	353.0	49.2	1.099	20.52	373.1	20.0	0.908
COC 40%	59.70	349.0	47.6	1.111	23.30	373.2	19.2	1.041
COC 50%	46.04	348.0	30.9	1.259	37.00	374.1	22.6	1.463
COC 60%	48.42	349.2	30.1	1.371	36.06	371.8	24.1	1.308
COC	60.84	341.5	36.6	1.468	38.27	376.5	20.9	1.506

ID: srinivasanv | Black Lining: [ON] | Time: 16:41 | Path: N:/Wiley/3b2/APP#/Vol00000/091972/APPFile/C2APP#091972

TABLE III
Methods Used in the Kinetic Analysis

Method	Expression	Parameters
Criado[a]	$\frac{z(\alpha)}{z(0.5)} = \frac{f(\alpha)g(\alpha)}{f(0.5)g(0.5)}$ Master curves (theoretical)	$f(\alpha)$
	$\frac{z(\alpha)}{z(0.5)} = \left(\frac{T_\alpha}{T_{0.5}}\right)^2 \cdot \frac{(d\alpha/dt)_\alpha}{(d\alpha/dt)_{0.5}}$ Master curves (experimental)	
Coats-Redfern	$\int_0^\alpha \frac{d\alpha}{f(\alpha)} = \ln\left[\frac{g(\alpha)-g(0)}{T^2}\right] = \ln\left(\frac{k_0 \cdot R}{b \cdot E_{CR}}\right) - \frac{E_{CR}}{R \cdot T}$	E_{CR}
Chang	$\ln\left[\frac{d\alpha/dt}{(1-\alpha)^n}\right] = \ln Z - \frac{E_{Ch}}{R \cdot T}$	n, E_{Ch}
Kissinger	$S = \frac{[d^2\alpha/dt^2]_l}{[d^2\alpha/dt^2]_r}$ $n_K = 1.88 \times S$	n_K

[a] $g(\alpha) = \int_0^\alpha \frac{1}{f(\alpha)} d\alpha$. α is the degree of conversion of the individual process.

$\alpha_i = \Delta H_i / \Delta H_{\exp i}$ for each phase transition i, which represents the COC fraction that remains forming a liquid crystalline phase in the films. The values of α for the two transitions observed in the DSC thermograms are displayed in Table I. The results indicate that there is a considerable amount of COC dissolved into the polymer substrate at any composition, revealing some kind of interactions between the liquid crystal and the polymer even at low COC concentrations.[24] These interactions, however, are not high enough to inhibit the COC mesomorphic behavior in the films.

The thermal stability of the films containing CA and COC was studied by TGA. Figure 6 shows their derivative thermogravimetric curves (DTG).

In the films with low COC concentrations it is possible to distinguish a main degradation process ($T_{max} \sim 370$°C) which can be attributed to the decomposition of CA.[18–20] In the DTG curves it is also possible to observe the appearance of new secondary processes at lower temperatures ($T > 280$°C). Such processes increase with the COC content and therefore can be associated to its presence in the films. At COC weight concentrations of 40% and higher, the degradation of the films seems to occur in at least two main steps (at $T_1 \sim 345$°C and $T_2 \sim 370$°C). The intensities and shapes of the two peaks vary with the COC concentration.

In Figure 6 the ideal DTG curves of the CA and COC films have been also plotted (dotted lines). The ideal curves were built by the adjusted

TABLE IV
Summary of the Results of the Kinetic Analysis (CA-COC Films)

	Coats–Redfern/Criado		Chang		Kissinger
Sample	Model	E_{CR} (KJ mol^{-1})	n_{Ch}	E_{Ch} (KJ mol^{-1})	n_K
		High temperature process			
CA	A3/$n = 1$	272	1.2	313	1.2
COC 10%	$n = 1$	331	1.1	368	1.4
COC 20%	$n = 0.75$	245	0.8	262	1.0
COC 30%	$n = 1.5$	497	1.5	514	1.5
COC 40%	$n = 1.5$	522	1.8	575	1.8
COC 50%	$n = 1.5$	460	1.8	508	1.7
COC 60%	$n = 2$	491	2.1	504	2.0
COC	D2	422	0.25	206	0.4
		Low temperature process			
COC 10%	$n = 2$	216	2	218	2.1
COC 20%	$n = 2$	193	2.4	216	2.5
COC 30%	$n = 1.5$	187	1.7	206	1.7
COC 40%	$n = 1.5$	196	1.8	216	1.9
COC 50%	R3	183	0.7	199	0.9
COC 60%	$n = 0.5$	172	0.5	181	0.8
COC	$n = 1.5$	239	1.5	252	1.5

J_ID: Z8E Customer A_ID: APP31376 Date: 13-October-09 Stage: Page: 8

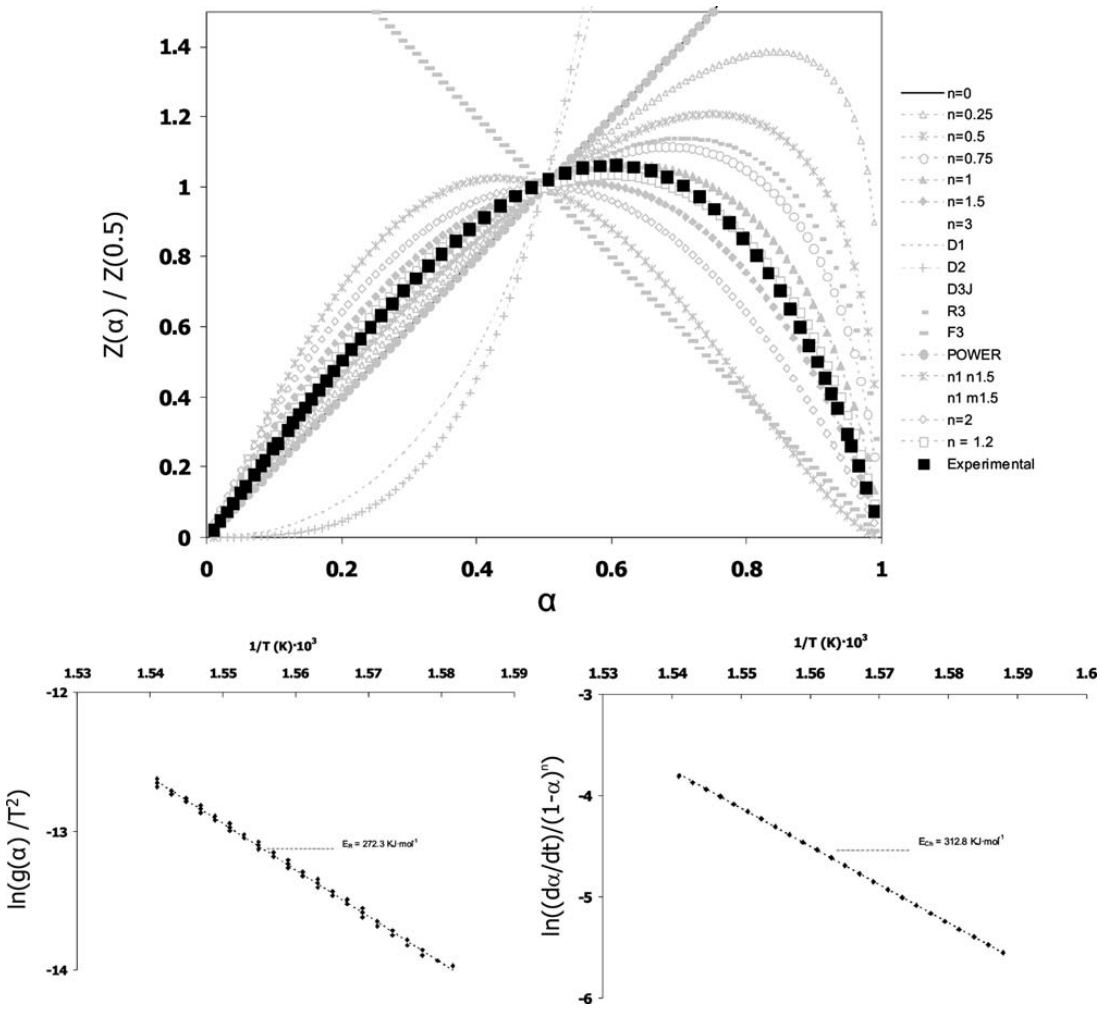

Figure 8 Results of the kinetic analysis applied to the DTG curve of CA: (a) Criado method, (b) Coat-Redfern method, (c) Chang method.

addition of the individual DTG curves of CA and COC at any composition. There are noticeable changes between the experimental and ideal curves shown in Figure 6, suggesting the existence of interactions in the thermal degradation of the CA-COC films.[27] Such interactions are stronger in the films with higher COC contents. This fact suggests the existence of more prominent bulk processes in the degradation of the films with higher COC concentration.[28]

On the other hand, it is worth highlighting that the deviations between the experimental and ideal DTG curves are stronger in the high temperatures range, where the intensity of the DTG experimental curves is lower than expected. It is well-known that the degradation of cellulose and its derivatives can be described as a process of consecutive and competing reactions that can be strongly influenced by the composition.[29,19,20] In this case, the existence of a second phase in the films (evidenced by the DSC results) seems to be responsible for the suppression of some of the decomposition reactions occurring at high temperatures. This fact is coherent with an increase in the residual values at 700°C, which was also observed for all the CA-COC films. All these results suggest that the interactions between CA and COC promote a certain inhibition of the degradation of the polymer substrate.

ID: srinivasanv | Black Lining: [ON] | Time: 16:41 | Path: N:/Wiley/3b2/APP#/Vol00000/091972/APPFile/C2APP#091972

J_ID: Z8E Customer A_ID: APP31376 Date: 13-October-09 Stage: Page: 9

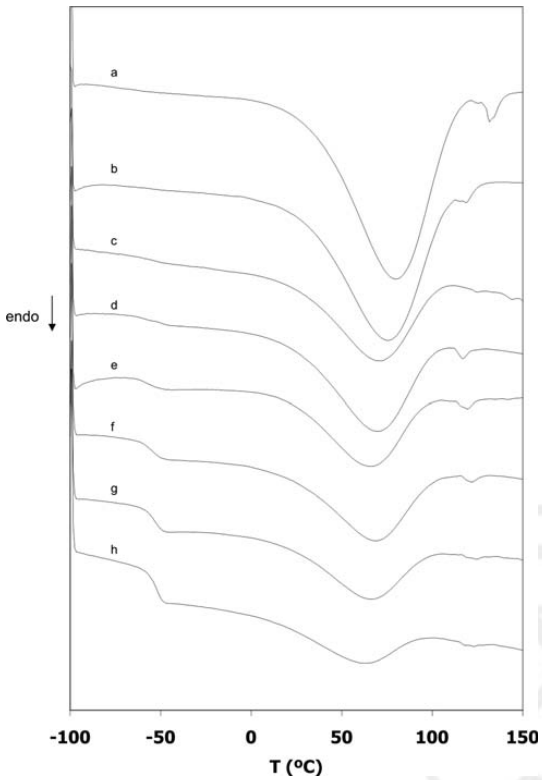

Figure 9 DSC thermograms corresponding to the first heating scan of the samples containing CA and MBBA with: (a) 0, (b) 10, (c) 20, (d) 30, (e) 40, (f) 50, (g) 60, and (h) 70% in weight percentage of MBBA.

As an attempt to perform a more accurate analysis of the thermal degradation of the COC and CA films, the experimental DTG curves were fitted to a sum of asymmetric peaks, according to the following equation:

$$y(x) = y_0 + \sum_{i=1}^{n} A_i \cdot \left(\frac{1}{1+\exp\left(\frac{-(x-x_{ci}+0.5)}{w_{2i}}\right)} \right) \times \left(1 - \frac{1}{1+\exp\left(\frac{-(x-x_{ci}-0.5)}{w_{3i}}\right)} \right)$$

where y_0 is the baseline of the DTG curve, x_{ci} is a position parameter related to the maximum in the curve, A_i is an amplification parameter and w_{2i} and w_{3i} describe the dispersion and symmetry of the individual curve i. All the DTG curves were satisfactorily fitted to two peaks ($n = 2$) except the curve corresponding to the degradation of pure CA, where only one peak was used.

The individual curves at each composition resulting from the deconvolution are shown in Figure 7(a,b) corresponding to the processes at high (peak *a*) and low (peak *b*) temperatures, respectively. As expected, there are slight changes in the individual curves as a function of the COC content. To quantify such changes, the area, temperature of the maximum (T_{peak}) and width at the maximum intensity were calculated by using the OriginLab software for each individual peak. The results are summarized in Table II. F7 T2

At low COC concentrations, it is possible to observe a decrease in the values of area of the peak at high temperatures (peak *a*) when the concentration of CA in the films decreases. However, the values of area of the peak at lower temperatures (peak *b*) are too high to be related only to the degradation of COC. This suggests that part of the CA degrades at temperatures lower than expected. On the other hand, the values of T_{peak_b} of the films are higher than those corresponding to the first COC degradation process ($T_{COC\_1} \sim 345$°C). This fact confirms that, in the decomposition of the films, this process

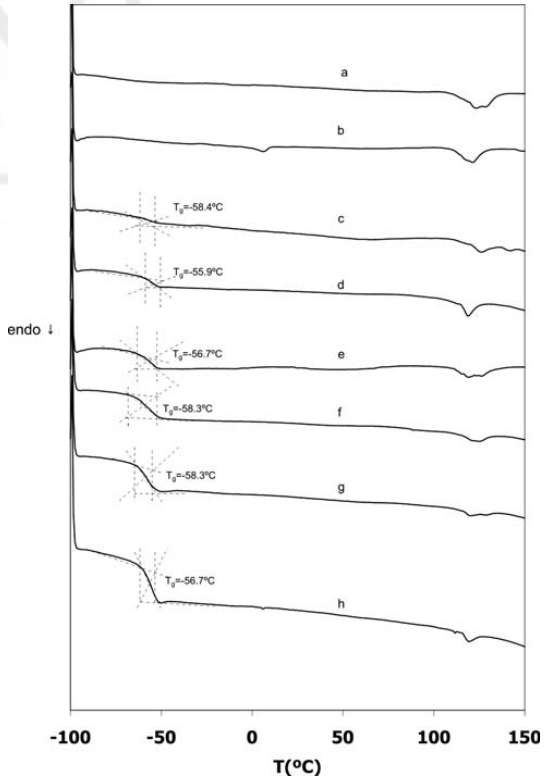

Figure 10 DSC thermograms corresponding to the second heating scan of the samples containing CA and MBBA with: (a) 0, (b) 10, (c) 20, (d) 30, (e) 40, (f) 50, (g) 60, and (h) 70% in weight percentage of MBBA.

ID: srinivasanv | Black Lining: [ON] | Time: 16:41 | Path: N:/Wiley/3b2/APP#/Vol00000/091972/APPFile/C2APP#091972

J_ID: Z8E Customer A_ID: APP31376 Date: 13-October-09 Stage: Page: 10

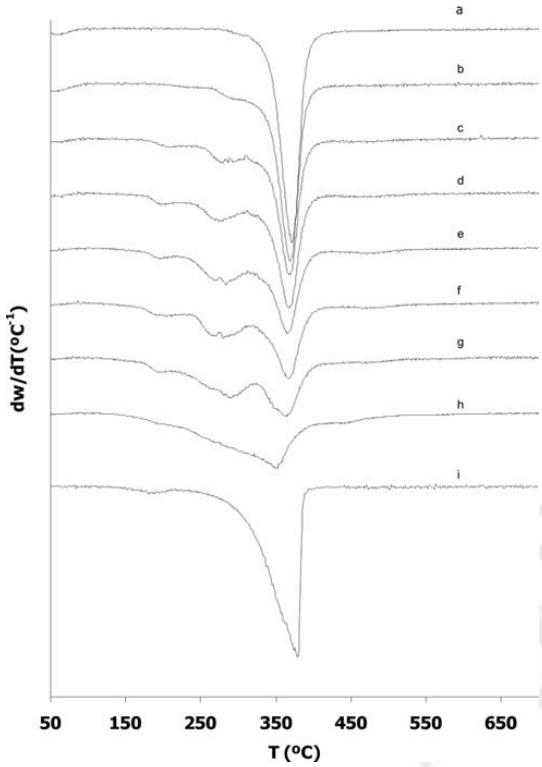

Figure 11 DTG curves of the membranes containing CA and MBBA with: (a) 0, (b) 10, (c) 20, (d) 30, (e) 40, (f) 50, (g) 60, (h) 70, and (i) 100% in weight percentage of MBBA.

may involve the degradation of polymeric chains and not only COC molecules. This result is in agreement with other authors who have previously reported that the existence of low molecular compounds can cause a destabilization of the polymer in PDLCs[29,30]

As it was expected, at high COC concentrations the evolution of the area of peak *b* seems to be more related to the composition of COC in the films. There are not large variations in the temperature range at which this decomposition process occurs. However, it is remarkable that the maximum values of the peak at high temperatures (peak *a*) corresponding to the films appear between those corresponding to the pure components (COC, $T_{COC\_2} \sim 378$°C and CA, $T_{CA} \sim 370$°C). This suggests that the high temperature process may reflect the effect of decomposition of both components

The previous results have shown that the interactions in the thermal degradation of CA and COC promote changes in the shape of the individual decomposition curves, suggesting that the processes of degradation may have changed in the films. To better describe the changes in the thermal degradation of the polymer, the different individual decomposition processes were studied by several methods of kinetic analysis. The Criado method[31] was applied to study the mechanism of decomposition $f(\alpha)$ which best fits to the experimental curves. With that aim, the master curves corresponding to some theoretical models are calculated and compared to those based in the experimental TGA results.

On the other hand, the expression of $f(\alpha)$ of the model which provided the best fit according to the Criado method was used to calculate an apparent activation energy (E_{CR}), by applying the Coats-Redfern method.[32] Additionally, the Chang method,[32] was also applied to estimate the order of the decomposition process, by finding the value of n that provided the best fit of the experimental data and its corresponding activation energy value (E_{Ch}). Finally, the Kissinger method was also used to estimate the values of reaction order (n_K) of the individual processes.[19] The expressions used in the four methods are shown in Table III. T3

The results of the application of the four kinetic methods to the individual curves obtained by deconvolution are summarized in Table IV. The curves T4 corresponding to the application of the methods to the pure CA are shown in Figure 8. F8

TABLE V
Summary of Thermogravimetric Results for the Films containing CA and MBBA

	Main process		Low temperature shoulder 1		Low temperature shoulder 2		High temperature shoulder		
	T_{max} (°C)	Weight-loss (%)	T_{max} (°C)	Weight-loss (%)	T_{max} (°C)	Weight-loss (%)	T_{max} (°C)	Weight-loss (%)	Residual (%)
0	370.8	78.35							10.53
10	369.4	63.52	231.4	1.41	303.1	9.55			16.68
20	368.3	52.54	211.2	4.37	287.2	16.51			20.56
30	368.3	48.94	203.8	4.64	277.8	19.03			22.85
40	367.2	39.77	197.4	4.91	279.8	25.96	467.6	2.33	22.75
50	368.6	36.66	199.2	6.94	279.6	26.16	463.7	6.19	22.58
60	363.7	22.03	197.8	6.23	285.6	36.18	405.2	12.40	22.49
70	351.0	7.39	223.2	11.65	319.7	51.48	443.0	8.88	20.82
100	379.6	94.01	188.0	3.37					

ID: srinivasanv | Black Lining: [ON] | Time: 16:41 | Path: N:/Wiley/3b2/APP#/Vol00000/091972/APPFile/C2APP#091972

J_ID: Z8E Customer A_ID: APP31376 Date: 13-October-09 Stage: Page: 11

According to the Criado method, the curve corresponding to the degradation of pure CA fits very well to an acceleratory process or to a reaction process with values of n slightly higher than $n = 1$ ($n \sim 1.2$) This is in good agreement with the references in which the CA decomposition process is described either as an auto-accelerated process or as a first order process.[21,33,34,35] The values of n calculated by Chang and Kissinger are in good agreement with the Criado method. Despite the slight differences between the activation energies, the values are in good concordance with those reported in the bibliography.[21,33]

However, the reaction order values of peak *a* display values of $n < 1.2$ for the films containing 10 and 20% of COC. Since these processes have been attributed mainly to the degradation of CA, it can be assumed that there is a change in the mechanism of degradation of the polymer in the films, even at low COC concentrations. It is remarkable that the presence of aggregates in the films avoids the random degradation typical in the degradation of long linear polymers.[33,36] The change in the mechanism could also explain the abrupt increase of the residual values. On the other hand, there is a clear increase in the values of n and E_a for this process when the concentration of COC increases in the films. This fact indicates a more complex and energetic degradation mechanism, probably including several species.

Films containing CA and MBBA

The DSC thermograms corresponding to the first heating scan of all the films containing CA and MBBA as well as the pure CA are plotted in Figure 9. All the films containing MBBA exhibit a glass transition in the $T_g \sim -50°C$ region in their first heating scans. All the DSC thermograms also show all the peaks related to CA and previously described. F9

Figure 10 displays the DSC thermograms corresponding to the second heating scans of the films containing CA and MBBA. All the thermograms in Figure 10 show the glass transition in the $T_g \sim -50°C$ region. However, the T_g values in the films are slightly higher than that observed for the pure component in Figure 3 ($T_g = -65.0°C$). On the other hand, unlike happened in the DSC thermograms of the COC-CA films, it is not possible to observe the phase transitions associated to MBBA at any composition.[14] This fact suggests that an inhibition of the F10

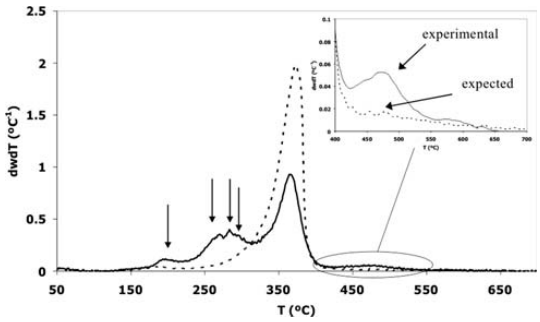

Figure 12 Thermal degradation of the membrane containing 40% of MBBA: (——) experimental and (-----) expected behavior.

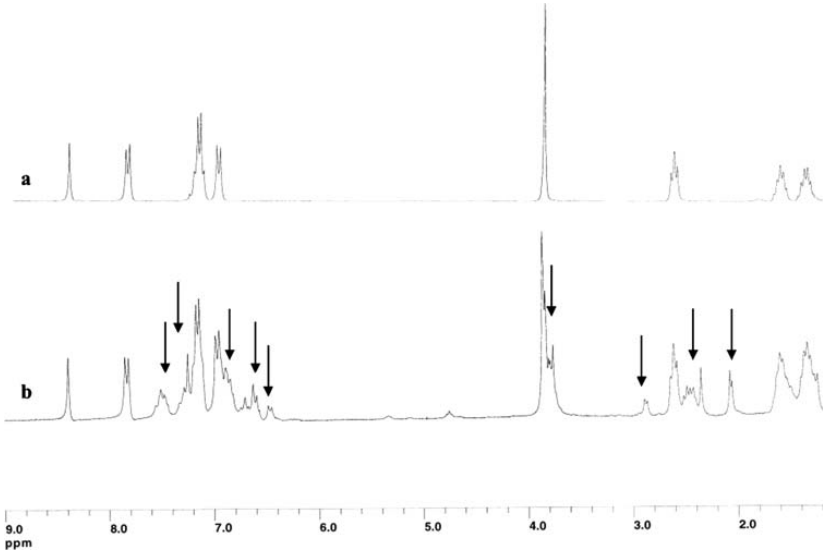

Figure 13 NMR spectra of MBBA: (a) without prior treatment; (b) after extraction from the films.

ID: srinivasanv | Black Lining: [ON] | Time: 16:41 | Path: N:/Wiley/3b2/APP#/Vol00000/091972/APPFile/C2APP#091972

J_ID: Z8E Customer A_ID: APP31376 Date: 13-October-09 Stage: Page: 12

mesomorphic behavior is taking place in these films.[25,26]

The suppression of some of the MBBA transitions studied by DSC suggests that the MBBA is interacting with the CA in the films even at low temperatures.[9] To study whether these interactions can affect the thermal stability, TGA of the films has been carried out.

The derivative thermogravimetric (DTG) curves corresponding to the films containing MBBA and CA are shown in Figure 11. The curves corresponding to the degradation of CA and MBBA are also displayed. The most representative parameters of the TG and DTG curves were calculated and are summarized in Table V. The main degradation process is observed at $T_{max} = 370°C$ and can be assigned to the decomposition of CA, since it appears at the same temperature region than the pure CA.[18–20] The DTG curves also show the appearance of new peaks at low temperatures (200 and 360°C) as well as at high temperatures (400–500°C).

The ideal DTG curves were built following the same procedure previously used for the COC-CA films. An example can be seen in Figure 12. There are significant differences between the DTG experimental and ideal curves of the CA-MBBA films, indicating the existence of strong interactions in the thermal degradation of the components.[27]

The differences between the curves are especially strong in the 200–360°C region. The appearance of the new processes in this region, where none of the individual components are expected to undergo decomposition processes, suggests that other compounds are present in the films. The fact that the weight-loss corresponding to the new shoulders increases with higher MBBA concentrations in the films suggests that compounds could be derived from the MBBA in the films. Nuclear magnetic resonance (NMR) was performed to a sample of MBBA extracted during the formation process of the films (see Fig. 13). The existence of new signals at 7.5, 7.4, 6.8, 6.6, 6.5, 3.6, 2.9, 2.4, and 2.1 ppm confirmed the existence of new compounds in the sample. The existence of such compounds could be responsible for the inhibition of the MBBA mesomorphic behavior studied by DSC[9]

CONCLUSIONS

Two series of PDLC films showed different behaviors depending on the nature of the liquid crystal and its interactions with the polymer substrate.

The films containing CA and COC maintained their mesomorphic behavior in all the range of compositions, indicating that these films behave as genuine PDLC. However, there was evidence of some interactions between the two components which altered the properties of the polymeric and liquid crystalline phases. Such interactions lead to a decrease in the thermal stability of the first stages of decomposition and also to a certain inhibition of the substrate degradation. The mechanisms of the different decomposition stages vary with the concentration of COC.

On the other hand, the presence of strong interactions was observed in the films containing CA and MBBA even at low temperatures. Such interactions promoted the inhibition of the mesomorphic properties of MBBA in these films. This fact was also accompanied by a decrease in the thermal stability of the samples.

Therefore, the membranes containing CA and COC are candidates for their use in electrolytic applications, since they maintain the mesomorphic properties and do not suffer a drastic decrease in their thermal stability, while the films containing CA and MBBA had poor chemical and thermal stability, which lead to a suppression of the liquid crystallinity.

References

1. Blomen, L. J.; Mugerwa, M. N., Eds. Fuel Cell Systems, Plenum Press: New York, 1993.
2. Dyer, C. K. J Power Sources 2002, 106, 31.
3. Kim, D. S.; Parka, H. B.; Rhim, J. W.; Lee, Y. M. Solid State Ionics 2005, 176, 117.
4. Shin, J. P.; Chang, B. J.; Kim, J. H.; Lee, S. B.; Suh, D. H. J Membr Sci 2005, 251, 247.
5. Schauer, J.; Kůdela, V.; Richau, K.; Mohr, R. Desalination 2006, 198, 256.
6. Collings, P. J.; Hird, M., Eds. Introduction to Liquid Crystals. Chemistry and Physics, Taylor & Francis: New York, 1997.
7. Demus, D.; Goodby, J.; Gray, G. W.; Spiess, H. W.; Vill, V., Eds. Handbook of Liquid Crystals. Fundamentals, Wiley-VCH: New York, 1998.
8. Mucha, M. Prog Polym Sci 2003, 28, 837.
9. Crawford, G. P.; Zumer, S., Eds. Liquid Crystals In Complex Geometries Formed by Polymer and Porous Networks, Taylor and Francis: New York, 1996.
10. Filip, D.; Simionescu, C. I.; Macocinschi, D. Polym Degrad Stab 2001, 72, 377.
11. Smitha, B.; Suhanya, D.; Sridhar, S.; Ramakrishna, M. J Membr Sci 2004, 241, 1.
12. Edgar, K. J.; Buchanan, C. M.; Debenham, J. S.; Rundquist, P. A.; Seiler, B. D.; Shelton, M. C.; Tindall, D. Prog Polym Sci 2001, 26, 1605.
13. Lin, Y. Y.; Chen, K. S.; Lin, S. Y. J Controlled Release 1996, 41, 163.
14. Sorai, M.; Nakamura, T.; Seki, S. Pramana Suppl 1975, 1, 503.
15. Kajiyama, T.; Nagata, Y.; Washizu, S.; Takayanagi, M. J Membr Sci 1982, 11, 39.
16. Kajiyama, T.; Kikuchi, H.; Shinkai, S. J Membr Sci 1988, 36, 243.
17. Shieh, J. J.; Chung, T. S. J Membr Sci 1998, 140, 67.
18. Arthanareeswaran, G.; Thanikaivelan, P.; Srinivasn, K.; Mohan, D.; Rajendran, M. Eur Polym J 2004, 40, 2153.
19. Huang, M. R.; Li, X. G. J Appl Polym Sci 1998, 68, 293.
20. Chatterjee, P. K.; Conrad, C. M. J Polym Sci, Part A: Polym Chem 1968, 6, 3217.
21. Lucena, M. C.; Alencar, A. V.; Mazzeto, S. E.; Soares, S. A. Polym Degrad Stab 2003, 80, 149.

ID: srinivasanv | Black Lining: [ON] | Time: 16:42 | Path: N:/Wiley/3b2/APP#/Vol00000/091972/APPFile/C2APP#091972

22. Alvarez, V. A.; Vázquez, A. Polym Degrad Stab 2004, 84, 13.
23. Rao, R. V.; Ashokan, P. V.; Shridhar, M. H. Polym Degrad Stab 2000, 70, 11.
24. Filip, D.; Simionescu, C. I.; Macocinschi, D.; Paraschiv, I. J Therm Anal Calorim 2001, 65, 821.
25. Smith, G. W. Mol Cryst Liq Cryst 1990, 180, 201.
26. Smith, G. W.; Ventouris, G. M.; West, J. L. Mol Cryst Liq Cryst 1992, 213, 11.
27. Turi, E. Thermal Characterization of Polymeric Materials, Academic Press: New York, 1997; Vol 2, p 864.
28. Zhou, Y. W.; Jaroniec, M.; Gilpin, R. K. J Colloid Interface Sci 1997, 185, 39.
29. Yang, P.; Kokot, S. J Appl Polym Sci 1996, 60, 1137.
30. Filip, D.; Simionescu, C. I.; Macocinschi, D. Thermochim Acta 2003, 395, 217.
31. Criado, J. M. Thermochim Acta 1978, 24, 186.
32. Chang, W. L. J Appl Polym Sci 1994, 53, 1759.
33. Capart, R.; Khezami, L.; Burnham, A. K. Thermochim Acta 2004, 417, 79.
34. Varhegyi, G.; Antal, M. J.; Szekely, T.; Piroska Szabo, P. Energy Fuels 1989, 3, 329.
35. Prout, E. G.; Tompkins, F. C. Trans Faraday 1944, 40, 488.
36. Wall, L. A.; Madorsky, S. L.; Brown, D. W.; Straus, S.; Simha;, R. J Am Chem Soc 1954, 76, 3430.

3 CONCLUDING REMARKS

Two series of Polymer Dispersed Liquid Crystals (*PDLC*) have been prepared and characterised by thermal analysis. The study has focused on the effect of composition on the thermal behaviour of the materials. The methodology, based on the use of DSC and TGA, has been successfully applied to obtain relevant preliminary information about the interactions between the components at low and high temperatures and the phase morphology.

The stability of the films represents an important issue in the applications of *PDLC*, since the presence of aggregates can decrease the thermal stability of the polymer substrate. In this chapter the use of ideal DTG curves and their comparison with the experimental ones showed the existence of deviations from the expected ideal behaviour. In particular, the high thermal stability observed for the polymer substrate in the *COC–CA* films is a good basis for now assessing potential applications at lower temperatures. The presence of interactions also promoted variations in the mechanism of the polymer decomposition, which deviates from the typical random degradation shown in linear polymers.

The phase behaviour of the liquid crystalline materials has been determined by DSC and PLM. It has been shown that, despite the occurrence of phase separation, there are interactions between the components which lead to deviations from the expected ideal behaviour. This fact can facilitate the design of the morphology, since the composition of the films affected the parameters of the phase separation.

The materials show a two-phase morphology and phase-separation has been monitored by thermal transitions of the dispersed phase (analogous to the cluster transition in Nafion). It is apparent that the *PDLC* systems may achieve a greater decoupling of the properties of the two components, and therefore maintain the liquid crystal of the dispersed phase yielding materials with controllable morphologies.

Another important difference between Nafion and *PDLC* is the driving force for the phase transition. In Nafion the molecular reorganization is related to the different chemical natures (repulsion) of the hydrophobic and hydrophilic regions of the material.

In *PDLC*, the phase transition occurs within the liquid crystalline phase. This fact, and the reversibility of the transitions, is attractive in designing materials for controlled applications. However, preliminary results from swelling tests performed with the *COC-CA* and *MBBA-CA* membranes revealed were partially soluble in the presence of alcohol and water mixtures. Therefore, these materials cannot be used as electrolytes in *DFMC* in their current form.

In the following chapters, attempts to prepare materials having solvent resitance will be described via crosslinking or using side-chain liquid-crystalline co-polymers (*SCLCcP*). The expectation is to obtain intermediate behaviours between Nafion and *PDLC* in terms of phase separation. Moreover, the use of copolymers should promote coupling between the different functionalities of the polymer.

REFERENCES CHAPTER 4

1. Mucha, M. Prog. Polym. Sci. 28 (2003) 837

2. Crawford, G.P.; Zumer, S. L*iquid crystals in complex geometries formed by polymer and porous networks*; Ed. Taylor and Francis: New York (1996)

3. D. Filip, D.; Simionescu, C. I.; Macocinschi, D. Polym. Degrad. Stab. 72 (2001) 377

4. Smith, G.W.; Mol. Crys. Liq. Crys. 180 (1990) 201

5. Smith, G.W.; Ventouris, G.M.; Wes, J.L. Mol. Cryst. Liq. Cryst., 213 (1992) 11

6. Turi, E. *Thermal characterization of polymeric materials*, Academic Press: New York (1997) Vol 2, p. 864

5

Synthesis and characterisation of Poly(vinyl alcohol)-based materials for DMFC

1 SUMMARY

Chapter 1 described the importance of the structure of Proton Exchange Membranes (*PEM*) used in Direct Methanol Fuel Cells (*DMFC*) [1]. In general terms the search for new materials which can reduce crossover in *DMFC* has focused on polymers with a biphasic structure containing a hydrophobic backbone and polar sites to facilitate the proton transfer [2]. In the previous chapter a first attempt to obtain externally controllable materials was carried out by preparing polymer dispersed liquid crystals (*PDLC*) based on a cellulose acetate (*CA*) substrate. Unfortunately, the resulting materials had poor thermal and chemical stability, particularly in the presence of alcohols. As an alternative design approach to prepare new materials with enhanced stability, in this chapter the preparation of new poly(vinyl alcohol) (PVA)-based materials is described. The characterisation of the materials includes an analysis of their physical-chemical properties and also a study of the diffusion of water and methanol in membranes prepared from them, following a similar methodology as in chapters 3 and 4.

Poly(vinyl alcohol) (PVA) is a non-ionic water-soluble polymer consisting of the repeat unit -(CH_2-CHOH)-. The presence of the OH groups provides highly hydrophilic behaviour and promotes water uptake. The high density of hydroxyl groups in the polymer chains promotes the existence of inter and intra molecular hydrogen bonds that determine the ultrastructure of the material. PVA is commercially produced on a scale of several hundred kton/year all over the world, and is the highest volume on scale of production of any water-soluble polymer [3].

PVA is not produced by direct polymerization of vinyl alcohol due to its tendency to convert spontaneously into the enol form of acetaldehyde. PVA is prepared instead from the homopolymer poly(vinyl acetate) (*PVAc*). Polymerisation of vinyl acetate takes place via a free-radical mechanism in MeOH or EtOH or in suspension, and the resulting polymer is hydrolyzed in alkaline conditions. The extent of remaining acetate groups determines the hydrolysis degree (*HD*), which usually varies from 70% to 99% in commercial PVA. The *HD* and the molecular weight of PVA are controlled by several reaction parameters such as the reaction time, the concentration of vinyl acetate, the amount of solvent, the concentration of the radical initiator and the temperature.

Even though PVA-based materials have shown interesting results in preliminary tests such as, proton conductivity, stability, ionic exchange capacity, it is necessary to increase their resistance to hydrolysis and their chemical stability. With that aim in mind, PVA materials have been crosslinked to obtain membranes with enhanced properties. Furthermore, the use of sulfonated crosslinkers provides the new PVA structures high proton conductivities as well as enhanced stability [4, 5].

The introduction of the crosslinker and the ion exchange sites in the same molecule is not always desirable, since both features are then coupled. PVA membranes with a low degree of crosslinking show a considerable increase in their proton conductivity, due to the presence of ionic conducting groups. However, at higher degrees of crosslinking the reduction of the free volume becomes limiting and the water swellability is dramatically reduced, and leads to a decrease in the proton conductivity. For such systems, it is necessary to establish a balance between the number of sulfonic groups and the hydrophilicity. It is also nothworthy that the proton conductivity is dependent on the water content and also on the resulting morphology (coupled system). Other non-sulfonated crosslinking agents have been used, such as glutaraldehyde [6, 7]. In these cases other groups must be added to the polymer to obtain high proton conductivities.

In this chapter a number of poly(vinyl alcohol) (PVA)-based materials have been prepared and characterised with the aim to obtain polymers with enhanced proton conductivity and potentially controllable morphologies. The design of the materials will be based on two different strategies. First, liquid crystal molecules will be attached to the PVA backbone to obtain side-chain liquid-crystalline polymers. Second, different PVA substrates will be crosslinked by using sulfo succinic acid (SSA) and the absorption of water and methanol will be assessed, following the same procedure as in chapter 3. The use of SSA as the crosslinking agent provides the PVA substrate anionic sites that enhance proton conductivity as well as effecting transport properties of solvents through the membranes.

The main aims of this chapter can be summarised as follows:

1. To obtain externally controllable PVA membranes with enhanced proton conductivity and stability for their use in *DMFC*.
2. To study the effect of the composition of PVA on the formation of the membranes.
3. To analyse the swelling properties of the materials with respect to water and methanol mixtures.

1.1 Preparation of Liquid Crystal Polymers with a PVA backbone

Given the good performance of PVA membranes [4, 5], and the aims of this thesis to develop new materials for application in *DMFC*, side-chain liquid-crystalline polymers based on a PVA backbone were synthesised as an attempt to obtain externally controllable materials.

Two different liquid crystalline polymers were prepared. The low molecular weight liquid crystals used were 4-pentoxybenzoic acid (POBA, **1**) and 6-[4-(4-methoxyphenylazo)phenoxy]hexanoic acid (Azo5, **2**). The synthetic schemes used to prepare these compounds is shown in *Figures 5.1* and *5.2* [8].

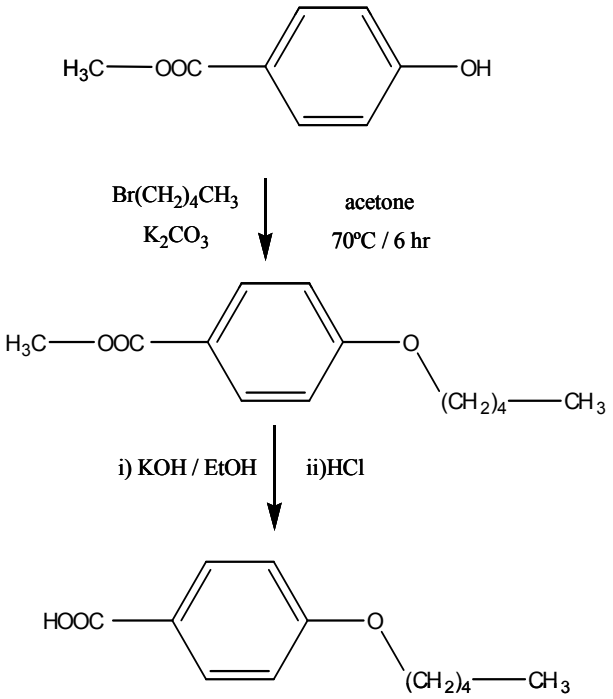

*Figure 5.1 Synthesis route of POBA, **1***

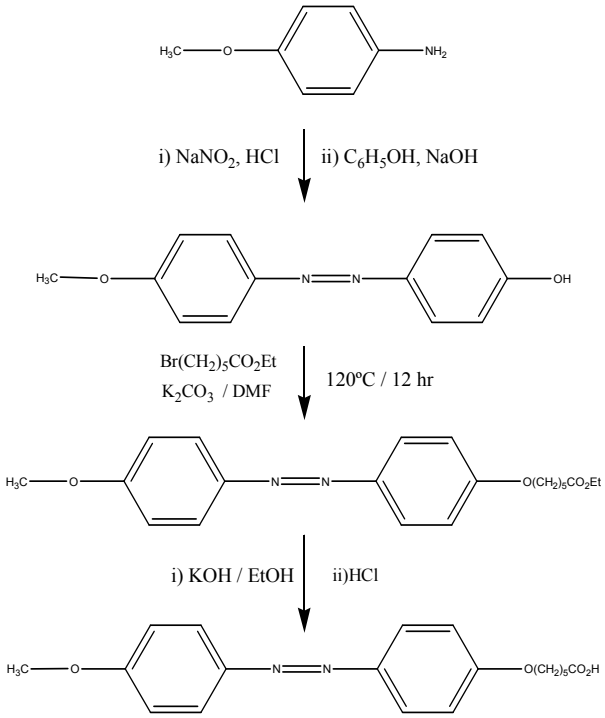

Figure 5.2 Synthesis route of Azo5, ***2***

The esterification of the polymer backbone was performed using the appropiate acid chloride in pyridine and dimethylformamide (*DMF*) [9]. The acid chloride was prepared by refluxing the acid in thionyl chloride ($SOCl_2$) and the excess $SOCl_2$ was subsequently removed by distillation (B_p = 79ºC). The esterification was catalysed by the presence of a weak base, pyridine. The general schemes of the reactions are shown in *Figures 5.3* and *5.4*.

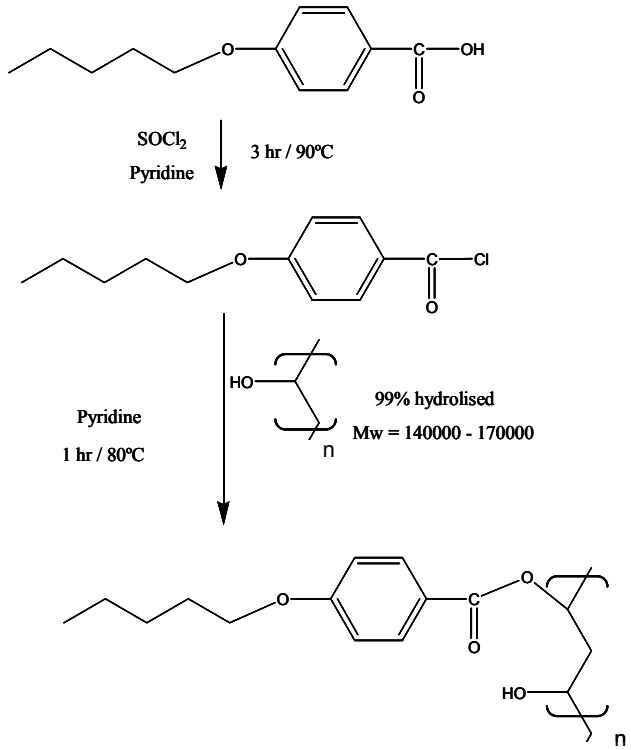

Figure 5.3 Synthesis of poly(vinyl 4-pentoxybenzoic acid)-co-(vinyl alcohol), PVA-POBA

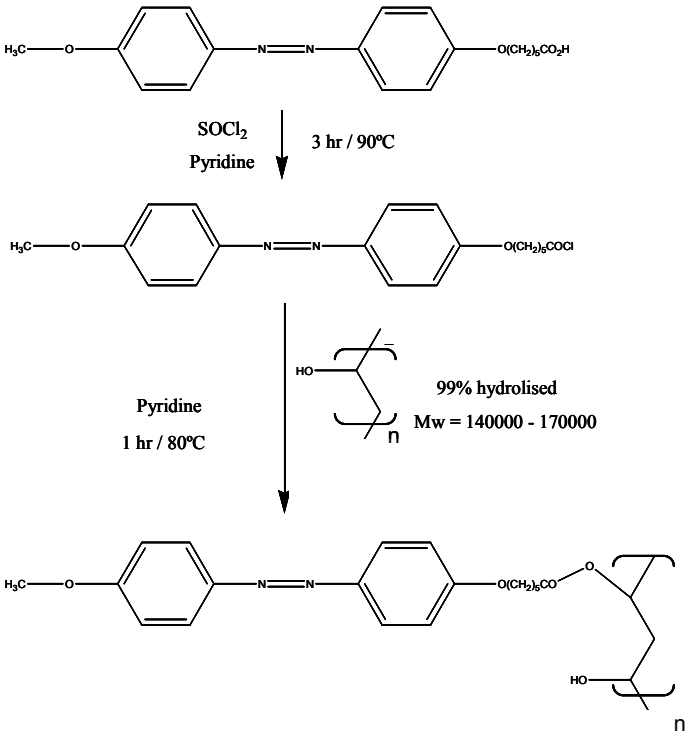

Figure 5.4. Synthesis of azo5, 6-[4-(4-methoxyphenylazo)phenoxy]hexanoic acid)-co-(vinyl alcohol), PVA- Azo5

The two polymers were successfully synthesised, although the synthesis of PVA-POBA proceeded with higher yields than that of PVA-Azo5. The esterification was verified by ^{1}H-nuclear magnetic resonance spectroscopy (NMR) and Infrared Spectroscopy (IR). The NMR spectra included the appearance of a peak in the vicinity of 5.1 ppm, which corresponded to the methyne protons of the PVA esterified groups and a broad peak at 1.8 ppm corresponding to the methylene groups of the PVA backbone (see *Figure 5.5*). Furthermore the appearance of the ester band at 1720 cm^{-1} in the IR spectra of the new materials was also seen (see *Figure 5.6*).

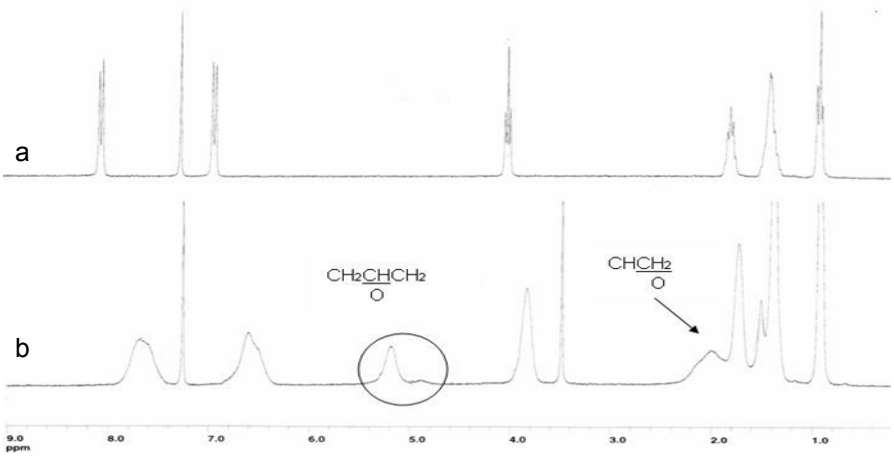

Figure 5.5 NRM spectra of (a) POBA and (b) PVA-POBA

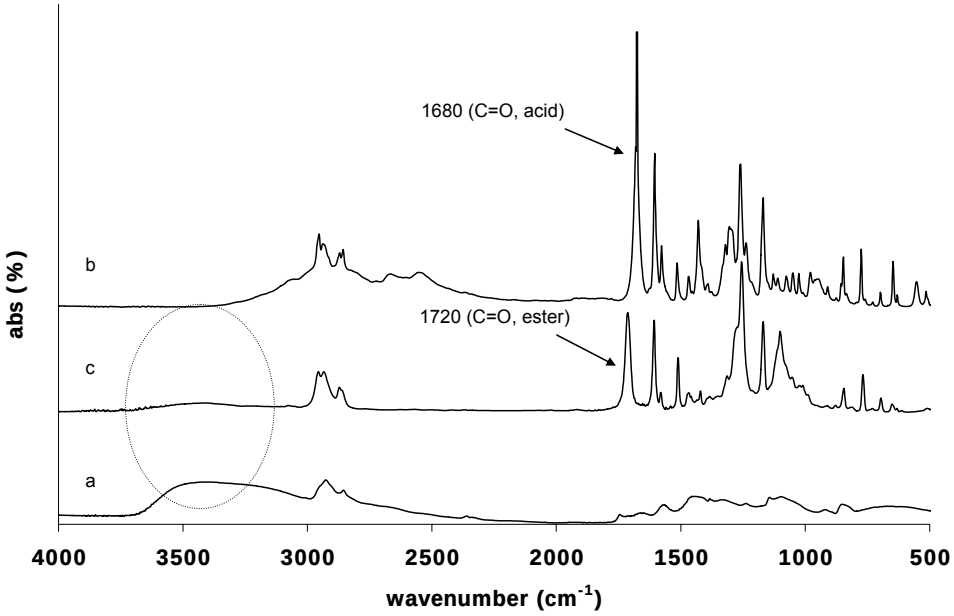

Figure 5.6 FTIR curves corresponding to (a) PVA, (b) POBA (c) PVA – POBA

As mentioned already, the reactions between PVA and Azo5 proceeded in low yields compared to the formation of the PVA-POBA polymers. In part, this was attributed to solubility limitations, arising from the different character of the two reactants. PVA is strongly hydrophilic and is easily dissolved in polar solvents such as water. However, it is soluble in few organic solvents, such as dimethylformamide (*DMF*), pyridine, 1-4 dioxan and dimethyl sulfoxide (*DMSO*) and their binary and ternary mixtures with water [10].

Pyridine was found to be a good solvent both for PVA and the liquid crystals. In the synthesis of new *PEM* for *DMFC*, the selection of the solvent is critical since the resulting structure of the polymers usually contains both hydrophobic and hydrophilic groups.

Another aspect which should be taken into account in future synthesis is the effect of the neighbouring groups to the carboxylic acid of the liquid crystals. Although it could have been predicted that the bulky phenyl group may have sterically impeded the yield of formation of the PVA-POBA polymer, the yield of this was actually higher than that of the PVA-Azo5 polymer. This suggests that the phenyl group acts as an activating site for the acid chloride. Therefore the structure of the liquid crystalline moiety can significantly affect the reaction rate and must be chosen carefully.

1.2. Preparation of PVA-SSA crosslinked membranes

Three commercial PVA polymers with different degrees of hydrolysis (*HD*), 89%, 96% and 99%, were used to prepare crosslinked membranes. The PVA substrates were crosslinked by the addition of sulfosuccinic acid (SSA). The structures of the four components are shown in *Figure 5.7*.

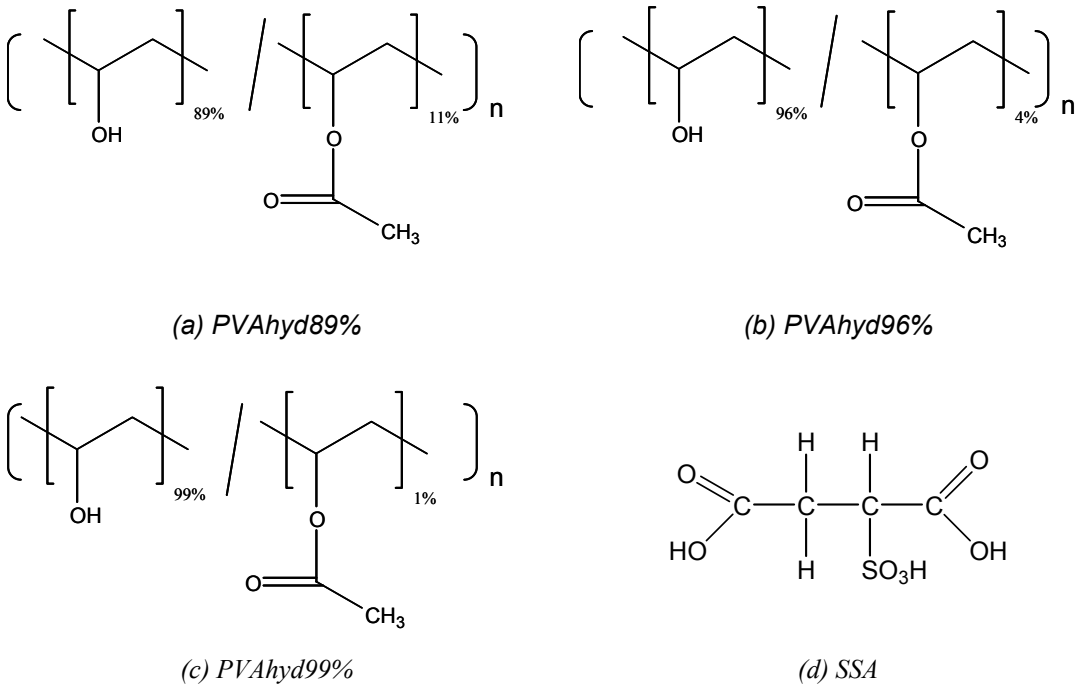

(a) PVAhyd89% *(b) PVAhyd96%*

(c) PVAhyd99% *(d) SSA*

Figure 5 7 Chemical structures of the materials used for the preparation of PVA-SSA crosslinked membranes

Sulfosuccinic acid (SSA) (*Figure 5.7d*) is a diacid commonly used to modify the PVA structure. Under some conditions, the OH groups of PVA and the carboxylic acid groups of SSA react in an esterification reaction. Since SSA has two reactive groups, the resulting polymer has a crosslinked structure in which two PVA chains are linked by a molecule of SSA. Since SSA possesses a sulfonic acid group (SO_2OH), it is expected that the resulting polymer has enhanced proton conductivity without further treatment. The scheme for the esterification is shown in *Figure 5.8*.

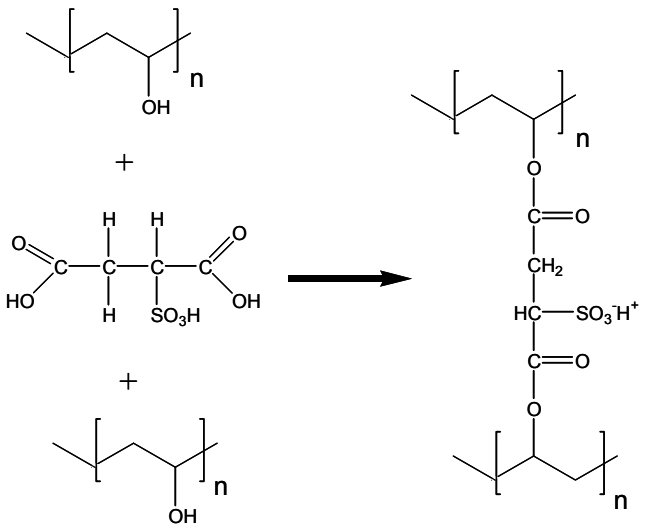

Figure 5.8. Crosslinking (esterification) of PVA – SSA

The membranes were prepared following a standard procedure described in the literature [6, 11]. PVA was dissolved in water at 90ºC, and SSA was added and mixed for 24 hours. The resulting solutions were then cast on a Teflon sheet and the water was allowed to evaporate at room temperature. Once the membranes were dry, they were peeled off the Teflon sheet and were heated at 110ºC for 2 hours. Samples of the membranes before and after being submitted to the thermal treatment were stored for further analysis. A dark coloration was observed after the thermal treatment. This coloration was attributed to a slight degradation probably caused by the release of sulphuric acid from SSA at 110ºC.

Three series of PVA-SSA membranes were obtained using the three different PVA polymers shown in *Figure 5.7a*, *5.7b* and *5.7c* (*PVA-89hyd*, *PVA-96hyd* and *PVA-99hyd*, respectively). The PVA-SSA membranes were obtained by using these polymers and varying the concentration of SSA. PVA-SSA membranes with 5%, 10%, 15%, 20%, 25% and 30% (weight percentage, wt. %) of SSA with respect to the initial PVA weight were prepared. The pristine PVA membranes were also prepared (so-called PVA substrates). The membranes were labelled as *PVAXhyd-Y%*, where *X* is the hydrolysis degree and *Y* the SSA concentration (C_{SSA}). The letters *bt* and *at* were added to the name of the membranes to denote *before treatment* and *after treatment*, respectively.

The PVA substrate membranes, the dried PVA-SSA membranes prior to thermal treatment and the thermally treated PVA-SSA membranes were analysed by Fourier

Transform Infrared Spectroscopy (FTIR) and Thermogravimetric Analysis (TGA). The FTIR experiments were performed using an Attenuated Total Reflectance (ATR) accessory (similarly as in chapter 3) in the usual range of frequencies (4000 – 400 cm^{-1}) with standard accuracy of 4 cm^{-1}. The FTIR curves were normalised using the CH_2 stretching vibration band at 2900 cm^{-1}. The TGA experiments were performed following standard conditions consisting of heating ramps from 25ºC to 700ºC, at a heating range of 10ºC/min under argon atmosphere.

The discussion of the results considers:

- The effect of the addition of SSA to the PVA membranes
- The effect of the thermal treatment on the PVA-SSA membranes
- The effect of the PVA substrate on the formation of the PVA-SSA membranes
- The effect of the concentration of SSA (C_{SSA}) on the PVA-SSA membranes

The FTIR results showed differences in the absorption bands associated with the representative groups of PVA as a consequence of the preparation processes. The bands corresponding to the stretching vibration of OH groups, the stretching of the C=O and C-O-C bonds of the acetate and other ester groups, and the sulfonate groups (SO_3^-) of SSA were studied in detail. The maximum absorbance (I_{OH}, I_{COO}, I_{COC} and I_{SO3}) and wavenumber (ν_{OH}, ν_{COO}, ν_{COC} and ν_{SO3}) of the bands were obtained for each curve. Furthermore, the relative intensity $I_{COO/OH} = \frac{I_{COO}}{I_{OH}}$, and $I_{COC/OH} = \frac{I_{COC}}{I_{OH}}$ and $I_{SO3/OH} = \frac{I_{SO3}}{I_{OH}}$ were also calculated.

The values of I_{OH}, I_{COO}, I_{COC}, and particularly those of $I_{COO/OH}$ and $I_{COC/OH}$ provide evidence of the esterification occurring between the OH groups of PVA and the COOH groups of SSA, even prior to the thermal treatment. However, there were also changes in the vibrations of the groups post thermal treatment, implying that the esterification was not completed only on mixing and drying. The results also showed that the process is dependent on the PVA substrate to some extent.

According to the results, the SSA concentration has different effects on the esterification reaction depending on the PVA substrate. In particular, the PVA-SSA membranes with lower degrees of hydrolysis (*89hyd* and *96hyd*) showed a more gradual increase in esterification on increasing SSA concentration.

The chemical environments of the functional groups were also deduced from the positions of the FTIR vibration bands. Opposite trends are observed for the residual *OH* groups of PVA and the ester and sulfonate groups in the membranes. These results suggest that while the SO_3^- groups and the ester bonds tend to form stronger intermolecular (or even intramolecular) interactions, the H-bonds formed by the hydroxyl groups seem to be somewhat weaker. Therefore, the results suggest the existence of phase separation to some extent. This behaviour is similar to that observed in the commercial membranes of Nafion.

The thermal stability of all the materials was studied using TGA. Clear differences were observed in the PVA-SSA membranes before and after thermal treatment, confirming the change in the chemical structure already verified using FTIR. The results suggest that the PVA-SSA membranes posses a more thermal and mechanically stable structure, and their stability is enhanced by the thermal treatment. This was attributed to the crosslinked structure. TGA also revealed the existence of tightly bound water in the PVA-SSA membranes, which did not depend to a great extent on the nature of the substrate or the SSA concentration.

Finally, it was found that the PVA substrates responded differently to the thermal treatment and the concentration of SSA. In general terms, the results suggest that low hydrolysed substrates do not tend to react well at high SSA concentrations, in contrast to the behaviour of high hydrolised PVA substrates. On the other hand, the increase in the thermal stability of the *PVA-96hyd* membranes on thermal treatment is more gradual. These membranes also showed high values of absorbed water, which is important for the behaviour of *PEM* electrolytes in *DMFC*. Therefore, and according to the previous results, the PVA substrate with a 96% hydrolysis degree (*PVA-96hyd*) seems to be the most suitable for the preparation of PVA-SSA membranes for the use as electrolytes in *DMFC*.

1.3. Characterisation of the absorption and desorption of water, methanol and their binary mixtures in PVA96hyd-SSA membranes

The PVA-SSA membranes prepared with a PVA substrate having a degree of hydrolysis of 96% (*PVA96hyd-SSA* membranes) were chosen for detailed characterisation of their diffusion properties with respect to water, methanol and their binary mixtures

The absorption of water and methanol in the *PVA96hyd-SSA* membranes has been studied by swelling tests at 35ºC, following a similar procedure as for the evaluation of the Nafion membranes in chapter 3. Rectangular samples of the membranes were submerged in water, methanol and binary mixtures of water and methanol containing 10%, 20%, 30% and 40% by weight of methanol, until equilibrium was reached. The absorption of the solvent was monitored gravimetrically. The results show that the *PVA96hyd-SSA* membranes absorb high amounts of solvent from pure water and the solutions containing binary mixtures, but very low amounts of pure methanol. The swelling capacity of the membranes decreased on increasing SSA concentrations, suggesting that crosslinking somehow inhibits the diffusion of the solvents.

The chemical structure of the membranes used in the swelling tests was studied by FTIR and TGA. The FTIR results indicate the presence of methanol in the samples submerged in the binary mixtures, which suggests that the presence of water somehow enhances the diffusivity of the methanol molecules through the polymer structure. The existence of interactions between methanol and water was also observed by the shift of the corresponding IR bands. On the other hand, according to the TGA results, there is not a big increase in the values of solvent tightly bound to the polymeric structure after the swelling tests are performed.

The cooperative behaviour of the transport mechanisms of water and methanol through the *PVA96hyd-SSA* membranes was also apparent in the desorption tests performed using time resolved FTIR-ATR. The results show that methanol is rapidly desorbed from the membranes. The diffusion rates corresponding to the membranes were also compared to the diffusion of bulk solutions containing binary mixtures of water and

methanol with the same composition. The results show that desorption of methanol from the membranes is delayed with respect to the bulk behaviour. It can also be seen that the rate of methanol diffusion depends on the structure of the polymer. Higher crosslinking degrees promote lower desorption rates, probably by the existence of physical barriers caused by a more dense structure. The composition of the solutions also influences the loss of methanol. Higher water contents in the methanol mixtures promote faster desorption of methanol. All these results prove the importance of the role of water in the transport of methanol through the PVA membranes.

2 COMMUNICATION I

Synthesis and characterisation of Poly(vinyl alcohol) membranes with different hydrolysis degrees for their use as electrolytes in Direct Methanol Fuel Cells

Title:

SYNTHESIS AND CHARACTERISATION OF POLY(VINYL ALCOHOL) MEMBRANES WITH DIFFERENT HYDROLYSIS DEGREES FOR THEIR USE AS ELECTROLYTES IN DIRECT METHANOL FUEL CELLS

[1]A. Martínez-Felipe, [1]L. Santonja-Blasco, [1]C. Moliner-Estopiñán, [2]C.T. Imrie, [1]A. Ribes-Greus

[1]Institute of Materials Technology, Universidad Politécnica de Valencia,
Camino de Vera s/n, 46022, Valencia, Spain

[2]Department of Chemistry, University of Aberdeen, Meston Walk, Aberdeen, Scotland, United Kingdom

ABSTRACT

The effect of the degree of hydrolysis in poly(vinyl alcohol) (PVA) used in the preparation of membranes having enhanced proton conductivity for DMFC applications has been studied using Attenuated Total Reflectance-Fourier Transform Spectroscopy (ATR–FTIR) and Thermogravimetric Analysis (TGA). Three PVA substrates with degrees of hydrolysis of 89%, 96% and 99% were crosslinked with sulfosuccinic acid (SSA) by thermal treatment at high temperatures. The FTIR results revealed that esterifications occurs in all the membranes and even before the membranes were heated. Also, the degree of crosslinking depended on both the SSA concentration and the composition of the PVA substrate. Thermogravimetric Analysis confirmed the increase in the thermal stability of the PVA-SSA membranes with respect to their PVA substrates arising from the formation of a crosslinked structure. In addition, TGA showed the existence of free and tightly bound water in the PVA-SSA membranes. It was seen that the thermal treatment had a greater effect on the PVA substrates with higher degrees of hydrolysis.

INTRODUCTION

Interest in Fuel Cells has strongly increased due to their high efficiencies, low environmental impact and flexibility of operation [1, 2, 3]. In Direct Methanol Fuel Cells (*DMFC*) methanol is oxidized at the anode and the protons generated are transferred through a polymeric electrolyte membrane (*PEM*). The protons react at the cathode with oxygen from the air, and the flow of electrons through an external circuit generates electrical power [4]. *DMFC* have attracted considerable resarch attention since methanol is a liquid at room temperature and thus avoids some of the shortcomings derived from the use of hydrogen. However, *DMFC* still have some disadvantages when compared to hydrogen fuel cells, and in particular, the poor oxidation of methanol and other mass transfer limitations [5].

One of the most pressing problems associated with *DMFC* is the so-called crossover phenomenon, which consists of the flow of unreacted methanol from the anode through the electrolyte. When crossover occurs, methanol reacts at the cathode with oxygen in a combustion type reaction. This reaction produces thermal energy but does not generate net electrical power, leading to fuel leakage and loss of cell efficiency [5, 6, 7]. Crossover is mainly attributed to the interconnections between the transport mechanisms through the polymeric electrolyte of water, methanol and protons. Research in *DMFC* has focused on obtaining *PEM* with high proton conductivity and low methanol solubility. However, attempts to reduce the methanol permeation usually lead to lower water contents and consequently the proton conductivity in the membranes decreases [5].

The use of poly(vinyl alcohol) (PVA) membranes in *DMFC* has been studied in recent years due to their high selectivity for water with respect to alcohols [7, 8, 9]. Poly(vinyl alcohol) (PVA) is a non-ionic water-soluble polymer consisting of the repeat -(CH_2-CHOH)- unit. The high concentration of OH groups in the polymer chains provides PVA with its strong hydrophilic character and inter and intra molecular hydrogen bonds that determine the primary, secondary, tertiary and quaternary arrays of the molecules. PVA is prepared by the hydrolysis of the homopolymer, poly(vinyl acetate) (PVAc). The number of hydroxyl groups after the hydrolysis in PVA defines the hydrolysis degree (*HD*), which usually varies from 70% to 99% in commercial PVA [10].

Prior to its use as an electrolyte in *DMFC*, PVA is usually submitted to crosslinking reactions. Sulfonic and sulfosuccinic acids containing two carboxylic acid groups are used to crosslink the main chains by the esterification of the hydroxyl groups. These reactions enhance the proton conductivity of PVA by the introduction of the sulfonic acid groups, as well as increasing the stability of the resulting membranes by the formation of a 3D interconnected network [11, 12, 13].

In this paper the effects of the PVA substrate, the SSA concentration and the thermal treatment on the preparation of PVA-SSA membranes for *DMFC* applications have been studied. Different PVA-SSA membranes have been prepared by varying the hydrolysis degree of PVA (*HD* = 89%, 96% and 99%) and the concentration of SSA in the 0 – 30% range (SSA weight percentage). The molecular interactions between the components have been studied by Fourier Transform Infrared Spectroscopy (FTIR) and the thermal stability of the membranes has been assessed by Thermogravimetric Analysis (TGA).

EXPERIMENTAL PROCEDURE

Materials

Three samples of poly(vinyl alcohol) (PVA) with different hydrolysis degrees (89% hydrolysed, MW ~ 85,000 – 124,000 g·mol^{-1}; 96% hydrolysed, MW ~ 85,000 – 146,000 g·mol^{-1}; 99% hydrolysed, MW ~ 85,000 – 124,000 g·mol^{-1}) and a commercial sulfosuccinic acid (SSA) solution (70%, weight. % in H_2O) were purchased from Sigma-Aldrich.

Membrane preparation

Three series of membranes were prepared based on PVA substrates with hydrolysis degrees of 89%, 96% and 99%. All the membranes were prepared following the same procedure. PVA was dissolved in distilled water to give a 10% (wt/wt %) solution by stirring at 90ºC for 6 hours. The commercial SSA solution was then added to the PVA solutions and the mixtures were stirred at room temperature for 1 day. The amount of the commercial SSA solutions varied to form PVA-SSA membranes containing 5%, 10%, 15%, 20%, 25% and 30% by weight percentage of SSA with respect to the amount of PVA. The resulting solutions were cast on a Teflon sheet and the water was removed by drying in ambient conditions until no further mass loss was observed in the membranes. The resulting PVA-SSA membranes were then heated at 110ºC for 2 hours.

The membranes were then denoted as *PVAXhyd-Y%SSA*, where *X* is the hydrolysis degree of the PVA substrate (*HD*) and *Y* the weight percentage of SSA. Membranes consisting of the three pure PVA substrates were also prepared.

Attenuated Total Reflectance - Fourier Transform Infrared Spectroscopy (ATR-FTIR)

The FTIR experiments were performed using a Thermo Nicolet 5700 spectrometer (MA, Waltham) with a ATR attachment. The samples were placed on a diamond crystal, and the experiments were performed using 1 bounce and an incident angle of 45ºC. The spectra were collected after 128 scans with an accuracy of 4 cm^{-1}. Background spectra were collected before each series of experiments. All the experiments were performed three times and the average was calculated.

Thermogravimetric Analysis (TGA)

The TGA thermograms were obtained using a Mettler Toledo TGA/SDTA 851 analyser (OH, Columbus). Measurements were performed following a dynamic program from 25ºC to 700ºC at a linear heating rate of 10ºC/min under inert argon (Ar) atmosphere with a flow rate of 50 ml/min. Sample masses were around 5 mg. All the experiments were performed three times and the average was calculated.

RESULTS AND DISCUSSION

1. Characterisation of the pure components

Figure 1 shows the FTIR spectra of the commercial SSA solution and the PVA substrates with different hydrolysis degrees. The assignment of the different absorption bands are summarised in *Table 1*.

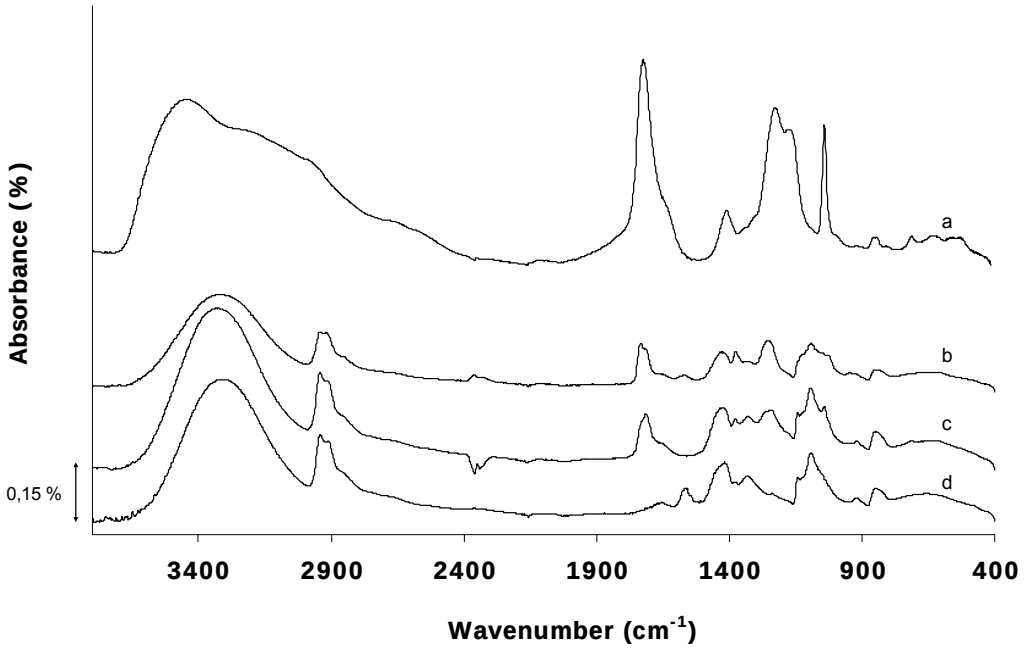

Figure 1. FTIR spectra of the pure components: (a) SSA commercial solution; PVA substrates: (a) PVA89hyd0%, (b) PVA96hyd0%, (c) PVA99hyd0%. (d) commercial SSA solution

In the FTIR curve of SSA (*Figure 1a*) it is possible to observe the bands associated with the carboxylic groups (COOH) at ν ~ 3000 – 3600 cm^{-1} (OH stretching) and 1730 cm^{-1} (C=O stretching) and a prominent peak in the vicinity of 1043 cm^{-1} which can be assigned to the SO_3^- groups. The high water contents in the solution is apparent in the H_2O bending band at 1650 cm^{-1} region overlapped with the C=O band, and the appearance of several bands in the OH stretching region [13]. The FTIR curves of the three PVA substrates (*Figure 1b, 1c and 1d*) contain bands associated with the groups in PVA [14-20], specifically:

- The different regions associated with OH group stretching (ν ~ 3000 – 3600 cm^{-1}, *OH* stretching; ν ~ 920 cm^{-1}, OH out of plane deformation [14, 17, 21].
- The deformation vibration of the CH_3 groups (ν~1340 cm^{-1}) [13].
- The alcohol groups (ν~1140 cm^{-1}, crystalline C-O stretching; ν~ 1090 cm^{-1}, C-O stretching) [20].
- The bending vibration of the water molecules (ν_{H2O}) of PVA in the vicinity of ν_{H2O}~ 1650 cm^{-1}. It is expected that the hydroxyl groups of water also contribute to the *OH* stretching band at 3600 – 3000 cm^{-1} [16, 21].
- In the substrates with lower hydrolysis degrees (*PVA89hyd* and *PVA96hyd*) it is also possible to observe the bands associated with the acetate groups at 1730 cm^{-1} (C=O stretching) and 1250 cm^{-1} (C-O-C stretching) [21].

Table 1. Assignment of the FTIR absorption bands of the PVA membranes

Region (cm^{-1})	Assigment	Contributions	References
3400 – 3000	**OH stretching**	Intermolecular hydrogen bonding PVA, H_2O, SSA	[13, 14, 17, 21]
1660 – 1640	**OH bending**	H_2O	
920	**OH out of plane**	Carboxylic group SSA	
2910 - 2950	**CH_2 stretching**	PVA structure, SSA	[13]
1420	**CH_2 scissoring**		
1330	**CH_2 deformation**		
850	**CH_2 rocking**		
1790 – 1660	**C=O stretching**	Acetate groups PVA, carboxyl groups SSA	[13, 20, 21]
1250	**C-O stretching**	Acetate groups PVA, SSA	
1140	**C-O stretching**	Crystalline form	
1090	**C-O stretching**	Acetate groups PVA, SSA	
1040	SO_3^- **stretching**	SO_3^- group SSA	[P14]

The curves corresponding to the three PVA substrates were normalised with respect to the stretching vibration of the CH_2 groups of the polymer backbone (ν~2950 cm^{-1}). The values of maximum absorbance and wavenumber of the hydroxyl groups (I_{OH}, ν_{OH}) and the ester groups (I_{COO}, ν_{COO} and I_{COC}, ν_{COC}) were calculated. The relative values $I_{COO/OH} = \frac{I_{COO}}{I_{OH}}$ and $I_{COC/OH} = \frac{I_{COC}}{I_{OH}}$ were also obtained.

The parameters related to the OH, C=O and COC stretching bands of the PVA substrates are summarised in *Table 2*. As expected, there is an increase in the absorbance values of the C=O and COC bands (I_{COO} and I_{COC}, respectively) with decreasing hydrolysis degrees, since the concentration of acetate groups increases.

Table 2. Position and absorption parameters of the IR bands corresponding to the PVA membranes

Sample	OH st		C=O st	
	ν_{max} (cm^{-1})	I_{max} (I_{OH}) (%)	ν_{max} (cm^{-1})	I_{max} (I_{COO}) (%)
PVA89hyd0%	3310	0.275	1733	0.132
PVA96hyd0%	3322	0.251	1717	0.055
PVA99hyd0%	3319	0.42	-	-

Sample	C-O-C st		I_{COO} / I_{OH}	I_{COC} / I_{OH}
	ν_{max} (cm^{-1})	I_{max} (I_{COC}) (%)		
PVA89hyd0%	1252	0.14	0.48	0.51
PVA96hyd0%	1260	0.082	0.22	0.33
PVA99hyd0%	-	-	-	

The thermal stability of the pure components has been also studied. *Figure 2* shows the Derivative Thermogravimetric (DTG) curves of the SSA commercial solution and the three PVA substrates. The DTG curve of SSA (*Figure 2a*) shows a mass loss peak at 100ºC, which is attributed to the loss of water, and a main decomposition process in the region 200ºC-330ºC, related to the desulfonation process. The degradation of PVA proceeds in at least, three steps (*Figure 2b*, *2c* and *2d*). At low temperatures (T_1~100ºC) a peak is observed which can be attributed to the loss of water (*peak 1*). In the 200ºC–400ºC region a strong peak (*peak 2*) is seen which is assigned to the loss of *OH* groups and to the deacetylation from the PVA chains. Finally, a weaker process is observed in the 400ºC – 500ºC region which is attributed to the degradation of the polymeric backbone (*peak 3*). The results are in agreement with the literature [6, 22, 23].

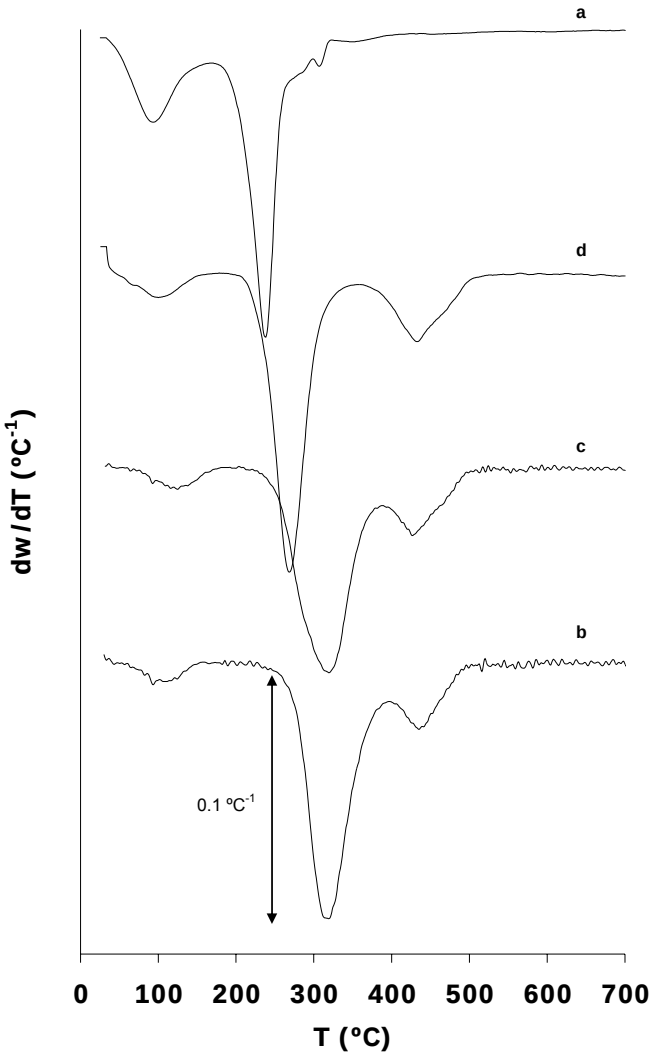

Figure 2. Derivative Thermogravimetric (DTG) curves of the commercial SSA solution (a) and the PVA substrates: (b) PVA89hyd0%, (c) PVA96hyd0%, (d) PVA99hyd0%.

The temperature at the maximum degradation rate (T_{peak}) and the mass loss ($\Delta\omega$) of the three main decomposition processes (*peaks 1, 2* and *3*) of the PVA substrates were calculated. The results have been plotted in *Figure 3* as a function of the hydrolysis degree. As expected, there is an increase in the water absorbed ($\Delta\omega_1$) in the substrates with higher hydrolysis degrees (*PVA99hyd*) due to the higher concentration of hydrophilic OH groups in the PVA chain [8, 20]. The mass loss related to *peak 2* ($\Delta\omega_2$) decreases at high hydrolysis degrees (*PVA99hyd*), probably due to the substitution of CH_3COO groups by lighter OH groups. This is also accompanied by a decrease in the temperatures of the degradation peak (T_2), which indicates that the acetate groups have higher stability than the hydroxyl groups in PVA [23]. Finally, there is a slight decrease

in the residual values on increasing hydrolysis degrees. This suggests that the decomposition of the PVA backbone is somehow promoted in samples with higher OH contents.

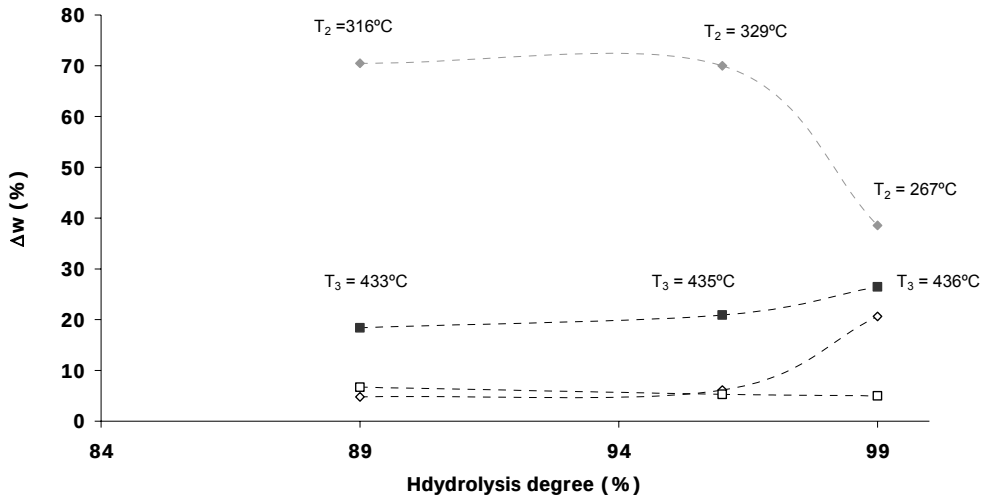

Figure 3 Weight loss of the degradation processes corresponding to the PVA substrates as a function of the hydrolysis degree: (◇) water - $\Delta\omega_1$, (◆) side groups decomposition ($\Delta\omega_2$), (■) main chains decomposition - $\Delta\omega_3$, (□) residual at 700ºC.

2 Characterisation of the PVA-SSA membranes before thermal treatment

The FTIR spectra of the PVA–SSA membranes prior to thermal treatment were obtained. In *Figure 4* the FTIR spectra of the *99hyd* series are shown, and the curve corresponding to the pure PVA membrane has also been included. Similar curves were obtained for the other two substrates but the results have not been shown for the sake of clarity. The values of I_{OH}, I_{COO}, I_{COC}, $I_{COO/OH}$ and $I_{COC/OH}$ and the corresponding frequencies (ν_{max}) were calculated from the FTIR spectra of the PVA-SSA membranes. The results are listed in *Tables 3, 4 and 5*.

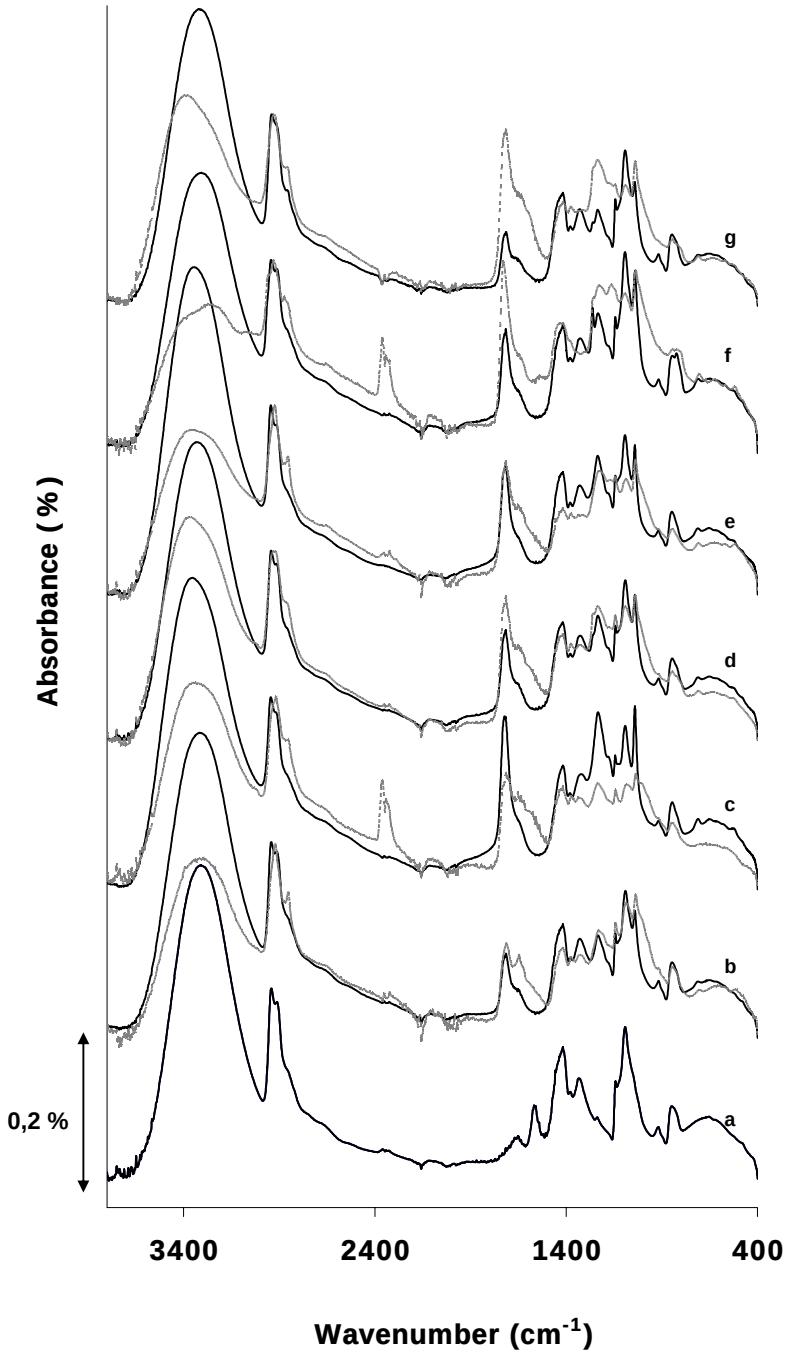

Figure 4 FTIR spectra of the 99hydPVA–SSA membranes before (black lines) and after (grey lines) thermal treatment: (a) PVA99hyd0%, (b) PVA99hyd5%, (c) PVA99hyd10%, (d) PVA99hyd15%, (e) PVA99hyd20%, (f) PVA99hyd25%, (g)PVA99hyd30%.

Table 3a. FTIR results. PVA89hyd PVA-SSA membranes before the heat treatment

C_{SSA} (wt. %)	ν_{OH} (cm^{-1})	ν_{COO} (cm^{-1})	ν_{COC} (cm^{-1})	ν_{SO3} (cm^{-1})	$I_{COO/OH}$	$I_{COC/OH}$	$I_{SO3/OH}$
0	3310	1733	1252	-	0,480	0,292	-
5	3338	1728	1262	1041	0,296	0,394	0,376
10	3346	1732	1258	1041	0,508	0,529	0,390
15	3330	1723	1242	1041	0,538	0,557	0,546
20	3309	1720	1250	1038	0,475	0,450	0,517
25	3350	1728	1238	1042	0,498	0,517	0,531
30	3342	1724	1234	1042	0,614	0,577	0,622

Table 3b. FTIR results. PVA89hyd PVA-SSA membranes after the heat treatment

C_{SSA} (wt. %)	ν_{OH} (cm^{-1})	ν_{COO} (cm^{-1})	ν_{COC} (cm^{-1})	ν_{SO3} (cm^{-1})	$I_{COO/OH}$	$I_{COC/OH}$	$I_{SO3/OH}$
0	3310	1724	1252	-	0,480	0,323	-
5	3362	1732	1258	1042	0,687	0,749	0,646
10	3358	1724	1242	1042	0,513	0,542	0,525
15	3367	1724	1238	1042	0,754	0,734	0,749
20	3375	1720	1234	1037	0,939	0,928	1,017
25	3387	1724	1234	1037	0,994	0,82	0,82
30	3367	1728	1237	1037	1,197	1,098	1,148

Table 4a. FTIR results PVA96hyd PVA-SSA membranes before the heat treatment

C_{SSA} (wt. %)	ν_{OH} (cm^{-1})	ν_{COO} (cm^{-1})	ν_{COC} (cm^{-1})	ν_{SO3} (cm^{-1})	$I_{COO/OH}$	$I_{COC/OH}$	$I_{SO3/OH}$
0	3297	1717	1260	-	0,219	0,323	-
5	3345	1715	1236	1040	0.323	0,146	0,149
10	3325	1723	1241	1041	0.146	0,366	0,388
15	3272	1712	1228	1036	0.366	0,319	0,487
20	3341	1723	1232	1040	0.319	0,399	0,430
25	3354	1719	1232	1041	0.399	0,592	0,604
30	3353	1719	1232	1041	0.592	0,477	0,498

Table 4b. PVA96hyd PVA-SSA membranes after the heat treatment

C_{SSA} (wt. %)	ν_{OH} (cm^{-1})	ν_{COO} (cm^{-1})	ν_{COC} (cm^{-1})	ν_{SO3} (cm^{-1})	$I_{COO/OH}$	$I_{COC/OH}$	$I_{SO3/OH}$
0	3297	1717	1260	-	0,219	0,323	-
5	3324	1721	1240	1039	1.534	0,227	0,310
10	3341	1727	1245	1040	1.329	0,596	0,522
15	3354	1728	1235	1035	1.072	0,548	0,653
20	3366	1723	1237	1041	0.888	0,602	0,670
25	3378	1723	1232	1037	1.101	0,592	0,657
30	3378	1727	1237	1041	0.979	0,618	0,658

Table 5a. FTIR results. PVA99hyd PVA-SSA membranes before the heat treatment

C_{SSA} (wt. %)	ν_{OH} (cm^{-1})	ν_{COO} (cm^{-1})	ν_{COC} (cm^{-1})	ν_{SO3} (cm^{-1})	$I_{COO/OH}$	$I_{COC/OH}$	$I_{SO3/OH}$
0	3310	-	1236	-	-	0,205	-
5	3313	1715	1233	1041	0.258	0,245	0,393
10	3354	1719	1233	1041	0.282	0,534	0,575
15	3329	1715	1233	1041	0.313	0,349	0,476
20	3342	1715	1233	1041	0.275	0,379	0,444
25	3309	1715	1233	1041	0.416	0,416	0,635
30	3317	1715	1233	1041	0.225	0,225	0,397

Table 5b. FTIR results. PVA99hyd PVA-SSA membranes after the heat treatment

C_{SSA} (wt. %)	ν_{OH} (cm^{-1})	ν_{COO} (cm^{-1})	ν_{COC} (cm^{-1})	ν_{SO3} (cm^{-1})	$I_{COO/OH}$	$I_{COC/OH}$	$I_{SO3/OH}$
0	3310	-	1236	-	-	0,323	-
5	3326	1712	1232	1036	0.226	0,570	0,789
10	3343	1717	1232	1036	0.347	0,491	0,539
15	3363	1721	1232	1036	0.286	0,593	0,633
20	3347	1716	1233	1036	0.389	0,742	0,811
25	3297	1729	1227	1036	0.618	1,168	1,281
30	3391	1712	1236	1040	1.165	0,679	0,675

The FTIR curves of the PVA-SSA membranes prior to thermal treatment shown in *Figure 4* show a remarkable increase of the 1700–1730 cm^{-1} region with respect to the

PVA spectrum. This change is accompanied with the appearance and growth of a prominent peak in the vicinity of ν~1040 cm^{-1} which is related to the stretching of the sulfonate group (SO_3^-) [24, 25]. The appearance of this peak confirms the presence of proton conducting groups in the PVA-SSA membranes.

Tables 3a, 4a and 5a also show shifts in some of the FTIR bands of the PVA-SSA membranes prior to thermal treatment with respect to the PVA curve, suggesting that the preparation of the membranes promote changes in the chemical environments of the groups. The OH stretching band shifts to higher wavenumbers, indicating the formation of weaker hydrogen bonds by the hydroxyl groups in the PVA-SSA membranes. On the other hand, the position of the COC band is shifted to lower frequencies with respect to the values shown by the acetate groups in the pure PVA substrates (1260 cm^{-1} and 1252 cm^{-1} for PVA96% and PVA89%, respectively). The increase in the COO and COC bands and the displacement of the bands indicate the occurrence of esterification reactions between the COOH groups of SSA and the OH groups of PVA, even prior to thermal treatment.

The DTG curves of the PVA–SSA membranes prior to thermal treatment were also obtained. *Figure 5* shows the results for the *PVA96hyd* series, and similar results were obtained for the other PVA substrates. The most notable change with respect to the DTG curves of the PVA substrates is the appearance of a very strong degradation peak in the 150ºC–200ºC region of all the PVA-SSA membranes. This peak has been observed by other authors and attributed to the existence of water tightly bound to the polymer structure and also to the water produced by the esterification reactions [17, 26]. The presence of bound water in the PVA-SSA membranes is very important to ensure proton conductivity in *DFMC* electrolytes. In the DTG curves of the PVA-SSA membranes without thermal treatment it is also possible to observe a shoulder at lower temperatures (T~100ºC) which indicates the presence of free water. Some weak processes are also visible in the 200ºC–320ºC temperature region and can be attributed to the desulfonation of the membranes and also to the loss of OH and acetate groups remaining in the polymer [17, 26].

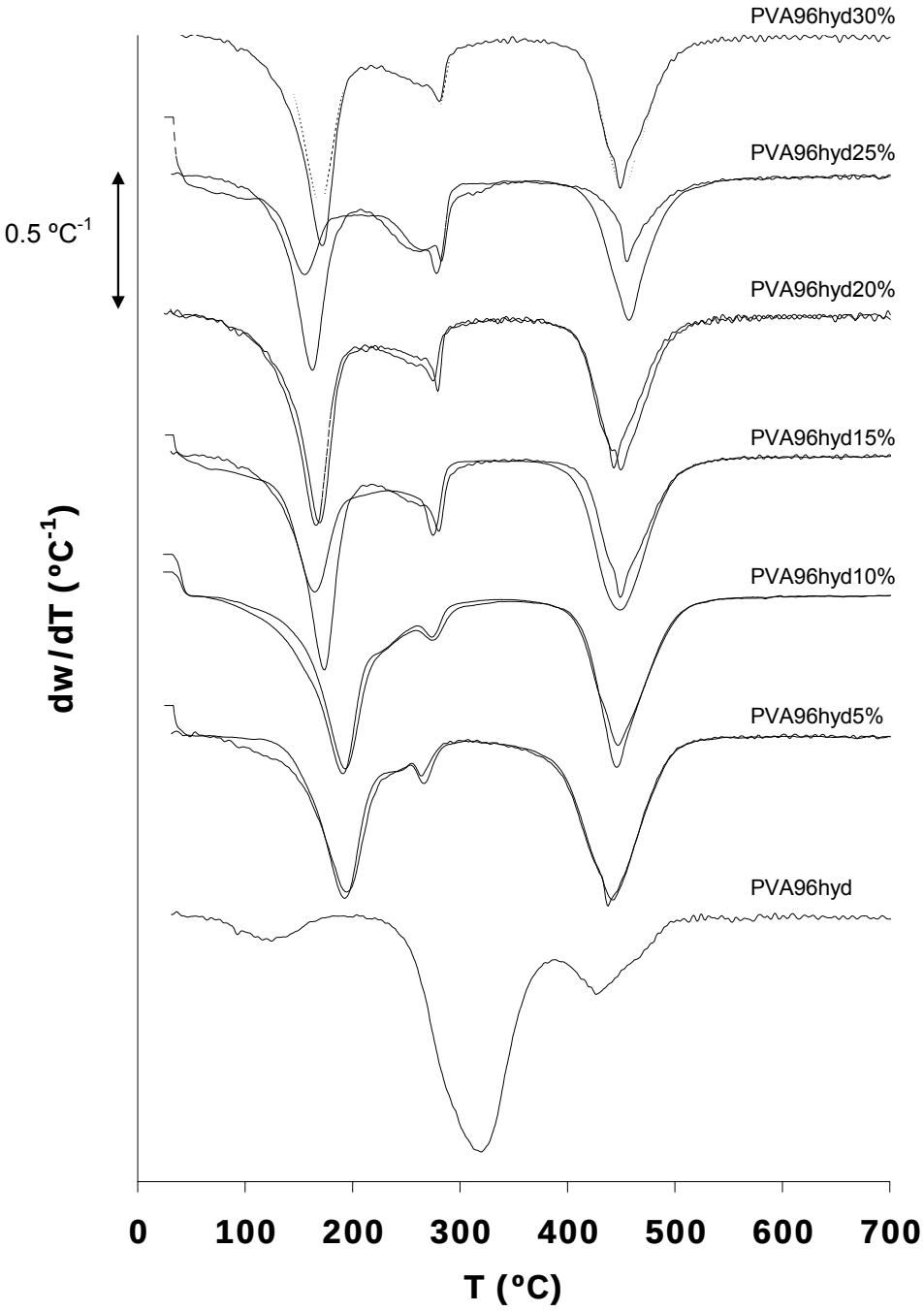

Figure 5 DTG curves of the 96hydPVA–SSA membranes before (black lines) and after (grey lines) thermal treatment: (a) PVA96hyd0%, (b) PVA96hyd5%, (c) PVA96hyd10%, (d) PVA96hyd15%, (e) PVA96hyd20%, (f) PVA96hyd25%, (g)PVA96hyd30%

The process related to the degradation of the main chains in the PVA-SSA membranes increases in the PVA-SSA membranes prior to thermal treatment with respect to the PVA substrates. Such as increase is also accompanied by an increase in the values of residual at 700ºC, which varies from the 5 – 7 % range in the PVA substrates, to the 23

– 30% range in the PVA-SSA membranes. These changes can be attributed to the formation of a crosslinked structure formed by esterification occurring even before the membranes are submitted to the thermal treatment [17, 23, 24]. Even though the thermal degradation of all the three series of PVA-SSA membranes prior to thermal treatment is similar, the values of water present and the residual are the highest for the membranes with higher hydrolysis degrees (*PVA-SSA 99%hyd*).

3 Characterisation of the PVA-SSA membranes after the thermal treatment

Figure 4 also shows the FTIR spectra of the membranes submitted to the thermal treatment (PVA-SSA crosslinked membranes). It is possible to observe that thermal treatment causes further changes in the FTIR spectra of the PVA-SSA membranes, particularly in the regions related to the OH, COO and COC vibration bands. In *Figure 6* the values of I_{OH} have been plotted as a function of the composition of the PVA-SSA membranes before and after the thermal treatment. There is a clear decrease of the values of I_{OH} after all the membranes are submitted to the thermal treatment, suggesting that a removal of the OH groups is taking place.

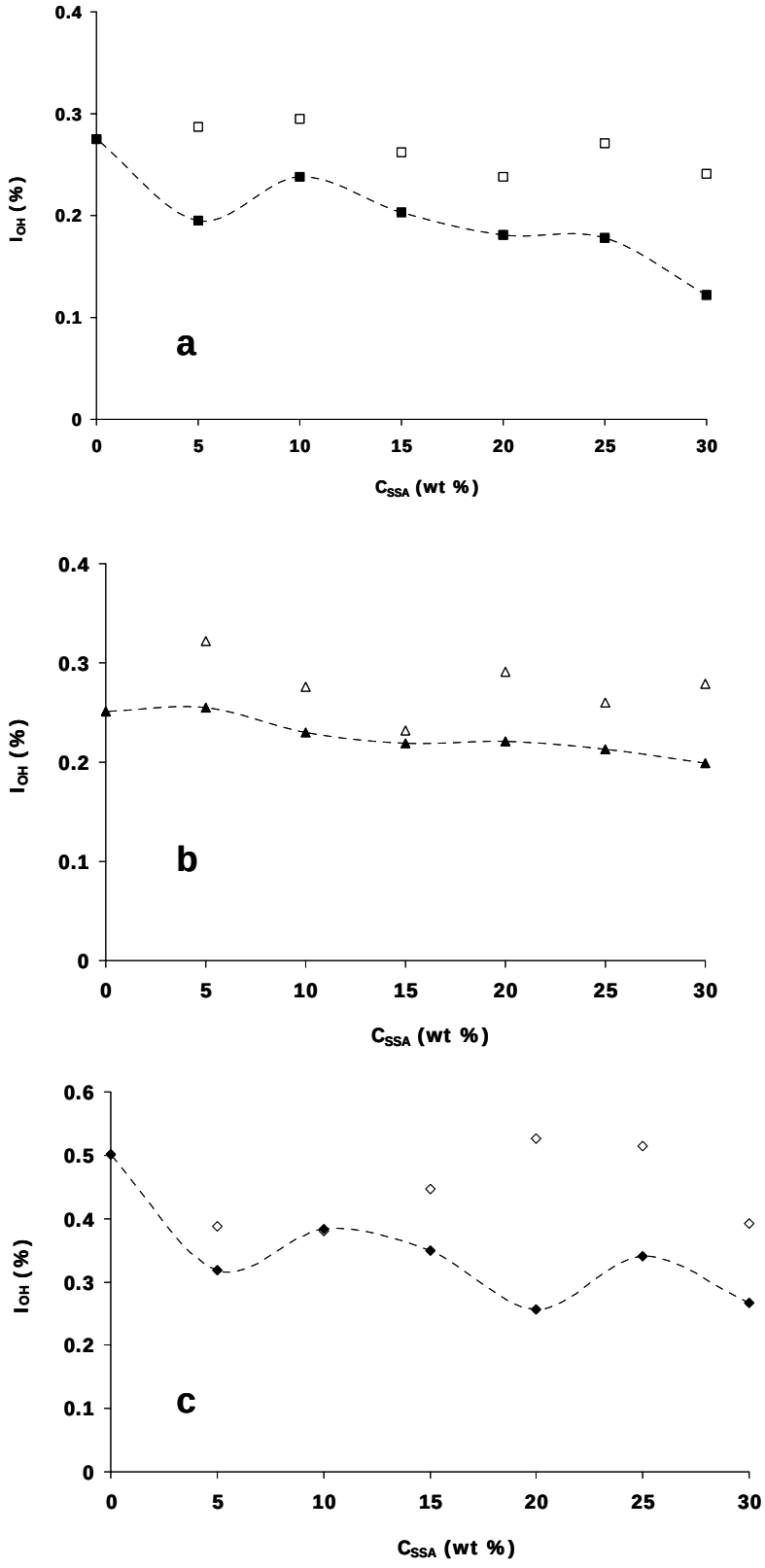

Figure 6 Maximum IR absorbance of the hydroxyl groups (I_{OH}): (a) 89hydPVA–SSA, (b) 96hydPVA–SSA and (c) 99hydPVA–SSA. Blank points correspond to untreated membranes and black points to thermally treated membranes.

The values of the relative intensity $I_{SO3/OH} = \frac{I_{SO3}}{I_{OH}}$ have been calculated and are listed in *Tables 3, 4* and *5*. *T*here is a clear increase in the values of $I_{COO/OH}$ and $I_{COC/OH}$ after the membranes are thermally treated. *Figure 7* shows the evolution of $I_{COO/OH}$ with the concentration of SSA in the membranes after heating. The increase of the COO band occurs for all three PVA substrates, but is greatest for higher SSA concentrations. These results suggest that the thermal treatment promotes the esterification reaction between PVA and SSA. This fact is also supported by the shift of the OH band to higher wavenumbers, which suggests the formation of weaker H-bonds [8, 27, 28].

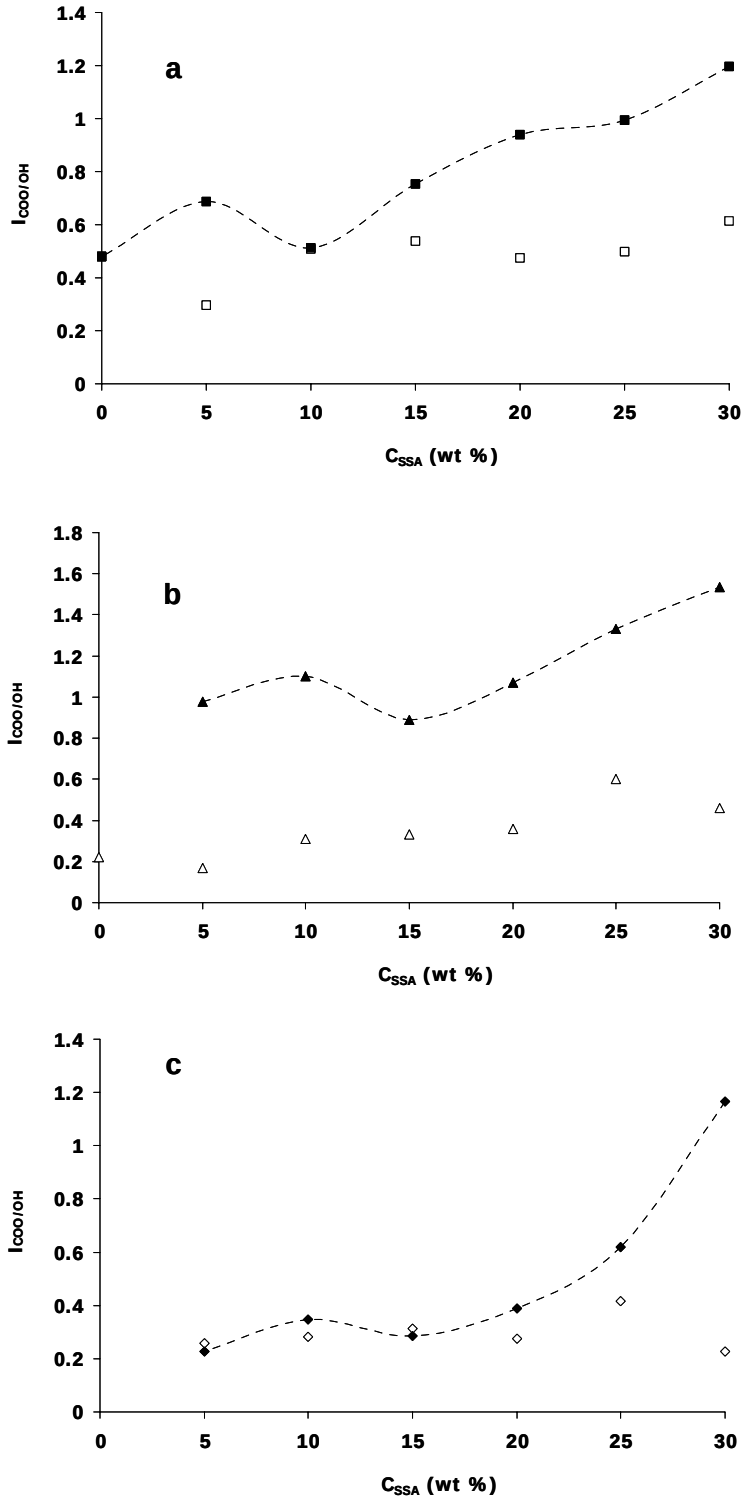

Figure 7 Relative IR absorbance of carbonyl groups to hydroxyl groups ($I_{COO/OH}$): (a) 89hydPVA–SSA, (b) 96hydPVA–SSA and (c) 99hydPVA–SSA. Blank points correspond to untreated membranes and black points to thermally treated membranes.

In general terms, all the PVA-SSA membranes show broadly similar structures. However, thermal treatment does have different effects in the three series of PVA-SSA membranes. *Figure 7* shows that the increase of $I_{COO/OH}$ is more regular in the *89hyd* and *96hyd* series (*Figures 7a and 7b*), while the esterification of the PVA-SSA membranes corresponding to the *99hyd* series is more effective above a certain value of SSA concentration (*Figure 6c)*. These results indicate that the PVA substrate (and therefore the initial concentration of OH groups in the polymer) can seriously affect the esterification process of the PVA-SSA membranes.

It is expected that the chemical environment of water in the polymers also depends on the substrate. The bending vibration band of water has been studied within detail (ν_{water}~1650 cm^{-1}) [15, 20]. Since this band overlaps the COO absorption band, a deconvolution of the 1750 – 1600 cm^{-1} IR region was performed by fitting the experimental FTIR curves to a sum of two Gaussian-Lorentzian peaks. *Figure 8* shows the average values of the frequency corresponding to the H_2O bending vibration band (ν_{water}) in the PVA-SSA membranes, before and after heating.

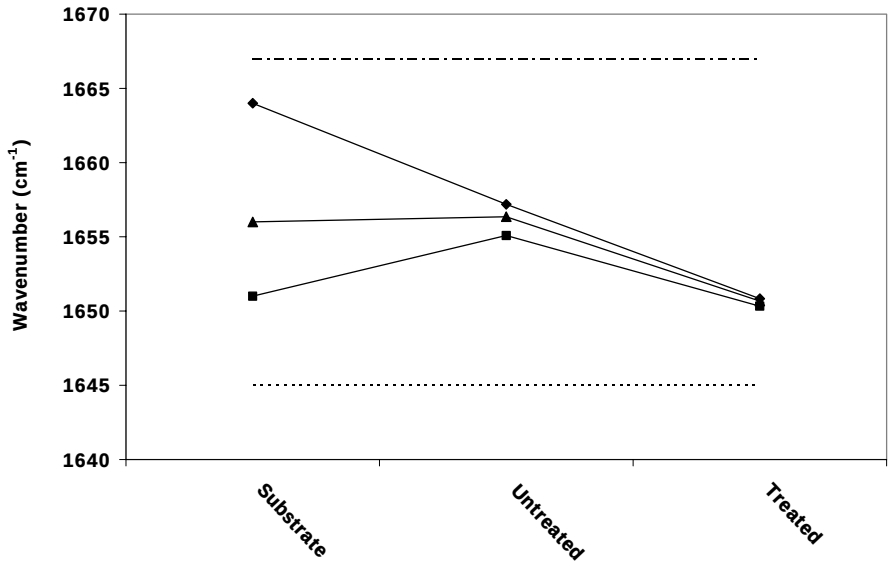

Figure 8 Effect of the membrane preparation and thermal treatment on the position of the H_2O bending vibration band (ν_{water}): (■) 89hydPVA–SSA, (▲) 96hydPVA–SSA, (◆) 99hydPVA–SSA membranes.

The bending vibration band of water appears at higher frequencies in the PVA substrates and the PVA-SSA membranes than in pure water (1645 cm^{-1}), indicating

strong intermolecular interactions between water and polymers. As expected, the number of stronger H-bonds increases in the polymers with higher hydrolysis degrees, due to the higher concentration of OH groups [8, 19]. The preparation of the PVA–SSA membranes and the thermal treatment tend to homogenise the values of ν_{water}. This fact indicates that the water molecules contributing to the band at 1650 cm^{-1} have similar chemical environments in the different PVA-SSA membranes. Moreover, the presence of a tail at $\nu < 3000$ cm^{-1} and at $\nu > 1700$ cm^{-1} in the FTIR spectra of the PVA-SSA membranes indicates the existence of water clusters in the PVA-SSA membranes, independently of the PVA substrate. The formation of polar aggregates in the crosslinked membranes is crucial to the development of proton conducting pathways in *DMFC* electrolytes [22, 29].

In order to study the effect of the thermal treatment on the stability of the membranes, the DTG curves of the *PVA-SSA crosslinked* membranes were obtained. The results corresponding to the *PVA96%hyd* series are shown in *Figure 5,* although similar results were obtained for all these series. The degradation of the PVA-SSA membranes is not changed to a great extent following thermal treatment. These results confirm that the main structure of the polymers is maintained after heating.

The hydrolysis degree of the substrate has some effect on the thermal stability of the different PVA-SSA crosslinked membranes. The values of dw/dT_{max}, T_{peak} and $\Delta\omega$ were obtained from the experimental DTG curves of all the PVA-SSA membranes. The average values of mass loss of the degradation processes ($\Delta\omega$) corresponding to the PVA substrates and the PVA-SSA membranes before and after heat treatment have been plotted in *Figure 9* for the three series.

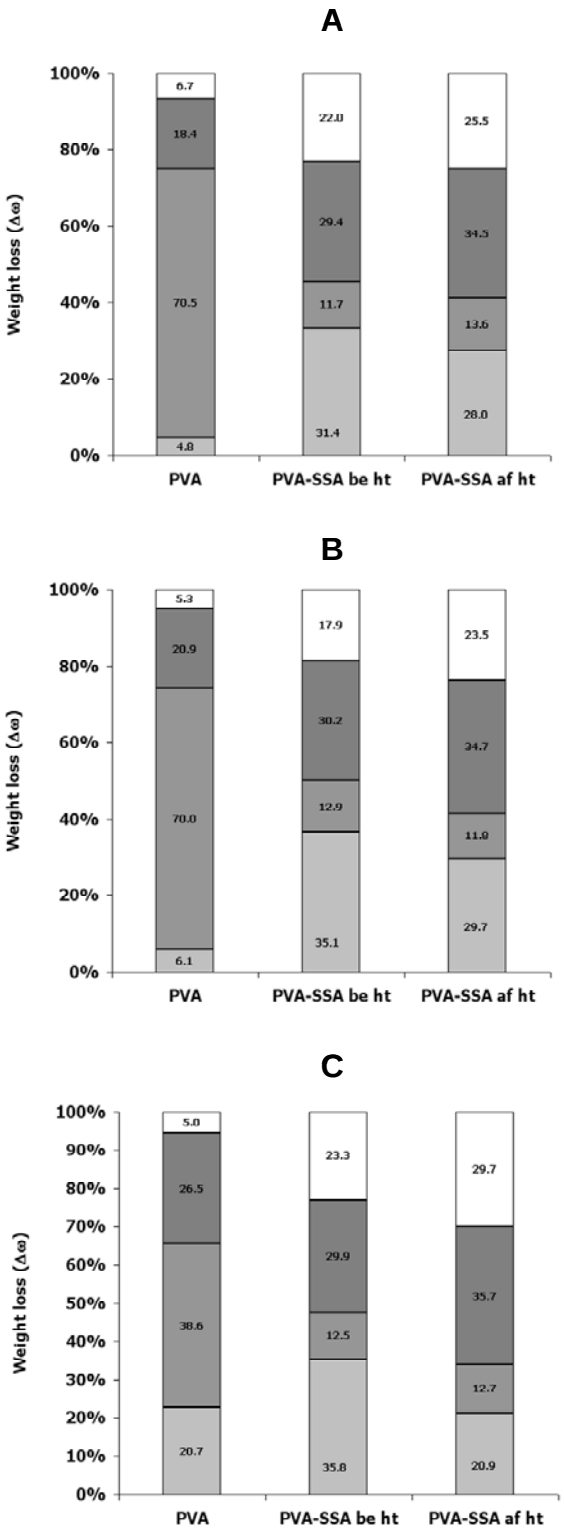

Figure 9 Average values of weigh loss and residual corresponding to the decomposition of: (a) 89hydPVA–SSA, (b) 96hydPVA–SSA, (c) 99hydPVA–SSA membranes. Left column corresponds to PVA substrates, central column to PVA-SSA membranes without thermal treatment and right column to PVA-SSA membranes after thermal treatment. (▫) water - $\Delta\omega_1$, (▪) side groups decomposition ($\Delta\omega_2$), (■) main chains decomposition - $\Delta\omega_3$, (□) residual at 700ºC.

It can be observed that the PVA-SSA membranes prepared with high hydrolysed substrates (*PVA99hyd% and PVA96hyd%*) are the most effected by the thermal treatment. The most thermally stable structures are the PVA-SSA crosslinked membranes prepared from the highest hydrolysis degrees (*PVA99hyd%*). However, the values of water content of *PVA99%hyd* is considerably lower than in the crosslinked membranes with lower hydrolysis degrees (*PVA96hyd and PVA89hyd*) [16, 24, 23].

The parameters corresponding to the thermal degradation of the crosslinked PVA-SSA membranes (after thermal treatment) have also been studied as a function of the concentration of SSA. The values of T_2, T_3 and residual have been summarised in *Table 6*. The results show that the stability of the polymeric chains in the PVA-SSA crosslinked membranes with low hydrolysis degrees (*PVA89hyd* and *PVA96hyd*) increases at higher SSA concentrations.

Table 6. Weight loss values of peak 2 and peak 3 (PVA-SSA membranes)

C_{SSA} (wt. %)	89hyd			96hyd		
	T_2 (ºC)	T_1 (ºC)	Residual (%)	T_2 (ºC)	T_1 (ºC)	Residual (%)
0	317	436	6.7	329	436	5.3
5	248	447	21.3	266	442	22.1
10	274	447	26.1	274	446	20.4
15	277	452	26.0	274	449	22.0
20	277	453	27.3	277	451	23.0
25	278	453	26.8	265	448	26.3
30	279	452	25.5	279	451	27.5

C_{SSA} (wt. %)	99hyd		
	T_2 (ºC)	T_1 (ºC)	Residual (%)
0	267	433	5.0
5	274	448	30.4
10	267	448	33.6
15	278	448	36.3
20	272	447	30.2
25	272	451	23.8
30	277	445	24.2

Moreover, the results corresponding to the water contents ($\Delta\omega_l$) indicate that there is not a clear relationship between the amount of water absorbed in the membranes and the SSA concentration. Although the addition of sulfonic groups is expected to promote an increase in the hydrophilicy of the membranes and thus their capability to absorb water, it is well know that the formation of a network polymer can inhibit the absorption of solvents to some extent [16, 24]. Therefore, water absorption in the PVA-SSA crosslinked membranes is a process which depends on a balance between both factors.

CONCLUSIONS

The hydrolysis degree of the PVA substrate had important effects on the preparation and the final structure of PVA-SSA membranes for *DMFC* applications prepared by thermal crosslinking. The occurrence of esterification between the hydroxyl groups of PVA and the carboxyl groups of SSA and the formation of a crosslinked structure with enhanced stability was observed for all the PVA substrates. The esterification occurred as the membranes were formed but was promoted by the thermal treatment.

The PVA-SSA membranes with highest hydrolysis degrees (*99hyd* and *96hyd*) were the most effected by the thermal treatment and the SSA concentration. The presence of tightly bound water and water clusters in the PVA-SSA membranes has been found. The highest values of water content were observed for the membranes prepared using a PVA substrate with a hydrolysis degree of 96%, which also exhibited the best processing properties in the preparation of crosslinked PVA membranes. These observations suggest that this PVA substrate is the most suited with which to prepare new PVA-SSA membranes electrolytes for *DMFC* applications.

REFERENCES

1. Blomen, L. *Fuel Cell Systems*, Ed. Plenum Press, New York (1993)

2. Hoogers, G. *Fuel Cell Technology Handbook*, CRC Press, Nueva York, (2003)

3. U.S. Department of Energy, *Handbook of Fuel Cells*, Fifth Edition, EG&G Services (2000)

4. DeLuca, N.W., Elabd, Y.A. J Polym. Sci. Part B: Polym. Phys. 44 (2006) 2201

5. Elmér, A.M.; Jannasch, P. J. Polym. Sci. 44 (2006) 2201

6. Shen, C.C.; Joseph, J.; Lin, Y.C.; Lin, S.H.; Lin, C.W.; Hwang, B.J. Desalination 233 (2008) 82

7. Pivovar, B.S.; Wang, Y.; Cussler, E.L. Journal of Membrane Science, 154, (1999) 155

8. Kang, M.S.; Kim, J.H.; Won, J.; Moon, S.H.; Kang, Y.S. J. Memb. Sci 247 (2005) 127

9. Rhim, J.W.; Lee, S.W.; Kim, Y.K. J Appl Polym Sci 85 (2002) 1867

10. Chiellini, E.; Corti, A.; D'Antone, S.; Solaro, R. Prog. Polym. Sci 28 (2003) 963

11. Yang, C.C.; Chiu, S.J.; Chien, W.C. J Power Sources 162 (2006) 21

12. Kim, D.S.; Guiver, M.D.; Nam, S.Y.; Yun, T.I.; Seo, M.Y.; Kim, S.J.; Hwang, H.S.; Rhim, J.W. J. Memb. Sci 281 (2006) 156

13. Socrates, G. *Infrared and Raman Characteristic Groups Frequencies*, Ed. J. Wiley. 2001 England

14. Rhim, J.W.; Yeom, C.K.; Kim, S.W. J. Appl. Polym. Sci. 68 (1998) 1717

15. Xiao, S.; Huang, R.Y.M.; Feng, X. J Memb Sci 286 (2006) 245

16. Hallinan Jr., D.T.; Elabd, Y.A. J Phys Chem B 111 (2007) 13221

17. Rhim, J.W.; Park, H.B.; Lee, C.S.; Jun, J.H.; Kim, D.S.; Lee, Y.M. J Membr Sci 238 (2004) 143

18. Lee, J.; Lee, K.J.; Jang, J. Polym Testing 27 (2008) 360

19. Huang, Y.F.; Chuang, L.C.; Kannan, A.M.; Lin, C.W. J Power Sources 186 (2009) 22

20. Herman S. Mansur, Rodrigo L. Oréfice, Alexandra A.P. Mansur Polymer 45 (2004) 7193

21. Lin, C.W.; Huang, Y.F.; Kannan, A.M. J Power Sources 164 (2007) 449

22. Zundel, G. *The Hydrogen Bond*. Schister, P. Zundel, G. Sandorf, C. Eds. Amsterdam, (1979) pp 655

23. Tury, A. *Thermal Characterization of Polymeric Materials*, Vol 1, Academic Press, San Diego (1997)

24. Qiao, J.; Hamaya, T.; Okada, T. Polymer 46 (2005) 10809

25. Ding, J.; Chuy, C.; Holdcroft, S. Chem. Mater. 13 (2001) 2231

26. Kim, D.S.; Park, H.B.; Rhim, J.W.; Lee, Y.M. Solid State Ionics 176 (2005) 117

27. Pandey, L.K.; Saxena, C.; Dubey, V. J. Memb. Sci. 227 (2003) 173

28. Carretta, N.; Tricoli, V.; Picchioni, F. J. Memb. Sci.166 (2000) 189

29. Zundel, G. *The Hydrogen Bond;* Schister, P. Zundel, G. Sandorf, C.,Eds. Amsterdam, (1979) pp 683

3 COMMUNICATION II

On the diffusion of water and methanol mixtures of Poly(vinyl alcohol) with enhanced proton conductivity for Direct Methanol Fuel Cells (DMFC)

Title:

ON THE DIFFUSION OF WATER AND METHANOL MIXTURES IN POLY(VINYL ALCOHOL) MEMBRANES WITH ENHANCED PROTON CONDUCTIVITY FOR DIRECT METHANOL FUEL CELLS

[1]A. Martínez-Felipe, [2]C.T. Imrie, [1]A. Ribes-Greus

[1]Institute of Materials Technology, Universidad Politécnica de Valencia,
Camino de Vera s/n, 46022, Valencia, Spain

[2]Department of Chemistry, University of Aberdeen, Meston Walk, Aberdeen, Scotland, United Kingdom

Keywords:
DFMC, TGA, FTIR

ABSTRACT

Poly(vinyl alcohol) (PVA) membranes crosslinked with sulfosuccinic acid (SSA) have been prepared as potential electrolytes for application in Direct Methanol Fuel Cells (*DMFC*). The diffusion of water and methanol in the PVA-SSA membranes has been studied using Fourier Transform Infrared Spectroscopy (FTIR) and Thermogravimetric Analysis (TGA). The results have shown that the degree of crosslinking of the polymers plays an important role in the diffusion of the solvents through the membranes. The transport of methanol in the membranes is enhanced by the presence of water through the existence of cooperative processes between the solvents and the polymer.

INTRODUCTION

In recent years, research in Direct Methanol Fuel Cells (*DMFC*) has focused on the reduction of the crossover phenomenon, which consists of the flow of unreacted methanol through the electrolyte [1]. Crossover can cause a drop of efficiency of up to 30% in *DMFC*, since the methanol transferred through the electrolyte reacts at the cathode with oxygen and there is no generation of net electrical power [2, 3, 4, 5, 6]. Along with other shortcomings, crossover represents a serious limitation for the development of commercial *DMFC*.

The development of new Polymer Electrolyte Membranes (*PEM*) to reduce crossover in *DMFC* has focused on the preparation of phase separated polymers with polar regions and non-polar regions. The polymer backbone is usually hydrophobic and provides mechanical strength and chemical stability to the membrane while the presence of polar groups enhances the hydrophilic properties of *PEMs* and also their proton conductivity by the creation of ionic channels. In *DMFC*, it is critical to study the diffusion of water (desired for high proton conductivity) and methanol (undesiredable to avoid crossover) through the electrolytes [1, 7].

Poly(vinyl alcohol) (PVA) membranes have been suggested as an alternative to the use of present commercial materials employed in Direct Methanol Fuel Cells (*DMFC*) electrolytes, due to its high selectivity for water with respect to alcohols. The introduction of polar groups in PVA substrates to obtain high proton conducting *PEM* for *DMFC* is usually carried out by the addition of sulfonated molecules [8, 9]. In particular, sulfosuccinic acid (SSA) has been extensively used as a crosslinking agent in the formation of PVA membranes having high proton conductivities. Under some conditions the esterification of the OH groups in PVA by the two carboxylic acids in SSA (COOH) leads to the formation of a 3D-structure with enhanced solvent resistance and thermal stability [10, 11, 12]. However, prior to the use of PVA membranes in *DMFC*, it is necessary to study the solubility of water and methanol within the membranes and also the state of the solvent inside the polymer structure. All these factors may play an important role in the reduction of crossover in *DMFC*, since the diffusion mechanisms of the solutes in *PEM* are highly interconnected and depend on the interactions between the solvent and the polymer [4, 13].

In this paper we have prepared a series of PVA membranes with different degrees of crosslinking, using SSA as the crosslinking agent. The membranes have been used in swelling tests in water, methanol and their binary mixtures at 35ºC in order to study the absorption of the solvents in the membranes. The composition of the membranes at equilibrium swelling as well as the chemical structure and the thermal stability of the membranes were studied by Fourier Transform Infrared Spectroscopy (FTIR) and Thermogravimetric Analysis (TGA). Finally, the kinetics of desorption of the solvents from the swollen membranes were also studied as a function of the time using time resolved FTIR.

EXPERIMENTAL PROCEDURE

1. Materials

Poly(vinyl alcohol) (PVA) (hydrolysis degree 96%; average molecular weight 85,000 – 146,000 g·mol^{-1}) and a commercial sulfosuccinic acid (SSA) solution (70 wt. % in H_2O) were purchased from Sigma-Aldrich.

2. Membrane preparation

PVA powder with a 96% hydrolysis degree was dissolved in distilled water to form a 10% (weight percentage) solution by stirring at 90ºC for 6 hours. The commercial SSA solution was added to the solution and the mixtures were stirred at room temperature for 1 day. The amount of the commercial SSA solutions varied to form PVA-SSA membranes containing 5%, 10%, 15%, 20%, 25% and 30% by weight percentage of SSA with respect to the amount of PVA in the dry membranes. The resulting solutions were cast on a Teflon sheet and the water was removed by drying in ambient conditions until no further mass loss was observed in the membranes. The resulting PVA-SSA membranes were then heated at 110ºC for 2 hours, and subsequently stored for further analysis. The thickness of the membranes was measured by a clock Comparator Stand (Mitutoyo) with ±1 μm accuracy. The thickness was calculated as the mean of triplicate measurements across different parts of the membranes.

3. Swelling tests

The *PVA96hyd-SSA* membranes were cut in 4x1 cm^2 rectangular films and were weighed (t = 0, w_0) using a Mettler Toledo balance (0.1 mg accuracy). The films were inmersed in test tubes with binary solutions of water and methanol containing 10%, 20% and 30% by weight of methanol. The samples were also inmersed in tubes containing pure water and pure methanol. The test tubes containing the water and methanol solutions of different concentrations and the films were submerged in a thermostated SELECTA Ultrasonic bath (accuracy 0.1ºC) at 35ºC, in order to simulate the behaviour of the materials at low temperatures. The absorption of the solvents in the membranes was measured gravimetrically at different times during the experiment following a standard procedure. First, the superficial liquid was drained from the

samples with a tissue and then the membranes were weighed. The membranes were then placed back into the test tubes and re-submerged in the isothermal bath.

The amount of solvent absorbed was monitored using the parameter M_t:

$$M_t(\%) = \frac{w_t - w_0}{w_0} \cdot 100$$

Membranes were inmersed in the solutions for a maximum time of one week in order to reach equilibrium (M_{eq}).

The different membranes were labelled as *PVAX%-Y%MeOH*, where *X* indicates the weight concentration of SSA in the membranes (C_{SSA}) and *Y* the weight percentage of methanol in the binary mixtures.

4. Attenuated Total Reflectance - Fourier Transform Infrared Spectroscopy (ATR-FTIR)

The chemical characterisation of the *PVA96hyd-SSA* membranes before and after the swelling tests was performed using a FTIR Thermo Nicolet 5700 spectrometer (MA, Waltham) equipped with an ATR modulus. The samples were placed on a diamond crystal, and the experiments were performed using 1 bounce and an incident angle of 45ºC. The spectra were collected after 128 scans with an accuracy of 4 cm^{-1}. Background spectra were collected before each series of experiments.

5. Thermogravimetric Analysis (TGA)

The TGA thermograms were carried out using a Mettler Toledo TGA/SDTA 851 analyser (OH, Columbus). Measurements were performed following a dynamic program from 25ºC to 700ºC at a linear heating rate of 10ºC/min under inert argon (Ar) atmosphere with a flow rate of 50 ml/min. Sample masses were around 5 mg.

6 Desorption tests

The loss of solvent from the swollen membranes was studied using time resolved FTIR-ATR in a Thermo Nicolet 5700 spectrometer (MA, Waltham) equipped with an ATR modulus. The swollen membranes were placed on the ATR surface and the FTIR spectra were acquired continuously with an accuracy of 32 cm^{-1} for 30 minutes. The study of the membranes was completed by means of TGA, using a Mettler Toledo TGA/SDTA 851 analyser (OH, Columbus), and following the same procedure described already.

RESULTS AND DISCUSSION

1. Absorption of water and methanol in PVA-SSA membranes.

The absorption of the solvents in the *PVA96hyd-SSA* membranes followed a typical diffusion process of solutes into a polymeric matrix: the values of M_t increase during the first few minutes of the tests and then stabilise to a maximum value (M_{eq}) rapidly [14].

The values of M_t/M_{eq} were plotted as a function of the normalised time ($t^{1/2}/L$), where L is the thickness of the dry membranes. The normalised curves corresponding to the membrane with C_{SSA}=5% (*PVA96hyd-5%SSA*) are shown in *Figure 1*. The absorption of water and its binary mixtures with methanol in the *PVA96hyd-SSA* membranes fit well to a typical Fickian profile [14]. However, the absorption of pure methanol in the membranes passes through a maximum value after the rapid initial weight increase, followed by an asymptotic decrease to the equilibrium value (M_{eq}). This deviation from Fickian behaviour in the absorption of methanol is observed for all the *PVA96hyd-SSA* membranes inmersed in pure methanol.

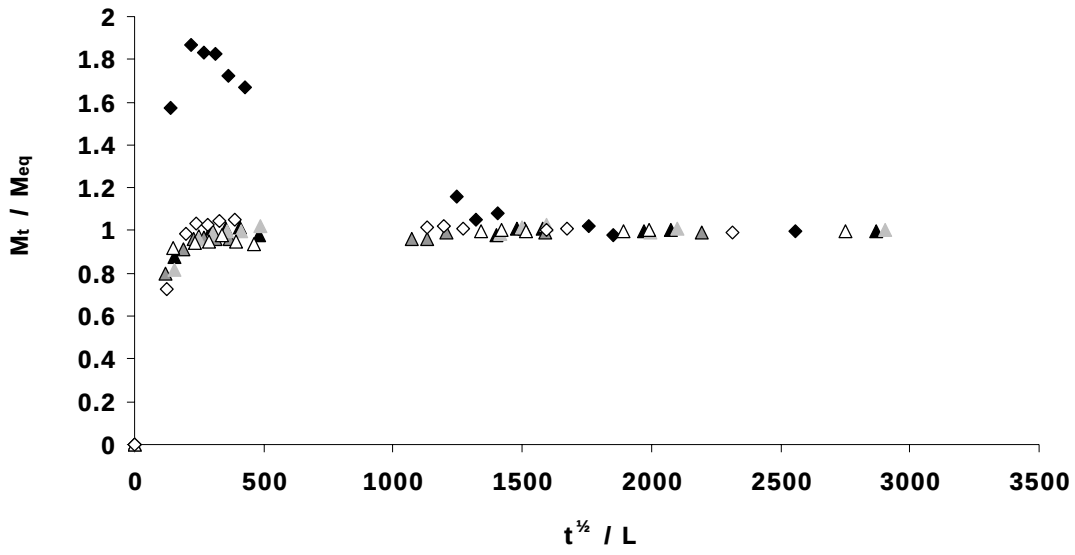

Figure 1. Values of M_t/M_{eq} as a function of the normalised time for the PVA-SSA membranes submitted to the swelling tests: ◇ PVA5%SSA0%MeOH, △ PVA5%SSA10%MeOH, △ PVA5%SSA20%MeOH △ PVA5%SSA30%MeOH, ▲ PVA5%SSA40%MeOH, ◆ PVA5%SSA100%MeOH

The maximum amount of solvent absorbed in the PVA96%hyd-SSA membranes (M_{eq}) depends on the composition of the polymers and the solutions. The values of M_{eq} for the *PVA96%hyd-SSA* membranes were calculated and are shown in *Figure 2* as a function of the SSA concentration (C_{SSA}). The results imply that the membranes absorb considerably less methanol than water, which is in good agreement with the literature [4, 10, 15, 16]. Unlike other commercial membranes used in *DMFC*, there is no apparent relationship between the composition of the mixtures and their solubility in the polymer [17, 18, 19]. Moreover, *Figure 2* also shows that M_{eq} decreases on increasing SSA concentrations suggesting that the absorption of solvent depends on the composition of the *PVA96%hyd-SSA* membranes.

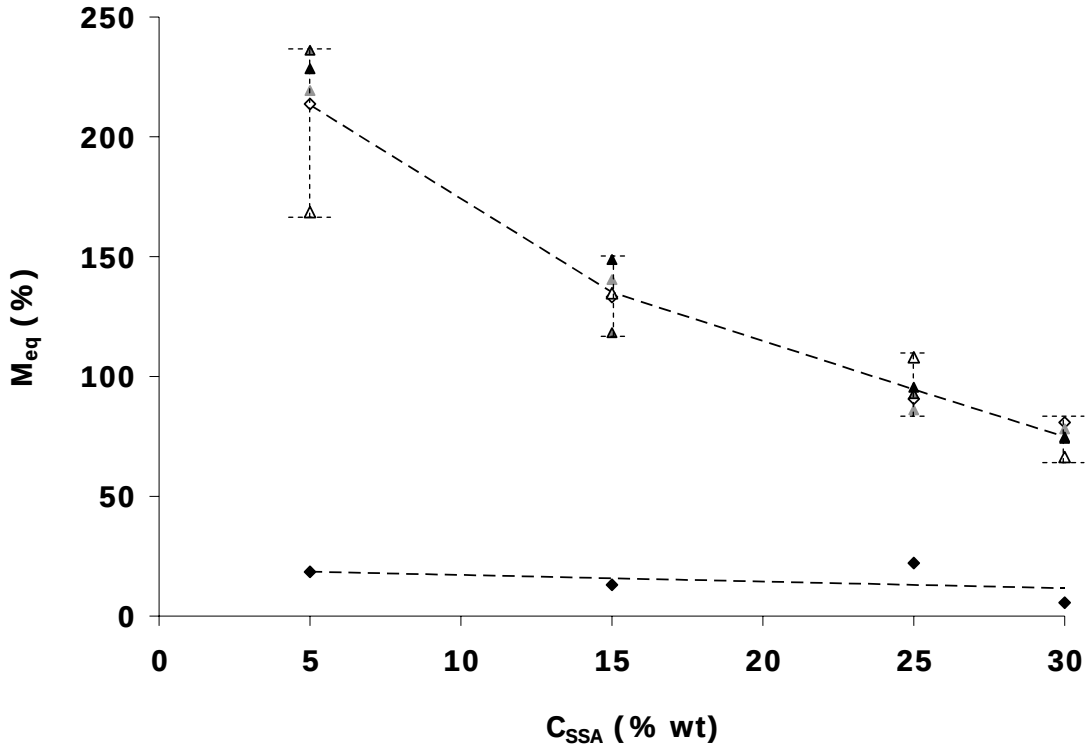

Figure 2. Solvent absorption at equilibrium by the PVA-SSA membranes at 35ºC: ◇ PVA5%SSA0%MeOH, △ PVA5%SSA10%MeOH, ▲ PVA5%SSA20%MeOH ◬ PVA5%SSA30%MeOH, ▲ PVA5%SSA40%MeOH, ◆ PVA5%SSA100%MeOH

The effect of the absorption of the solvents on the chemical structure of the *PVA96hyd-SSA* membranes was studied by FTIR. *Figure 3* shows the FTIR spectra of the *PVA96%hyd-5%SSA* membrane before (curve *a*) and after being inmersed in pure water (*PVA-5%SSA-0%MeOH,* curve *b*) or in pure methanol (*PVA96%hyd-5%SSA-*

100%MeOH, curve *c*) for one week. The FTIR spectra of pure water and methanol are also displayed in *Figure3* (curves *d* and *e*, respectively).

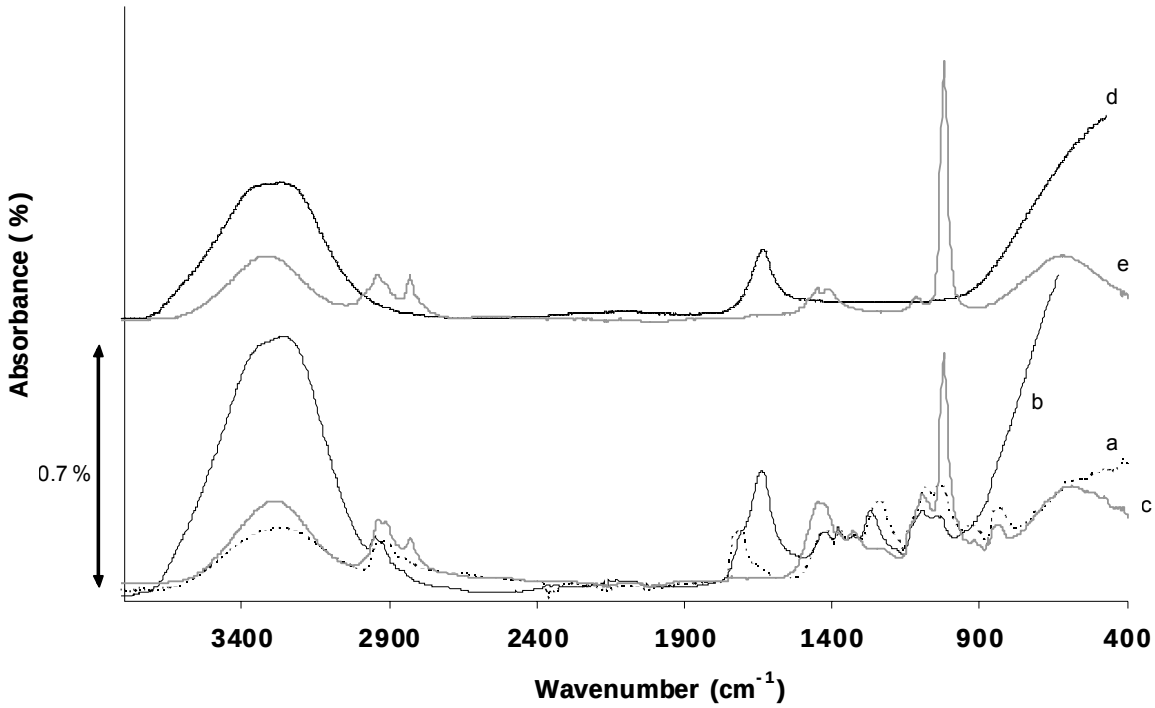

Figure 3. FTIR curves corresponding to (a) PVA5%SSA, (b) PVA5%SSA0%MeOH, (c) PVA5%SSA100%MeOH, (d) water and (e) methanol.

The curve corresponding to the *PVA96%hyd-5%SSA* membrane (*Figure 3a*) shows the characteristic IR bands associated with the functional groups of PVA, including the stretching vibration band of the hydroxyl (OH) groups in the ν_{OH} 3600 – 3000 cm^{-1} region, the bands corresponding to the acetate groups of PVA at ν_{COO}~1710 cm^{-1} (COO *st*) and ν_{COC} ~1260 cm^{-1} (COC *st*) and a prominent peak in the vicinity of ν~1080 cm^{-1} related to the vibration of the CHOH groups of the PVA main chain. Moreover, the presence a low intensity peak at ν ~1650 cm^{-1} associated with the bending of the H_2O molecule denotes the presence of water in the *PVA96%hyd-SSA* membranes [8, 12, 20-24].

The bands at 1710 cm^{-1} and 1260 cm^{-1} can also be attributed to the ester bonds formed by the reaction between the OH groups of PVA and the COOH groups of SSA during the preparation of the *PVA96%hyd-%SSA* membranes [8, 25]. This can be seen in *Figure 4*, in which the FTIR spectra of the different *PVA96%hyd-%SSA* membranes

have been plotted. The growth of the COO band (1710 cm^{-1}) and the appearance and growth of the band at ν~1034 cm^{-1} associated with the sulfonic groups (SO_3^-) on increasing SSA concentration imply the introduction of proton conductive groups in the *PVA96%hyd-%SSA* membranes by the formation of esters.

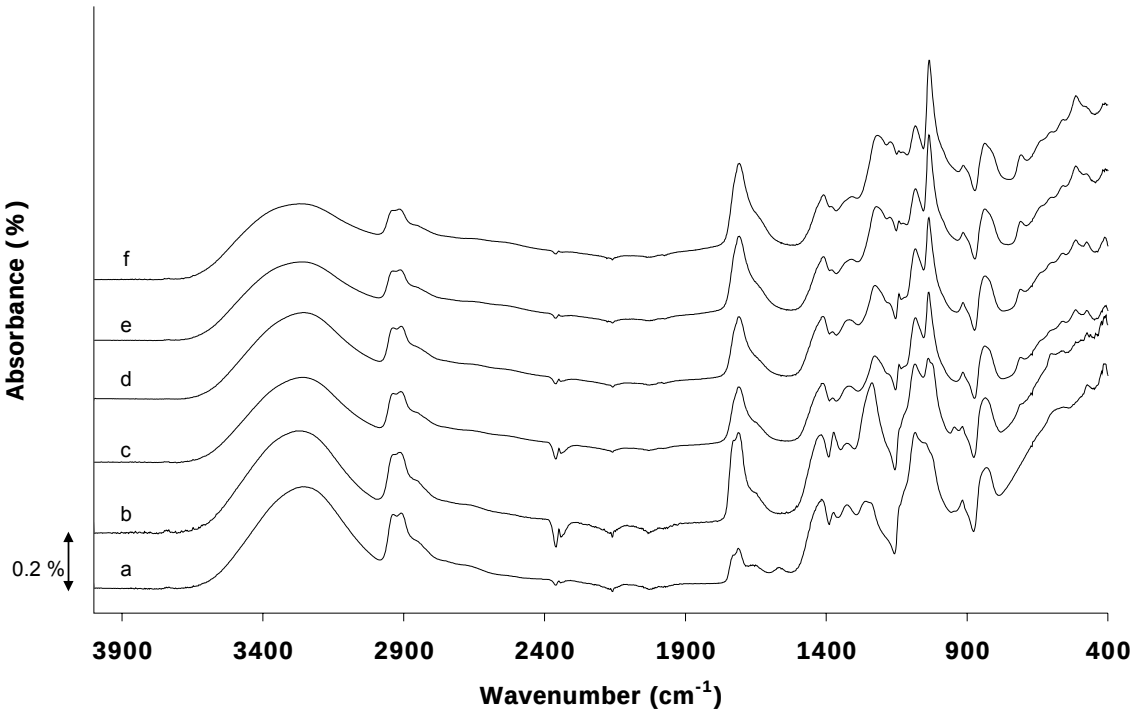

Figure 4. FTIR – ATR curves corresponding to the PVA-SSA membranes: (a) PVA0%; (b) PVA5%SSA, (c) PVA15%SSA, (d) PVA20%SSA, (e) PVA25%SSA, (f) PVA30%SSA.

Figure 3 shows that there is a clear increase of the bands associated with the OH stretching and the bending modes of H_2O (ν ~1650 cm^{-1}) in the curve corresponding to *PVA-5%SSA-0%MeOH* (curve *b*), due to the absorbance of water in the membrane compared with curve (a), the spectra of the dry membrane. On the other hand the samples inmersed in pure methanol (*PVA-5%SSA-100%MeOH*) show a prominent peak at ν~ 1020 cm^{-1}. This band is associated with the C-O stretching vibration in methanol (curve *c*) and its presence is critical in the study of absorption of alcohols in *DMFC* electrolytes [22]. These three bands will be used to establish the presence and composition of the solvents absorbed by the *PVA96%hyd-%SSA* membranes.

The FTIR spectra of the samples inmersed in the binary mixtures show the bands corresponding to absorbed water and methanol, see *Figure 5.* The intensity of the band at 1016 cm^{-1} increases on increasing methanol concentration in the solutions, suggesting that methanol is absorbed from the binary mixtures. Since the absorbance of pure methanol in the PVA-SSA membranes was found to be very low, this strongly suggests that water somehow enhances the methanol diffusion. The changes in the intensity of the stretching CH_3OH band in the membranes inmersed in binary mixtures are accompanied with a shift in its position (from ν_{MeOH} ~1021 cm^{-1} to 1016 cm^{-1}) and suggests the existence of interactions between water and methanol [26]. The differences in the values of ν_{MeOH} observed in the *PVA96%hyd-%SSA* membranes with respect to those observed in the binary solutions suggest that the polymer structure disrupts the interactions existing between the solvents.

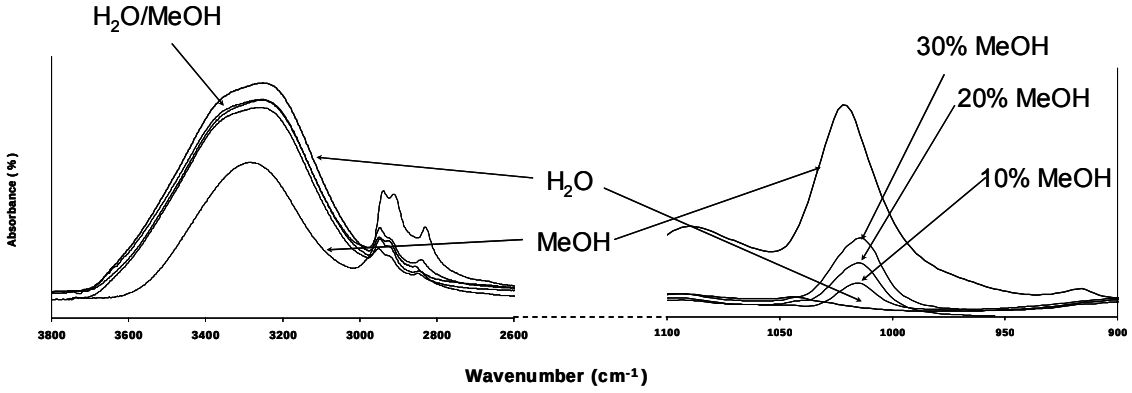

Figure 5. FTIR curves corresponding to PVA5%SSA submerged in pure water, pure methanol and water and methanol binary mixtures with different compositions.

The changes accompanying the absorption of the solvents in the thermal stability of the *PVA96%hyd-%SSA* membranes have been studied by TGA. *Figure 6* shows the DTG curves corresponding to the *PVA96%hyd-30%SSA* membrane before and after swelling tests in water, methanol and a binary mixture containing 30% by weight of methanol.

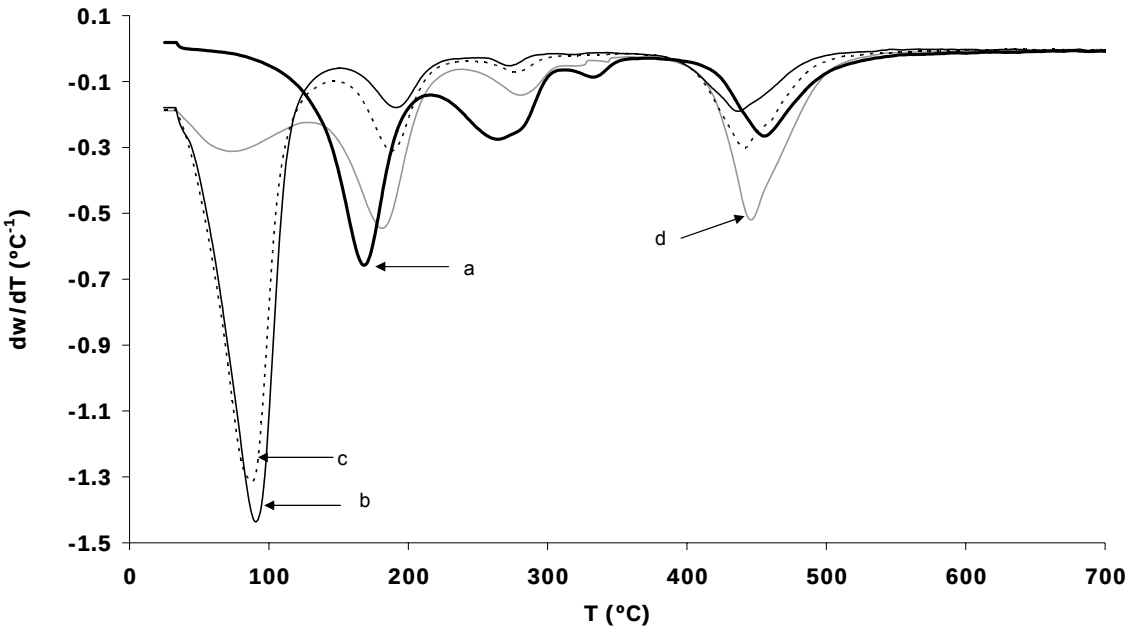

Figure 6. DTG curves corresponding to the membranes (a) PVA-30%SSA, (b) PVA-30%SSA-0%MeOH, (c) PVA-30%SSA-30%MeOH, (d) PVA-30%SSA-100%MeOH.

The thermal degradation of the *PVA96%hyd-30%SSA* membrane proceeds in several steps corresponding to different mass loss processes. A prominent process in the vicinity of T=175ºC is observed which has been previously attributed by other authors to the loss of tightly bound water in the *PVA96%hyd-SSA* membranes, [8]. This process may obscure the presence of a weak peak at lower temperatures (T~100ºC) which is related to the loss of free solvent from the membranes. In the 250 – 350ºC region additional mass loss processes can be seen related to desulfonation and the loss of hydroxyl groups from the membranes. Finally, the decomposition of the main chain of the membranes occurs at higher temperatures (400 – 500ºC). The high values of residue in the *PVA96%hyd-SSA* membranes are around $\Delta\omega$~20%, which confirm the existence of a crosslinked structure formed by esterification (PVA substrates have residual values around $\Delta\omega$~5%) [8, 11].

Figure 6 shows a clear increase in the values of the loss of free solvent (T~100ºC), and a decrease in the values of the peaks previously related to the loss of tightly bound solvent in the membranes inmersed in water and in binary mixtures. This indicates a preferential absorption of free solvent in the *PVA96%hyd-SSA* membranes and is in good agreement with the values obtained for M_{eq} in the swelling tests (see *Figure 2*). However, on increasing methanol contents in the binary solutions there is a relative

increase of the mass loss at 175ºC with respect to the process at lower temperatures. This fact suggests that the presence of methanol somehow promotes the absorption of tightly bound solvent in the membranes [27, 28].

3. Desorption of water and methanol from the swollen PVA-SSA membranes.

The maximum intensity of the IR bands related to methanol (C-O stretching at ν~1016 cm^{-1}) and water (OH stretching, ν~3600-3000 cm^{-1} and H_2O bending at ν~1650 cm^{-1}) were monitored as a function of the time for the *PVA96%hyd-%SSA* membranes after being removed from the swelling solutions. The results of maximum absorption $(Abs_{max})_t$ at a certain time *t* of desorption were normalised by the initial intensity $(Abs_{max})_{t=0}$, according to the following expressions:

$$I_{OHStretch} = \frac{Abs_{\max}(3200cm^{-1})_t}{Abs_{\max}(3200cm^{-1})_{t=0}} \cdot 100$$

$$I_{H2OBend} = \frac{Abs_{\max}(1650cm^{-1})_t}{Abs_{\max}(1650cm^{-1})_{t=0}} \cdot 100$$

$$I_{Met} = \frac{Abs_{\max}(1016cm^{-1})_t}{Abs_{\max}(1016cm^{-1})_{t=0}} \cdot 100$$

Similar experiments were also carried out to measure the loss of solvent from droplets of water/methanol binary mixtures containing 10%, 20% and 30% by weight of methanol, and also from pure water and methanol.

Figure 7a shows the evolution with the time of I_{Met}, $I_{H2OBend}$ and $I_{OHStretch}$ for the diffusion of solvents from a membrane previously inmersed in a binary solution containing 20% of methanol (PVA-*SSA5%-20%MeOH*).

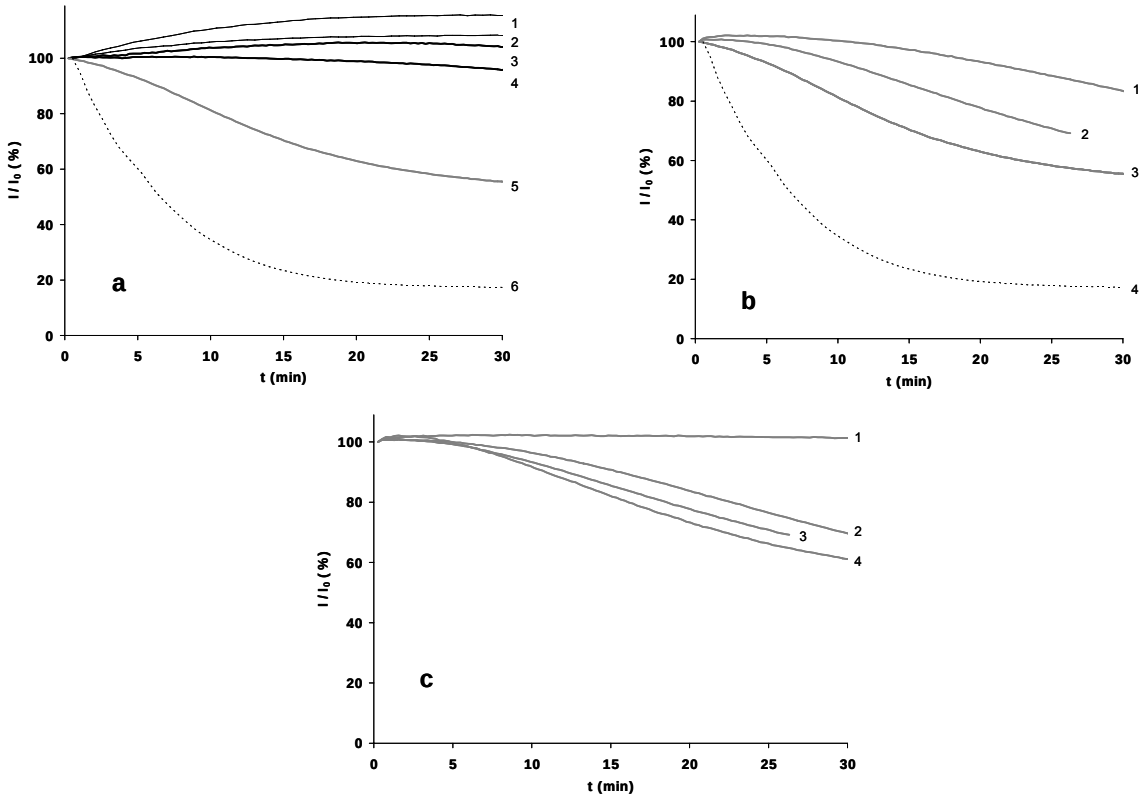

Figure 7. Study of the desorption process through the curves of normalised FTIR absorbance (I/I_0) of different membranes.

(a) Curves corresponding to PVA-20%SSA-20%MeOH: (a1) $I_{H2Obend}$(solution 20%MeOH), (a2) $I_{OHStretch}$(solution 20%MeOH), (a3) $I_{H2Obend}$(PVA5%SSA 20%MeOH), $I_{OHStretch}$ (PVA5%SSA 20%MeOH), IMet (PVA5%SSA 20%MeOH), I_{Met}(solution 20%MeOH.

(b) Effect of the membrane composition: (b1) I_{Met} (PVA25%SSA 20%MeOH), (b2) I_{Met} (PVA15%SSA 20%MeOH), I_{Met}(PVA5%SSA 20%MeOH) and (b3) I_{Met} (solution 20% MeOH) solution.

(c) Effect of the concentration of the solution (c1) I_{Met} (PVA-15%SSA-100%MeOH), (c2) I_{Met} (PVA-15%SSA-30%MeOH), (c3) I_{Met} (PVA-15%SSA 20%MeOH) and (c4) I_{Met} (PVA-15%SSA-10%MeOH)

The diffusion of the corresponding solution has been also included. While the values of I_{Met} decrease with the time, the bands related to water ($I_{H2OBend}$ and $I_{OHStretch}$) slightly increase, indicating a rapid loss of methanol from the membranes [22]. This effect is also observed in the diffusion from the solutions non-confined in the polymer (dotted lines in *Figure 7*) and in the FTIR spectra at different times (see *Figure 8*), and can be attributed to the low vapour pressure of methanol and the high affinity between water and methanol. In *Figure 7a* it is also possible to observe that the diffusion of *MeOH* from the binary solutions proceeds following a 1st order process, while the transport

from the *PVA96%hyd-%SSA* membranes tends to a zero order process. These results suggest that the diffusion of methanol probably involves molecular dynamics of the polymeric chains of the membranes [29]

Figure 7b shows the results of loss of methanol for *PVA96%hyd-%SSA* membranes with different SSA percentages inmersed in binary mixtures with 20% of methanol weight percentage. The shapes of the curves tend to a first-order process on decreasing SSA contents, which indicates that high crosslinking degrees promotes a deviation from the behaviour observed in the diffusion of methanol from the binary mixtures.

Finally, *Figure 7c* shows that the solvent composition has an important effect on the desorption profiles of methanol. The diffusion of methanol is promoted at lower methanol concentrations (*PVA-15%-10%MeOH*), while the curves tend to become flatter on increasing methanol contents in the binary mixtures. These results are in accord with the values of swelling tests which indicated very low methanol absorption from pure methanol. [22, 29].

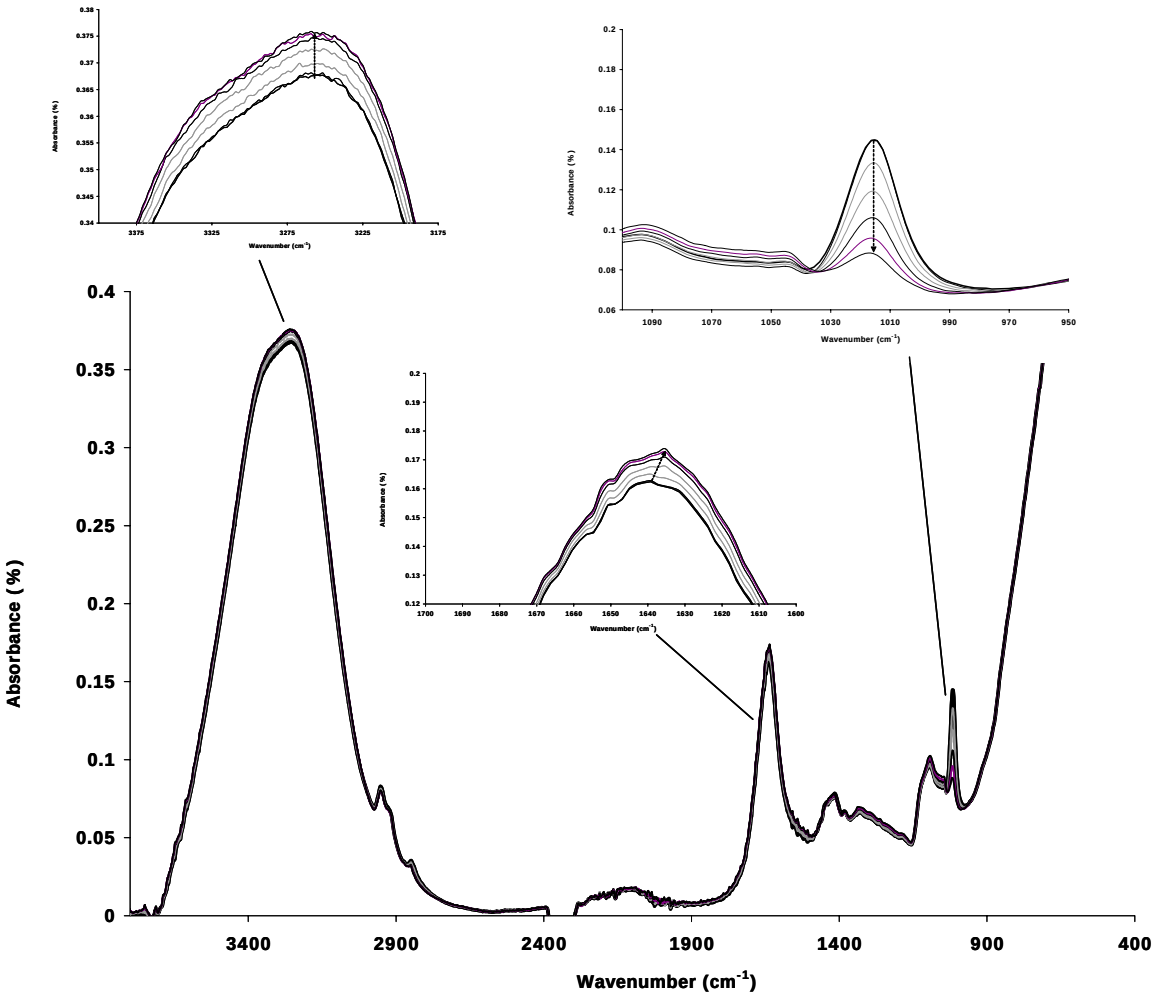

Figure 8. FTIR curves corresponding to the desorption of the solvents from the sample PVA-15%SSA-10%MeOH. The arrows indicate the evolution of the FTIR regions with time up to 30 minutes.

CONCLUSIONS

FTIR and TGA revealed that the transport properties of water, methanol and their binary mixtures through crosslinked poly(vinyl alcohol) (PVA) membranes having enhanced proton conductivity were strongly dependent on the composition of the membranes and the solvent. This information is important in evaluating their application as portential electrolytes in Direct Methanol Fuel Cells (*DMFC*) in order to reduce crossover.

While the *PVA96%hyd-%SSA* membranes absorbed high amounts of solvent from the water and water/methanol binary mixtures, the diffusion of pure methanol was very low and deviated from ideal behaviour. Moreover, the methanol was tightly bound to the polymeric structure.

The composition of the binary mixtures and the polymer structure greatly affected the transport mechanism of the solvents in the *PVA96%hyd-%SSA* membranes. The results suggest that the presence of water promotes the diffusion of methanol by the occurrence of molecular dynamic processes involving the polymeric chains. Moreover, it was observed that high degrees of crosslinking tend to reduce the diffusion of methanol through the *PVA96%hyd-%SSA* membranes, probably by the reduction of free volume in the polymers.

REFERENCES

1. Elmér, A.M.; Jannasch, P. J. Polym. Sci. 44 (2006) 2201

2. Pivovar, B.S.; Wang, Y.; Cussler, E.L. Journal of Membrane Science, 154, (1999) 155

3. Kang, M.S.; Kim, J.H.; Won, J.; Moon, S.H.; Kang, Y.S. J. Memb. Sci 247 (2005) 127

4. Rhim, J.W.; Lee, S.W.; Kim, Y.K. J Appl Polym Sci 85 (2002) 1867

5. Kim, D.S.; Park, H.B.; Rhim, J.W.; Lee, Y.M. Solid State Ionics 176 (2005) 117

6. Larminie, J.; Dicks, A. *Fuel Cell Systems Explained* 2nd ed.,Wiley: New York (2003)

7. Adam Z. Weber and John Newman Chem Rev 104 (2004) 4679

8. Ji-Won Rhim, Ho Bum Park, Choong-Sub Lee, Ji-Hyun Jun, Dae Sik Kim, Young Moo Lee J. Membr. Sci. 238 (2004) 143

9. Chia-Chin Shen, Jorphin Joseph, Yun-Chih Lin, Sheng-Horng Lin, Chi-Wen Lin, Bing Joe Hwang Desalination 233 (2008) 82

10. Yang, C.C.; Chiu, S.J.; Chien, W.C. J Power Sources 162 (2006) 21

11. Kim, D.S.; Guiver, M.D.; Nam, S.Y.; Yun, T.I.; Seo, M.Y.; Kim, S.J.; Hwang, H.S.; Rhim, J.W. J. Memb. Sci 281 (2006) 156

12. Rhim, J.W.; Yeom, C.K.; Kim, S.W. J. Appl. Polym. Sci. 68 (1998) 1717

13. P. Costamagna; S. Srinivasan, J Power Sources 102 (2001) 242

14. P. Neogi, Marcel Dekker, *Diffusion in Polymers*, New York (1996) p 186

15. Rhim, J.W. Kim, Y.K. J Appl Polym Sci 75 (2000) 1699

16. Ji-Won Rhim, Min-Young Sohn, Hyeok-Jong Joo, Kew-Ho Lee J Appl Polym Sci 50 (1993) 679,

17. W. Vieth, *Diffusion in and through polymers, principles and applications* Hanser Publishers (1991)

18. Venturi, M.T.; Tosi, C. J. Mol. Struct. 14 (1972) 293

19. Hietala, S.; Maunu, S.L.; Sundholm, F. J. Polym. Sci. Part B: Polym. Phys. 38 (2000) 3277

20. Xiao, S.; Huang, R.Y.M.; Feng, X. J Memb Sci 286 (2006) 245

21. Hallinan Jr., D.T.; Elabd, Y.A. J Phys Chem B 111 (2007) 13221

22. Lee, J.; Lee, K.J.; Jang, J. Polym Testing 27 (2008) 360

23. Y.F. Huang, L.C. Chuang, A.M. Kannan, C.W. Lin J Power Sources 186 (2009) 22

24. Mansur, H.S.; Oréfice, R.L.; Mansur, A.P. Polymer 45 (2004) 7193

25. Qiao, J.; Hamaya, T.; Okada, T. Polymer 46 (2005) 10809

26. Wakisaka, A.; Abdoul-Carime, H.; Yamamoto, Y.; Kiyozumi, Y. J. Chem. Soc. Faraday Trans. 94 (1998) 369

27. Duplessix, R.; Escoubes, M.M.; M. Rodmacq, B.; Volino, F.; Roche E J. J. Therm. Anal. Calorim. 58 (1999) 569

28. Eisenberg, A.M.; Pineri, M., *Water in Polymers* Rowlands ACS Symposium Series 127; ACS Washington DC (1980) p 469

29. Tarcha, P.J. *Polymers for Controlled Drug Delivery* Boca Raton: CRC Press (1990)

4 CONCLUDING REMARKS

In this chapter different PVA materials were prepared with the aim to obtain externally regulated membranes for *DMFC*. First, carboxylic acid liquid crystals were reacted with a PVA substrate to obtain side-chain liquid-crystalline polymers by esterification. The syntheses had very low yields and the resulting materials poor processability (high melting point, high viscosity). This synthetic route was discarded. As an alternative, the preparation of polymeric dispersions such as those obtained in chapter 4 was proposed. In order to increase the thermal stability of the dispersions and to enhance the proton conductivity of the membranes, PVA was crosslinked with sulfosuccinic acid (SSA) by means of thermal treatment.

The effect of the chemical composition of the PVA substrate used to prepare the crosslinked membranes was studied by FTIR and TGA. The results showed that PVA substrates with intermediate hydrolysis degrees (*HD* ~ 96%) were the most suitable for the preparation of the PVA-SSA membranes by thermal treatment. Considering these results, the absorption of water and methanol and their binary mixtures in PVA-SSA membranes with a 96% hydrolysis degree was studied through absorption (swelling tests) and desorption (time resolved FTIR-ATR) tests.

The results indicated that the transport of methanol in the membranes was strongly dependent on the presence of water, and also on the polymeric structure. It is notable that the behaviour of the PVA-SSA membranes differed with respect to the commercial samples studied in chapter 3, since the absorption of pure methanol was hindered to a great extent. It is also worth noting the low degrees of absorption of methanol and also the effect of the polymeric structure on the solvent absorption shown by these membranes. However, the interrelationship between the transport properties of water and methanol may be an important drawback in this attempt to reduce crossover in potential *DMFC* applications. The results in this chapter have also shown that the amount of solvent tightly bound to the polymer structure does not increase to any great extent during the swelling tests.

A similar methodology to the previous chapters was applied to the preparation and characterisation of PVA-SSA membranes to evaluate their potential application in

DMFC. Fourier Transform Infrared Spectroscopy (FTIR) and Thermogravimetric Analysis (TGA) has provided information about the chemical processes involved in the preparation of the materials.

FTIR focused on the chemical environment of the different groups in the membranes. The calculation of relative values of absorbance ($I_{COO/OH,}$ $I_{COC/OH}$…) was very useful in studying variations in the composition of the materials. All the results were normalised and were compared within the series. The study of the frequencies of the bands provided a good description of the intermolecular and intramolecular interactions between the groups in the membranes. The TGA results gave evidence of structural changes through the thermal stability of the materials. It was also possible to study the state of solvent, showing the existence of free and bound water, as also observed in the Nafion membranes.

Swelling tests were used to characterise the absorption of water, methanol and their binary mixtures by the membranes. The analysis procedure of the data was similar to that performed for the Nafion membranes, although remarkable differences were obtained between the materials. All the tests were performed at 35ºC although the effect of temperature on the transport of the solvents could be easily carried out by performing tests at different temperatures. Following the same methodology as in chapter 3, the membranes used in the swelling tests were analysed by FTIR and TGA. The combination of the swelling tests, FTIR and TGA analyses has provided relevant information about the state of the solvents in the membranes. In this case, the study has focused on the evolution of the IR bands of the solvents (ν=1650 cm^{-1} for water bending and ν=1016 cm^{-1} for the methanol C-O stretching band). The study of the hydroxyl stretching band of the solvents (ν=3600-3000 cm^{-1}) was obscured by that associated with the OH groups of the PVA chain.

The study of the transport properties of methanol and water was completed by undertaking desorption tests using time resolved FTIR-ATR. These studies provided relevant information about the dynamics of desorption of the solvents from the membranes. Moreover, additional desorption tests using solutions of water and methanol binary mixtures non-confined into the polymers. The results shed important

light on the diffusion of the solutes into the membranes which are relevant for the design of materials with controlled release properties.

REFERENCES CHAPTER 5

1. Nácher, A.; P. Escribano, P.; Del Río, C.; Rodríguez, A.; Acosta, J. L J. Polym. Sci. Part A: Polym. Chem. 41 (2003) 2809

2. Mauritz, K.A.; Robert B. Moore, R.B. Chem Rev 104 (2004) 4535

3. Chiellini, E.; Corti, A.; D'Antone, S.; Solaro, R. Prog. Polym. Sci 28 (2003) 963

4. Yang, C.C.; Chiu, S.J.; Chien, W.C. J Power Sources 162 (2006) 21

5. Rhim, J.W.; Yeom, C.K.; Kim, S.W. J. Appl. Polym. Sci. 68 (1998) 1717

6. Rhim, J.W.; Park, H.B.; Lee, C.S.; Jun, J.H.; Kim, D.S.; Lee, Y.M. J Membr Sci 238 (2004) 143

7. Shen, C.C.; Joseph, J.; Lin, Y.C.; Lin, S.H.; Lin, C.W.; Hwang, B.J. Desalination 233 (2008) 82

8. Stewart, D.; Paterson. B.J.; Imrie, C.T. Eur. Polym. J. 33 (1997) 285

9. Janietz, D.; Bauer, M. Makromol. Chem. 192 (1991) 2635

10. Yamaura, K.; Ideguchi, S.; Tanigami, T. J. Appl. Polym. Sci. 70, 1998, 1661

6

New side-chain liquid-crystalline copolymers containing proton conducting groups

1 SUMMARY

Side-chain liquid-crystalline polymers (*SCLCP)* are materials containing mesogenic groups attached to a polymeric backbone through side chains [1-9]. The main parts of a *SCLCP* are shown schematically in *Figure 6.1*.

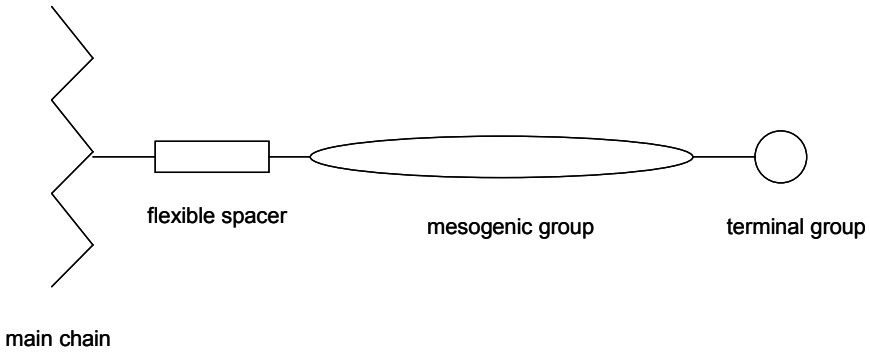

Figure 6.1 Schematic representation of a Side-Chain Liquid-Crystalline Polymer (SCLCP)

The properties of *SCLCP* depend on various factors, such as the backbone flexibility, the length of the spacer, the structure of the mesogenic group (core and terminal groups), the molecular weight and so on. *SCLCP* usually form well ordered mesophases, such as *smectic* phases, although other structures can be eventually formed.

Over a number of years *SCLCP* based on polymethacrylate backbones have been synthesised and studied. The general structure of a polymethacrylate based SCLCP is shown in *Figure 6.2*.

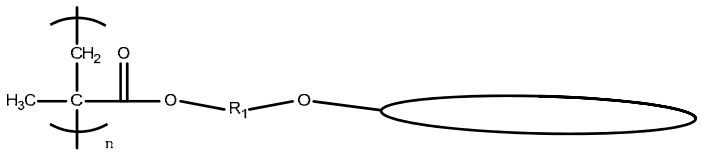

Figure 6.2 Schematic representation of a polymethacrylate-based SCLCP

Polymethacrylate-based *SCLCP* are usually prepared from the corresponding methacrylic acid by radical polymerisation.

The properties of the material depend on the structures of the backbone, the flexibility of the spacer, and the side groups. It is very common to introduce other groups into the methacrylate main chain in order to vary the properties, including, for example, copolymers which include repeating unit with methacrylate or acrylic acid units along the backbone (*Figure 6.3*).

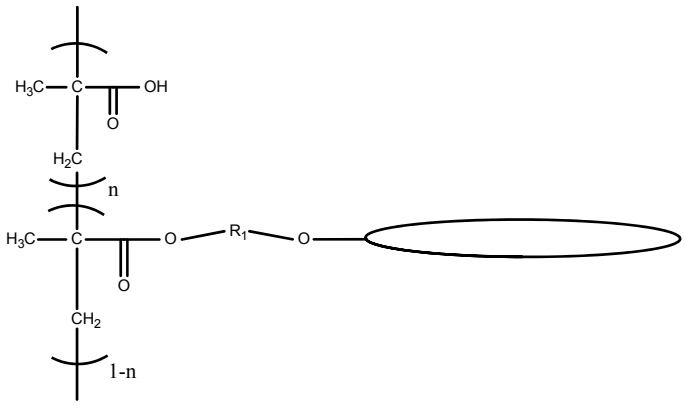

Figure 6.3 Schematic representation of a polymethacrylate-based SCLCP containing non-mesogenic units in the backbone.

The introduction of these non-meseogenic units in the main chain has important effects on the properties of the resulting copolymers. For example, the glass transition temperature is modified while the liquid crystal-siotropic transition temperature is reduced. Indeed the liquid crystallinity of the polymers is maintained only up to a certain concentration of the non-mesogenic compound. Some studies have also reported changes in phase type on increasing the non-mesogenic unit content [10].

Different mesogenic groups have been used to prepare side-chain liquid-crystalline polymethacrylates, including azobenzene and cyanobiphenyl units, see *Figure 6.4*. The terminal groups of the liquid crystal moieties have also been varied in order to study their effect on the properties of the resulting polymers.

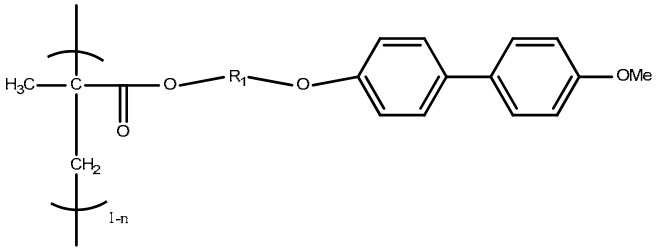

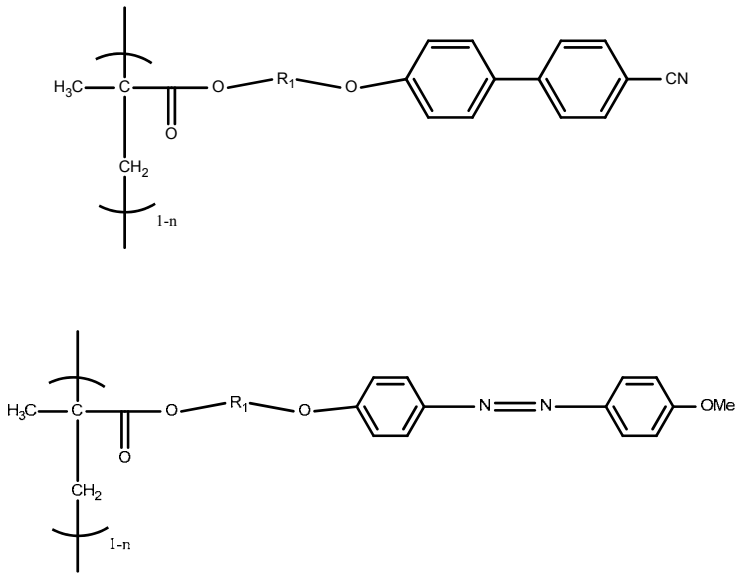

Figure 6.4 Examples of different polymethacrylate-based SCLCPs

The chain length of the spacer R_1 also plays an important role in determining the properties of polymethacrylate-based *SCLC* polymethacrylates. An increase in the chain length generally decreases the clearing point, liquid crystalline transitions and glass transition temperature. An odd-even effect is also observed in the polymers when the chain length and parity is varied, as also seen for low molecular weight compounds. All these effects are attenuated as the spacer is increased.

In this chapter, a series of new side-chain liquid-crystalline copolymers (*SCLCP)* with enhanced proton conductivity has been prepared and characterised. Considering the low yields obtained for the preparation of side chains polymers by polymer modification of a PVA main chain, in this chapter the materials have been prepared by copolymerisation of mesogenic and non-mesogenic monomer units. The materials are based on poly methacrylates containing azobenzene moieties (10-(4-methoxy-4'-oxy-azobenzene) decyl methacrylate) (*10-MeOAzB*). The proton conductivity of the polymer is enhanced by copolymerisation with 2-acrylamido-2-methyl-1-propanesulfonic acid (*AMPS*), thus introducing terminal sulfonic acid groups as in Nafion membranes [11]. The resulting copolymers (*10-MeOAzB/AMPS*) containing both mesogenic and proton conducting units are shown in *Figure 6.5*.

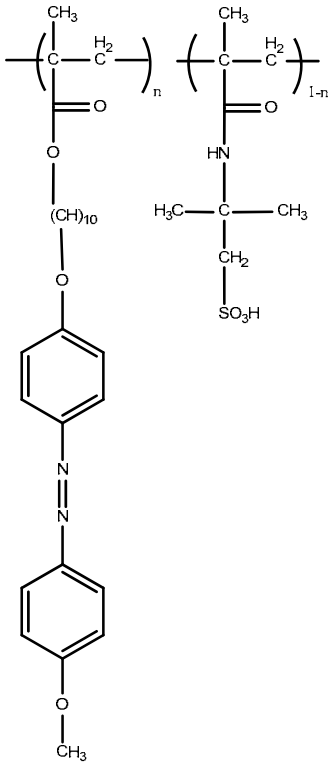

Figure 6.5 (10-(4-methoxy-4'-oxy-azobenzene) decyl methacrylate)-co-2-acrylamido-2-methyl-1-propanesulfonic acid

As already discussed, appropriatly designed copolymerisation can be profitable to obtain new materials *SCLCP* with enhanced properties. However, the introduction of non-mesogenic units can change and even inhibit the liquid crystallinity and thus, it is important to systematically study the effect of the addition of new components on the liquid crystallinity of the copolymers.

The aims of this chapter are:

1. To prepare new side-chain liquid-crystalline copolymers (*SCLCP*) with enhanced proton conductivity.
2. To characterise the new materials by spectroscopy and thermal analysis.

The synthesis of the copolymers has been carried out by radical polymerisation under an inert nitrogen (N_2) atmosphere. This necessarily involves the preparation and purification of the liquid crystal monomers. The synthetic route used to obtain the liquid crystal monomer is summarised in *Figure 6.6*.

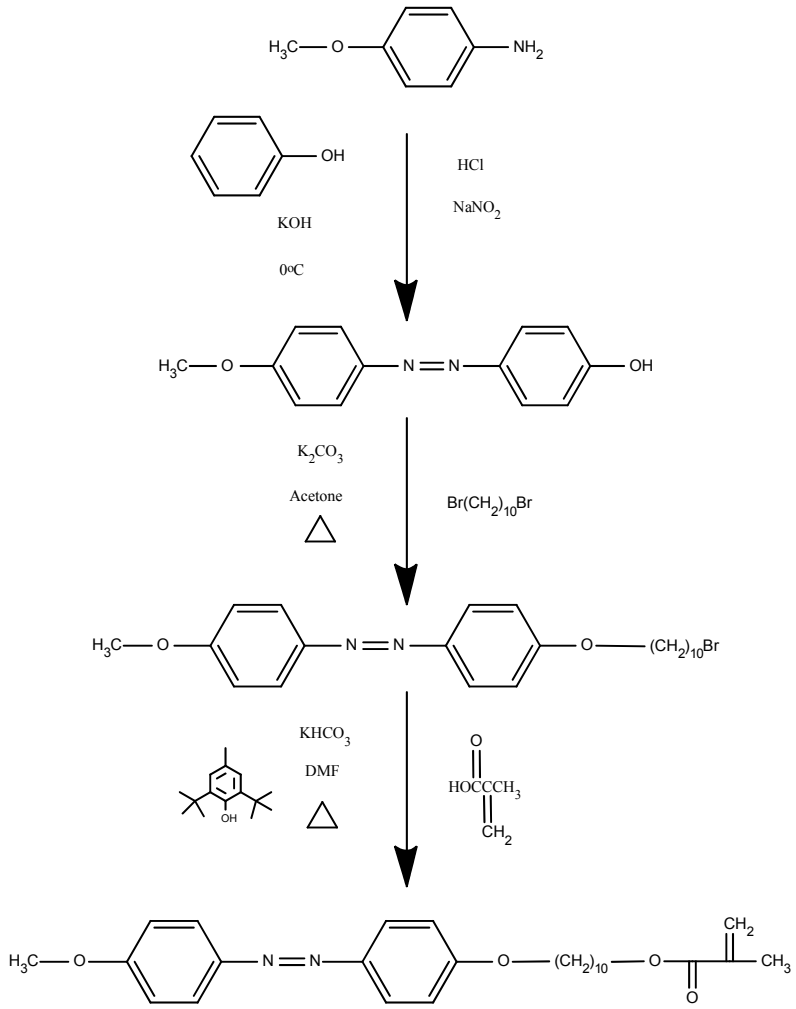

Figure 6.6 Synthetic route for the preparation of the 10-MeOAzB polymers

Commercial 2-acrylamido-2-methyl-1-propanesulfonic acid (*AMPS*) has been used in the copolymerisation without further purification (*Figure 6.7*):

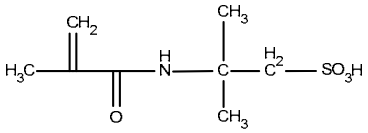

Figure 6.7 2 -acrylamido-2-methyl-1-propanesulfonic acid (AMPS)

The synthesis of polymethacrylate-based *SCLCP* has been extensively studied for many years [10, 12, 13]. However modifications were required in the experimental conditions, due to the difference in the polarities of the two monomers. Thus a common solvent was used (*n, n'*-dimethylformamide *DMF*) instead of toluene or water and the precipitation

and purification usied diethylether (*DE)* and dichlorometane (*DCM)* rather than methanol or pretroleoum ether. The main reaction scheme is shown in *Figure 6.8*.

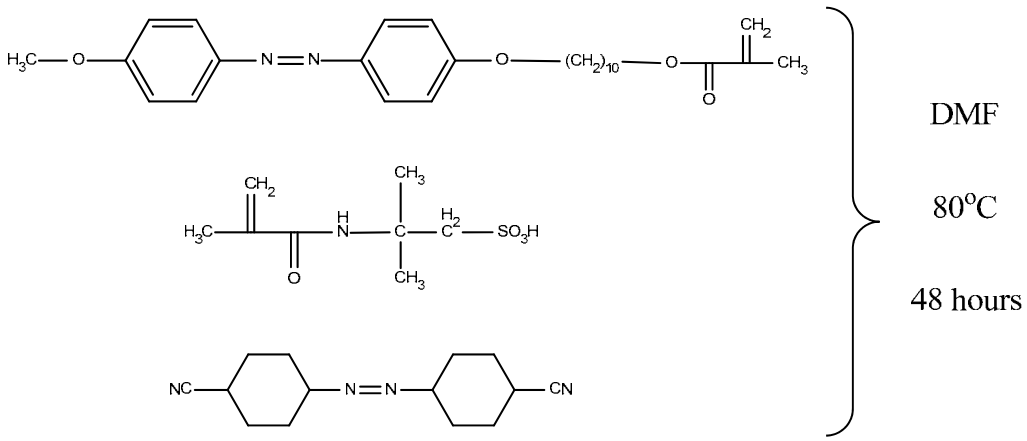

Figure 6.8 Copolymerisation of 10-MeOAzB with AMPS

A series of copolymers containing between 0.10 and 0.66 mole fraction of *AMPS* (x_{AMPS}) in the feed solution have been prepared. The homopolymers have been also prepared. The chemical structures and compositions of the copolymers were verified by NMR and IR spectroscopies.

The characterisation of the copolymers and homopolymers has been performed using a similar methodology as in previous chapters using DSC, FTIR and TGA. As in chapters 4 and 5, the behaviour of the individual homopolymers is very useful in comparing the expected and experimental results for the copolymers.

Differential Scanning Calorimetry (DSC) was used to characterise the thermal behaviour of the new copolymers. Three scans were performed on each sample: two heating ramps and a cooling scan, all of them at 10ºC·min^{-1} under a nitrogen atmosphere. The DSC curves show *smectic* to isotropic (clearing) transitions for all the copolymers, and their liquid crystallinity is observed even at high *AMPS* concentrations. The type of mesophase was confirmed by the texture of the copolymers using polarised light microscopy.

The results suggest the existence of interactions between the components. The strongest deviations from the ideal behaviour have been found for the copolymers with x_{AMPS}~0.3. The DSC results also exhibit a high degree of phase segregation probably occurring between the hydrophobic regions formed by the liquid crystalline units and the hydrophilic regions containing the sulfonic groups.

The Fourier Transform Infrared (FTIR) spectra have been obtained using KBr discs containing 0.5% by weight of the samples. The FTIR curves of the copolymers show the characteristic bands corresponding to the groups of the homopolymers. There are clear variations in the intensity of the bands with composition, showing good agreement with the NMR results.

The IR study has focused on the most representative bands of the two homopolymers. Two regions have been studied in further detail:

- The 1800 – 1500 cm^{-1} region. In this region different bands appear, including:
  - The ester group (1726 cm^{-1}, *10-MeOAzB*)
  - The C=H stretching vibrations from the aromatic rings (1600 and 1580 cm^{-1}, *10-MeOAzB*).
  - The C-O bond of the amide group (1652 cm^{-1}, *AMPS*)
  - The N-H bond of the amide group (1549 cm^{-1}, *AMPS*)

- The 628 cm^{-1} band. Corresponding to the sulfonate group (SO_3^-)

As in chapters 3 and 5, it has been necessary to perform a deconvolution of the 1800 – 1500 cm^{-1} region following the methodology described in chapter 2, since several peaks overlap. The study of the individual bands reveals shifts in the peaks which imply changes in the chemical environment of the components with composition. An increase in the strength of the intermolecular forces of the ester and ether groups of *10-MeOAzB* and *AMPS* has been found on increasing *AMPS* concentrations. This indicates a major interaction between the components in the main chain at higher *AMPS* contents.

From the point of view of the *AMPS* units, the results also show that the more polar groups (NH and sulfonate groups) form stronger interactions at higher *10-MeOAzB* concentrations. This fact can be an indication of the formation of intermolecular interactions. These interactions may be responsible for the destabilisation of the s*mectic* phase seen by DSC.

Thermogravimetric Analysis (TGA) has revealed changes in the thermal stability of the polymers with composition. The samples have been submitted to heating ramps at $10ºC \cdot min^{-1}$ in an argon atmosphere, from 25ºC to 700ºC. The Derivate Thermogravimetric curves (DTG) have been used to study the different mass loss processes more accurately.

Following similar strategies as described in chapters 4 and 5 ideal curves were constructed from the weighted averages of the individual curves, and compared to the experimental ones. Although the temperature range of the thermal degradation does not vary greatly, the comparison of the DTG curves shows that the copolymerisation promotes an increase in the thermal stability of the copolymers.

An increase in the onset temperatures of the polymer decomposition has been also found. This is evident from the values at which 1% and 10% of the whole mass is lost (T_α). The degradation of the polymeric chains is also displaced to higher temperatures and is accompanied by an increase of the residual mass at 700ºC. All these results suggest that the degradation of the copolymers is inhibited when compared to the behaviour of the homopolymers.

The copolymers prepared in this chapter were obtained as fine powders, and not as films. This represents a shortcoming because an additional processing stage is required prior to their use as electrolytes in *DMFC*, but at the same time provides an opportunity to consider the construction of the membranes.

Several aspects must be considered to obtain *SCLCP* membranes:

- The selection of a substrate to prepare self-standing films to either support or embed the active material (the copolymers)

- Pre-treatment can be a key factor in the behaviour of liquid crystal materials, therefore the processing conditions must be selected carefully.
- The solvent contents must be controlled through all the preparation process.

During the final stages of this PhD thesis some self-standing films were prepared using the *10-MeOAzB/AMPS* copolymers. Two slides of non-woven poly(propylene) (*PP*) were used as substrates, and a certain amount of copolymer was cast between them. The films have been prepared from the melt (110ºC) at high pressure (15 $Kg \cdot cm^2$) for 10 minutes and were subsequently cooled to room temperature and held for 10 minutes. The resulting films show good mechanical integrity but variable thickness. To date, alternative procedures are being studied using similar substrates but varying parameters such as the minimum amount of copolymer, the size of the films or the processing conditions.

2 COMMUNICATION

Synthesis and thermal and spectrometric characterisation of new side chains liquid crystal co-polymers containing sulfonic groups for their future use as electrolytes in Direct Methanol Fuel Cells

Title:

SYNTHESIS AND CHARACTERISATION OF NEW SIDE CHAIN LIQUID CRYSTAL CO-POLYMERS CONTAINING SULFONIC GROUPS FOR POTENTIAL APPLICATION AS ELECTROLYTES IN DIRECT METHANOL FUEL CELLS.

[1]A.Martinez-Felipe, [2]PA. Henderson, [2]CT. Imrie and [1]A. Ribes-Greus*
[1]School of Industrial Design Engineering
Universidad Politecnica de Valencia
Camino de Vera S/N, 46022 Valencia (Spain)
*E-mail: aribes@ter.upv.es

[2]Department of Chemistry, Meston Walk University of Aberdeen
Aberdeen AB24 3FX Aberdeen, Scotland (UK)
Phone/Fax number: +44 (0)1224-272000

ABSTRACT

New liquid side-chain liquid-crystalline copolymers poly[10-(4-methoxy-4'-oxy-azobenzene) decyl methacrylate]–co-poly[2-acrylamido-2-methyl-1-propanesulfonic acid]s (*10-MeOAzB/AMPS*) were prepared by free radical copolymerisation for potential application as electrolytes in Direct Methanol Fuel Cells (*DMFC*). The new materials were characterised by Differential Scanning Calorimetry (DSC), Fourier Transform Infrared Spectroscopy (FTIR) and Thermogravimetric Analysis (TGA). The copolymers exhibit liquid crystalline behaviour and the formation of phase separated aggregates over a broad range of compositions. However, it was found the existence of interactions between the components which caused a partial inhibition of the liquid crystallinity and a reduction of the mesogenic range. Such interactions were also present at high temperatures and promoted the inhibition of the polymer degradation and an enhancement of the thermal stability of the copolymers.

INTRODUCTION

Fuel Cells have emerged as an alternative to other more conventional systems of energy conversion due to their high efficiencies and low environmental impact [1, 2]. In particular, in Direct Methanol Fuel Cells (*DMFC*) methanol is oxidized at the anode and the protons produced are transferred through an electrolyte to the cathode, where they react with oxygen from the air. The overall reaction leads to the generation of *DC* power with high yields. Methanol is usually supplied to the anode in aqueous mixtures at low temperatures, which avoids the problems derived from the storage and delivery of fuel in hydrogen fuel cells. Furthermore, methanol can be obtained from renewable sources (bio-alcohol), which represents an important additional advantage [3].

This application potential, however, has still to be realised and there are serious challences to be overcome prior to their use on an industrial scale. One of the most significant problems of *DMFC* is the so-called crossover phenomenom. Crossover occurs when methanol flows from the anode to the cathode and reacts directly with the oxygen. This produces thermal energy but no net electrical power, causing an efficiency drop of up to 30% in the cell [4, 5, 6, 7]. The occurrence of crossover is associated with the links between the transport mechanisms of water, methanol and protons through the electrolyte. For this reason, it is critical to control the morphology of the polymers used in *DMFC* in order to reduce the alcohol permeability without causing a significant decrease in the proton conductivity. This is normally achieved by using materials with a biphasic structure and creating specific sites for the ionic transport and physical barriers for the alcohols transfer [8].

In this paper we propose the use of side-chain liquid-crystalline based on a polymethacrylate backbone as potential electrolytes for *DMFC* applications. The formation of liquid crystalline phases in these materials allows for a certain control over the resulting morphology and selective pathways for the diffusion of the different components [9]. A series of poly[10-(4-methoxy-4'-oxy-azobenzene) decyl methacrylate]s-co-poly[2-acrylamido-2-methyl-1-propanesulfonic acid] copolymers, **1**, were prepared by free radical copolymerisation over a broad range of composition of the comonomers.

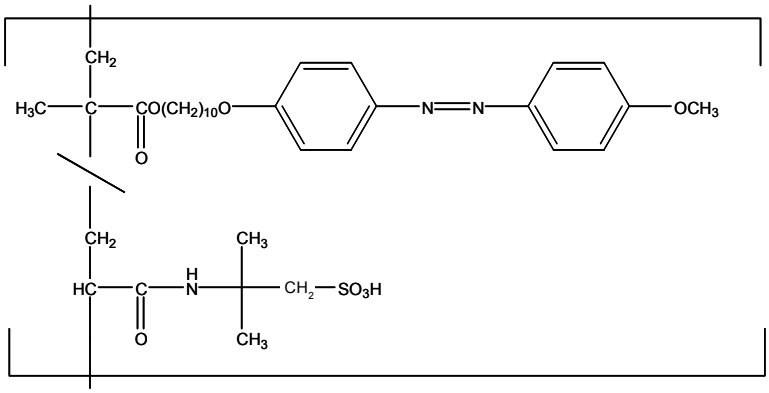

1

The acronym *10-MeOAzB/PAMPS-X* is used to refer to series 1, where *X* denotes the molar fraction of *AMPS* units in the copolymers. The introduction of 2-acrylamido-2-methyl-1-propanesulfonic acids intended to enhance the proton conductivity of the materials. The mesogenic properties, the chemical structure and the thermal stability of the resulting materials were studied by Differential Scanning Calorimetry (DSC), Fourier Transform Infrared Spectroscopy (FTIR) and Thermogravimetric Analysis (TGA), respectively.

EXPERIMENTAL SECTION

Synthesis and materials

The *10-MeOAzB/PAMPS* copolymers series, **1**, was prepared by radical copolymerisation of 10-(4-methoxy-4'-oxy-azobenzene) decyl methacrylate and 2-acrylamido-2-methyl-1-propanesulfonic acid (*AMPS*).

AMPS, **6**, was purchased from Sigma-Aldrich and used without further purification:

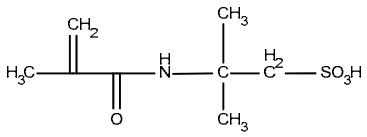

6

The preparation of 10-(4-methoxy-4'-oxy-azobenzene) decyl methacrylate is shown in *Scheme 1*. All the chemicals used in the synthesis of the monomer were purchased from Sigma and used without further purification.

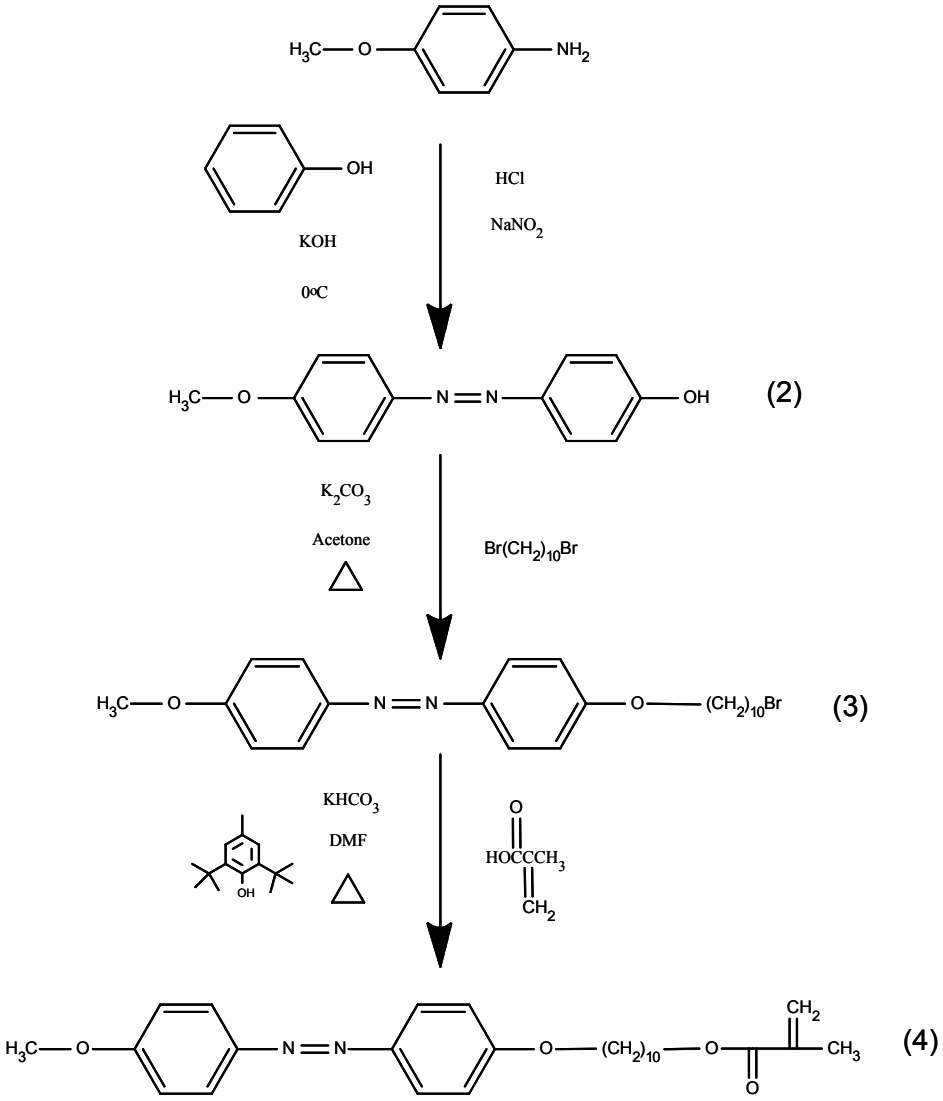

Scheme 1

4-Hydroxy-4'-methoxy-azobenzene (2) [10]

A solution of sodium nitrite (28.9 g, 419 mmol) in distilled water (150 ml) was added slowly with vigorous stirring to a solution of *p*-anisidine (50.4 g, 409 mmol) in 3 M hydrochloric acid (500 ml) at 0°C. The resulting diazonium salt solution was then slowly added to a stirred solution of phenol (39.4 g, 419 mmol) in 10% aqueous sodium hydroxide (400 ml). The dark brown suspension was then acidified and the precipitate collected. The crude product was washed with copious amounts of water and dried.

IR. (KBr) ν cm^{-1}: 3428 (OH). ^{1}H-NMR ($CDCl_3$) δ (ppm): 7.0, 7.9 (m, aromatic, 8 H), 3.9 (s, $ArOCH_3$, 3H)

1-Bromo-10-(4-methoxy-azobenzene-4'oxy) decane (3) [11]

A mixture of **2** (11.5 g, 50.2 mmol) 1,10-dibromodecane (103.3 g, 423 mmol), potassium carbonate (30.2 g, 218.2 mmol) and acetone was refluxed with stirring for 48 hours. Then the reaction was allowed to cool down to room temperature and filtered after 2 hours. A yellow solid was obtained and washed with methanol and water, recrystallised from ethanol and dried.

^{1}H-NMR ($CDCl_3$) δ (ppm): 7.0, 7.9 (m, aromatic, 8 H), 4.0 (t, OCH_2, 2 H), 3.9 (s, $ArOCH_3$, 3H), 3.4 (t, $BrCH_2$, 2), 1.0 – 2.0 (m, $CH_2(CH_2)_8CH_2$, 16)

10-(4-Methoxy-4'-oxy-azobenzene) decyl methacrylate (4) [12]

Methacrylic acid (3.7 g, 42.7 mmol) was added to $KHCO_3$ (5 g, 50 mmol) and stirred at room temperature for 5 minutes to form potassium methacrylate. The potassium methacrylate was then added to a solution of **3** (6.8 g, 15.2 mmol) and 2,6-ditertbutyl-4-methyl-phenol (0.007g, 0.032 mmol) in n,n'-dimethylformamide (40.0 g) and the resulting mixture was stirred at 100^{o}C for 24 hours. The solution was then allowed to cool to room temperature and water was added to the mixture (500 ml). The yellow powder was then collected by filtration, washed with copious amounts of water, recrystallised from ethanol and dried.

Yield: 6.3 g, 13.9 mmol, 92.0 %, IR. (KBr) ν cm^{-1}: 1714 (C=O), 1637 (C=C), ^{1}H-NMR ($CDCl_3$) δ (ppm): 7.0, 7.9 (m, aromatic, 8 H), 5.5, 6.1 (s, CH_2=C-, 2 H), 4.2 (t, CH_2-OOC, 1.26 H), 4.0 (t, OCH_2, 1.61 H), 3.9 (s, $ArOCH_3$, 2.98H), 3.4 (t, $BrCH_2$, excess), 1.0 – 2.0 (m, $CH_2(CH_2)_8CH_2$, $CH_3C(COO)$ excess)

Poly[10-(4-Methoxy-4'-oxy-azobenzene)decyl methacrylate] (5)

The polymerisation of 10-(4-Methoxy-4'-oxy-azobenzene)decyl methacrylate, **5**, was performed using a reaction procedure described elsewhere [13]. 0.5 g (1.10 mmol) of **4** were weighted in a two necked 100 ml flask, together with 0.0132 g of 1,1'-Azobis(cyclohexane carbonitrile) and 12.1 g of *DMF*. The mixture was then flushed with N_2(g) for 45 minutes, then heated at 80ºC in absence of oxygen and left for 24 hours. The product was precipitated into methanol and collected. The polymer was purified by several precipitations from dichloromethane into diethyl ether.

Yield: 68.0 %, IR (KBr) ν cm^{-1}: 1726 (C=O), ^{1}H-NMR ($CDCl_3$) δ (ppm): 7.0, 7.9 (m, aromatic, 8 H), 4.1 – 3.9 (m, CH_2-OOC, OCH_2, 4H), 3.8 (s, $ArOCH_3$, 3H), 1.0 – 2.0 (m), 0.7 – 1.1 (CH_3C(CO.O), 3 H)

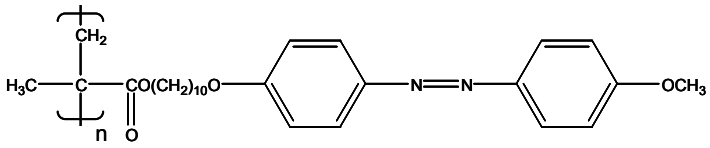

5

Poly[2-Acrylamido-2-methyl-1-propanesulfonic acid] (PAMPS) (7)

1 g (4.48 mmol) of **6** was weighted in a two necked 100 ml flask, together with 0.0328 g of 1,1' azobis(cyclohexane carbonitrile) (3% mol) and 10.0 g of *DMF*. The mixture was then flushed with N_2 (g) for 60 minutes, then heated at 80ºC in absence of oxygen and left overnight (24 hours). The reaction was stopped by addition of diethyl ether, and a precipitate was obtained. The product was dried for several days.

IR (KBr) ν cm^{-1}: 628 (SO_3^-), ^{1}H-NMR (D_2O) δ (ppm): 1.5 (s, CH_3, 3H), 2.1 (s, main chain CH_2), 3.7 (s, $\underline{CH_2}SO_3H$, 2H)

***10-MeOAzB/PAMPS* copolymers (1)**

The appropiate amounts of **4**, **7** and 1,1' azobis(cyclohexane carbonitrile) in a 3% molar concentration were weighed in a two necked 100 ml flask, together with 20 ml of DMF. The mixture was flushed with N_2(g) for 60 minutes, and then heated at 80ºC in absence of oxygen for 24 hours. Diethyl ether (500 mL) was added. The resulting yellow precipitated was collected and purified by several precipitations from dichloromethane into diethyl ether. The product was dried at 80ºC for several days. Copolymers containing mole fractions of 0.1, 0.2, 0.3, 0.4, 0.5 and 0.66 in the feed of *AMPS* were prepared, and designated as *Copol X*, with *X* is the corresponding actual molar fraction, as seen in *Table 1*. The homopolymers (**5** and **7**) were also prepared.

Yield *Copol 0.56* (AMPS molar fraction) 63 %, IR (KBr) ν cm^{-1}: 1726 (C=O), 628 (SO_3^-),^{1}H-NMR ($CDCl_3$) δ (ppm): 8.5 (s, NH, 1H) 7.0, 7.9 (m, aromatic, 8 H), 4.1 – 3.9 (m, CH_2-OOC, OCH_2, 4H), 3.8 (s, $ArOCH_3$, 3H), 2.8 (s, $CH_2 – SO_3$, 2H) 1.0 – 2.0 (m), 0.7 – 1.1 (m, CH_3C(CO.O), H main chain *AMPS*)

Table 1. Feed and actual compositions of the 10-MeOAzB/PAMPS copolymers

Sample	X_{AMPS} Feed	X_{AMPS} Copolymer
10-MeOAzB	0	1
Copol 0.06	0.1	0.06
Copol 0.27	0.2	0.27
Copol 0.3	0.3	0.3
Copol 0.34	0.4	0.34
Copol 0.56	0.5	0.56
Copol 0.78	0.66	0.78
PAMPS	1	0

Characterisation

The proposed structures of all the compounds were verified using ^{1}H NMR and IR spectroscopy. The ^{1}H-NMR spectra were measured in $CDCl_3$ (except for **6,** which was measured in D_2O) on a Bruker AC-F 250 MHz spectrometer. All the copolymers (as well as the homopolymers) were characterised by Differential Scanning Calorimetry (DSC), Fourier Transformed Infrared Spectroscopy (FTIR) and Thermogravimetric Analysis (TGA). Phase identification was performed by polarised light microscopy using an Olympus BH-2 optical microscope equipped with a Linkam THMS 600 heating stage and TMS 91 control.

Differential Scanning Calorimetry (DSC)

The DSC thermograms were obtained using a Mettler Toledo DSC 822 analyser. The samples of around 5 mg were heated up from 25ºC to 220ºC, held at 220ºC for 3 minutes, cooled to 25ºC, held for 3 minutes, and re-heated to 220ºC. All the scans were performed at 10ºC/min in a nitrogen atmosphere and using liquid nitrogen as the coolant. Additional phase recognisation was performed using polarised light microscopy with an Olympus BH-2 optical microscope equipped with a Linkam THMS 600 heating stage and TMS 91 control unit.

Fourier Transform Infrared Spectroscopy (FTIR)

The FTIR experiments were performed using a Thermo Nicolet 5700 spectrometer and KBr discs (1 mg sample / 200 mg background). The spectra were collected after 128 scans with an accuracy of 4 cm^{-1}. Background spectra were collected before each series of experiments.

Thermogravimetric Analysis (TGA)

The TGA experiments were carried out using a Mettler Toledo TGA/SDTA 851 analyser. Measurements were performed following a dynamic program from 25ºC to 700ºC at a heating rate of 10ºC/min under an inert Argon (Ar) atmosphere with a flow rate of 80 ml/min. Sample masses were around 5 mg.

RESULTS AND DISCUSSION

Differential Scanning Calorimetry (DSC)

The DSC traces for *10-MeOAzB/PAMPS* copolymers, **1**, poly[10-(4-Methoxy-4'-oxy-azobenzene)decyl methacrylate], (*10-MeOAzB*), **5**, and poly[2-Acrylamido-2-methyl-1-propanesulfonic acid], (*PAMPS*), **7**, corresponding to their cooling scans are shown in *Figure 1*. The most important parameters corresponding to the thermal transitions of all the samples have been summarised in *Table 2*.

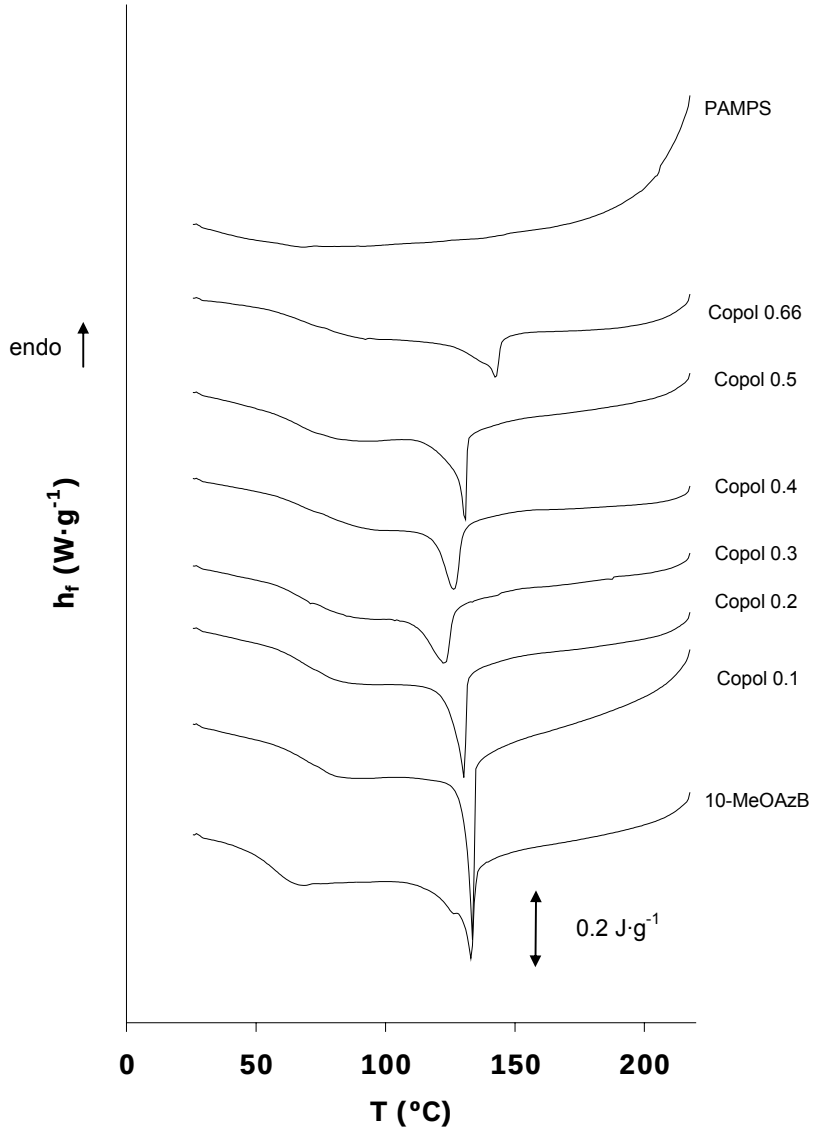

Figure 1. DSC thermograms of the 10-MeOAzB/PAMPS copolymers. Cooling scan.

Table 2. DSC transitional properties of the 10-MeOAzB/PAMPS copolymers

Sample	T_g (ºC)	$T_{SmA - I}$ (ºC)	$\Delta H_{SmA - I}$ ($J \cdot g^{-1}$)	$\Delta H(LC)_{SmA - I}$ (kJ /·mol LC)	$\alpha_{Sma - I}$
10-MeOAzB	57	139	12.2	5.53	1.00
Copol 0.1	76	134	9.7	4.53	0.82
Copol 0.2	76	130	9.1	4.74	0.86
Copol 0.3	70	123	7.9	4.17	0.75
Copol 0.4	77	126	6.2	3.36	0.61
Copol 0.5	65	131	5.3	3.32	0.60
Copol 0.66	78	143	3.8	2.77	0.50

The homopolymer *10-MeOAzB* shows a glass transition at T_g = 57ºC and an endothermic process at T_p = 135ºC, which was attributed to a *smectic A* to isotropic transition (clearing temperature) [13, 14, 15]. It is possible to observe a change in the slope of the curve corresponding to the *PAMPS* homopolymer at high temperatures, which can be attributed to the presence to the glass transition of *PAMPS* in the vicinity of T_{p2}~196ºC [16]. The thermal behaviour of all the *10-MeOAzB/PAMPS* copolymers is similar to that of the homopolymer *10-MeOAzB*, indicating that the copolymers show liquid crystalline behaviour over all the composition range studied. The textures observed under the microscope confirmed the formation of the *smectic A* phase, as seen in *Figure 2*.

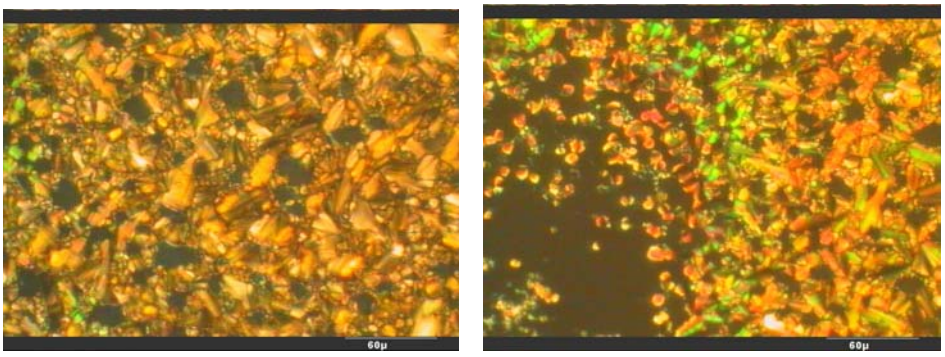

(a) **(b)**

Figure 2. PLM images of Copol 0.05: (a) showing the smectic A phase, (b) showing the smectic A phase and homeotropic regions.

The phase diagram of the copolymers is shown in *Figure 3*. The appearance of the thermal transitions of the homopolymer in the DSC curves in the heating and cooling scans suggests the existence of a certain degree of phase separation in the copolymers [17, 18]. The values of T_g of all the copolymers are higher than that of the *10-MeOAzB* hompolymer. This fact has been already observed in previous liquid crystal ionomers and has been attributed to the increase of the interactions between molecules promoted by the ionic groups [17, 19, 20].

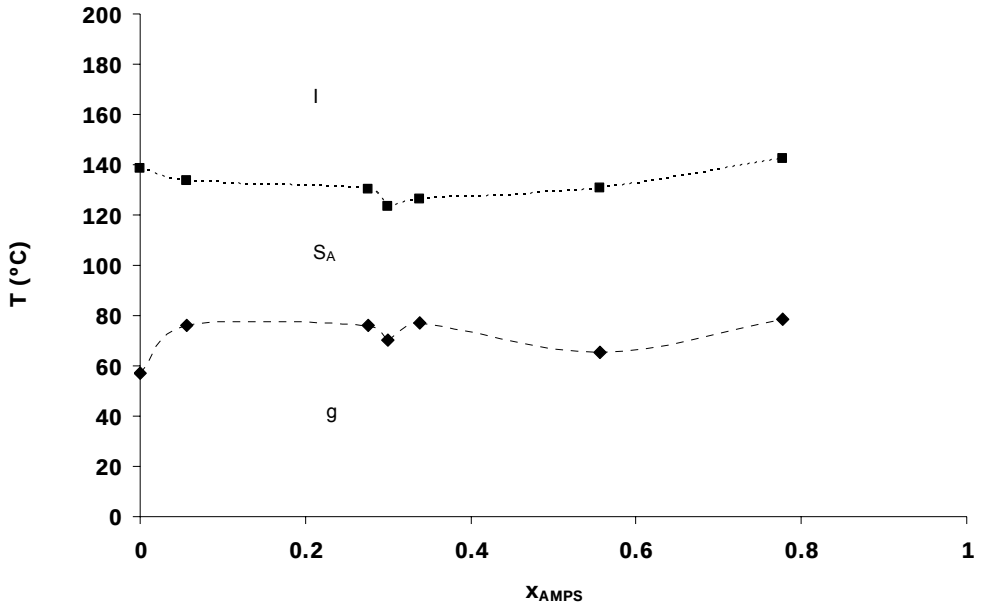

Figure 3. Phase diagram of the 10-MeOAzB/PAMPS copolymers: (◆) glass transition, (■) smectic A to isotropic transition

The clearing temperatures of the copolymers with low *AMPS* concentrations ($x_{AMPS} < 0.5$) are lower than that of the homopolymer *10-MeOAzB*. It is well known that the addition of non-mesogenic units to side chain liquid crystal polymers can promote a destabilisation of the smectic phase, which can even lead to the destruction of the liquid crystallinity [14, 16]. The variation of the liquid crystal range in polymer liquid crystals is generally rationalised in terms of the backbone flexibility and also of the microphase separated morphology exhibited by the smectic phase [21, 22, 23]. The slight increase of the clearing temperatures observed at higher AMPS concentrations ($x_{AMPS}>0.5$) suggests that the liquid crystalline behaviour of these copolymers is more similar to that of the homopolymer.

Table 2 also lists the enthalpy values of the clearing transition per gram of dry copolymer (ΔH_{SmA-I} , J/g), which have been obtained from the areas of the endothermic peaks in the second heating scan thermograms. The values of enthalpy of the transition per mole of liquid crystal unit ($\Delta H(LC)_{SmA-I}$, KJ/mol *LC*) were also calculated:

$$\Delta H(LC)_{SmA-I} = \Delta H_{SmA-I} \cdot \frac{MW_{LC} / 1000}{(1-\chi)} \qquad (1)$$

where MW_{LC} is the molecular weight (452.6 g·mol^{-1}) and χ the mass fraction of the non-mesogenic unit in the copolymers, respectively.

The results for $\Delta H(LC)_{SmA-I}$ are shown in *Figure 4*. There is a decrease in the enthalpy per mole of mesogenic unit at decreasing liquid crystalline concentrations in the copolymers. This difference indicates that part of the mesogenic units does not contribute to the mesomorphism of the copolymers.

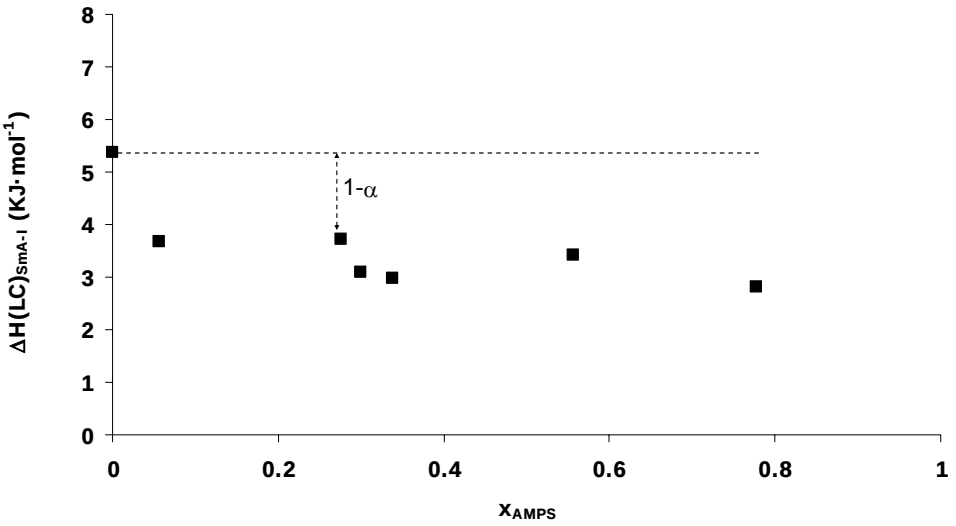

Figure 4. Enthalpy values of the liquid crystal transition ($\Delta H(LC)_{SmA-I}$) of the 10-MeOAzB/PAMPS copolymers.

The fraction of liquid crystal contributing to the liquid crystalline phase in the copolymers can be expressed by the distribution coefficient α, which is the ratio

between $\Delta H(LC)_{SmA-I}$ in the copolymers and in the *10-MeOAzB* homopolymer [24, 25]:

$$\alpha = \frac{\Delta H(LC)_{SmA-I}(copolymers)}{\Delta H(LC)_{SmA-I}(10-MeOAzO)}$$

The results of the distribution coefficient (α) as a function of the composition of the copolymers are also shown in *Table 2*. The fraction of liquid crystal contributing to the transition decreases rapidly even at low *AMPS* concentrations. This suggests that the mesomorphism of a fraction of the liquid crystal units is hindered by the presence of the molecules of *AMPS*. At high *AMPS* concentrations (x_{AMPS}>0.4) the values of α stabilise.

Fourier Transform Infrared Spectroscopy (FTIR)

Figure 5 displays the FTIR spectra of the *10-MeOAzB/PAMPS* copolymers and the two homopolymers. The FTIR spectra of all the copolymers show characteristic absorption bands consistant with the structures of the homopolymers. The assignments of the key absorption bands in the spectra are listed in *Table 3* and the associated values of wavenumber and maxim absorption given in *Table 4*.

Table 3. FTIR results. Assignation of the vibration bands

Group	Region (cm^{-1})	References
	Regions related to 10-MeOAzB	
Ester	1726 (C=O st), 1147 (C-O, st asym), 1104 (C-O, st. sym)	13, 29, 30
Aromatic rings	1600 (st), 1580 (st), 1500 (st) 841 (CH bend oop), 756 (CH bend oop), 729 (CH bend oop)	30
Ether (aromatic)	1248 (st), 1030 (st)	30
	Regions related to AMPS	
Amide	3444 NH strech (amide, II) 1650 COO (amide, I) 1549 NH (amide, II)	30
Sulfonic group	3000 (O-H), 1210 (SO_2, st), 1042 (SO_2, st), 628 (S-O st)	30, 31
Amide	1650 COO (amide, I) 1549 NH (amide, II)	30
	Common regions	
C-H stretching	2930 (CH_3), 2850 (CH_2), 2810 (CH)	16, 30
C-H bending	1470 (CH_3), 1380 (CH_2), 1298 (CH)	16, 30

Table 4. Values corresponding to the FTIR absorption peaks of the 10-MeOAzB/PAMPS copolymers.

Sample	1726 (C=O)		1600 (arC-C)		1580 (arC-C)	
	Position (cm^{-1})	Intensity (Abs %)	Position (cm^{-1})	Intensity (Abs %)	Position (cm^{-1})	Intensity (Abs %)
10-MeOAzB	1726	0.429	1600	0.714	1581	0.598
Copol 0.1	1726	0.541	1600	0.808	1581	0.664
Copol 0.2	1725	0.258	1600	0.399	1582	0.317
Copol 0.3	1724	0.261	1600	0.404	1582	0.318
Copol 0.4	1724	0.188	1600	0.285	1582	0.221
Copol 0.5	1723	0.168	1601	0.260	1582	0.211
Copol 0.66	1719	0.132	1601	0.239	1582	0.176

Table 4 (cont)

Sample	1500 (arC-C)		1248 (C-O)		1030 (C-O)	
	Position (cm^{-1})	Intensity (Abs %)	Position (cm^{-1})	Intensity (Abs %)	Position (cm^{-1})	Intensity (Abs %)
10-MeOAzB	1248	1.168	1248	1.168	1030	0.374
Copol 0.1	1250	1.237	1250	1.237	1030	0.496
Copol 0.2	1251	0.614	1251	0.614	1032	0.244
Copol 0.3	1251	0.626	1251	0.626	1033	0.248
Copol 0.4	1252	0.433	1252	0.433		
Copol 0.5	1251	0.387	1251	0.387		
Copol 0.66	1253	0.347	1253	0.347		

Sample	3444 (amide, II)		1650 (amide, I)		1549 (amide, II)	
	Position (cm^{-1})	Intensity (Abs %)	Position (cm^{-1})	Intensity (Abs %)	Position (cm^{-1})	Intensity (Abs %)
10-MeOAzB	3434	0.044				
Copol 0.1	3448	0.061	1655	0.070	1542	0.067
Copol 0.2	3435	0.054	1670	0.07	1541	0.074
Copol 0.3	3447	0.089	1655	0.089	1541	0.079
Copol 0.4	3335	0.081	1653	0.093	1541	0.082
Copol 0.5	3442	0.335	1653	0.217	1545	0.147
Copol 0.66	3442	0.779	1653	0.635	1549	0.401

Sample	1210 (SO_3)		1042 (SO_3)		628 (S-O)	
	Position (cm^{-1})	Intensity (Abs %)	Position (cm^{-1})	Intensity (Abs %)	Position (cm^{-1})	Intensity (Abs %)
10-MeOAzB						
Copol 0.1					626	0.036
Copol 0.2					625	0.044
Copol 0.3			1036	0.184	626	0.045
Copol 0.4	1211	0.205	1038	0.200	627	0.055
Copol 0.5	1212	0.325	1042	0.307	628	0.128
Copol 0.66	1211	0.843	1042	0.834	628	0.369

As expected, the intensity of the peaks related to *10-MeOAzB* tends to decrease with increasing contents of *AMPS* in the copolymers. Specifically, the dependence of the spectra on the composition of the copolymers can be most clearly observed in the 1800 – 1520 cm^{-1} region, by considering the different contributions of the homopolymers:

- The ester group (1726 cm^{-1}) and the *C=H* stretching vibrations from the aromatic rings (1600 and 1580 cm^{-1}) of *10-MeOAzB* [13, 26, 27].
- The *C-O* (1652 cm^{-1}) and the N-H (1549 cm^{-1}) vibration bands of the amide group of *AMPS* [32].

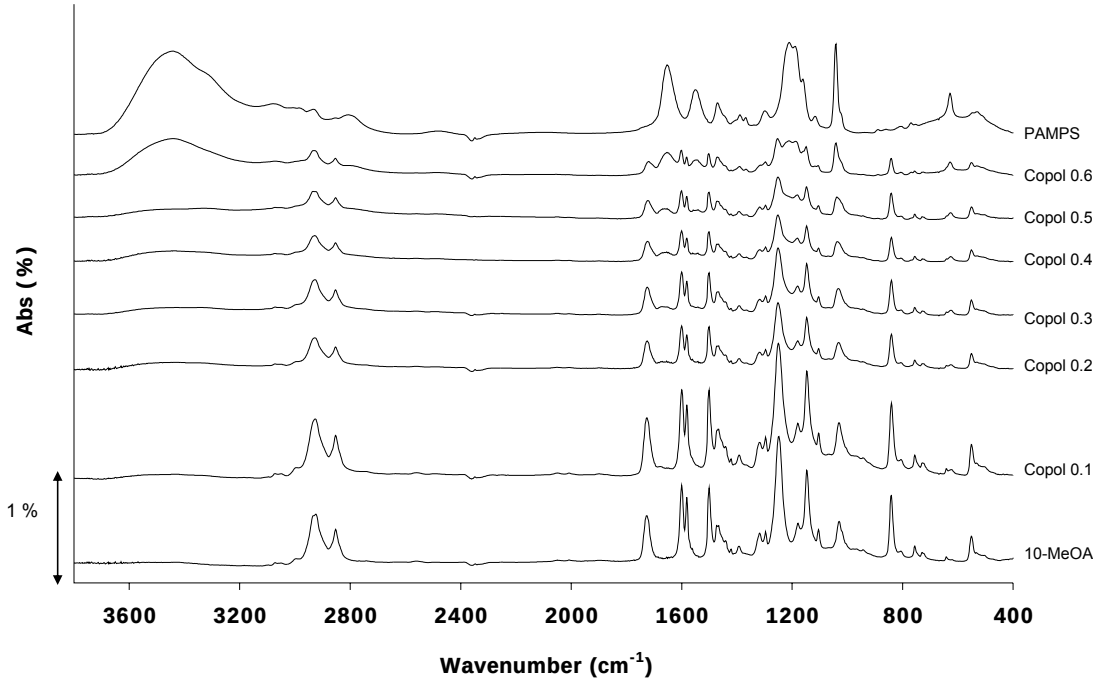

Figure 5. FTIR spectra of the 10-MeOAzB/PAMPS copolymers.

In order to study this region in further detail, the experimental FTIR curves were fit to a sum of Lorentzial/Gaussian peaks. An example of the deconvolution is shown in *Figure 6*. While the bands related to *10-MeOAzB* were fitted to only one peak, two contributions were found in the bands corresponding to the amide groups (C-O and N-H) of *AMPS*. This fact suggests that the sulfonated units may be found in different chemical environments in the *10-MeOAzB/PAMPS* copolymers. The values of position and area were calculated for each individual peak obtained by deconvolution and the results have been plotted in *Figure 7*.

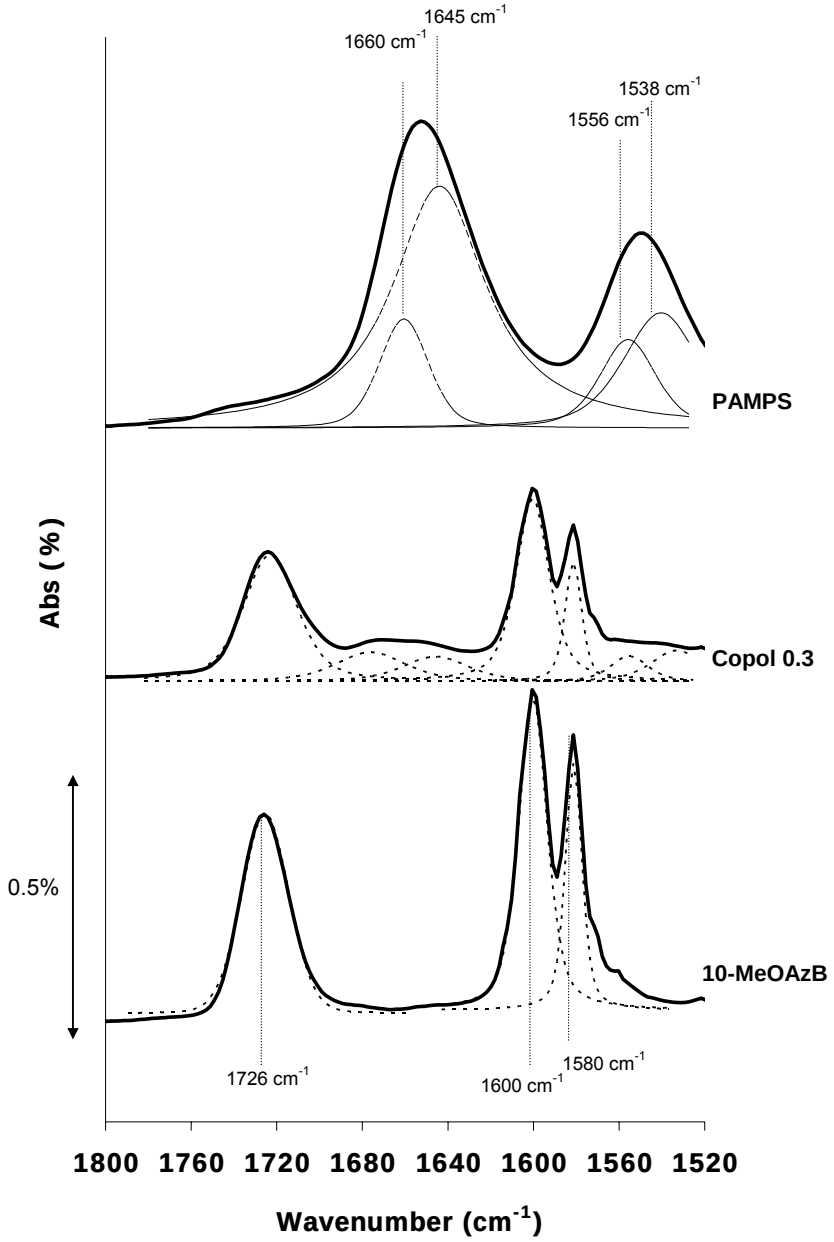

Figure 6. Detail of the FTIR spectra of 10-MeOAzB, Copoly 0.3 and PAMPS in the 1800 – 1500 cm^{-1} region. Dotted lines indicate the individual peaks of the deconvolution.

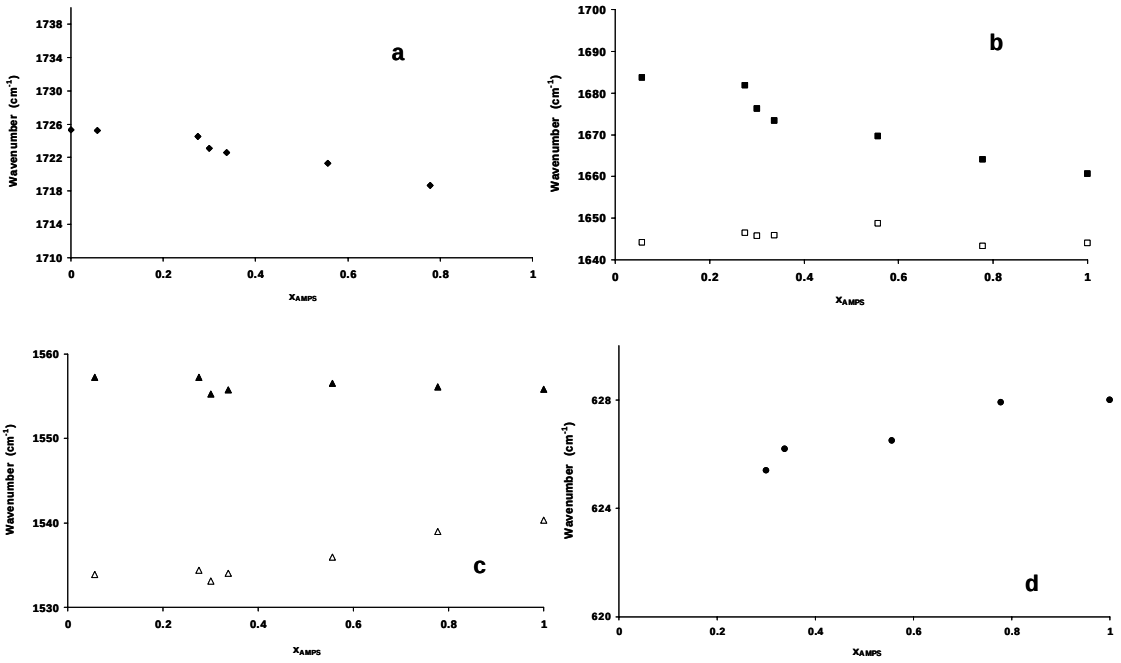

Figure 7. Values of position of the individual peaks corresponding to: ester bond (a), CO amide I group (b), N-H amide II group (c) and the sulfonic group (d).

The IR vibration band of the ester group of *10-MeOAzB* at 1726 cm^{-1} (*Figure 7a*) progressively shifts to lower wavenumbers at higher *AMPS* concentrations, and a similar trend is observed for the amide peak (C-O) at 1660 cm^{-1} (*Figure 7b*). These facts suggest that the presence of this secondary band can be related to the formation of interactions between *AMPS* and *10-MeOAzB* units in the copolymers. These interactions tend to be more prevalent as the mesogenic units dilute in the copolymers and could be responsible of the inhibition of the liquid crystallinity observed in the DSC results (see Figure 4).

It is also possible to observe a blue-shift of the peak at 1580 cm^{-1} corresponding to the *NH* group at increasing *AMPS* concentrations (*Figure 7c*). This trend is also observed for the bands related to the sulfonic group at 628 cm^{-1} and 1042 cm^{-1} (see *Table 3* and *Figure 7d*). These results suggest the formation of stronger hydrogen bonds involving the amide and sulfonate groups of *AMPS* and could be indicative of the formation of polar aggregates at higher concentration of non-mesogenic groups [28, 29, 30].

Thermogravimetric Analysis (TGA)

The Derivative Thermogravimetric (DTG) curves of the *10-MeOAzB/PAMPS* copolymers and the two homopolymers are shown in *Figure 8*. The degradation of 10-*MeOAzB* occurs following two main processes centred at $T_{MeOAzB-1}$=360ºC and $T_{MeOAzB-2}$= 419ºC, which can be related to the decomposition of the side chains and the degradation of the main chains, respectively [33, 34]. The decomposition of *PAMPS* occurs through several processes. In the low temperatures region (T < 240ºC) it is possible to observe the loss of absorbed water (T ~ 100ºC) and at slightly higher temperatures (T ~ 200ºC) a low intensity process assigned to the loss of solvent tightly bound to the polymer structure [35]. The desulfonation can be found at temperatures around T~240ºC. The degradation of the polymer structure of *PAMPS* occurs through a main decomposition process at $T_{PAMPS-1}$ = 288ºC and a secondary process observed at temperatures slightly higher (T_s~310ºC). Finally, the decomposition of undegraded fractions of the polymer takes place at higher temperatures $T_{PAMPS-2}$=411ºC [31, 36].

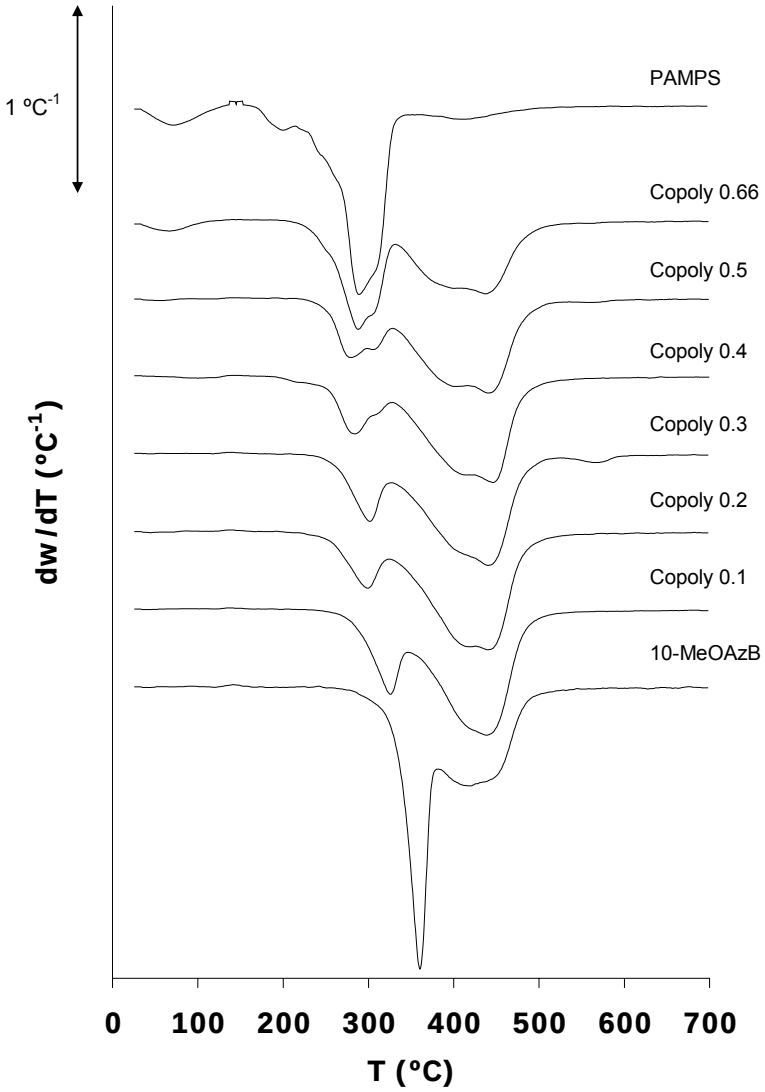

Figure 8. DTG curves of the 10-MeOAzB/PAMPS copolymers.

The decomposition of the *10-MeOAzB/PAMPS* copolymers proceeds following several degradation processes in the same temperature range as seen for the two homopolymers. The decomposition seems to occur in two main regions: from 200ºC to 320ºC (*region 1*) and from 320ºC to 500ºC (*region 2*). The parameters corresponding to the thermal degradation of the copolymers and the homopolymers were obtained and are summarised in *Table 5*. It is possible to assign *region 1* to the degradation of *PAMPS* and *region 2* to the decomposition of the *10-MeOAzB* fractions.

Table 5. Summary of the thermogravimetric parameteres

	Loss of solvent		Low temperatures process (1)		High temperatures process(2)		Residual (%)
	T_{peak1} (ºC)	dw/dT_{max} ($ºC^{-1}$)	T_{peak1} (ºC)	dw/dT_{max1} ($ºC^{-1}$)	T_{peak2} (ºC)	dw/dT_{max2} ($ºC^{-1}$)	
10-MeOAzB	-		360	14.53	419	5.10	8.0
Copol 0.1	-		326	4.40	439	6.50	16.4
Copol 0.2	45	0.09	299	2.94	440	6.11	16.7
Copol 0.3	43	0.15	284	2.63	445	5.77	16.79
Copol 0.4	100	0.15	284	3.01	446	5.51	18.7
Copol 0.5	56	0.16	279	3.08	440	4.91	19.8
Copol 0.66	66	0.58	288	5.63	437	3.81	17.3
PAMPS	71	1.14	289	9.85	411	0.84	15.3

The DTG curves and the thermal parameters reveal that the decomposition of the *10-MeOAzB/PAMPS* copolymers has changed with respect to the homopolymers. The increase in the mass of residue at 700ºC and the temperature of degradation of region 2 (T_2) indicates that the degradation of the polymer chains is somehow inhibited in the copolymers. [34]. The copolymer structure also affects the first steps of decomposition. The values of the degree of conversion of the decomposition processes α, were calculated, according to the following expression:

$$\alpha = \frac{w - w_0}{w_\infty - w_0} \qquad (2)$$

with w, w_0 and w_∞ the current, initial and final mass of the samples, respectively). The temperatures at which α = 0.01, 0.1 and 0.9 ($T_{\alpha=0.01}$, $T_{\alpha=0.1}$ and $T_{\alpha=0.9}$, respectively) were obtained for the copolymers and the homopolymers. The results are shown in *Figure 9*. All the copolymers show values of $T_{\alpha=0.01}$, and $T_{\alpha=0.1}$ higher than those expected from the homopolymers in all the range of compositions. This result indicates that the thermal stability of the copolymers is higher than that of the corresponding homopolymers [31, 33].

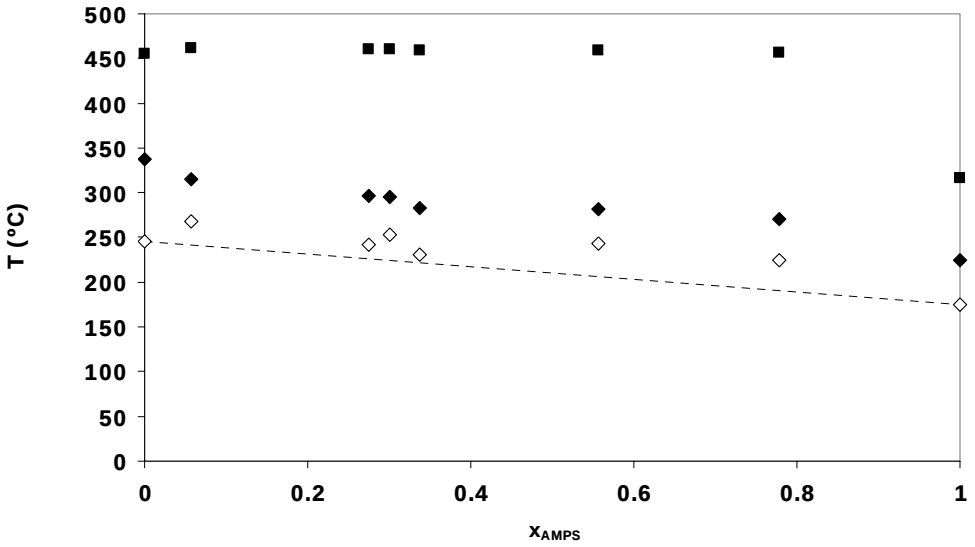

Figure 9. Values of $T_{\alpha=0.01}$ (◇), $T_{\alpha=0.1}$ (◆) and $T_{\alpha=0.9}$ (■) corresponding to the thermal degradation of the 10-MeOAzB/PAMPS copolymers.

CONCLUSIONS

A series of mesogenic/non-mesogenic new side-chain liquid-crystalline copolymers containing sulfonic acid groups has been synthesised over a broad range of compositions. All the copolymers exhibited liquid crystal behaviour and also the formation of hydrophilic aggregates, and therefore have application potential as new electrolytes for Direct Methanol Fuel Cells having controllable morphology.

However, there was evidence of interactions between the polar sites of the components, especially through the sulfonate groups, which promoted partial inhibition of the liquid crystallinity of the copolymers. The presence of interactions at high temperatures also caused enhancement of the thermal stability of the copolymers respect to that showed for the respective homopolymers.

REFERENCES

1. Blomen, L. *Fuel Cell Systems*, Ed. Plenum Press, New York, (1993)

2. Hoogers, G. *Fuel Cell Technology Handbook*, CRC Press, Nueva York, (2003)

3. Service, R. F. Science 296 (2002) 1222

4. Rhim, J.W.; Park, H.B.; Lee, C.S.; Jun, J.H.; Kim, D.S.; Lee, Y.M. J Membr Sci 238 (2004) 143

5. Ravikumar, M.K.; Shukla, A.K. J Electrochem Soc 143 (1996) 260

6. Scott, K.; Taama, W.; Cruickshank, J. J. Appl Electrochem 28 (1998) 289

7. Ge, J.; Liu, H. J Power Sources 142 (2005) 56

8. DeLuca, N.W., Elabd, Y.A. J Polym. Sci. Part B: Polym. Phys. 44 (2006) 2201

9. Every, H.A.; Janssen, G.J.M.; Sitters, E.F.; Mendes, E.; Picken, S.J. J.Power Sources 162 (2006) 380

10. Steinstrasser, R.; Pohl, L. Naturforsch 26b (1971) 577

11. Attard, G.S.; Imrie, C.T.; Karasz, F.E. Chem. Mater. 4 (1992) 1246

12. Craig, A.A.; Imrie, C.T. J. Mater. Chem. 1 (1994) 1705

13. Stewart, D.; Imrie, C.T. Polymer 37 (1996) 3419

14. Imrie, C.T.; Karasz, F.E.; Attard, G.S. Macromolecules 25 (1992) 1278

15. Craig, A.A.; Imrie, C.T. J. Polym. Sci. Part A. Polym. Chem. 34 (1996) 421

16. Zhong, C.; Huang, R.; Zhang, X.; Dai, H. J. Appl. Polym. Sci. 103 (2007) 4027

17. Zhang, B.Y.; Sun, Q.J.; Tian, M.; Ren, S.C. J. Appl. Polym. Sci. 104 (2007) 304

18. Turi, E. *Thermal characterization of polymeric materials*; Academic Press: New York (1997) Vol 2

19. Zhao, Y.; Lei, H. Macromolecules 27 (1994) 4525

20. Hu, J.; Zhang, B.; Feng, Z.; Wang, H.; Zhou, A. J. Appl. Polym. Sci. 80 (2001) 2335

21. V. Percec, V.; Hahn, B.; Ebert, M.; Wendorff, J. H. Macromolecules 23 (1990) 2092

22. Diele, S.; Oelsner, S.; Kuschel, F.; Hisgen, B.; Ringsdorf, H.; Zentel, R. Makromol. Chem. 188 (1987) 1993

23. Westphal, S.; Diele, S.; Mädicke, A.; Kuschel, F.; Scheim, U.; Rühlmann, K.; Hisgen, B.; Ringsdorf , H. Makromol. Chem. Rapid. Commun. 9 (1988) 489

24. Filip, D.; Simionescu, C. I.; Macocinschi, D.; Paraschiv, I. J Therm. Anal. Calorim. 65 (2001) 821

25. Smith, G.W. Mol. Cryst. Liq. Cryst. 180 (1990) 201

26. Craig, A.A.; Imrie, C.T. Polymer 38 (1997) 4951

27. Morishima, Y.; Nomura, S.; Ikeda, T.; Seki, M.; Kamachi, M. Macromolecules 28 (1995) 2874

28. Eisenberg, A.; Hird, B.; Moore, R. B. Macromolecules 23 (1990) 4098

29. Gohy, J. F.; Vanhoorne, P.; Jérôme, R. Macromolecules 29 (1996) 3376

30. Zhang, B.Y.; Meng, F.B.; Li, Q.Y.; Tian , M. Langmuir 23 (2007) 6385

31. Hwu, J.M.; George J.; Gao, Z.M.; Xie, W.; Pan, W.P. J Appl Polym Sci 83 (2002) 1702

32. Hatada, K.; Kitayama, T.; Fujimoto, N.; Nishiura, T. J Macromol. Sci. Part A: Pure Appl. Chem. 30 (1993) 645

33. de Almeida, S.H.; Kawano, Y. J. Therm. Anal. Calorim. 58 (1999) 569

34. Sebastien Viale, S.; Li, N.; Schotman, A.H.M.; Best, A.H.M.; Picken, S.J. Macromolecules 38 (2005) 3647

35. Chuan, K.Y.; Yao, W.G.; Yi, W. European Polymer Journal 44 (2008) 2448–2457

3 CONCLUDING REMARKS

A synthetic route for the preparation of *SCLCP* with enhanced proton conductivity has been designed and carried out. The route consists of only a few stages of synthesis and purification which are readily reproducible. This route has the advantage of being highly versatile and other methacrylate-based units can be easily incorporated such that new copolymers can be prepared to enhance the properties of the resulting materials.

The liquid crystallinity of the new copolymers is maintained even at low mesogenic concentrations. This can be explained by the formation of a phase separated structure, more similar to block-copolymers rather than to random-copolymers. This structure may be driven by the large difference in the polarity of the monomers. Moreover, the presence of sulfonic acid aggregates such those observed in pefluorinated membranes strongly suggest that these new materials will show high proton conductivity.

As mentioned previously, the synthesis of *SCLCP* provides flexibility in the preparation of new customised materials with enhanced properties. In this chapter, potentially highly conducting materials with liquid crystalline properties have been prepared. By separating the two main properties (conductivity and structural control) the new systems appear to be decoupled, which is advantageous when compared to the perfluorinated and PVA-crosslinked materials described earlier.

Another alternative to introduce morphology control using liquid crystals in high conducting materials is to prepare mesogenic units containing sulfonate groups, such the one shown in the following *Figure 6.9*:

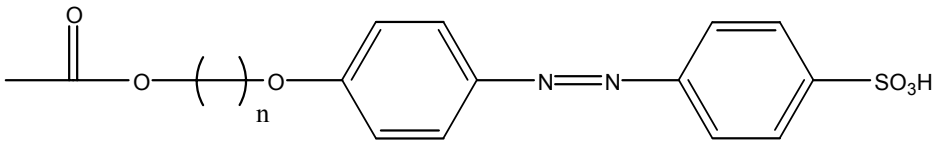

Scheme 6.9 Example of a sulfonated mesogenic unit

The introduction of the sulfonate unit in the mesogen will probably cause a higher dependency of the sulfonic group on the liquid crystal morphology, since the reorientational process will be more affected due to the existence of intra and inter

molecular bonds between the sulfonate groups and the rest of the polar sites of the molecule (N=N, bonds or ester groups). Therefore, a proper examination of the mesomorphism must be carried out.

In this context, some experiments have already been performed for the preparation of new sulfonated mesogenic materials, during the last stages of this PhD thesis. The preparation and analysis of the resulting properties will provide interesting results and will also give valuable information about the reorientation and phase morphology occurring in other *SCLCP*.

Apart from the synthesis of sulfonated mesogenic materials, different strategies have been proposed for the preparation of high proton conductive *SCLCP*. This includes:

- The preparation of ter-copolymers (the inclusion of methacrylate acid units among others can vary the flexibility of the backbone and also the reactivity ratios).
- The sulfonation of mesogenic copolymers, the study of the effect of different mesogenic units (length of the spacer, terminal groups, nature of the core).
- The search for new sulfonated units and even the use of different backbones (such as polysyloxanes or polystyrenes).

Finally, it would also be profitable to perform more detailed studies on the reactivity of the monomers in different conditions, since the reactions conditions can seriously affect the final chemical structure of the resulting copolymers.

REFERENCES CHAPTER 6

1. Percec, V.; Lee, M. J Mater. Chem. 2 (1992) 617

2. Ringsdorf, H.; Schneller, A. Makromol. Chem. Commun. 3 (1982) 557

3. Starnes Jr, W. H. Pure Appl. Chem. 57 (1985) 1009

4. Gray, G.W., *In Side Chain Liquid Crystal Polymers*, C.B. McArdle, Ed., Blackie and Sons, Glasgow (1989) chapter 4

5. Percec, V.; Hahn, B. Macromolecules 22 (1989) 1588

6. Percec, V.; Hahn, B.; Ebert, M.; Wendorff, J.H. Macromolecules 23 (1990) 2092

7. Braun, D.; Neumann, H. J.; Hellmann G. P. Makromol. Chem. 194 (1993) 2349

8. Neumann, H.J.; Jarek, M.; Hellmann, G.P. Macromolecules 26 (1993) 2489

9. Craig, A.A.; Imrie, C.T. J. Polym. Sci. Part A: Polym. Chem. 34 (1996) 421

10. Walker Jr., C.W.Electrochem Soc 151 (2004) A1797

11. P Stewart, D.; Imrie, C.T. Polymer 37 (1996) 3419

12. Craig, A.A.; Imrie, C.T. Polymer 38 (1997) 4951

7

Preliminary diffusion tests on the membranes

The final scope of this PhD thesis is to prepare new membranes for their use as Polymeric Electrolytes Membranes (*PEM*) in Direct Methanol Fuel Cells (*DMFC*) and to characterise their physical-chemical properties and also their diffusion properties for water and methanol mixtures. In the previous chapters the absorption of water, methanol and their binary mixtures in the materials has been studied through the combination of swelling tests and spectroscopic and thermal analysis techniques. These results must be analysed with those from diffusion tests. In this chapter, preliminary results obtained for some of the materials prepared in this PhD thesis are shown.

1 Materials

As described in chapter 6, the materials studied in chapters 3, 4 and 5 (Nafion, *PDLC* and PVA-SSA materials, respectively) are obtained as self-standing films. Examples of such materials are shown in *Figures 7.1 and 7.2*. However, the new side-chain liquid-crystalline copolymers (*SCLCP*) studied in chapter 6 were obtained as fine powders, as seen in *Figures 7.3 and 7.4*.

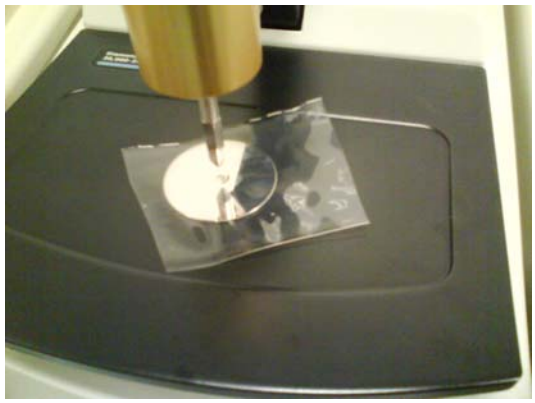

Figure 7.1 Example of a PVA-SA membrane under the FTIR-ATR accessory

Figure 7.2.Picture of Nafion membrane

Figure 7.3.Texture and appearance of the 10-MeOAzB monomer.

Figure 7.4.Examples of the 10-MeOAzB/AMPS copolymers

In order to obtain self-standing films, the *10-MeOAzB/AMPS copolymers* were cast from the melt at ambient conditions, as described in the previous chapter. The resulting films were brittle and had poor mechanical integrity. In order to enhance their mechanical properties, an inert support has been used. The copolymers have been cast on non-woven poly(propylene) (PP*)* from the melt and at high pressure. An example of the *SCLCP* films is shown in Figure 7.5. Although the first results have shown good compatibility between the copolymers and PP, new materials will be sourced to enhance the mechanical properties of the films.

Figure 7.5 Examples of the SCLCP films on non-woven PP

2 Experimental results

Some results on the diffusivity of water and methanol in the membranes prepared in this PhD thesis are described in this chapter. *Figure 7.6* shows the set-up of the diffusion test using the *10-MeOAzB/AMPS* copolymers. The membranes prepared on a non woven PP substrate were supported on two supports (*Figure 7.6a*) and were sandwiched between the two modules (*Figures 7.6b* and *7.6c*). The two reservoirs contained a mixture of water and methanol (in the blue module, left in *Figures 7.6b* and *7.6c*) and water (in the red module, right in *Figures 7.6b* and *7.6c*). The final set-up can be seen in the following *Figure 7.7*.

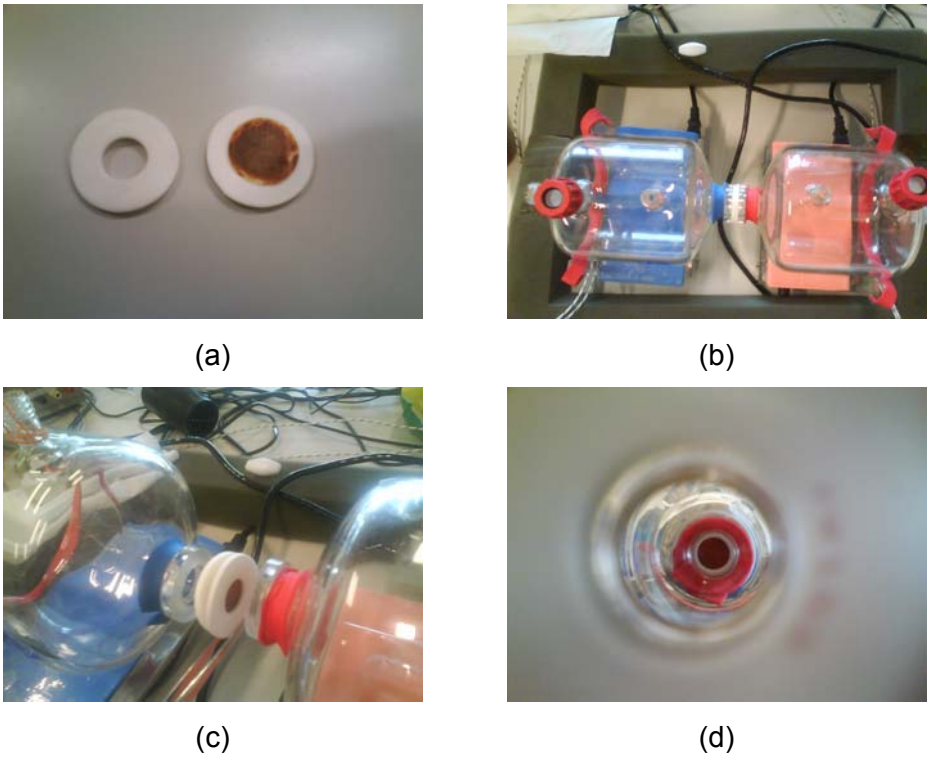

Figure 7.6 Set up of the diffusivity experiment with SCLCcP (chapter 6). (a) Membrane supported by two foam supports; (b) Upper view of the module; (c) Detail of the central part of the module; (d) Inside view of the module with the membrane.

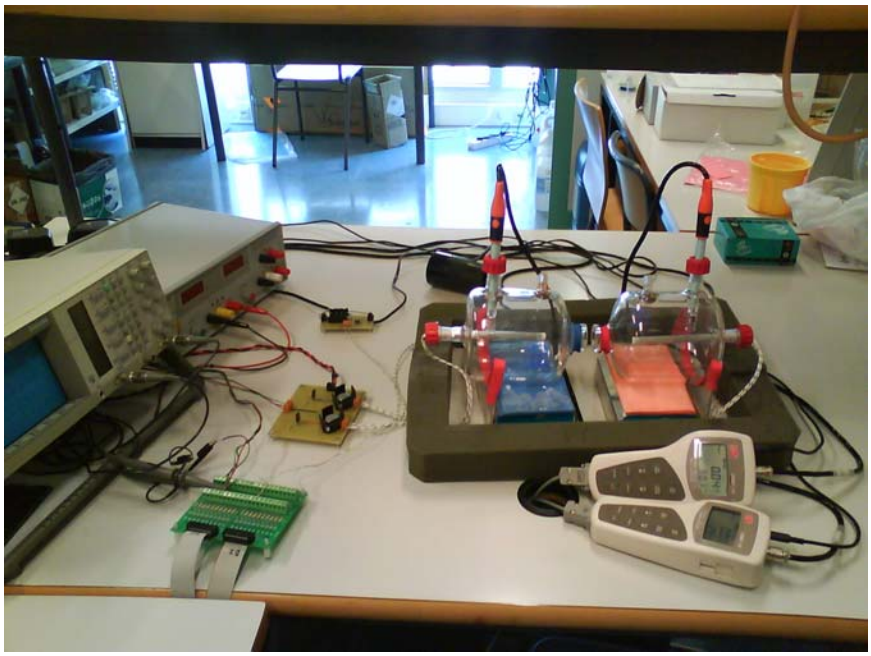

Figure 7.7 Diffusivity experiment

The conductivity of the solutions in both tanks was monitored (*Figure 7.8a*) and data collected by the computer through the conductimeters (*Figure 7.8b*). The signals were processed with a *LabView* program (*Figure 7.8c*) and the results were monitored in real time (*Figure 7.8d*) being automatically saved in a *.txt* file, according to the procedure explained in chapter 2.

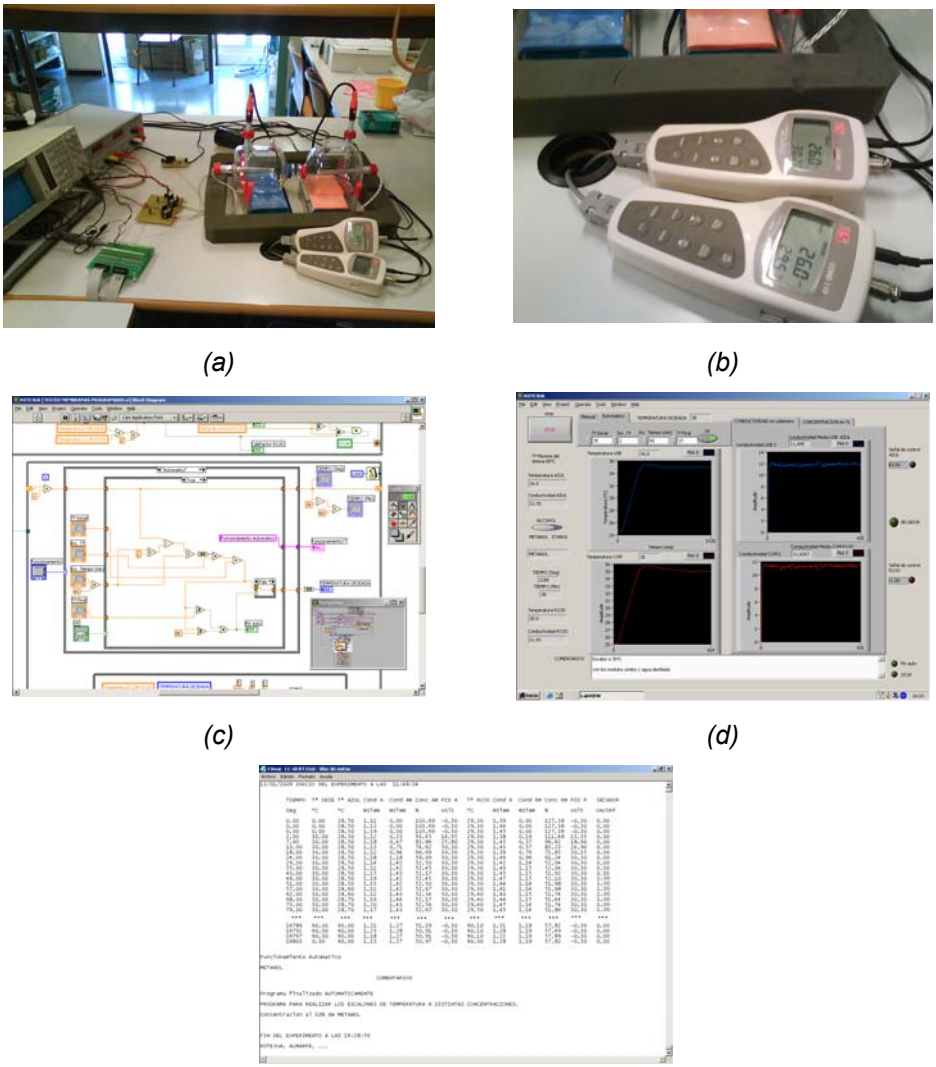

(a) *(b)*

(c) *(d)*

(e)

Figure 7.8.Steps in the data acquisition

Figure 7.9 shows the results of a test performed to measure the free diffusion of a mixture of 30% by weight of methanol from the blue tank to the red one, in the absence of a membrane. This curve gives an indication of the maximum diffusion rate in the conditions of the experiments.

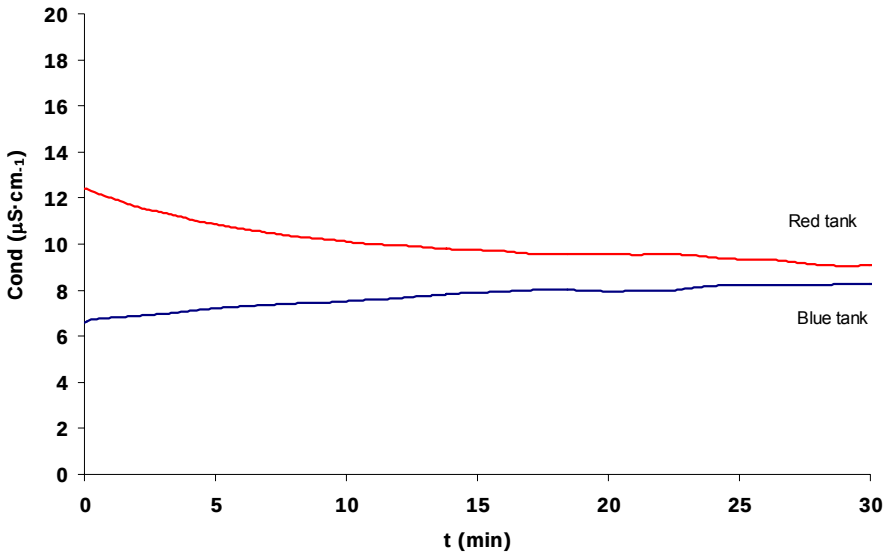

Figure 7.9 Diffusion test (open tanks with no transport resistance)

The results corresponding to the diffusion tests through different membranes of a solution of water/methanol containing 30% by weight of methanol were also obtained. The normalised curves with respect to time (t) and the square root of the time ($t^{1/2}$) are shown in *Figures 7.10* and *7.11*, respectively. The figures show the curves corresponding to a Nafion commercial membrane, a *PVA96hyd-10%SSA* membrane and a membrane prepared on non-woven PP with *10-MeOAzB/AMPS 0.3*. The curve corresponding to the diffusion of methanol from a solution containing 30% by weight in the absence of a membrane (*Figure 7.9*) is also shown.

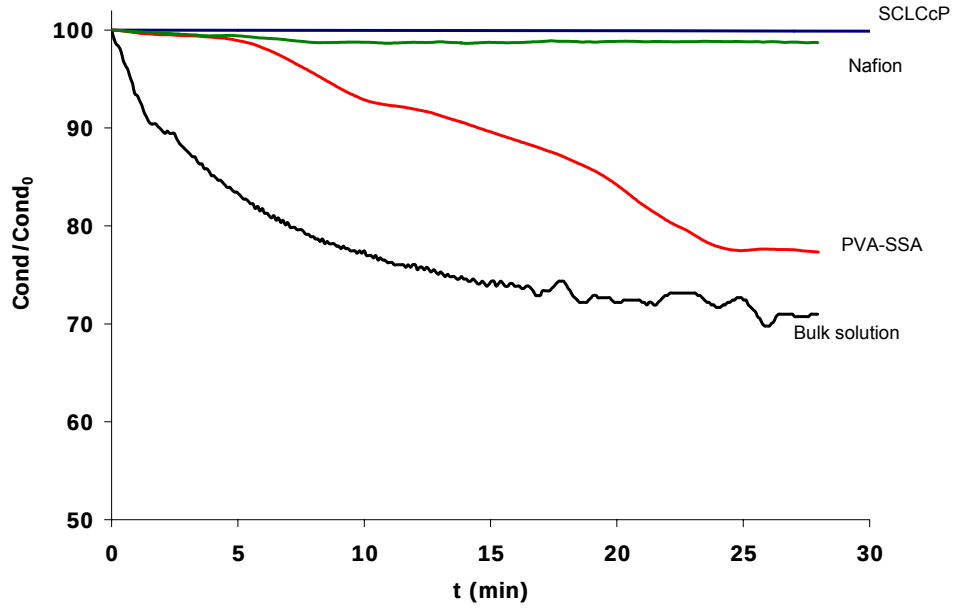

Figure 7.10 Diffusion tests of different membranes (1). Values of relative conductivity (Cond) respect to the initial value ($Cond_0$)

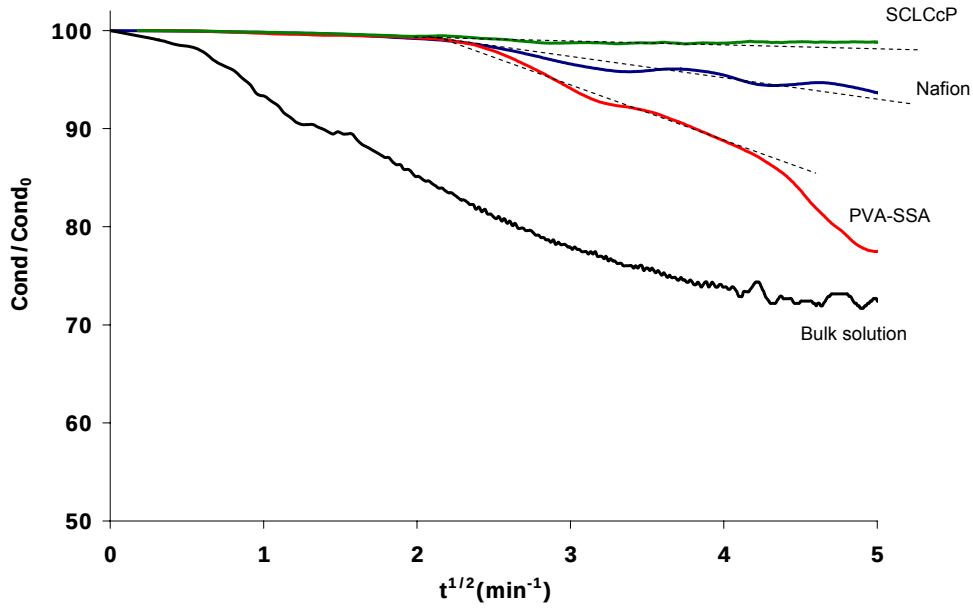

Figure 7.11 Diffusion tests of different membranes (2). Values of relative conductivity (Cond) respect to the initial value ($Cond_0$)

As expected, the normalised conductivities behave differently for each type of membrane and in the absence of one (black curve). The diffusion of methanol in the

absence of a membrane follows a first order profile. In contrast, the diffusion through the membranes seems to occur following at linear profile close to zero order, suggesting that diffusion is controlled by relaxation processes of the polymer chains of the membranes, or the so-called Case II (non-Fickian) [1]. A similar dependence was also found in the results of the desorption tests for PVA-SSA membranes prepared in chapter 5, see *Figure 7.12* indicates.

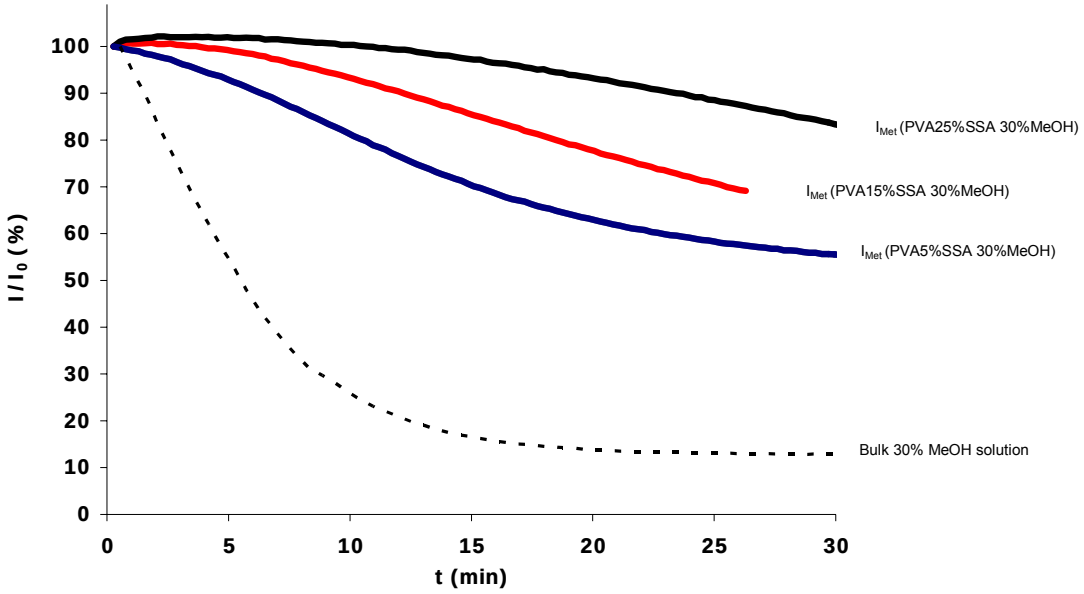

Figure 7.12 Desorption tests corresponding to PVA-SSA membranes

It is notable that all the membranes shown in *Figure 7.10* contain an initial period of time during which the conductivity decreases very slowly, approximately *5* minutes (*see Figure 7.13*).

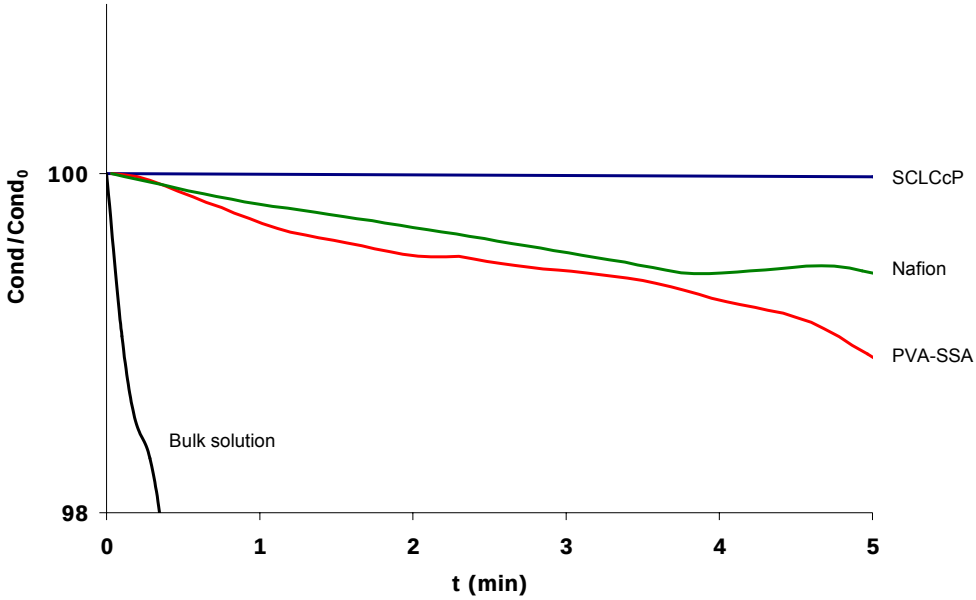

Figure 7.13 Curves corresponding to the first moments of diffusion through the membranes

After 5 minutes, the conductivity of the red tank (initially fed with water) starts to decrease at a greater rate (see *Figures 7.10* and *7.11*). These results indicate that methanol is transferred through the membranes very slowly during the initial stages, but then starts to diffuse more rapidly. This can also be seen in Figure 7.12 for the highly crosslinked PVA-SSA membranes, and may be attributed to a transport process based on an initial swelling of the membrane followed by diffusion through the swollen membrane. This may imply the so-called vehicular mechanism of mass transfer, as previously discussed in chapter 1 [2]. As described elsewhere, this mechanism is strongly implicated in the crossover phenomena in *PEM* used in *DMFC*.

Another important feature seen in *Figures 7.10, 7.11* and *7.13* is that the diffusion rate in the zero-order region varies from one membrane to another, indicating that the chemical composition has some effect on the diffusivity of methanol through the membranes. It is clear that, while the PVA-SSA membrane shows a high methanol diffusion rate, the membrane prepared with the *10-MeOAzB/AMPS 0.3* copolymer shows very low methanol permeability, even lower than Nafion.

Moreover, FTIR analysis of the *10-MeOAzB/AMPS 0.3* membrane after the diffusivity test revealed the presence of water absorbed in its structure, see *Figure 7.14*.

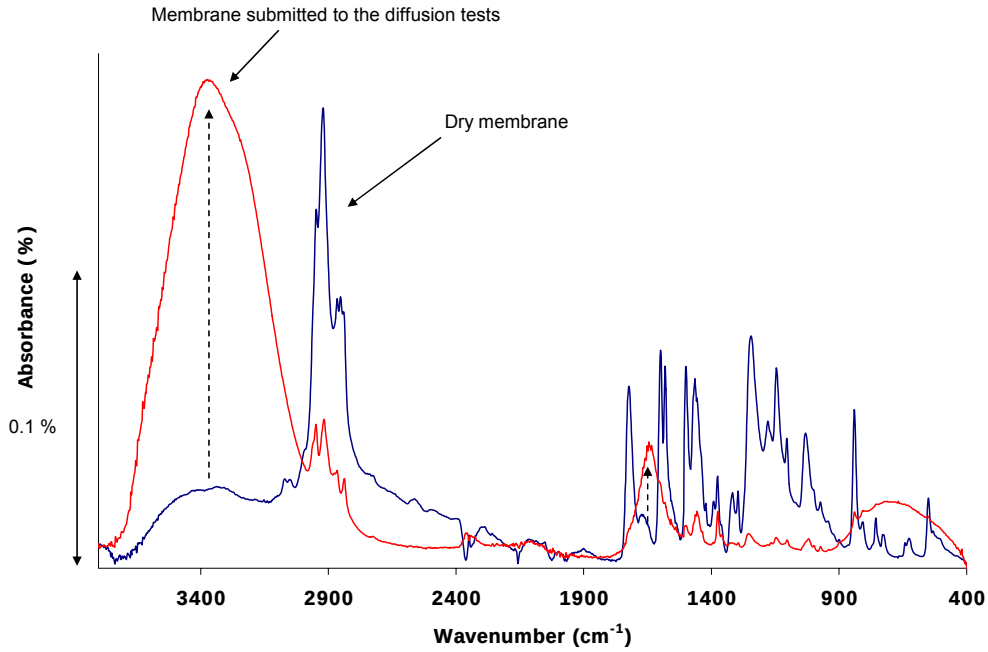

Figure 7.14.FTIR curves corresponding to the10-MeOAzB/AMPS 0.3 copolymer before (blue line) and after (red line) being submitted to the diffusion test in a binary mixture containing 30% of methanol (weight percentage)

These data suggest that the liquid crystal copoly(methacrylate)s containing azobenzene moieties (10-(4-methoxy-4'-oxy-azobenzene) decyl methacrylate) and 2-acrylamido-2-methyl-1-propanesulfonic acid (*AMPS*) do have potential application as Polymer Electrolyte Membranes in Direct Methanol Fuel Cells, since they show low methanol diffusivity but do absorb water in their structure. These are the target properties of materials designed to reduce the so-called crossover phenomenon.

3. Conclusions

Some of the materials prepared in this PhD thesis have been submitted to diffusion tests. The results have shown differences between the diffusion of methanol through the different membranes. As expected, all the membranes retard the transport of methanol. In general terms, there are two diffusion regimes. During the initial stage, the diffusion of methanol seems to be very slow, which was attributed to the swelling of the membranes. After some minutes, there is a more accelarated decrease in the conductivity with time, which was related to a faster diffusion of methanol through the membranes. This fact is attributed to a change in the transport mechanism of methanol through the swollen membrane, more similar to a zero order (constant) diffusion profile. The results also reveal that the *10-MeOAzB/AMPS 0.3* membrane shows the lowest methanol diffusion rates, which suggests that this type of membranes may be suitable for use as *PEM* in *DMFC*, in order to reduce the crossover phenomenon and hence increase their efficiency.

REFERENCES CHAPTER 7

1. Tarcha, P.J. *Polymers for Controlled Drug Delivery*, Boca Raton: CRC Press (1990)

2. Kreuer, K.D.; Rabenau, A.; Weppner, W. Angew. Chem. In. Ed. Engl. 21 (1982)

8

Conclusions

This PhD thesis has investigated new polymeric materials for their potential use as electrolytes in Direct Methanol Fuel Cells (*DMFC*). In particular, the study has focused on the preparation of polymers with enhanced proton conductivity and having controllable morphology, with the aim of reducing the so-called crossover phenomenon.

1 Final conclusions

Different design strategies for achieving new materials with controllable morphology for potential use as electrolytes in Direct Methanol Fuel Cells (*DMFC*) have been employed in this PhD thesis, including:

- The preparation of polymer dispersions of liquid crystals.
- The preparation of crosslinked poly(vinyl alcohol) membranes with enhanced proton conductivity.
- The synthesis of side-chain liquid-crystalline copolymers incorporating sulfonic acid groups in their structure.

A methodology by which to undertake the structural and morphological characterisation of the new materials has been developed involving spectroscopic and thermal analysis techniques. The joint application of Fourier Transform Infrared Spectroscopy (FTIR), Differential Scanning Calorimetry (DSC) and Thermogravimetric Analysis (TGA) provides highly complementary information about the chemical structure, the cluster morphology and the thermal stability of the materials prepared in this PhD thesis.

The spectroscopic analysis focused on a study of the FTIR bands related to the most characteristic groups of the materials. The intensity and displacement of the bands were used to analyse the formation and strength of intermolecular interactions between the components of the membranes and the solvents. This approach was very useful in studying the process of formation of the membranes and also the contents and state of solvents inside them. Particular attention was paid to the formation of hydrogen bonds between water and methanol with the different regions of the polymer, and their strength as a function of the solvent composition and polymer structure.

In the TGA experiments, the different mass loss regions provided information about the stability of the proton conducting groups, the side groups, the membranes and the interactions between the polymeric components of the membranes and the solvents. In particular TGA was very useful to reveal and study solvents with different degrees of association with the polymer, mainly free and bound solvent.

DSC was used to analyse the morphology of the polymers. This technique provided information about the phase separation in the materials, and also the possible existence of a morphology based on cluster aggregates. These two structural features are crucial for the performance of polymer electrolytes in *DMFC*. Moreover, DSC was used to study the phase behaviour of the polymeric materials having enhanced morphology control. In *DMFC* electrolytes, the interactions and cooperative effects occurring between the polymer backbone and the side groups is very important to obtain morphological control and to separate the functionality of each phase.

A methodology to evaluate the diffusion properties of the materials with respect to water and methanol has been devised, based on the performance of swelling, desorption and diffusion tests. A plant has been designed, built and set-up to measure the diffusivity properties of polymeric electrolytes for *DMFC*, and particularly those with morphological control. The plant measures the concentration changes produced in two solutions when water and alcohol (methanol or ethanol) permeate through a membrane under test. The module incorporates two mesh electrodes that can be used to simulate the electro-osmotic conditions in a *DMFC* and also to test membranes with controlled morphology, such as those prepared in this PhD thesis.

This methodology for evaluating structural and diffusion characteristics was first applied to commercial Nafion membranes. The absorption tests of water in the Nafion membranes revealed a typical Fickian behaviour but the absorption of methanol and its binary mixtures in water was more complex. The values of mass flux indicated that the absorption of solvent was faster in the solutions containing methanol than in pure water.

The variation of the IR vibrations in the regions of 3000 cm^{-1} and 1650 cm^{-1} corresponding to the OH groups in the swollen membranes were chosen to analyse the strength of the interactions between the solvent and the hydrophobic groups of Nafion. The variations in these bands on increasing methanol concentration showed that the solvent composition had notable effects in the polymer groups of the membranes. The physical-chemical analysis also showed that two types of solvent were absorbed in the membranes: free or loosely absorbed solvent and tightly bound solvent. The results indicated that the amount of solvent bound to the polymer structure increased gradually with the methanol concentration in the binary mixtures.

The study of the morphology revealed changes in the morphology of the polymer with the composition of the solutions absorbed in the Nafion membranes. While the membrane submerged in water tended to follow a typical coalescence process by forming large clusters, this process seemed to be modified by the presence of methanol in the solutions. The differences in the mechanisms observed for the absorption of methanol and water could be responsible, at least in part, for crossover in *DMFC*.

As an alternative to perfluorosulfonic acid polymers (*PFSA*), new polymers were prepared during this PhD thesis. In order to reproduce the cluster structure observed in Nafion membranes, films consisting of Polymer Dispersed Liquid Crystals were prepared. Cellulose Acetate (*CA*) was used as the polymeric substrate and two different commercial liquid crystals (cholesteryl oleyl carbonate (*COC*) and *n*-(4-methoxybenzylidine)-4-butylaniline (*MBBA*)) as the dispersed phase.

The two series of Polymer Dispersed Liquid Crystals films showed different behaviour depending on the nature of the liquid crystal and its interactions with the polymer substrate. The films containing *CA* and *COC* exhibited liquid crystal behaviour across the range of compositions, indicating that these films behave as genuine liquid crystals polymer dispersions. However, there was evidence of some interactions between the two components which did alter the properties of the polymeric and liquid crystalline phases. Such interactions lead to a decrease in the thermal stability of the first stages of decomposition but also to a certain inhibition of the substrate degradation. The random degradation mechanism of *CA* was somehow inhibited in the films.

On the other hand, the presence of strong interactions was observed in the films containing *CA* and *MBBA* even at low temperatures. Such interactions promoted the inhibition of the mesomorphic properties of *MBBA* in these films and a drastic decrease in the thermal stability of the samples.

Unlike the films containing *CA* and *MBBA*, the application of the physical-chemical analysis concluded that the membranes containing *CA* and *COC* are candidates for their use in electrolytic applications, since they maintained the mesomorphic properties. However, some swelling and diffusion tests performed to the *CA-COC* membranes

showed very little stability of the dispersed phase respect to alcohols and also high amounts of methanol permeation. All these facts represent serious limitations and some modifications must be carried out prior to their use as electrolytes in *DMFC* applications.

With the aim of obtaining materials with enhanced stability and controllable morphology, the preparation and properties of poly(vinyl alcohol) (PVA) materials were investigated. PVA materials with enhanced morphology control were prepared by the esterification of PVA backbone with two different liquid crystal molecules, (4-pentoxybenzoic acid-POBA and 6- [4-(4-methoxyphenylazo)phenoxy]hexanoic acid-Azo5) through the corresponding acid chlorides. Unfortunately the polymer modification reactions proceeded with very low yield. The properties of the resulting materials (high melting point and low decomposition temperature, high viscosity and low solubility in common solvents) were not suitable for the preparation of *DMFC* membranes.

As an alternative, the preparation of dispersions of liquid crystals in crosslinked PVA membranes was proposed. PVA membranes with different degrees of hydrolysis (89%, 96% and 99%) were prepared using sulfosuccinic acid (SSA) as the crosslinking agent (PVA-SSA membranes) by thermal treatment. The occurrence of esterification between the hydroxyl groups of PVA and the carboxylic acid groups of SSA and the formation of a crosslinked structure with enhanced stability was observed for all the PVA substrates. The esterification reaction began as soon as the membranes were formed but was accelerated by the thermal treatment.

The study of the membranes using FTIR revealed distinct chemical environments comprising of the polar and non-polar regions in the PVA-SSA membranes. The 3700 – 3000 cm^{-1} region was chosen to analyse the contributions of the OH groups, and a blue-shift of the OH stretching band corresponding to the polymer backbone was observed. The formation of water clusters of ionic aggregates in the PVA-SSA membranes was also demonstrated by the presence of a tail in the $\nu<3000$ cm^{-1} region, as seen for the commercial Nafion commercial membranes. Another region of interest was that corresponding to the OH bending vibration of the water molecules ($\nu\sim1650$ cm^{-1}). This

region also underwent characteristic changes with the chemical composition of the polymer backbone and the presence of tightly bound water.

The hydrolysis degree of the PVA substrate also had important effects on the preparation and the structure of the PVA-SSA membranes. It was found that the PVA-SSA membranes with higher hydrolysis degrees (99% and 96% hydrolysed) were the most affected by the thermal treatment and the SSA concentration. The presence of tightly bound water and water clusters in the PVA-SSA membranes was also observe and similar to that seen for the Nafion membranes. The highest values of water content were observed for the membranes prepared using a PVA substrate with a hydrolysis degree of 96%, which also showed the best processing properties in the preparation of the crosslinked membranes.

These suggest that the PVA-SSA membranes prepared using the PVA substrate with 96% hydrolysis degree (96% *HD*) have the greatest potential as electrolytes for *DMFC*. The diffusion properties of the PVA-SSA membranes (96% *HD*) were also investigated, and the results were compared to those obtained for the commercial Nafion membranes.

The transport properties of water, methanol and their binary mixtures through the PVA-SSA crosslinked membranes (96% *HD*) were strongly dependent on the composition of the polymer and the solvent. While the membranes absorbed high amounts of solvent from the water and water/methanol binary mixtures, the diffusion of pure methanol was very low and deviated from ideal behaviour. Moreover, it was found that methanol was tightly bound to the polymeric structure, as observed for the commercial Nafion membranes.

The composition of the binary mixtures and the polymer structure greatly affected the transport mechanisms of the solvents in the membranes. The results suggest that the presence of water promotes the diffusion of methanol by the occurrence of molecular dynamic processes involving the polymeric chains. Moreover, it was observed that high crosslinking degrees tend to reduce the diffusion of methanol and water through the PVA SSA membranes (96% *HD*).

The results also indicated that the balance of free and bound solvent depends on the composition of the solvent and also on the morphology of the polymer. The PVA membranes showed higher contents of tightly bound water than Nafion. This suggests that the process of formation of the polymers may have an important effect on the water content. The absorption tests indicated that the absorption of pure methanol was much lower than the absorption of water in the PVA membranes. However, the diffusion of methanol through the PVA membranes was very high from the binary mixtures with water, which may be an significant shortcoming for their future use in *DMFC*.

The results of some diffusivity tests performed on the PVA-SSA membranes showed that the diffusion of methanol was still very high compared to the results obtained for the Nafion membranes. Therefore, although the PVA-SSA membranes showed a certain control by the morphology on the diffusion process by varying crosslinking degree, further modifications must be made in order to reduce the methanol diffusion in water binary mixtures prior to their use in *DMFC*. This will involve achieving a better balance between polar and non-polar regions and the crosslinking degree.

In order to obtain materials with high degree of morphology control enhanced thermal and chemical stability and improved selectivity with respect to the methanol transport, new side-chain liquid-crystalline copolymers were designed, synthesised and characterised. Poly[10-(4-methoxy-4'-oxy-azobenzene) decyl methacrylates]–co-poly[2-acrylamido-2-methyl-1-propanesulfonic acid]s were prepared by free radical copolymerisation. The synthesis procedure involved several experimental steps and was carried out in mild conditions using a relatively polar organic solvent (*DMF*). Unlike the esterification of PVA, the preparation of these copolymers showed high yields and the resulting materials have appropriated processing conditions to obtain films from the melt by using an adequate substrate. Moreover, the use of copolymers can combine the properties of different materials by varying the chemical composition of the monomers used. Therefore, these reactions are suitable to obtain tailor made materials with enhanced properties. The proton conductivity, the backbone flexibility as well as other parameters can be readily varied by simply changing the nature of the molecules, adding new groups or varying the feed ratios.

As with Nafion and the PVA-SSA membranes, sulfonic acid groups were used as proton conductive sites in the materials. The introduction of the *SO_3* groups was successful, as shown by FTIR, NMR and TGA. The study of the chemical environment of these groups focused on the frequency shift and intensity of the bands at ν~1042 cm^{-1} and ν~1230 cm^{-1} (SO_3^- *st*), although this latter band is usually overlapped by other contributions (*COC* or CF_2 stretching). The IR results also showed that the acid group was found in the dissociated form ($SO_2OH + H_2O \rightarrow SO_3 + H_3O^+$) in all the materials, promoting the formation of proton clusters in superacid structures. These species are responsible of the so-called vehicular mechanism of water and methanol through *DMFC* electrolytes, and their study is important in order to analyse and optimise the proton conductivity processes and to reduce crossover.

There was also evidence of interactions between the polar sites of the copolymers which promoted partial inhibition of the liquid crystallinity. The interactions were studied through the variations in the IR bands of the polar and non-polar groups of the copolymers, since the frequency of the bands as well as their intensity changed depending on the composition.

The most characteristic bands were chosen to analyse the polymer backbone (CF_2 in Nafion, OH and CH_2 in PVA and C-O and C=O in the copolymers) and the groups responsible for the proton conductivity (SO_3^-). There were notable differences between the behaviour of the polar and non-polar regions, and also between the groups related to the polymer backbone and the side groups. The formation of covalent bonds promoted an increase in the stability to solvents of the resulting copolymers with respect to the dispersions.

Important differences in the thermal stability of the side and main chain components of the different materials were observed. All the sulfonated materials followed a similar decomposition pattern. The desulfonation of the materials took place at low temperatures (250ºC – 350ºC) and can be used as a parameter to define the thermal stability of the membranes. Another indicator of the stability of the materials is the decomposition of the side chains, which was observed in the 400ºC – 490ºC region for Nafion, and at lower temperatures for the copolymers (~300ºC), due to the different

chemical composition of the materials. The degradation of the polymeric main chain (occurring at higher temperatures 350ºC – 550ºC) and the residual values have also shown different behaviours depending on the composition of the materials.

The diffusion properties of the membranes prepared using the side-chain liquid-crystalline copolymers on a non-woven poly(propylene) substrate were also studied with respect to methanol and water binary mixtures. The diffusion of the solvents through the membranes took place through two main steps. During the first moments of the tests, the diffusion of methanol seemed to be very slow, which was attributed to the swelling of the membranes. After some minutes, there was a more pronounced decrease in the conductivity with time, which was related to a faster diffusion of methanol through the membranes. This fact can be attributed to a change in the transport mechanism of methanol through the swollen membrane, more similar to a zero order (constant) diffusion profile, and could be observed in all the membranes prepared in this PhD thesis.

The side-chain liquid-crystalline copolymers showed the lowest methanol diffusion rates and high water absorption, compared to the commercial Nafion membranes and the other membranes prepared in this PhD thesis. The introduction of sulfonate groups (which ensures high proton conductivities) indicates that these membranes can be used as electrolytes in *DMFC*. Moreover, the liquid crystal behaviour of the copolymers indicated that the morphology of the copolymers can be somehow controlled by external factors. All these facts suggest that the use of these materials as electrolytes with morphological control can help reduce the crossover phenomenon and to increase the efficiency of Direct Methanol Fuel Cells.

2 Further work

All the different materials prepared in this PhD thesis have shown interesting properties and several have real application potential in *DMFC*.

The properties of the PVA materials can be enhanced by the preparation of blended copolymers using a hydrophobic polymeric substrate. This can be achieved by using alternative crosslinking agents (such as glutaraldehide, *GA*) following a similar methodology as the one proposed in this PhD thesis. On the other hand, the preparation of polymer dispersed liquid crystals could be a simple and effective method to obtain electrolytes with enhanced properties. However, a deep analysis on the interactions between the substrate and the liquid crystals must be carried out, in order to choose the materials to prepare the dispersions.

Among all the materials prepared in this PhD thesis, the liquid crystal copolymers have shown the most promising behaviour. Several approaches to improve the performance of these materials have been proposed, including the use of a tertiary component to modify the flexibility in the main chain, or the use of mesogenic units containing sulfonate groups, such the one shown in *Figure 6.2:*

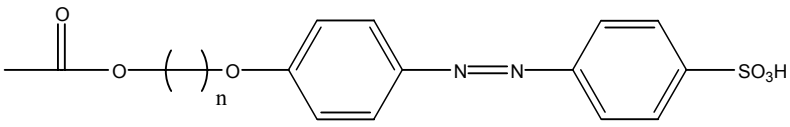

Figure 6.2. Example of a sulfonated mesogenic unit

Different swelling tests and diffusion techniques to characterise the solubility and selectivity of membranes against water and methanol mixtures have been used in this PhD thesis. The presence of water and other solvents in the polymers has been related with the structure through the use of FTIR, TGA and DSC. The use of all the dielectrical techniques together with the methodology of morphological characterisation proposed in this thesis will give a complete description and analysis of the new polymeric electrolytes membranes (*PEM*) with morphological control for Direct Methanol Fuel Cells (*DMFC*). It is especially important to study the effect of the reorientation of liquid crystalline materials on the morphology of the polymers and their

diffusion properties respect to water and methanol. Therefore, during the development of this PhD several techniques have been designed and set-up to test the electrical response of the materials, including:

- The incorporation of electrodes in the diffusion plant to apply electrical fields through the membranes under test. This also includes the implementation of the control elements by PC.
- The design and set-up of a device to obtain the polarisation and depolarisation curves of membranes at different temperatures. The system includes an electrometer, a power source and a measurement cell. A program has been prepared for the performance of the tests and the data acquisition. The scheme and a picture of the plant is shown in *Figures 8.1* and *8.2*, respectively:

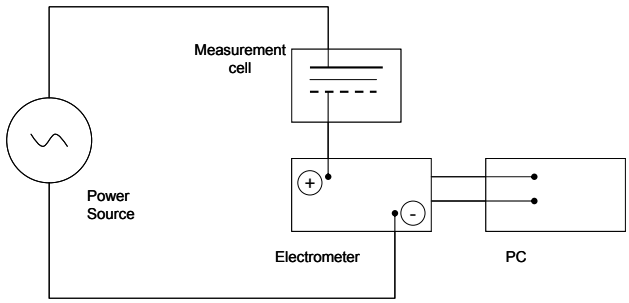

Figure 8.1 Schematic of the test fixture to test polarisation and depolarisation curves

Figure 8.2 Test fixture to test polarisation and depolarisation curves

- The dielectrical relaxation spectra of side-chain liquid-crystalline copolymers will also be obtained by a dielectrical module, at different temperatures and frequencies. The tests will help analyse the reorientation of the mesogenic units and discriminate the coupling effects between the polymeric backbone and the side groups through the study of the different molecular relaxations.
- The results will be completed by measuring the proton conductivity of the electrolytes at several conditions. This will be carried out with a proton conductivity fixture using a Frequency Response Analyzer coupled with an electrochemical interface. The proton conductivity (σ^+) will be calculated from the measures of complex impedance ($Z^* = Z + iZ$) by obtaining the intersection with the real axis. The results will be complemented with experiments on the Ionic Exchange Capacity (*IEC*) and hydrolytic stability.

3 Other Institutional Benefits of the PhD thesis

As it was mentioned in the first sections of this thesis report, these PhD studies have been performed in the framework of a co-supervised partnership between the Universitat Politècnica de València (UPV, Valencia, Spain) and the University of Aberdeen (UOA, Aberdeen, Scotland, UK). Therefore the scientific results and the cooperation frameworks consolidated during the past years will be very useful for future PhD students and also to enhance the collaboration between both universities.

Other positive aspects resulting from the work in this PhD studies are related to the development of several research projects in the fuel cells area with other universities from Spain (Universitat Politècnica de Catalunya, Universidad Politécnica de Madrid) and from other European countries (University of Genova, Italy). The development of some of these projects, among other research actions and collaborations, has promoted the implementation of a laboratory to prepare and characterise new electrolytes for Direct Methanol Fuel Cells which is now active and in continuous growth.

From a scientific point of view, this PhD thesis has shown interesting results on the preparation of complex polymeric materials for advanced applications. In particular, the work has been focused on the search of new electrolytes for their application in the field of fuel cells. During the duration of this PhD thesis, the number of publications and the investment on research in science and technology related to fuel cells has enormously increased, which is a clear indication of the great interest that this technology has these days.

Moreover, during the preparation of this PhD thesis, relevant information about new hydrophobic / hydrophilic materials has been obtained. The research on this topic can be very useful not only for the development and characterisation of electrolytes, but also in other fields of materials science. The synthesis of new polymers with polar and non-polar regions usually presents several limitations due to the different chemical nature of the components. Such limitations usually concern solubility and reactivity problems. Copolymerisation results a good alternative for the preparation of liquid crystalline materials with enhanced proton conductivity, but the results can be also applied in other systems where polar and non-polar groups must be present in the same structure.